Spring 1990

The petrogenesis of the Agamenticus complex and late Paleozoic and Mesozoic tectonics in New England

John A. Brooks
University of New Hampshire, Durham

Order Number 9027424

The petrogenesis of the Agamenticus complex and late Paleozoic and Mesozoic tectonics in New England

Brooks, John A., Ph.D.

University of New Hampshire, 1990

U·M·I
300 N. Zeeb Rd.
Ann Arbor, MI 48106

THE PETROGENESIS OF THE AGAMENTICUS COMPLEX AND LATE PALEOZOIC AND MESOZOIC TECTONICS IN NEW ENGLAND

BY

JOHN A. BROOKS
Bachelor of Arts, Boston University, 1974
Master of Science, University of New Hampshire, 1986

DISSERTATION

Doctor of Philosophy

in

Earth Sciences

May, 1990

This dissertation has been examined and approved.

Dissertation Co-Director, Dr. Wallace A. Bothner
Professor of Geology
University of New Hampshire

Dissertation Co-Director, Dr. David A. Gust
Adjunct Associate Professor of Geology
University of New Hampshire
Associate Professor and Head
Department of Applied Geology
Queensland University of Technology

Dr. Francis S. Birch
Professor of Geophysics
University of New Hampshire

Dr. Jo Laird
Associate Professor of Geology
University of New Hampshire

Dr. O. Donald Hermes
Professor of Geology
University of Rhode Island

April 19, 1990
Date

Dedicated to Dr. C. Wroe Wolfe and all geologists like in heart:

The Himalayas

Rock!
Jagged, sculptured rock!
Where air is thin,
Too thin to breathe.

Where mind and blood congeal
And sky is just a step away.

There you stand,
Mighty monuments-ramparts rising-
Born from out a Tethys sea
You reach for Heaven from Earth.

Young you are
As mountains go.
Only yesterday the waters crossed your face;
But deep below the waters your strength was growing.

Then-
Quake by quake, fault by fault
You rose-
To claim the sky.

And now 'tis yours.
Drink deep of that ethereal blue,
For as your winter snows
Melt and fade away,
So will your form and power decay,
And you will sink to prepare the way
For a loftier, nobler range of yet another day.

From the unpublished collection of C. Wroe Wolfe
(Lyons and Brownlow, 1976)

ACKNOWLEDGEMENTS

Funding for this research is gratefully acknowledged; UNH (CURF and Hubbard Fellowships), GSA (Grants 3728-87 and 3941-88), AFMS (1988-1990),and Sigma XI, and National Science Foundation (Dr. D. Gust - Grant EAR-8817184). Geochemical labs at the University of Rhode Island, Boston College, and the USGS (Denver) were instrumental in obtaining geochemical analyses required for this study. Irradiation costs were covered under a US DOE reactor sharing grant (DE-FG02 ER10770) to the MIT reactor. My thanks to Mathew Paige and Nancy Niven for their guidance at the geochemical labs of Boston College and the University of Rhode Island, respectively. The support, encouragement, and education offered by my advisors laid the foundation for the completion of this dissertation. With Linda Hoadley at the helm, the office staff, past and present, helped smooth over many a bump in my progress. But most of all my gratitude is extended to the my wife, Janice, for her years of loving support.

TABLE OF CONTENTS

DEDICATION....iii

ACKNOWLEDGMENTS....iv

LIST OF FIGURES....x-xii

LIST OF PLATES....xiii

LIST OF TABLES....xiv

ABSTRACT....xv-xvii

CHAPTER 1 INTRODUCTION....1

CHAPTER 2 GEOLOGY AND GEOPHYSICS OF CENTRAL COASTAL NEW ENGLAND AND WEST-CENTRAL MAINE: IMPLICATIONS FOR MESOZOIC IGNEOUS COMPLEXES....7

I. INTRODUCTION....7

II. REGIONAL SETTING....13

Massabesic-Merrimack-Rye Blocks....13

Central Maine Terrane....19

Terranes of southeastern New England....19

Casco Bay Block....20
Gulf of Maine....21
III. DATA COMPILATION AND PROCESSING....24
IV. RESULTS....26
Mesozoic Plutons....32
Massabesic-Merrimack-Rye Block....36
Casco Bay Block....38
Kearsarge Central Maine Synclinorium....39
Zones of the Boston Platform....39
Nashoba Zone....40
Marlboro-Newbury Zone....40
Esmond-Dedham Zone....41
Offshore Lithotectonic-Geophysical Correlations....43
V. DISCUSSION....45
IMPLICATIONS FOR REGIONAL TECTONICS....45
IMPLICATIONS FOR MESOZOIC IGNEOUS ACTIVITY....51

CHAPTER 3 PETROGENESIS OF THE AGAMENTICUS COMPLEX: SOUTHWESTERN MAINE....54

I. INTRODUCTION....54
Previous Work....55
Geologic Setting....58
Models for the petrogenesis of A-type magmas....60
II. ANALYTICAL TECHNIQUES....61
III. RESULTS....63
Petrography and mineral chemistry....64

Biotite Granite....64
Alkalic Granite to Quartz Syenite....68
Aegirine Alkalic Granite....71
Alkalic Syenite....79
Porphyritic Aenigmatite Syenite....84
Syenite to Quartz Syenite Zone (SQSZ)....87
Dikes....90
Mafic Dikes....90
Trachyte Dikes....90
Mafic Syenite Dikes....91
Geochemistry....91
Major Elements....91
Trace Elements....97
Rare Earth Elements....108
Discrimination Diagrams....111
IV. DISCUSSION....111
Sequence of Intrusion....111
Depth of Emplacement....118
Petrology of the Agamenticus Complex....122
Magma Mixing....124
Assimilation....126
Fractional Crystallization....128
SQSZ and Aenigmatite Syenites....132
Alkalic Syenite....147
Quartz Syenite to Alkalic Granite Zone....156
Aegirine Granite....166
Biotite Granite....170

Controls on HFS element abundances.....171
Source Considerations.....175
Petrogenesis of the Agamenticus Complex.....185

CHAPTER 4 Summary.....194

I. COMPARISON OF TRIASSIC AND CRETACEOUS COMPLEXES....194
II. IMPLICATIONS FOR THE PETROGENESIS OF MESOZOIC MAGMATISM IN SOUTHWESTERN MAINE.....202

REFERENCES.....206

APPENDICES.....226
II.I Location of gravity measurements.....226
II.II Power spectra of aeromagnetic and gravity data and filter responses.....228
II.III Matched filters.....231
II.IV Plotting and Digitizing Programs.....234

III.I Analytical techniques.....248
III.II FeO/Fe2O3 ratios for selected samples.....252
III.IIII Microprobe mineral analyses. 254
III.IV EXCELL Macros.....272
III.V Least squared mixing models and trace element calculations.....282
III.V.I SQSZ.....286

III.V.II Alkalic Syenite.....300
III.V.III Alkalic Granite to Quartz Syenite.....308
III.V.IV Aegirine Granite.....315

LIST OF FIGURES

1.1 Linear trends and magmatic provinces of Mesozoic magmatism in New England and Quebec....2
1.2 Geologic map for southeastern Maine....4

2.1 Lithotectonic boundaries for eastern New England....8
2.2 Aeromagnetic map for eastern New England and the Canadian Maritimes....10
2.3 Location map of salient features referred to in text....14
2.4 Offshore geology and terrane boundaries....22
2.5 High-pass filtered aeromagnetic map with overlay of interpreted lithotectonic blocks. 28
2.6 Band-pass filtered gravity residual map with overlay of interpreted lithotectonic blocks....30
2.7 Lithotectonic map based on interpretation of aeromagnetic and gravity residual maps....33
2.8 Interpretation of fault motion within Gulf of Maine transpressional zone....48

3.1 Simplified geology of southwestern Maine....56
3.2 Photomicrograph of biotite granite....65
3.3 Photomicrograph of alkalic granite....69
3.4 Representative amphibole microprobe analyses....72
3.5 Backscatter image of amphibole, zircon, and magnetite clots in alkalic granites....73

3.6 Photomicrograph of aegirine granite....76
3.7 Representative clinopyroxene microprobe analyses....78
3.8 Photomicrograph of alkalic syenites....80
3.9 Photomicrograph of amphibole overgrowths on olivine....82
3.10 Photomicrograph of aenigmatite syenite....85
3.11 Photomicrograph of subsolvus augite syenite....88
3.12 Major element vs SiO2 plots....92
3.13 Agpaitic vs. Pulmaskitic index diagram and Agpaitic vs peraluminous index diagram....98
3.14 Trace element Harker diagrams. 99
3.15 Eu* and Ga/Al vs LIL diagrams....100
3.16 Rb-Sr-Ba diagram....102
3.17 Zr,Nb,Th,U vs. SiO2 diagrams....105
3.18 Th-U, Zr-Y, and Sc-Co diagrams....106
3.19 Ga/Al, Nb/Ta, and Th/U vs Zr/Hf. 107
3.20 REE diagrams....109
3.21 Eu*, La/Yb, and sum REE vs. SiO2 diagram. 110
3.22 Tectonic discrimination diagrams....112
3.23 Plan view of the intrusion of the Agamenticus Complex....114
3.24 Qtz-Alb-Or-Ne diagram....121
3.25 Overlay of composition of Kittery Fm. on major element Harker plots....129
3.26 Mineral compositional overlay on major element Harker diagram....130
3.27 Plots of trace element model for SQSZ and aenigmatite syenite....136
3.28 Mg-(Fe-Na)-Na ternary plot of clinopyroxene compositions..139

3.29 fO2 vs T diagram....142
3.30 Amphibole cation plots....146
3.31 Sr/Ba vs Ga/Al Plot....148
3.32 Trace element model for alkalic syenites....150
3.33 Calculated cumulate compositions compared to alkalic syenites....155
3.34 Plot of trace element data for the alkalic granites-Model I..158
3.35 Plot of trace element data for the alkalic granites-Model II....159
3.36 Rb-Sr, Rb-Ba, and Sr-Ba diagrams....161
3.37 Zr-M plot....173
3.38 Comparison of geochemistry of the Agamenticus Complex to alkalic complexes with a basalt lineage....177
3.39 Rb/Sr isochron for the Agamenticus Complex....179
3.40 Selected trace elements compared to other A-type granite suites....184
3.41 Flow diagram of the interrelationship of rocks within the Agamenticus Complex....187
3.42 Cross-sectional view of the intrusion of the Agamenticus Complex....188

4.1 Geology of southwestern Maine....195
4.2 LIL-LIL variation diagrams....199
4.3 LIL ratio-LIL and Ga-Zn plots....200

LIST OF PLATES

Plate 2.1 Lithotectonic overlay.

Plate 3.1 Sample Locations for the Agamenticus Complex.

Plate 3.2 Geologic map of the Agamenticus Complex.

LIST OF TABLES

2.1 Susceptibility measurements of selected rocks.....27

3.1 Point counts of representative samples.....67
3.2 Major element compositions and CIPW normative assemblages.....95
3.3 Trace element concentrations.....104
3.4 Results of least squares analyses.....134
3.5 Aenigmatite compositions expressed as end members.....144
4.1 Major and trace element analyses for additional Mesozoic Complexes in southwestern Maine.....198

Petrogenesis of the Agamenticus Complex and late Paleozoic and Mesozoic tectonics in New England.

by

John A. Brooks

University of New Hampshire, May, 1990

The Mesozoic opening of the Atlantic Ocean was associated with the emplacement of subalkalic to alkalic complexes along a linear trend that extends southeasterly from Montreal, Canada, into the Gulf of Maine. The portion of this trend within southwestern Maine consists of Triassic and Cretaceouscomplexes. The central complexes were emplaced within three different lithotectonic blocks or terranes and thus provide a number of unique opportunities for the investigation of Mesozoic anorogenic magmatism.

Proposed terrane boundaries in southwestern Maine and adjacent regions were investigated by a detailed analysis of maps of regional aeromagnetic and gravity data. Significant aeromagnetic anomalies associated with lithologic units and fault zones onshore (i.e. the Nonesuch River, Calef, and Portsmouth faults) provide the basis for offshore fault zone indentification and the interpolation of coastal New England geology and terrane boundaries into the western and west-central portions of the Gulf of Maine. Within the western Gulf of Maine north-south

aeromagnetic linears deflect westward, become segmented, and merge with the offshore extension of the Bloody Bluff and Clinton-Newbury Fault Zones. The regional pattern can be explained in terms of regional dextral transpression resulting from the late Paleozoic (Alleghanian (?)) deformation of previously accreted lithotectonic packages to the north and northwest of the Bloody Bluff and Clinton-Newbury fault zones.

Early Mesozoic rift-related magmatism was investigated through a detailed petrogenetic study of the Triassic Agamenticus Complex. Least squares models suggest that the aegirine granite and, possibly, the alkalic granite can be derived by fractional crystallization from a subsolvus augite syenite parent. Trace element modeling suggests that processes other than liquid-crystal equilibrium fractionation, such as volatile fluxing and deuteric alteration, also played a role in the development of the magmas. An alkalic syenite and biotite granite cannot be modeled as either cumulate or fractionate phases from this process and are considered to be separate magmatic pulses derived by partial melting of the lower crust.

The Triassic and Cretaceous felsic complexes in southwestern Maine can be separated on the basis of trace element and potential field data: eg. Triassic complexes are depleted in Sr and Ba and lack the positive aeromagnetic and gravity anomalies associated with the Cretaceous complexes. These data are interpreted to reflect the transition from dominantly crustally derived magmas in the Triassic to mantle derived melts in the Cretaceous. Significantly different petrogenetic processes operating at the beginning and end of the

rifting cycle resulted in the emplacment of mantle derived melts at progressively higher levels within the crust as Mesozoic taphrogenesis evolved.

CHAPTER 1

INTRODUCTION

The Mesozoic opening of the Atlantic Ocean was accompanied by subalkalic to alkalic plutonism along linear trends in a number of localities on either side of the Atlantic Ocean (Morgan, 1981). Among these is a linear array of sub-volcanic to volcanic bodies located in Quebec, New England, and offshore that includes the Monteregian Hills, the White Mountain Magma Series, and the New England Seamounts, respectively (Fig. 1.1). Emplacement of these bodies occurred in three major pulses (Foland and Faul, 1977). The earliest phase consisted of the alkalic, middle to late Triassic intrusives of the Coastal New England Province (McHone and Butler, 1984), which was synchronous with emplacement of dolerite dikes in the coastal region and the development of the nearby Hartford and Bay of Fundy rift basins (Fig. 1.1) (Bedard, 1986). Basaltic magmatism associated with the rift basins occurred at approximately the Triassic-Jurassic boundary (DeBoer, 1987; Bedard, 1986). The second major magmatic pulse is manifest by the early to middle Jurassic plutonic and volcanic White Mountain Magma Series (Billings, 1956) and basalt dikes of the Eastern North American Dolerite Province (Fig. 1.1) (McHone and Butler, 1984). The final phase of magmatic activity comprises the nearly synchronous, early Cretaceous emplacement of the Monteregian Hills, a number of

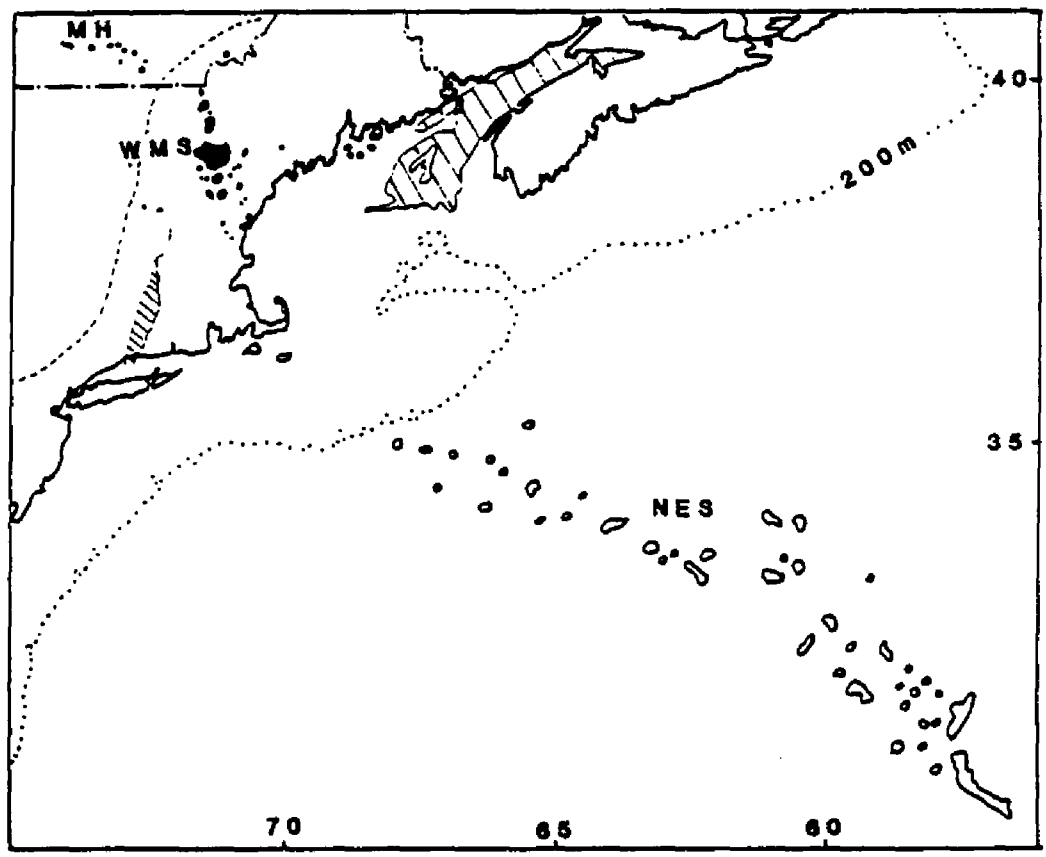

Fig. 1.1 Provinces of anorogenic Mesozoic magmatism in Canada, New England, and offshore (after Foland and Faul, 1977; Abbrv. MH- Monteregian Hills, WMS- White Mountain Magma Series, NES, New England Seamounts). The western limit of the Eastern North American Dolerite Province (after McHone and Butler, 1985) is shown as a dashed line. Diagonal lines show the extent of the Hartford and Fundy Triassic rift basins (after Hermes and Zartman, 1985).

mafic and felsic alkalic complexes and stocks in New Hampshire andsoutheastern Maine, and the New England Seamounts (Fig. 1.1) (Foland et al. 1989; McHone and Butler, 1984).

The origin of the New England-Quebec magmatic linear trend remains unclear. It has been suggested that this anorogenic , sub-alkalic to alkalic, igneous series is related to the trace of a mantle hotspot (Morgan, 1981; Crough, 1981; Foland et al., 1985, 1988; Duncan, 1984; McHone, 1981). However, Uchupi et al. (1970) noted that a well defined, NW to SE, age progression, as would be expected for a hotspot trace, is not present and proposed magma generation below a "leaky" transform fault system. Alternate mechanisms such as doming and/or passive rifting have also been proposed to explain both the type and location of the magmatism observed (McHone and Butler, 1984; Bedard, 1985).

All of these hypotheses suggest that the emplacement of the Quebec-New England magmatic trend is partly or wholly controlled by basement structure (See also Chapman, 1968). This is supported by the common occurrence of A-type magmas (alkalic, anorogenic, anhydrous (Loiselle and Wones, 1979)) along reactivated zones of crustal weakness worldwide (Sorensen, 1974; Bowden et al., 1987).

Testing the various petrogenetic models proposed for the Mesozoic plutons is made difficult by the disparity of geochemical data available. Noteworthy in this instance is the paucity of geochemical data available for the Mesozoic bodies located in southwestern Maine (Fig. 1.2). For example, only a limited number of

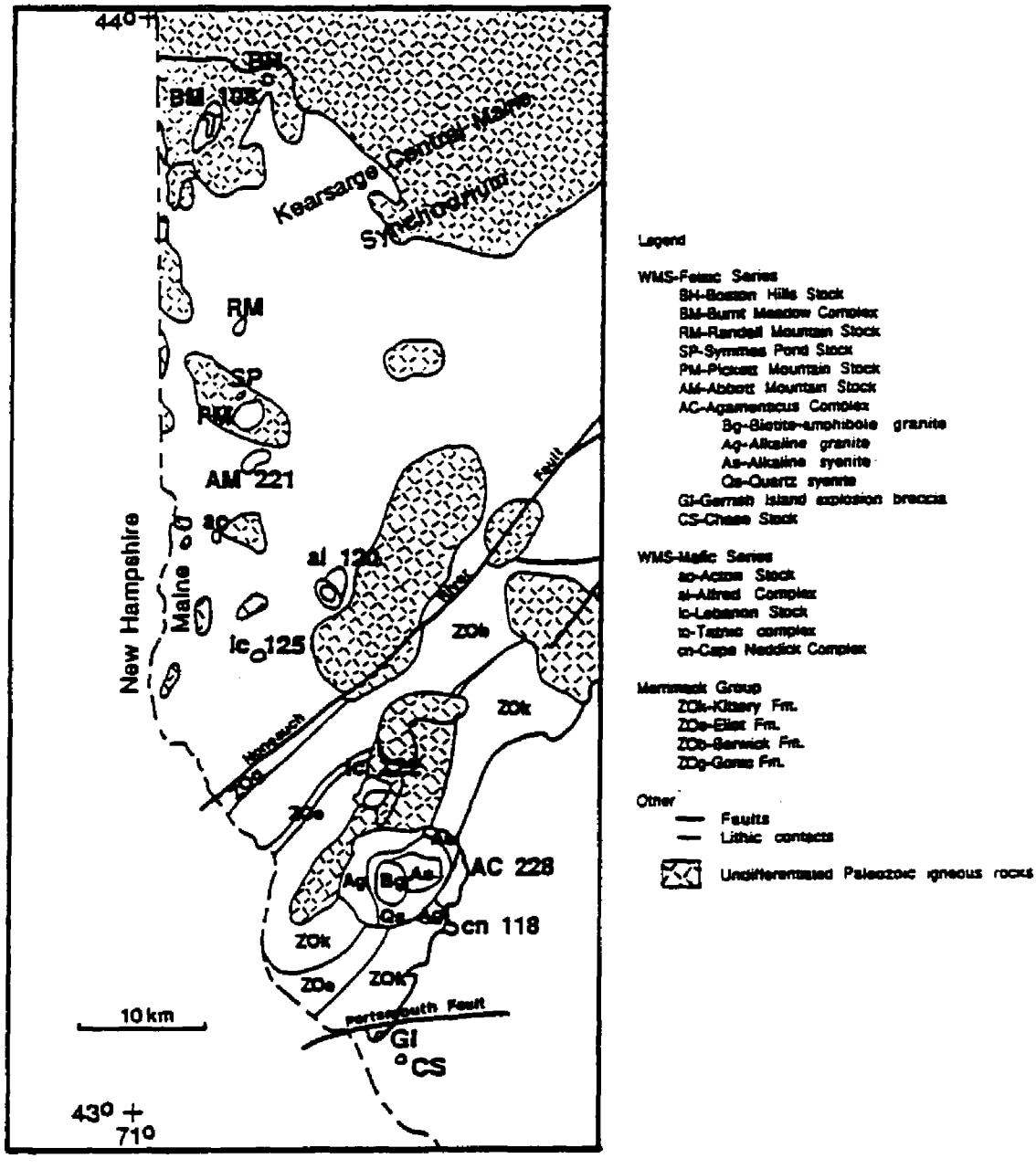

Fig. 1.2 Simplified geology of southwestern Maine. Adapted from Hussey 1985. Ages (Ma) indicated where known (Foland and Faul, 1977; Foland et al., 1977; Hoefs, 1967). Except for the Merrimack Group the metamorphic rocks are undifferentiated.

isotopic studies have been reported for these rocks (Foland and Faul, 1977 and references therein; Foland et al., 1989) and only the Abbot Complex has been analyzed for major and trace element geochemical data (Gilman, 1989).

This long overlooked region of Mesozoic magmatism provides several unique opportunities for study. The Mesozoic rocks of southwestern Maine form a NNW-trending linear which crosses a number of regionally significant faults interpreted as terrane boundaries (*i.e.* the Nonesuch River and Portsmouth Faults (Lyons et al., 1982; Carrigan, 1988) (Fig. 1.2). The occurrence of similar rock types that have intruded rocks of different lithotectonic affiliation provides an opportunity to evaluate the possible geochemical influence of different hosts and potentially different basements on the petrogenesis of the exposed Mesozoic rocks. The presence of the through-going fault systems in addition holds promise for evaluating the role of preexisting crustal structures on the emplacement of the plutons and stocks. The occurrence of Triassic plutonic rocks in southwestern Maine (Fig. 1.2) may provide insight into early rift-related, intracrustal magmatism. Coexisting Cretaceous plutons (Fig. 1.2) provides additional insight on compositional variations of both magma and source from the beginning to the end of the Mesozoic rifting cycle.

These issues are addressed using both geophysical and geochemical methods. Regional gravity and aeromagnetic residual maps are analyzed to evaluate the surface and subsurface configuration of Paleozoic terranes and Mesozoic plutons within the research area. Such analyses help constrain possible sources for

crustally derived magmas and allow an evaluation of the role Paleozoic structures played during magma emplacement. Early rift related magmatism is viewed in light of a detailed petrogenetic study of the Agamenticus Complex, the largest Triassic complex. Additional major and trace element data obtained for representative rocks of all the felsic, Triassic and Cretaceous plutons in southwestern Maine provide a means of comparison between magmas of different age and terrane affiliation.

CHAPTER 2

GEOLOGY AND GEOPHYSICS OF CENTRAL COASTAL NEW ENGLAND AND WEST-CENTRAL MAINE: IMPLICATIONS FOR MESOZOIC IGNEOUS COMPLEXES

INTRODUCTION

The Mesozoic plutons in southwestern Maine are exposed as a NNW-trending belt of small (1 to 10 km^2) oval, Triassic to Cretaceous plutons and stocks (Gilman, 1972,1979; Hussey, 1962, 1985; Osberg et al.,1985) (Fig. 1.2). They intrude the metasedimentary rocks of the Kearsarge-Central Maine Synclinorium, Merrimack Trough, and Rye Anticlinorium as well as Devonian and Carboniferous biotite and two-mica granites (Figs. 1.2 and 2.1) (Gilman, 1985; Lyons et al, 1982; Hussey, 1985; Brooks, 1986 and 1988). These Precambrian to Paleozoic metasedimentary and igneous rocks have been variably subdivided. Carrigan (1984) and Brooks (1986) referred to the Merrimack Trough and Rye Anticlinorium as lithotectonic "blocks" to emphasize that these units have distinct geologic histories. Both have been subsequently placed within the regional Nashoba-Casco-Miramichi Block (Zen et al., 1986) and Avalonian Composite Terrane (Bothner et al. 1988; Stewart, 1988; Hutchinson, 1988) (Fig. 2.1). Following the approach of Bothner et al. (1988), components of the Merrimack Trough and Rye Anticlinorium are grouped together as the Massabesic-

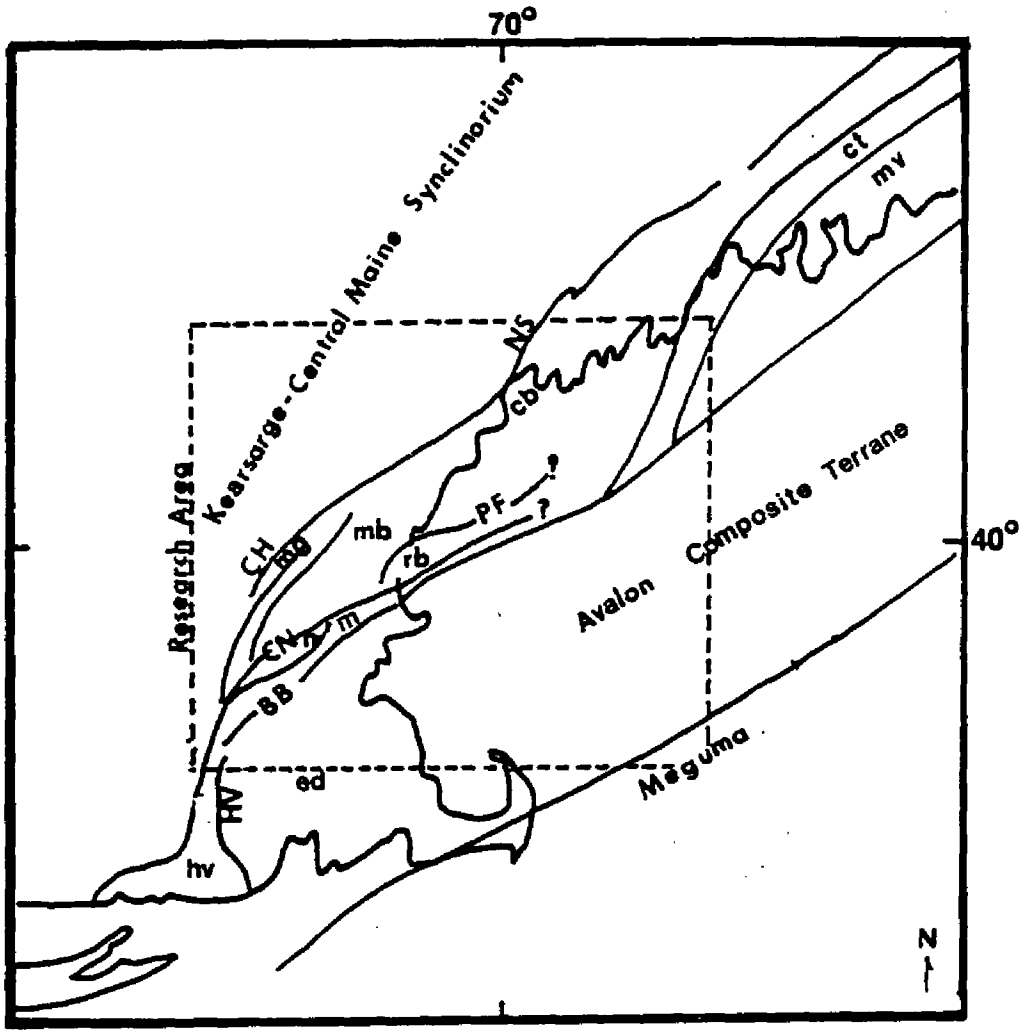

Fig. 2.1 Lithotectonic boundaries for southeastern New England (after Hutchinson et al., 1988; Stewart et al., 1988). Abbrv. CH- Campbell Hill Fault, NS- Nonesuch River Fault, CN- Clinton-Newbury Fault Zone, PF- Portsmouth Fault Zone, BB- Bloody Bluff Fault Zone, HV- Hope Valley Shear Zone, mv- Maine Volcanic Province, ct- Croix Terrane, cb- Casco Bay Block, mb- Merrimack Block, m- Marlboro Block, n-Nashoba Block, es- Esmond-Dedham Terrane, hv-Hope Valley Terrane.

Maine Synclinorium are considered to be part of the Gander (Lyons et al., 1982) or Central Maine Terrane (Eusden and Barreiro (1989) (Fig. 1.2 and 2.1).

The accretionary history of and geologic relationships between these terranes and the nature of the bounding faults is still unclear. Because crustal composition and structure created during the Paleozoic can affect the chemistry (Collins et al., 1982; Clemens and Valieuz, 1988) and emplacement of Mesozoic magmas (Chapman, 1968; Bowden et al., 1987), a more thorough understanding of the relationships between and within the Avalonian Composite Terrane and adjacent terranes is desired. The recent compilation of a new geologic map of New Hampshire (Lyons et al., 1986), detailed field mapping in the coastal (Carrigan, 1984; Brooks, 1986; Bothner, unpublished) and central New Hampshire regions (Fagan, 1985; Eusden, 1984; 1988), and compilations of aeromagnetic (Fig. 2.2, Shih et al., 1988) and gravity (Bothner et al., 1980) data provide the bases for reevaluation of the Avalon Composite Terrane within coastal New Hampshire and southwestern Maine.

The analysis of potential field data, in particular aeromagnetic data, is a useful and often powerful tool for interpretation of geology and terranes at both large and small scales. Birch (1984) mapped local bedrock geology to approximately 40 km offshore coastal New Hampshire using seismic reflection and detailed shipborne magnetic data. Harwood and Zietz (1977) and Castle et al. (1976) have shown that individual lithic units within the Boston Platform region can be correlated to specific magnetic anomalies

Fig. 2.2 Shaded relief aeromagnetic map for the Gulf of Maine and adjacent areas (Shih et al., 1988). The large positive, oval anomaly in the center of map is associated with the Ordovician Cashes Ledge anorogenic granite. The western end of Nova Scotia is outline by NE- and NS-trending aeromagnetic linears in the upper right portion of the map. The coastal Maine volcanics are associated with the NE-trending, oblate linears to the east of the Nova Scotian linears. The research area is outlined by solid line.

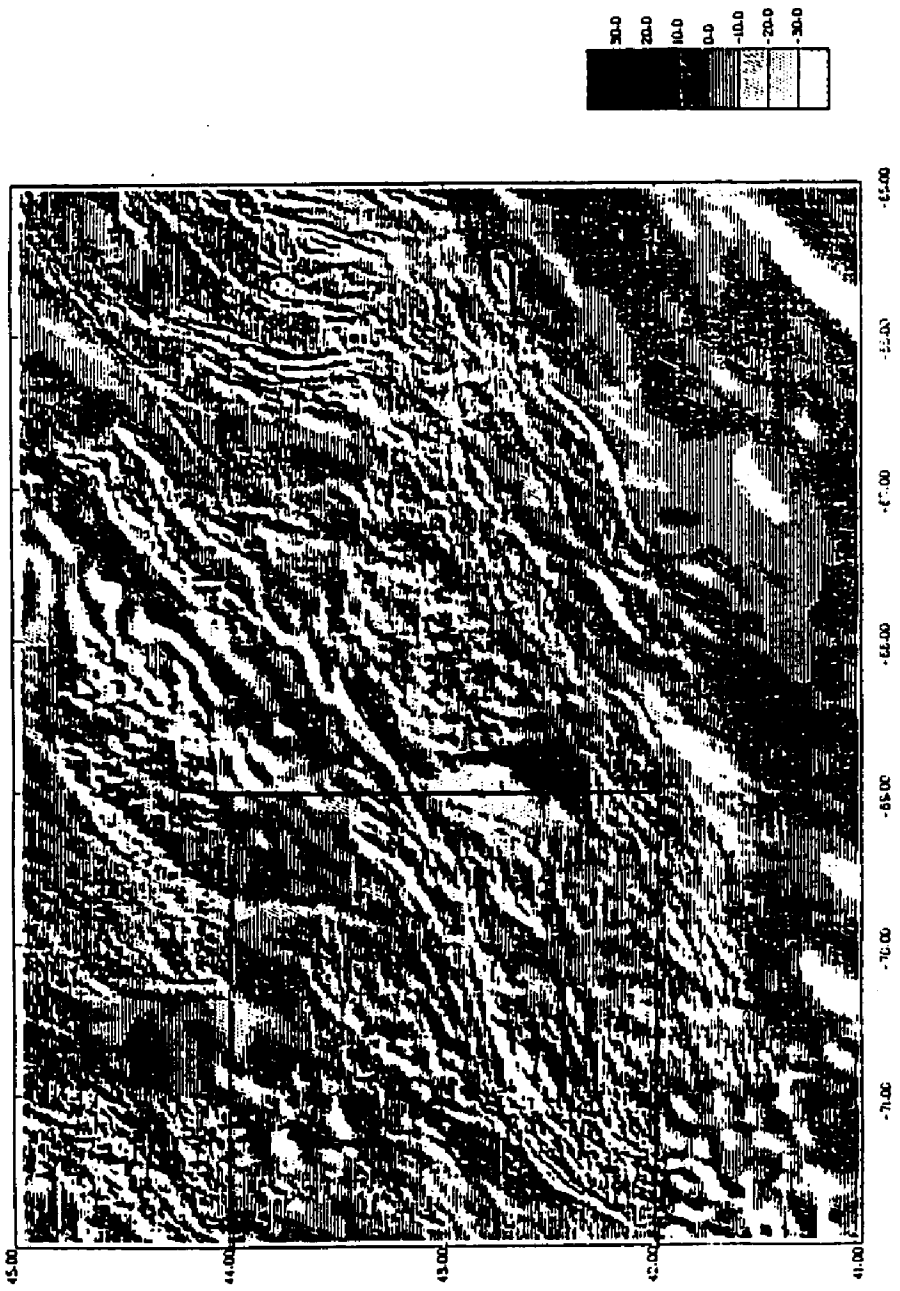
30.0
20.0
10.0
0.0
-10.0
-20.0
-30.0
45.00
44.00
43.00
42.00
41.00

and that major structural discontinuities can be mapped using magnetic signatures (e.g. the Clinton-Newbury and Bloody Bluff-Burlington Mylonite Fault Zones). The analysis of aeromagnetic data has also contributed to the investigation of regional shear fabrics (Hoffman,1987; Chandler and Southwick, 1990), to locating and modeling the sub-surface configuration of suture zones (Haworth and Jacobi, 1983; Miller,1988), and
the delineation of lithotectonic zones (Shih et al., 1989; Stettler et al., 1989; Miranda et al., 1989; Rivers et al., 1989).

Magnetic and gravity analysis in this study follows the same qualitative approach as those above. Linear and closed magnetic anomalies are compared to specific lithologies and/or fault boundaries with geologic map overlays. Possible correlations are tested by using measured bulk susceptibilities and by shape/magnitude analysis. Resulting correlations are then used to extrapolate onshore geology into regions of poor or inaccessible exposure offshore (Brooks, 1986).

Although the main focus of this research is the area defined as MMR, the Paleozoic history of this region must be considered in relationship to the adjacent lithotectonic zones. The geologies of all of these lithotectonic zones are reviewed to emphasize those features that distinguish each zone from the other and are most strongly represented in the potential field data. Following this introduction, salient characteristics of the potential field for each lithotectonic zone and for the Mesozoic igneous rocks are presented. The implications of these characteristics for Paleozoic imprints on the tectonic fabric of the MMR are discussed.

REGIONAL SETTING

Massabesic-Merrimack-Rye Blocks

The MMR occupies the region north and west of the Clinton-Newbury and Bloody Bluff fault zone in northeastern Massachusetts and its offshore extension (Simpson et al., 1980; Shih et al., 1988; Hutchinson et al., 1988) (Fig. 2.1). The northwest boundary is marked by the Campbell Hill-Nonesuch River fault system in New Hampshire and southwestern Maine (Lyons et al., 1982; Figs. 1.2 and 2.1). In Massachusetts, the continuation of this fault system is masked by Devonian granites and substantial glacial overburden. Zen (1989) proposed that it emerges at the southern terminus of the Fitchburg intrusive complex and separates rocks of the Merrimack Trough and the Kearsarge-Central Maine Synclinorium (Figs. 2.1 and 2.3).

The Massabesic-Merrimack-Rye Zones consist almost wholly of late Precambrian metasedimentary and metaigneous rocks that are polydeformed and successively intruded by late Precambrian, Paleozoic, and Mesozoic plutons (Figs. 1.2 and 2.3) (Bothner et al., 1984; Olszewski et al., 1984; Barreiro and Eusden, 1988; Brooks, 1986). The earliest intrusions (Precambrian, Ordovician, and Silurian?) were emplaced prior to final accretion of MMR onto the Kearsarge - Central Maine terrane. Devonian and Carboniferous plutons common to both terranes, are mostly "stitching plutons" (Lyons et al., 1986) and in part conceal the regionally significant tectonic boundaries (Figs. 1.2 and 2.3). Strongly discordant Mesozoic alkalic magmatism, including the Agamenticus Complex, reflect the

Fig. 2.3 Simplified geology of the research area with emphasis on the Massabesic, Merrimack, and Rye Blocks.

LEGEND

Mesozoic plutons

MR- Randall Mt. Stock
Mp- Pickett Mt. Stock
Ko- Ossipee Complex
Kg- Green Mt. Stock
Kb- Burnt Meadow Stock
Km- Merrymeeting Complex
Kp- Pawtuckaway Mt. Complex
Ka- Alfred Complex
Kt- Tatnic Complex
Jr- Red Hill Complex
Trag- Agamenticus Complex
Tra- Abbott Complex

Paleozoic Plutons

Cb- Biddeford Pluton
Cl- Lyman Pluton
Cs- Sebago Pluton
Dw- Webhannet Pluton
Oe- Exeter Pluton
Od- Dracut Diorite
On- Newburyport Complex
Oca- Cape Ann Complex
Zs- Salem Diorite/Gabbro

Metamorphic rocks

Casco Bay Area

DOb- Bucksport Fm.
OZsc- Scarboro Fm.
OZce- Cape Elizabeth Fm.

MMR Zones

ZOk- Kittery Fm.
ZOe- Eliot Fm.
ZOec- Calef Member
ZOb- Berwick Fm.
ZOmg- Massabesic Gneiss
ZOr- Rye Fm.

Esmond-Dedham Zone

DSv- Newbury Volcanics
ZOn- Nashoba Fm.
ZOnb- Boxford Member
ZOm- Marlboro Fm.

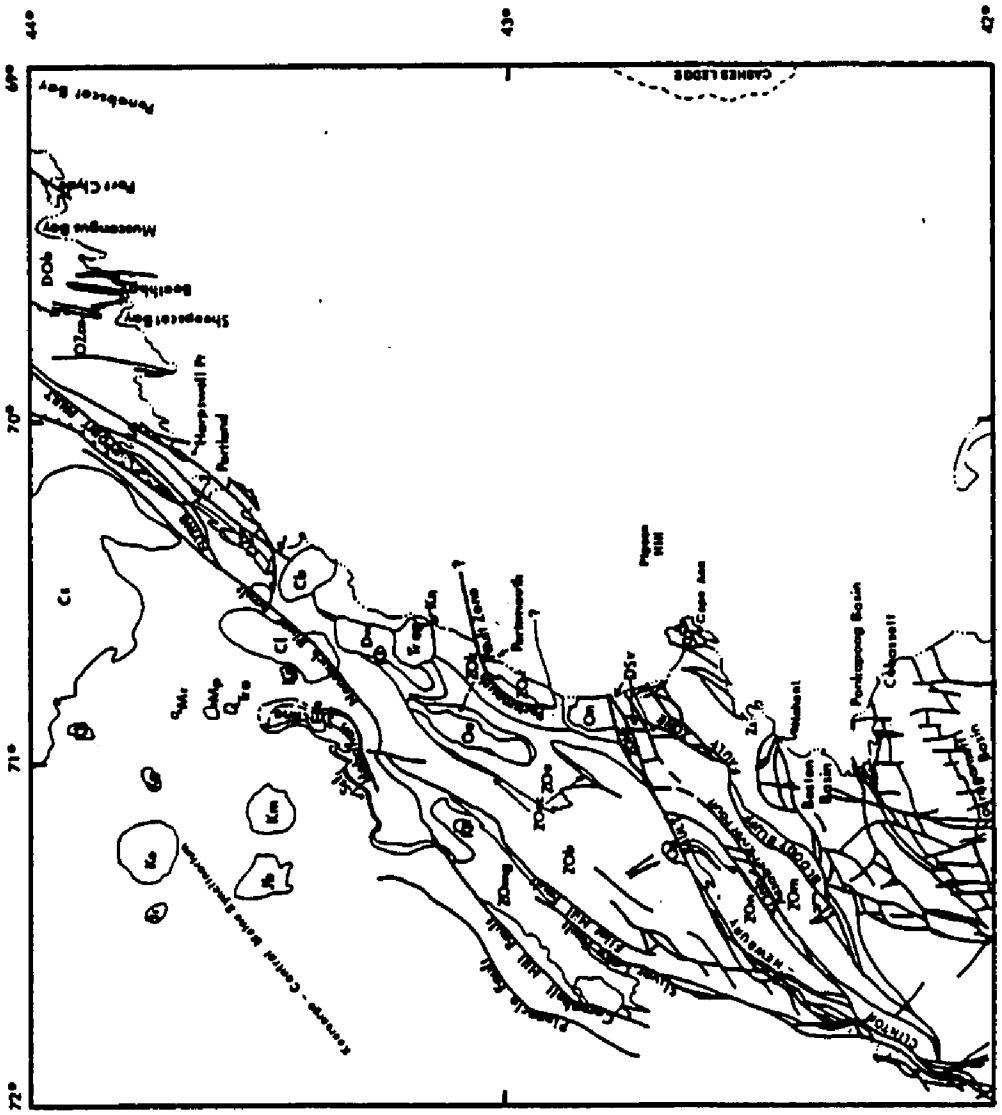
44°
43°
42°
70°
71°
72°
Penobscot Bay
Portland
Pigeon Hill
Cape Ann
Boston Basin
Cohasset
Hingham Basin
Canada Basin - Central Maine Basin Boundary
Blue Hill Fault
Clinton

subsequent effects of continental separation during the opening of the Atlantic Ocean.

The Merrimack Trough contains continental slope and rise rocks (Rickerich, 1983) of the Merrimack Group which are considered to be stratigraphically continuous with the ortho- and paragneisses of the Massabesic Gneiss Complex (Bothner et al, 1984). The age of orthogneiss from the Massabesic Gneiss is constrained by 650 Ma Rb/Sr whole rock isochrons (Bescancon et al., 1977; Olszewski et al., 1984) and a 650 Ma U/Pb zircon age (Aleinikoff et al., 1979). Another orthogneiss from the Massabesic Complex has yielded a 450 Ma isochron (Aleinikoff et al., 1979). A Permian U/Pb monazite 270 Ma age from the Massabesic Gneiss paragneiss and sillimanite grade Berwick Fm. records the latest peak metamorphism (Barreiro and Eusden, 1988). A provenance age for the Massabesic Gneiss is inferred by an approximate 1400 Ma age of detrital zircon from the paragneiss member (Aleinikoff et al., 1979).

A Precambrian Z to lower Ordovician age is assigned to the Merrimack Group based on radiometric age determinations for the undeformed, unmetamorphosed, cross-cutting Exeter Pluton (473 $\pm$ 37 Ma Rb/Sr whole rock, Olszewski et al., 1984; Olszewski and Gaudette, 1988) and Newburyport Quartz Diorite (450 $\pm$ 15 Ma $^{207}Pb/^{206}Pb$ zircon, Zartman and Naylor, 1986) and the interpreted gradational contact between the Berwick Fm. and Massabesic Gneiss (Bothner et al. 1984; Fagan,1985). On the basis of lithologic and structural data, which suggest that the Kittery Fm. is the youngest unit in the sequence, the previously defined stratigraphic sequence

of Kittery - Eliot - Berwick (from oldest to youngest; Hussey, 1985) is reversed (Bothner, in prep.).

Rocks of the Massabesic Gneiss Complex (Figs. 1.2 and 2.3) and the lower portion of the Berwick Formation are polydeformed, polymetamorphosed sillimanite to 2nd sillimanite grade migmatitic, dominantly calcareous quartzofeldspathic gneisses and minor mafic and pelitic gneisses (Lyons et al. 1982; Fagan, 1985). The upper portion of the Berwick Formation is a fine-grained, well-layered biotite granofels containing discontinuous calc-silicate intercalations and minor pelitic interbeds (Bothner et al., 1984). The Eliot Formation (Figs. 1.2 and 2.3), everywhere at biotite or lower grade, is composed of interbedded, but partly transposed, calcareous metasiltstone and non-carbonaceous phyllite. The boundary between the Berwick and Eliot Formations is marked by a fine-grained, rusty carbonaceous phyllonite originally described as the Calef Member of the Eliot Formation (Novotny, 1969). The Kittery Formation (Figs. 1.2 and 2.3) completes the Merrimack Group. It is dominated by biotite grade, fine-grained calcareous quartzite interbedded with minor pelitic phyllite or slate. Primary sedimentary features and structural analysis suggest that this formation is an easterly derived turbidite sequence (Rickerich, 1983; Hussey et al., 1984), perhaps the western margin of Avalon (Africa?).

At the eastern side of the MMR, Precambrian Z(?) mylonitized quartzofeldspathic, calc-silicate, pelitic, and mafic schists and gneisses of the Rye Block are juxtaposed against the Merrimack Group along the Portsmouth Fault zone (Hussey, 1980; Carrigan,

1984; Swanson and Carrigan, 1984; Brooks, 1986) (Figs. 1.2 and 2.3). Offshore, the Portsmouth Fault zone can be traced to the Boon Island region (Fig. 2.3) (Brooks, 1986). The Rye Formation extends for at least 16 km offshore of the New Hampshire coastline (Brooks, 1986; Birch, 1984) and underlies the Kittery Formation within southern New Hampshire (Public Service Company of NH, 1981). Metamorphic grade both onshore and offshore decreases from sillimanite and 2nd-sillimanite grade in the northern portion of the Rye Complex to garnet grade in the south (Carrigan, 1984; Brooks, 1986). The age of the Rye Block is constrained by the cross-cutting 483 ± Ma (whole rock Rb/Sr) metadiorite on the Isles of Shoals (Olszewski et al., 1984). A poorly constrained 383 ± Ma Rb/Sr whole rock age obtained for the granitic gneiss within the Rye Complex is tentatively interpreted by Olszewski et al. (1984) as a metamorphic age.

Although shearing within the Rye Formation was most intense near the Portsmouth Fault Zone, the presence of protomylonitic to mylonitic rocks at least 16 km offshore (Brooks,1986) suggests that the Rye Block represents a significant regional shear zone. The brecciation of early ductile structures within the Portsmouth region by a myriad of brittle faults indicates multiple, probably time-separated, deformational events within the Rye Block (Swanson, 1982, 1989; Swanson and Carrigan, 1984; Carrigan, 1984). Augen gneiss xenoliths within the metadiorite on the Isles of Shoals and strong shear along the metadiorite contact also show that the rocks of the Rye Block have experienced a long history of strain. The parallel alignment of mineral lineations and fold axes in the

Portsmouth region suggests that at least a portion of this deformation was transpressional.

Central Maine Terrane

At the western side of the MMR Silurian-Devonian turbiditic, sulfidic, and pelitic schists and gneisses of the Kearsarge-Central Maine synclinorium or Central Maine Terrane crop out across the Campbell Hill-Nonesuch River fault trace (Figs. 2.1 and 2.3). Recent detailed mapping along that fault from Massachusetts to southwestern Maine confirms structural discordance (i.e., the truncated Lebanon antiformal syncline, Eusden et al., 1987; Fig. 2.3) of this mostly westerly-derived sequence of rocks with those of the MMR. The truncation of the Lebanon Syncline against the the Campbell Hill fault argues effectively that the MMR was juxtaposed after Acadian folding. However, major motion along the Campbell Hill-Nonesuch River Fault system must predate the emplacement to the 364 MA (Barreiro and Eusden, 1988) Barrington Pluton. Subsequent Permian metamorphism (to 2nd sillimanite zone) of the late Precambrian Massabesic Gneiss Complex and MMR did not affect Acadian metamorphic signatures of the Kearsarge-Central Maine Synclinorium (Lyons et al., 1982; Barreiro and Eusden, 1988). This sequence of metamorphism and plutonism suggests late Permian uplift of the western portion of the MMR and the Massabesic Gneiss Complex (Eusden,1988).

Terranes of southeastern New England

To the south, rocks of the MMR are juxtaposed along the Clinton-Newbury Fault Zone against the Precambrian to Silurian rocks (Lyons and Brownlow and references therein, 1976; Hanson and

references therein, 1984; Fig.1) of the Nashoba-Marlboro Zones (Fig. 2.1 and 2.3). The dominant rocks are mafic and felsic volcanics and interbedded metasediments and associated Ordovician to Silurian granites. The Bloody Bluff fault separates this zone from the Esmond-Dedham Terrane. This terrane is composed of late-Precambrian dominantly marine and terrestrial metasediments and volcanic rocks that in places pass upward into Cambrian shales containing Eurobaltic trilobite fauna, *Paradoxides* (Rast and Skehan, 1983). These rocks are correlative with the Avalon rocks of coastal Maine, New Brunswick, and Newfoundland (Rast et al., 1976). The Avalon terrane in southeastern New England has been intruded by Ordovician to Devonian anorogenic plutons and has experienced Carboniferous extension and Alleghanian metamorphism and compressional deformation (Zartman,1988; Hermes and Zartman, 1985). The southwestern portion of the Avalon terrane can be subdivided into two terranes separated by the Hope Valley shear zone; the Hope Valley and Esmond-Dedham terranes (Fig. 2.1; O'Hara and Gromet, 1985; Hermes and Zartman, 1985; Zartman and Naylor, 1984).

Casco Bay Block

To the northeast the MMR is juxtaposed (Hussey, 1985) or perhaps, in part, transitional (Olzsewski et al., 1988) to the late Precambrian to Ordovician metasediments and metavolcanics of the Casco Bay Group (Fig. 2.1). This sequence of rocks experienced mid-Cambrian to Ordovician metamorphism which distinguishes them from all adjacent lithotectonic zones but the Merrimack and Massabesic Blocks (Olzsewski et al.,1988). The Casco Bay Group and

other rocks of coastal Maine have been cross-cut by a number of faults which have experienced a long history of reactivation (Hussey, 1985; Hogan et al., 1988). $^{40}Ar/Ar^{39}$ hornblende ages indicate that the rocks to the west (Falmouth-Brunswick Block) and east (Saco-Harpswell Block) of one these faults, the Flying Point Fault (Fig. 2.3), experienced differing thermal histories until the late Paleozoic (≈ 250 Ma) (West et al., 1988).

Gulf of Maine

Offshore, within the Gulf of Maine, the location of terrane boundaries is based on geophysical data and on the analyses of a very small number of bedrock samples (Fig. 2.4) (Kane et al., 1972; Hutchinson, 1988; Shih et al., 1988; Ballard 1974a, 1974b). Bedrock samples were obtained by SCUBA divers (Ballard, 1974b), with the use of submersibles (Ballard, 1974 b), and through drilling (Leo and Phillips, 1989; Scholle and Wenkam,1982; King and MacLean, 1976; Koteff and Cotton, 1962).

As in southern coastal New England, the major geomorphic features within west and west-central Gulf of Maine are primarily due to Carboniferous and Mesozoic extensional tectonics and subsequent deposition of sediments (Ballard, 1974a; Ballard and Uchupi, 1972, 1975; Shih et al., 1988). Sinistral rifting during the Carboniferous resulted in the development of the onshore Narragansett (Fig. 2.3) and the offshore Wilkinson pull-apart basins . Subsequent Mesozoic extension overprinted Paleozoic and Carboniferous features of western Gulf of Maine with a number of normal faults (e.g., the Fundy Fault and its onshore continuation as

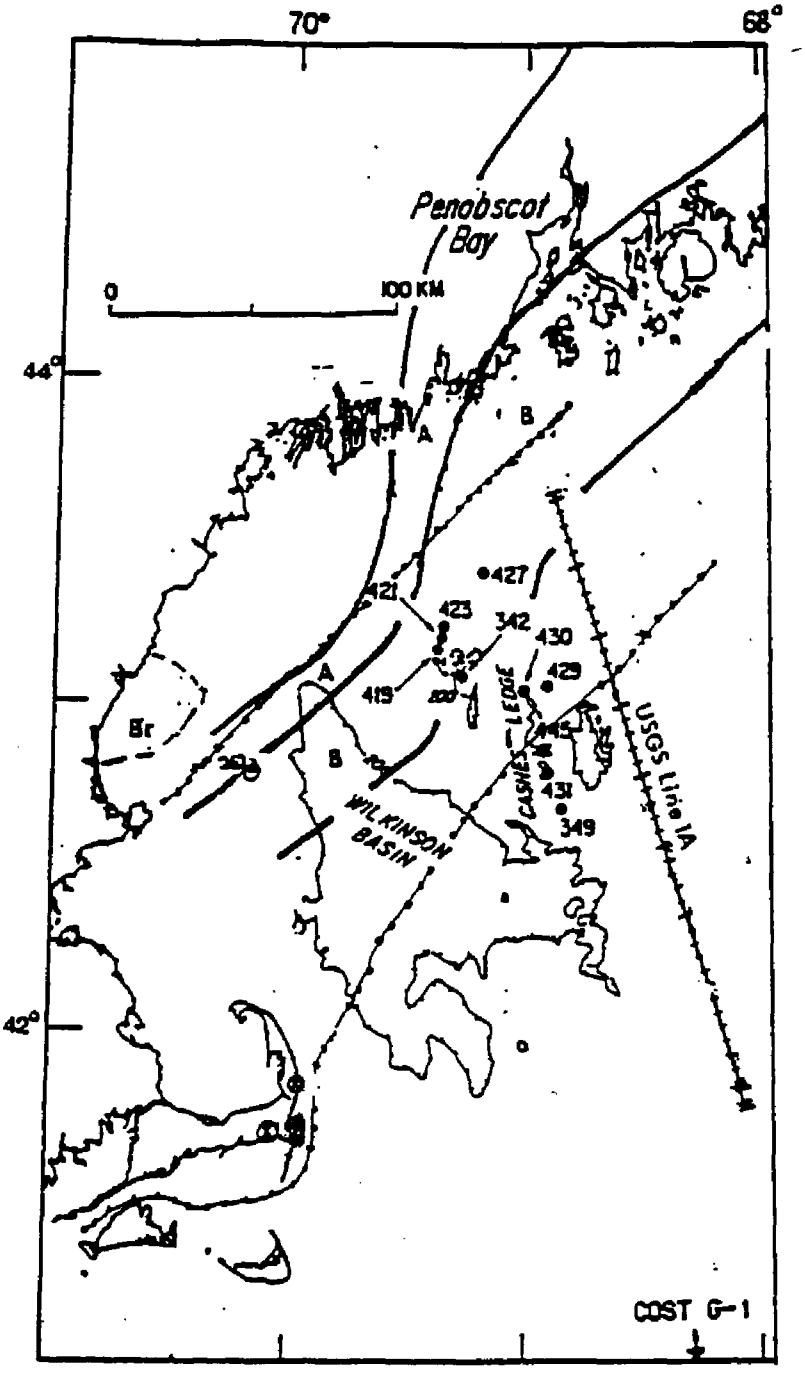

Fig. 2.4 Bedrock samples (Ballard, 1974, numbered locations; Brooks, 1985, region labeled Br), seismic boundaries (dotted lined, Ballard, 1974), and aeromagnetic zones (A and B; after Kane et al., 1972) within the western Gulf of Maine. USGS seismic line 1A is from Hutchinson et al. (1988). Circles with crosses are drill hole locations of bedrock samples (Koteff and Cotton, 1962; Leo and Phillips, 1989).

the Ponkapoag Fault in southeastern Massachusetts; Shih et al, 1988).

Geochemical and isotopic analysis of Ordovician alkalic and calc-alkalic granitic rocks from Cashes Ledge and other nearby ledges suggests that the central portion of the Gulf of Maine is located within the Avalon terrane (Hermes et al., 1978; Hermes and Zartman, 1985). Analysis of core samples from the Scotian Shelf indicate that the Meguma terrane extends at least 100 km to the southwest of Nova Scotia (King and MacLean, 1976; Pe-Piper and Loncarevic, 1988). The Cost G-1 well bottomed in low grade metasedimentary rocks that yielded a metamorphic age of 400 $\pm$ 50 Ma (Scholle and Wenkam, 1982). The inferred age, metamorphic grade, and rock type are compatible with either Avalon or Meguma terranes. Bedrock penetrated in a drill hole near Harwich, MA. is correlated to rocks of either the Carboniferous Narragansett basin or to the Precambrian Blackstone Series of the Avalon terrane (Koteff and Cotton, 1962). Two recent bedrock cores on Cape Cod recovered sheared and unsheared granitic rocks (Leo and Phillips, 1989) that correspond to two distinct basement types identified by Hutchinson et al. (1988).

Seismic and potential field data have placed further constraints on the location of terrane boundaries within the Gulf of Maine. Crustal seismic velocities obtained from refraction surveys (Ballard, 1974a) indicate the presence of three crustal zones (Fig. 2.4). The northernmost contact roughly corresponds with the offshore extension of the Bloody Bluff/Clinton-Newbury fault zone and to the northwestern boundary of the Avalon terrane proposed by

Hermes and Zartman (1985) (Fig. 2.4). Kane et al. (1972) were able to subdivide the Gulf of Maine on the basis of qualitative analysis of potential field data (Fig. 2.4). The contact between their zones A and B approximately corresponds to the western boundary of the Avalon terrane proposed by Hutchinson et al. (1988) (Fig. 1.2) and Stewart et al. (1985 and 1989).

DATA COMPILATION AND PROCESSING

Potential field analyses were conducted primarily at a scale of 1/500,000 using computer generated maps of total field, lowpass filtered, and highpass filtered gravity and aeromagnetic data. Several key areas were analyzed at larger scale.

Complete Bouguer gravity onshore and free air gravity offshore were compiled from a variety of sources (Bothner et al., 1980 and references therein; unpublished USGS gravity data). Bouguer corrections were not calculated for offshore data due to inadequate bathymetric control. Onshore data have an average station spacing of 1.5 km, while offshore station spacing is about 5 km for seabottom stations within localized regions and <0.5 km along ship tracks for shipboard meters (Appendix II.I). Errors onshore from position, elevation, and gravity meter do not exceed 1 Mgal. Offshore errors may be as large as 5 Mgal as determined by ship crossings. Most of the latter error stems from Eotvos corrections (calculated by the USGS-Woods Hole) and uncertainty of ship position (particularly for older data). It is estimated that <5% of the offshore data are off by 5 Mgal. These data were gridded

using a minimum curvature algorithm (MINC, Webring, 1977) at 5 km to compensate for greater data spacing offshore and then regridded to 1 km for filtering, contouring, and analysis.

Aeromagnetic data for the region are from digitized USGS analog maps covering eastern Massachusetts (Simpson et al., 1980), an unpublished Boston Edison digital set, and USGS compilations. Data from all three sources were collected along flight lines spaced $\leq$1 km apart and flown at 500 ft. above terrain. After removal of appropriate IGRF and level adjustments (conducted by USGS-Woods Hole), the data were gridded at 1.0 km and then regridded to 0.5 km for contouring and analysis. Reduction to pole was made to eliminate geographic shifts of anomalies using FFTFIL (a fast Fourier transform filtering algorithm; Hildenbrand, 1978), a declination of 16.5°, and an inclination of 70°. Shipborne magnetic data for nearshore areas off Massachusetts and New Hampshire (Bothner et al., 1983; Birch, 1984), not included in this compilation, have provided additional detail across major units.

Spectral analysis and filtering of the gravity and aeromagnetic data (Appendix II.II) were conducted with MFILT (Phillips, unpublished; Phillips, in prep). Filters are calculated within this program from data input to match segments of the curved total field power spectra (see Appendix II.III). Because estimates of apparent average depth to magnetic source are based on the slope of the total field power spectra and ignore the contribution of body size vs. body depth (Spector, 1979), they are greater than the actual average depth to the deeper magnetic sources. For this study, the apparent

depths are used only as an estimate of the crustal regions within which the magnetic bodies occur.

Contours maps were plotted on the UNH Calcomp plotter using CONTOUR (Godson, written comm.,1977) and VEC2PLOT (Appendix II.IV). To aid in interpretation, color shaded relief maps were generated on USGS color plotters. Although some detail is lost in this presentation, the enhancement of the anomaly shapes more than compensates for the loss of other information.

Geologic data were digitized from the Massachusetts state geologic map (Zen, 1983), preliminary New Hampshire state geologic map (Lyons et al., 1986), Portland 2^{0} sheet (Hussey, 1985), and Eusden (unpublished and 1988). Geologic overlays were plotted at appropriate scale and projection for anomaly-geology correlations.

Susceptibilities of selected samples (Table 2.1) were measured with a GEOINSTRUMENTS JH-8 susceptibility meter. Measurements were made at approximately 3 to 6 cm intervals depending on bedding thickness and/or lithic variation. Areas with a high degree of weathering were not included in the survey. Measurements on hand-samples were multiplied by a factor of 2. Units were converted from SI to CGS for modeling in SAKI (Webring, written comm., 1986).

RESULTS

In general, the maps of high-frequency aeromagnetic (apparent depth = 4 km) (Fig. 2.5) and gravity (apparent depth = 6 km) (Fig. 2.6) data enabled the analysis of geologic-anomaly correlations. As

TABLE 2.1 - SUSCEPTIBILITY MEASUREMENTS
Measurements in SI x10^5 units = 4 Pi cgs or emu units

#	formation/terrane	# meas	average	std dev
	KCM			
1	Rangeley	11	20.00	2.14
2a	2mica granite	66	3.82	1.46
2b	Mz basalt	10	2030.00	794.49
3a	Rangeley	84	26.30	9.61
3b	"	16	9.69	1.78
3c	Mz basalt	22	101.36	39.07
4a	Rangeley	84	21.95	6.68
4b	"	13	6.69	3.07
5a	"	104	36.01	13.32
6a	"	114	25.27	8.06
52a	Lower Rangeley	17	29.53	4.99
52b	Lower Rangeley	15	30.87	5.93
54a	Upper Rangeley	124	163.01	101.63
7a	Perry Mt	224	21.23	8.07
7b	"	3	71.33	27.15
8a	Smalls Falls	137	69.14	108.61
8b	" "	13	1507.69	442.46
50a	" "	43	33.05	17.20
50b	" "	60	69.98	25.77
50c	" "	51	43.37	60.84
50d	" "	44	28.25	7.33
50e	" "	15	66.60	80.23
53b	Blackwater Pluton	26	20.04	3.09
53a	Madrid Fm	10	30.20	4.26
55a	Littleton FM	89	39.63	9.89
56a	Kinsman Qtz Monzonite	44	28.45	6.41
57a	Madrid Fm	57	26.53	7.53
58a	Upper Littleton Fm/Mt	46	36.15	7.99
59a	Massesecum tonalite	11	4.55	1.04
59b	Kinsman	21	48.90	10.49
60a	Garnitte layer	6	151.33	38.92
49a	**Massabesic Gneiss**	68	61.34	44.25
49b	" "	102	964.06	703.11
49c	" "	106	871.59	795.55
49d	" "	58	27.38	16.56
49e	" "	92	765.60	964.49
	Merrimack Block			
9a	Kittery Fm	110	28.76	9.75
9b	Mz dike	20	2494.00	1591.88
9a	"	87	26.20	11.64
9b	"	15	1713.33	1184.95
10a	Kittery Fm	15	41.71	16.41
47a	Calef Fm	35	16.43	3.81
47b	" "	73	19.29	9.46
48a	Berwick Fm	15	25.60	5.94
48b	" "	76	33.89	12.78
48c	" "	59	24.24	5.13
48d	" "	52	27.06	6.26
	Rye Block			
15a	Rye Fm	90	12.03	6.84
15b	" "	15	6533.33	1184.82
15c	" "	18	591.17	1757.34
15d	Mz dikes	18	1944.44	537.12
16a	Rye FM	122	25.66	23.97
17a	" "	77	2184.61	2082.67
17b	" "	15	46.27	41.44
18a	" "	102	25.16	19.49
19a	" "	41	19.61	5.62
19b	Mz dikes	23	454.91	676.78
20a	Rye Fm	20	59.35	6.24
20b	" "	41	56.27	40.03
20c	" "	25	74.60	78.71
21a	" "	80	28.85	13.08
21b	Mz ? dike	9	74.89	3.92
21b	"	10	64.50	5.21
	Boston Basin			
11a	Roxbury conglomerate	15	11.67	3.04
12a	" "	59	8.68	2.78
13a	" "	15	11.07	1.87
14a	" "	24	9.46	1.56
35a	Rox Cong	8	11.75	2.12

#	formation/terrane	#meas	average	std dev
	Agamenticus Complex			
22a	mag -26	15	15.50	2.43
23a	mag-43	10	44.80	15.68
24a	mag44-a	10	13.10	1.97
25a	mag-45	10	441.00	121.42
77	mag-3	13	268.462	119.22
78	MAG-1	16	23.1875	4.48
79	MAG-20	12	9.25	7.61
80	MAG-17	15	31.1333	8.53
81	MAG-4	10	7.9	1.60
82	MAG-44B	9	29.6667	4.87
84	MAG-45	14	500.714	124.56
85	MAG-67	20	69.9	41.84
86	MAG-66E	13	67	13.76
	Abbot Mt			
27a	AB-8	7	701.43	160.77
28a	85-1	9	31.44	4.85
28b	85-1	15	0.00	0.00
29a	85-2	9	82.22	35.70
30a	85-3	13	30.77	5.96
31a	86-17	6	1916.67	231.66
32a	87-2	7	7.86	7.38
	Other Mesozoic Plutons			
33a	cape neddick	12	6291.67	906.00
26a	Chase Stock1211-A	7	39.29	7.41
76	Pickett Stock-2	22	400	66.33
51a	**Exeter Pluton**	52	777.12	915.85
51b	" "	46	1553.91	376.01
87	Ex15	12	53.6667	8.13
88	Ex7b	9	11.4444	3.64
89	Ex7a	12	120.75	41.57
90	Ex2a	14	10228.6	1913.69
91	Ex28	12	36.4167	10.98
	Dracut Diorite			
92	Dr1	9	62.7778	7.82
93	Dr2	10	14.3	5.52
94	Dr3	14	127.643	46.40
95	Dr4	9	79.2222	47.80
96	Dr5	14	664.286	122.08
	Gulf of Maine			
68	ALV 447 1-1a	16	504.375	176.52
74	ALV 447 1-1-8	20	556	156.35
71	ALV 445 1-5	18	365	50.67
73	ALV 445 2-2	14	639.286	168.36
69	ALV 431 2-4d	11	246.364	64.54
75	ALV 430 2-2b	9	194.444	49.78
72	ALV 429 1-1-3	15	271	108.47
70	ALV	10	92.9	34.30
	Milford-Dedham Zone			
61a	either Pzgb or "New	46	47.19	5.60
62a	Pzgb	34	3035.29	1587.24
62a	Pzgb	6	185.17	236.06
63a	Burlington mylonite	51	835.55	1106.32
64a	Pzgb	38	955.74	1012.47
65a	Lexington Volcanics	11	422.50	809.39
66a	Lexington Volcanics	36	5086.11	2560.04
34a	cape anne dike	9	59.89	12.78
	Esmond-Dedham			
36a	Oakdale FM	83	27.23	14.78
37a	Tower Hill Quartzite	26	6.27	3.24
38a	Nashoba FM	103	18.55	7.17
39a	Boylston schist	48	16.44	9.56
40a	Rocky Pond granite	16	2.50	1.26
41a	Tadmuck Brooks Sch	73	37.73	13.59
42a	Nashoba FM	125	2726.08	1817.99
43a	Nashoba Fm	78	794.44	812.34
44a	Straw Hill diorite ?	18	6.72	1.64
44b	" "	21	4719.05	2044.90
45a	Andover granite	17	17.76	2.86
46a	Marlboro FM	50	50.28	19.87

Fig. 2.5 Color contoured, shaded relief, filtered aeromagnetic map of southestern New England and eastern Gulf of Maine with lithotectonic overlay. Lithotectonc overlay also shown in Figure 2.7 and Plate 2.1 for clarity. Color scale intervals are 30 nT.

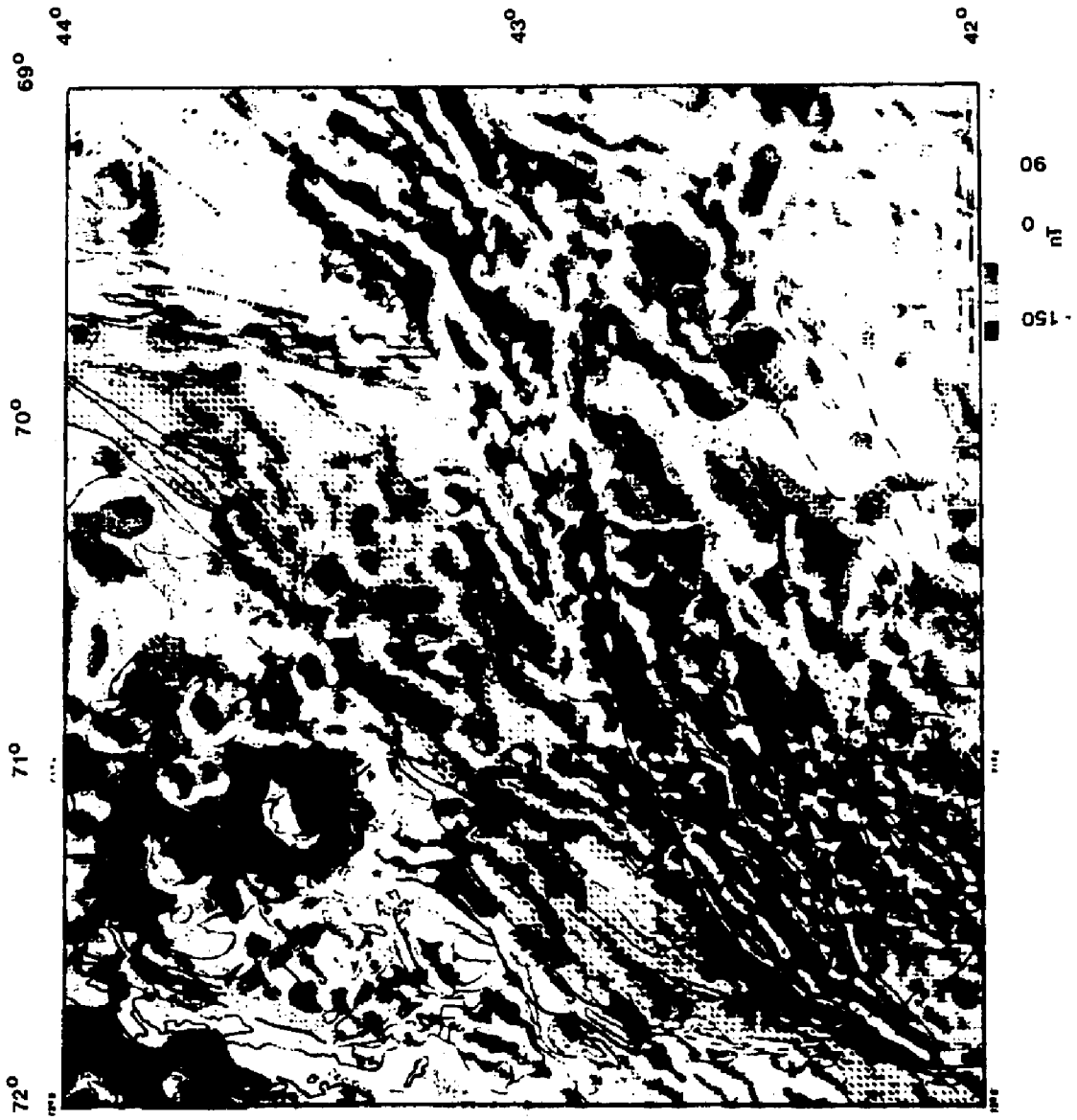
44°
43°
42°
69°
70°
71°
72°
90
0
nT
-150

Fig. 2.6 Color contoured, shaded relief, filtered gravity map of southestern New England and eastern Gulf of Maine with lithotectonic overlay. Gravity data onshore are Bouguer and offshore are free-air. Lithotectonc overlay also shown in Figure 2.7 and Plate 2.1 for clarity. Color scale intervals are 3 mgal.

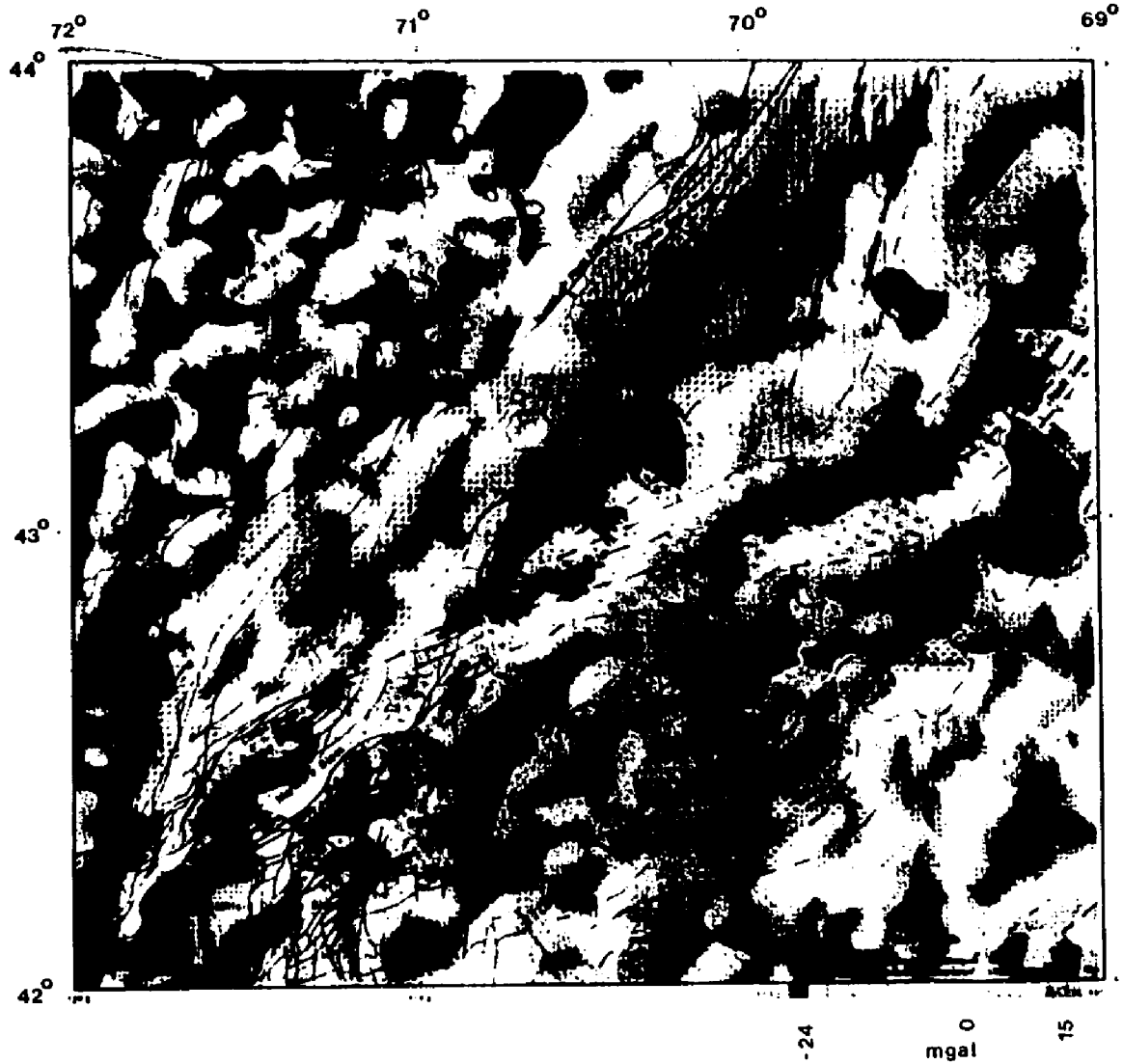
72°
71°
70°
69°
44°
43°
42°
-24
0
15
mgal

observed in other studies (Harwood and Zeitz, 1977; Castle, et al., 1976), the high-frequency aeromagnetic anomalies show acceptable agreement with the map pattern of appropriate metamorphic and igneous rocks. Structural discontinuities are readily apparent on the aeromagnetic map as truncated linear and oval aeromagnetic anomalies or by the juxtaposition of regions with differing aeromagnetic characteristics. The high-frequency gravity anomalies correlate to the igneous rocks within the research area and commonly cross lithic contacts. In places, the gravity anomalies overprint the terrane boundaries defined by the aeromagnetic anomalies suggesting the presence of stitching plutons. Specific features of the residual potential field maps are presented below by lithotectonic groups. Because the Mesozoic plutons are not confined to any one lithotectonic region, they are presented separately. Figure 2.7 shows the lithotectonic interpretation of the aeromagnetic and gravity residual maps. Specific geographic and geologic locations referred to in text are shown in figure 2.3.

Mesozoic Plutons

The Jurassic and Cretaceous plutons are associated with very high amplitude (up to 1100 nT) closed positive anomalies that disrupt the field over the Kearsarge-Central Maine Synclinorium and the MMR. These bodies and associated anomalies confirm the existence of the NW/SE-trending corridor of Mesozoic plutons (Billings, 1956; Foland and Faul, 1977) in the north central portion of the aeromagnetic map. Closed gravity highs are associated with a

Fig. 2.7 Lithotectonic interpretaion of research area. Unpatterned areas with solid boundaries are undifferentiated Paleozoic and Mesozoic igneous rocks. Unpatterned areas with dashed boundaries refer to Ordovician and Mesozoic anorogenic rock boundaries inferred from aeromagnetic data. Refer to figure 2.3 for geographic and geologic names.

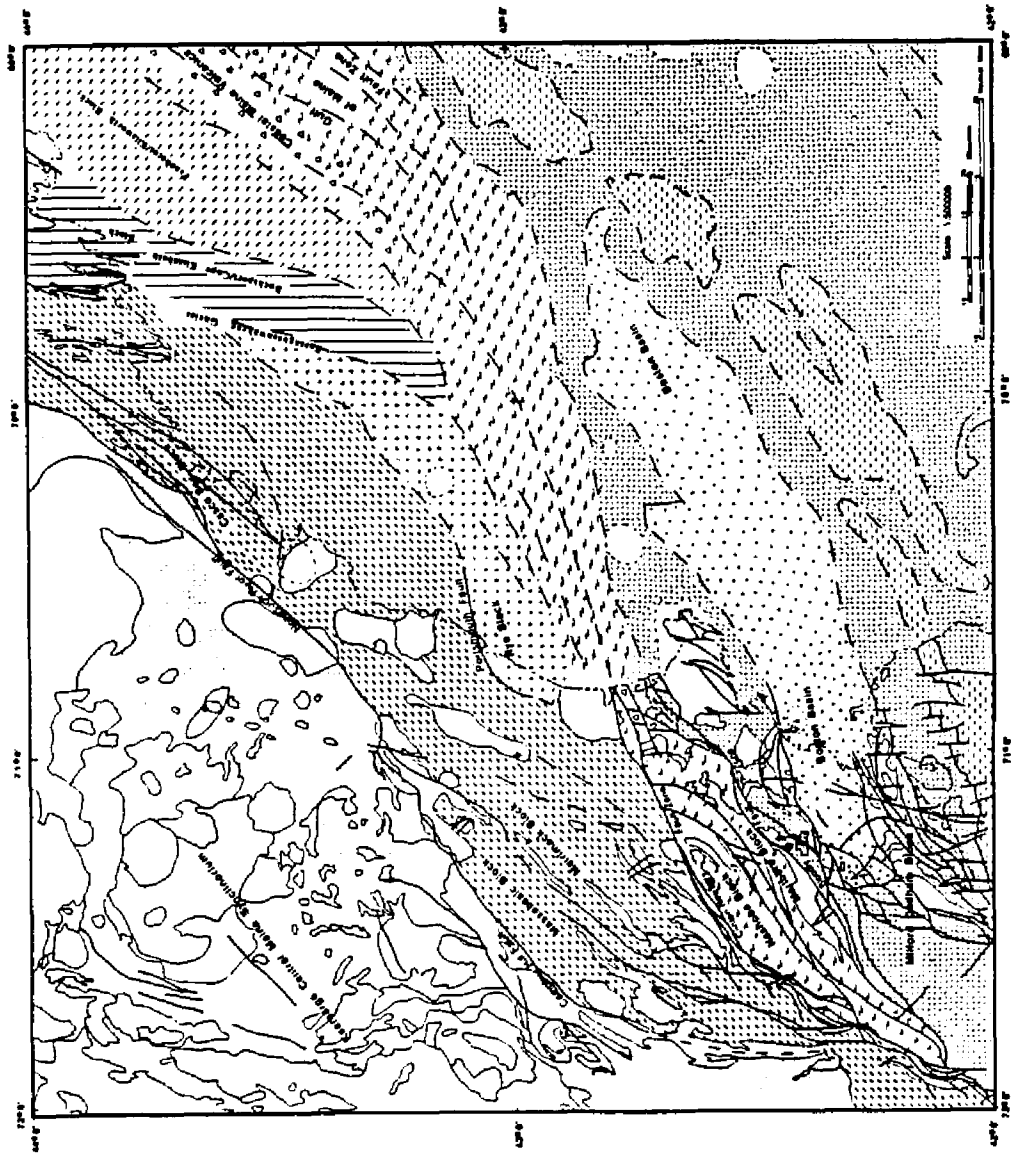

number of the WMS bodies; the Merrymeeting, Belknap, Red Hill, and Ossipee Complexes.

Within the research area, the Burnt Meadow, Randall Stock, Alfred Complex, Tatnic Complex, and Cape Neddick Complex are all associated with large aeromagnetic anomalies but, with the exception of the Cape Neddick Complex, lack associated gravity anomalies. Notably, the Triassic Abbott Complex lacks aeromagnetic and gravity signatures and the Agamenticus Complex has only small aeromagnetic highs associated with the alkalic syenite and syenite to quartz syenite zone (see Chapter 3 for complete description of these rocks). The biotite granite core of the Agamenticus Complex has an associated circular negative aeromagnetic anomaly. A closed aeromagnetic high to the east of the Tatnic Complex and north of the Agamenticus Complex is suggestive of an unexposed Tatnic-like body. A gravity high located in the eastern portion of the Merrimack Block partially overprints the Agamenticus Zone.

Aeromagnetic anomalies that are suggestive of subsurface Mesozoic igneous plutons (i.e., 8 to 10 km wide, oval highs) are present under the Biddeford Granite and within the offshore extensions of the Rye and Esmond-Dedham Blocks. The Ordovician anorogenic complexes in the Esmond-Dedham Zone (i.e., Cape Ann Complex, Nahant Granite, Cashes ledge (just on eastern edge of map) and Pigeon Hill (offshore of Cape Ann)) are also overprinted by circular highs similar to those of the Mesozoic anorogenic complexes.

Massabesic-Merrimack-Rye Blocks

The southwest portion of the aeromagnetic field over the Merrimack Block is different from that associated with the rest of the block. In the southwest, the aeromagnetic field is an undulating surface of approximately -30 to 0 nT with a NE-trending fabric comprised of 30 to 90 nT linears. To the northeast the background field deceases to -60 to 0 nT and is dominated by oval and NNE- to NE-trending linear anomalies with magnitudes greater than 90 nT. The southernmost two of these linear anomalies are loosely aligned with the phyllonitic Calef Formation. The oval highs are related to the Paleozoic (Exeter, Newberryport, Biddeford, and Dracut Plutons) and Mesozoic (Tatnic and Agamenticus Complexes) igneous rocks located within the Merrimack Block. The offshore extension of the Merrimack Block is associated with several elongate oval anomalies (to the east of the Agamenticus Complex) and somewhat randomly oriented linear highs (30 to >90 nT). The gravity field overlying the Merrimack Block appears as a subdued pattern that is lower than that of the adjacent Kearsarge-Central Maine and Nashoba Blocks. Juxtaposed on this field are several oval and linear gravity highs associated with the Paleozoic Plutons (Exeter, Newberryport and Dracut Plutons) and possible unexposed equivalents (i.e., under the Merrimack Block label, Fig. 2.6). A positive gravity plateau located in the eastern portion of the Merrimack Block, to the north of the Portsmouth Fault Zone, is continuous with a gravity high associated with the western portion of the Rye Block.

The Merrimack-Rye Block contact is defined by a steep aeromagnetic gradient whose curvilinear trend is located along the

Portsmouth Fault Zone onshore and along the southern portion of an irregular positive aeromagnetic plateau offshore. The offshore extension of this inferred boundary cross-cuts a large gravity low (-15 mgal). The Portsmouth Fault Zone aeromagnetic anomaly is disrupted by the Mesozoic Chase Stock (Brooks, 1986) just offshore of the New Hampshire/Maine border. The location of the southern terminus of the Portsmouth Fault Zone aeromagnetic anomaly is unclear. It either ends at the northern contact of the Newburyport Quartz Diorite, is truncated by EWE linear anomalies that trend offshore, or is offset by dextral motion. The latter suggests that the easternmost Calef Formation aeromagnetic anomaly is instead related to the Portsmouth Fault Zone.

The gently undulating to flat aeromagnetic field of -90 to 0 nT overlying the Rye Block is segmented by a 60 to 90 nT linear that parallel the coastline of New Hampshire and by an approximately 8 km wide, greater than 90 nT, oval high. Offshore, the eastern border of this relatively flat aeromagnetic field is truncated by major N/S to NNE-trending linears (under the Passagassawakeag Gneiss label, Fig. 2.5). Its southeastern edge is located along a series of smaller, segmented NE- to EWE-trending linears.

The western portion of the Merrimack Block is bounded by a prominent NE/SW aeromagnetic gradient, that corresponds to the Silver Lake, Flint Hill, and Nonesuch River faults. To the west of this gradient the Massabesic Block is associated with a aeromagnetic linear high (> 90 nT) and a flat -6 to 0 mgal gravity plateau. The western boundary of the Massabesic Gneiss is defined as a change from the relatively flat, low gravity pattern of the

Massabesic Gneiss to the highly undulating gravity field associated with the Kearsarge-Central Maine Synclinorium. The terrane boundary defined by the gravity field is coincident with the trace of the Campbell Hill-Nonesuch River faults and underlies the Fitchburg Pluton at its' southern terminus (located at the southern end of the Massabesic Block).

Casco Bay Block

The southern portion of the Casco Bay Block is dominated by two segmented 20 to 70 km long, 60 to 110 nT linear anomalies that in part are associated with sulfidic schists (Scarboro Formation) within this block (Figs. 2.3 and 2.5, Table 2.1). The linear anomalies are bounded in part by major faults (e.g. the Portland and Cape Elizabeth Faults) within the Casco Bay Region indicating that juxtaposition of different lithologies along these faults has contributed to the observed anomalies. The northern portion of the Casco Bay Block characterized by a relatively flat -30 to 30 nT plateau. The subdued character of the northern portion of the Casco Bay Block partly reflects wider data spacing. All but the northernmost portion of the Casco Bay Block is underlain by a gently undulating 3 to 15 mgal plateau. This plateau has similar characteristics to, and may be continuous with, that overlying the Merrimack and western Rye Blocks.

The aeromagnetic anomalies of the southern portion of the Casco Bay Block is similar to, and may be transitional with, the offshore extension of the Merrimack Block. This is supported by recent findings which suggest that the Merrimack Block and Casco Bay Block onshore are lithically transitional (Fargo, in prep) and by

the similarities in metamorphic and igneous histories (Olzsewski et al., 1988). Although these data justify grouping these two blocks and the Massabesic Block together as one lithotectonic zone on the map, the gravity high over the Casco Bay Group and the eastern portion of the Merrimack Block indicates that the rocks underlying these regions may be different from those in the southern portion of the Merrimack Block.

Kearsarge-Central Maine Synclinorium Zone

The Kearsarge-Central Maine Synclinorium Zone contains 30 to 90 nT, 10 to 30 km long aeromagnetic linears that generally trend NE/SW. Many of the aeromagnetic anomalies can be directly related to sulfidic, pyrrhotite bearing units such as the Smalls Falls Formation or the upper unit of the Rangeley Formation. The presence of these units allows the delineation of some regional fold patterns (i.e., the Lebanon Nappe, Fig. 2.3 and 2.5) and the truncation of units against faults (i.e. Smalls Falls Formation against the Campbell Hill Fault). Relatively flat, often low, aeromagnetic plateaus are associated with the Paleozoic granites within the Kearsarge-Central Maine Synclinorium. The gravity field associated with this region is comprised of highly undulatory and lobate -30 to 17 highs and lows. Although these anomalies cross-cut a large number of lithic contacts, the highs generally overlie the regions with the largest proportion of metasediments and the lows reflect the dominance of Paleozoic granites within a region.

Zones of the Boston Platform

The regional, total field anomalies associated with the Nashoba, Marlboro-Newbury, Esmond-Dedham, and Boston Basin Zones

have previously been analyzed by Harwood and Zietz (1977) and Castle et al. (1976). A detailed analysis of this region is therefore unnecessary, and the reader is referred to them for such a report. However, the tectonic importance of the Clinton-Newbury and Bloody Bluff fault zones makes a review of some of the distinguishing features observed within these regions important. As noted by Castle et al. (1976) many of the fine details of the aeromagnetic data are observable only on the scale of a 7.5 - minute quadrangle. The regional scale of this report results in a number of different anomaly-geology correlations compared to Castle et al. (1976).

The Nashoba Zone

The magnetically well-characterized Nashoba Zone is dominated by 30 to 60 km long, 1100 nT linear anomalies that are bounded on the north and northwest by a well defined negative trough. These linears correspond roughly to the Nashoba subdivisions of Abu-Moustafa and Skehan (1976) (not shown). Susceptibility measurements indicate that the source for these anomalies are the biotite-rich, quartz-plagioclase gneisses and schists of the Nashoba Formation (Table 2.1; samples 42a and 43a) rather than the mafic members (e.g., the Boxford Member). As noted by Castle et al. (1976), these well defined linears are subdued and truncated by the Silurian Andover Granite in the northern portion of the Nashoba Zone.

The Marlboro-Newbury Zone

Although the Marlboro Formation is stratigraphically related to the rocks of the Nashoba Zone, it is separated here on the basis of its aeromagnetic signatures. A steep gradient can be traced along

the southern extension of the Assabet River Fault (ARL) that separates the Nashoba Boxford Member from the Marlboro Formation. The Marlboro-Newbury Block itself is comprised of 6 to 12 km long , NE/SW-trending linear and oval anomalies that overprint lithologic contacts. The random orientation and shorter length of the anomalies in the Newbury region reflect its highly faulted nature. Contrary to Castle et al. (1976), the anomalies at this scale do not correspond to the mafic Marlboro Formation.

The Marlboro-Newbury and Nashoba Blocks are juxtaposed against the Merrimack and Rye Blocks along the Clinton-Newbury Fault Zone. The trace of this fault on the aeromagnetic map is readily apparent along the northern border of the Nashoba Block, where it overprints a steep gradient between the Nashoba Block and an adjacent aeromagnetic trough, but is harder to see along the northern border of the Marlboro-Newbury Block. The offshore trend of the Clinton-Newbury Fault System can be traced along segmented, positive, ENE-trending, aeromagnetic linears that truncate the N-S-trending linears that extend into the Gulf of Maine from eastern coastal Maine (see below). Aeromagnetic anomalies between this gradient and the offshore extension of the Bloody Bluff Fault System have a similar blocky appearance as, and are correlated, with the Marlboro-Newbury lithotectonic-magnetic zone.

The Esmond-Dedham Zone

The northern boundary of this zone lies along the Bloody Bluff/Burlington mylonite fault zone and is well defined by a nearly continuous, 1100 nT aeromagnetic linear. This linear cross cuts the contacts between Precambrian gabbros and volcanic rocks of the

Esmond-Dedham Zone and does not follow the northward deflection of this fault zone to the South Boundary fault (Morency, 1986) near Newburyport as proposed by Castle et al. (1976). Susceptibilities for both the volcanic and gabbro rocks are sufficiently high to produce this anomaly. Offshore this fault zone can be traced along the northern edges of segmented aeromagnetic and linear gravity highs.

Intrazone anomalies within the Esmond-Dedham zone are 2 to 12 km ovals and segmented linears with amplitudes that range from approximately 200 to 1100 nT. These anomalies generally cross cut lithic boundaries and are often bounded by brittle faults.

Prominent aeromagnetic highs are associated with the Salem Gabbro and the Cape Ann alkalic Complex. The Salem Gabbro anomaly can be traced offshore to its termination approximately 12 km to the east along the northern border of the Boston Basin. The latter is characterized on- and offshore by a relatively subdued aeromagnetic field that is punctuated by ovals similar to those associated with the gabbros of the Esmond-Dedham Zone.

The magnetic pattern in the southern portion of the Esmond-Dedham Zone has been segmented by anomalies associated with Carboniferous extensional features. Linears are observed along the northern and southern edges of the Ponkapoag Basin. The northern border of the Narragansett Basin is marked by the truncation and/or absence of Esmond-Dedham type anomalies.

The Esmond-Dedham Zone can be traced offshore as segmented regions of aeromagnetic, oval and linear highs segmented by low amplitude magnetic troughs interpreted as Precambrian and

Mesozoic rift basins (Shih, 1988; Hutchinson, 1988; Uchupi, 1966) and interrupted by the Cashes Ledge high.

Offshore Lithotectonic-Geophysical Correlations from Coastal Maine

The aeromagnetic and gravity anomalies in the northeastern portion of figures 2.5 and 2.6, respectively, are related to lithotectonic packages within coastal Maine. As noted earlier, the offshore extension of the aeromagnetic fields that overlie the Rye and Merrimack Blocks are truncated by a major N/S-trending aeromagnetic linear. This major N/S-trending aeromagnetic anomaly trends into the Boothbay region of coastal Maine where the Cape Elizabeth and Bucksport Formations occur (Figs. 2.3 and 2.5). North of the Boothbay region the aeromagnetic anomaly (Fig. 2.2) follows the Passagassawakeag Formation, composed of high grade, felsic to mafic volcanic rocks (Osberg et. al, 1985; Hussey, 1985).

A roughly triangular shaped aeromagnetic plateau, with an intervening low trough, is located to the east of the Passagassawakeag anomaly (Fig. 2.5). This plateau is located offshore of the Muscongus and Penobscot Bay regions of coastal Maine. The subdued, undulating, central portion of this plateau, partly the result of wider data spacing, correspond to the offshore extension of the Penobscot and Ellsworth Formations. The intervening trough approximately traces the Bucksport and/or the Cape Elizabeth Formations. The western border of the plateau parallels the Penobscot/Bucksport contact which is mapped onshore as an east-dipping thrust. The eastern border of the plateau trends onshore near to the contact of the Silurian to Devonian volcanics of downeast Maine and the Avalonian Precambrian rocks of Penobscot

Bay. Because the Precambrian rocks within Penobscot Bay have only limited exposure, the western border of the plateau offshore is correlated with the contact between Cambro-Ordovician rocks of the Penobscot-Ellsworth Formations. The eastern border of the plateau delineates the western limit the Silurian-Devonian volcanics extending offshore from eastern coastal Maine.

East of the plateau is a region of high amplitude (up to 400 Nt), NE/SW- to ENE/WSW-trending aeromagnetic linears (Fig. 2.5). In the gravity field this plateau is located within a trough partially bounded by 12 to 15 Mgal linears. To the northeast of the research area this package of linears can be traced along aeromagnetic linears (Fig. 2.2, see also Zietz et al., 1980) associated with the Gulf of Maine Fault Zone (Stewart et al., 1989; Hutchinson, 1988), and the coastal volcanics of southeastern coastal Maine . It is proposed that this aeromagnetic plateau is a zone of complex thrusting/transpression in which rocks of the coastal Maine volcanics and the Avalon Platform have been tectonically juxtaposed. Similarity of aeromagnetic patterns occur in southeastern Maine, where major through-basement, east-dipping thrusts (Hutchinson, 1988), rocks with Avalonian (Cashes Ledge and Three Dory Ridge) and coastal volcanic ? (samples from Fundy Fault and Sigsby Ridge) affinities (Hermes et al., 1978), and the tectonic juxtaposition of these lithologies in coastal Maine (Stewart, 1974) have been recognized.

DISCUSSION

Implications for regional tectonics

Analysis of maps of potential field data strongly supports the offshore extension of coastal New England lithotectonic zones into west and west-central Gulf of Maine. The coastal lithotectonic-magnetic zone, which includes the MMR, is truncated to the east by a major N/S linear that is correlated with the Passagassawakeag Gneiss. The southward extensions of this and other linears farther to the east are terminated by westward deflection, segmentation, and truncation against the offshore extension of the Bloody Bluff Fault Zone and/or the Clinton-Newbury Fault Zone.

This regional aeromagnetic anomaly pattern mirrors those associated with dextral transpressional regimes elsewhere (i.e. the Great Slave Lake shear zone, Canada, (Hoffman, 1987) and Nadj shear zone, Africa (Sultan et al., 1988)) and reflects the superposition of Alleghanian transpressional structures on preexisting Acadian or older structural fabrics. It is suggested that this transpression resulted from the impingement of a relatively local salient within the Avalon Terrane, the Esmond-Dedham zone, upon the previously accreted litho-tectonic packages to the north and northwest of the Bloody Bluff and Clinton-Newbury fault zones.

Accretion of the latter in the eastern coastal region of Maine is constrained by the late Devonian sealing of thrust faults by S-type plutons (Stewart, 1984; Keppie, 1988; Hogan, 1988). Eusden (1988) and Barreiro and Eusden (1988) suggest that the Massabesic and Merrimack Blocks were juxtaposed against the Kearsarge-

Central Maine Synclinorium by middle Devonian. Lyons et al. (1986) and Thompson (in press) suggest that this juxtaposition occurred by west directed thrusting of the Massabesic and Merrimack Blocks over the rocks of the Kearsarge-Central Maine Synclinorium. These emplacements ages are coeval with the docking of the Hope Valley Terrane in southern New England (O'Hara and Gromet, 1985; Rast and Skehan, 1988). Although poorly constrained, the development of the pervasive, ductile mylonitic fabric and epidote-amphibolite facies metamorphism (Brooks, 1986) (tentatively dated as Devonian by Olszewski et al., (1984)) within the Rye Complex were likely synchronous with the above accretionary events.

As oblique dextral transpression continued in response to the accretion of Gondwana (Keppie, 1988), dextral strike-slip motion (approximately 270 km of relative motion, Keppie, 1982) occurred during the late Devonian to early Pennsylvanian along NE-trending faults within and bounding the coastal Maine lithotectonic zone (i.e., the Norumbega and Belleisles Faults) (Bradley,1988). Synchronous with this motion was the development of Carboniferous pull apart basins (i.e., the Magdalen Basin (Keppie, 1982; Bradley, 1988) and the Narragansett Basin) and bimodal magmatism in the coastal Maine lithotectonic zone (Hogan, 1988). Within southeastern Maine, major strike-slip motion along the southern extension of the Norumbega Fault, the Nonesuch River Fault, had ceased by late Carboniferous (fault is sealed by the Saco Pluton, 307 Ma; Gaudette et al., 1982).

Following this period of NE directed strike slip motion, the continued encroachment of Meguma (the Nova Scotian platform), along the E/W-trending Minas Geofracture (approximately 160 km

dextral motion; Keppie, 1982), resulted in the NE-trending dextral transpression within coastal New Brunswick during mid to post late Pennsylvanian (Bradley, 1988; Manuel and Nance, 1988). This zone of dextral transpression, described by Manuel and Nance (1988) and Caudill and Nance (1986) as a positive flower structure, extends along strike into and is likely coeval with the west directed thrusting within the Gulf of Maine Fault Zone (Fig. 2.5 and 2.8; see also Hutchinson, 1988). In southern New England, this deformation was synchronous with the emplacement of the Esmond-Dedham or Boston-Avalon Terrane (Getty and Gromet, 1988; Rast and Skehan, 1988; O'Hara and Gromet, 1985) along the Hope Valley - Bloody-Bluff Fault Zones onshore and the offshore dextral strike-slip fault zone delineated by the aeromagnetic anomalies.

The amount and style of deformation along the Hope Valley-Bloody Bluff - Gulf of Maine Fault system can be related to the position of the lithotectonic zones in the collision zone. The degree of deflection and segmentation of the aeromagnetic anomalies suggests that deformation increases towards the offshore extension of the Bloody Bluff and Clinton-Newbury fault zones and is concentrated between their offshore extensions. Based on fault geometry inferred from the aeromagnetic data, dextral transpression within the Gulf of Maine would result in dominantly strike slip motion along approximately NNE/SSW-trending faults and oblique to orthogonal thrusting or underplating along NE/SW to N/S faults (Fig. 2.8). Within the central Gulf of Maine this resulted in northwest-directed oblique (?) thrusting (Hutchinson, et al., 1988) and imbrication of the Esmond-Dedham and coastal Maine volcanic

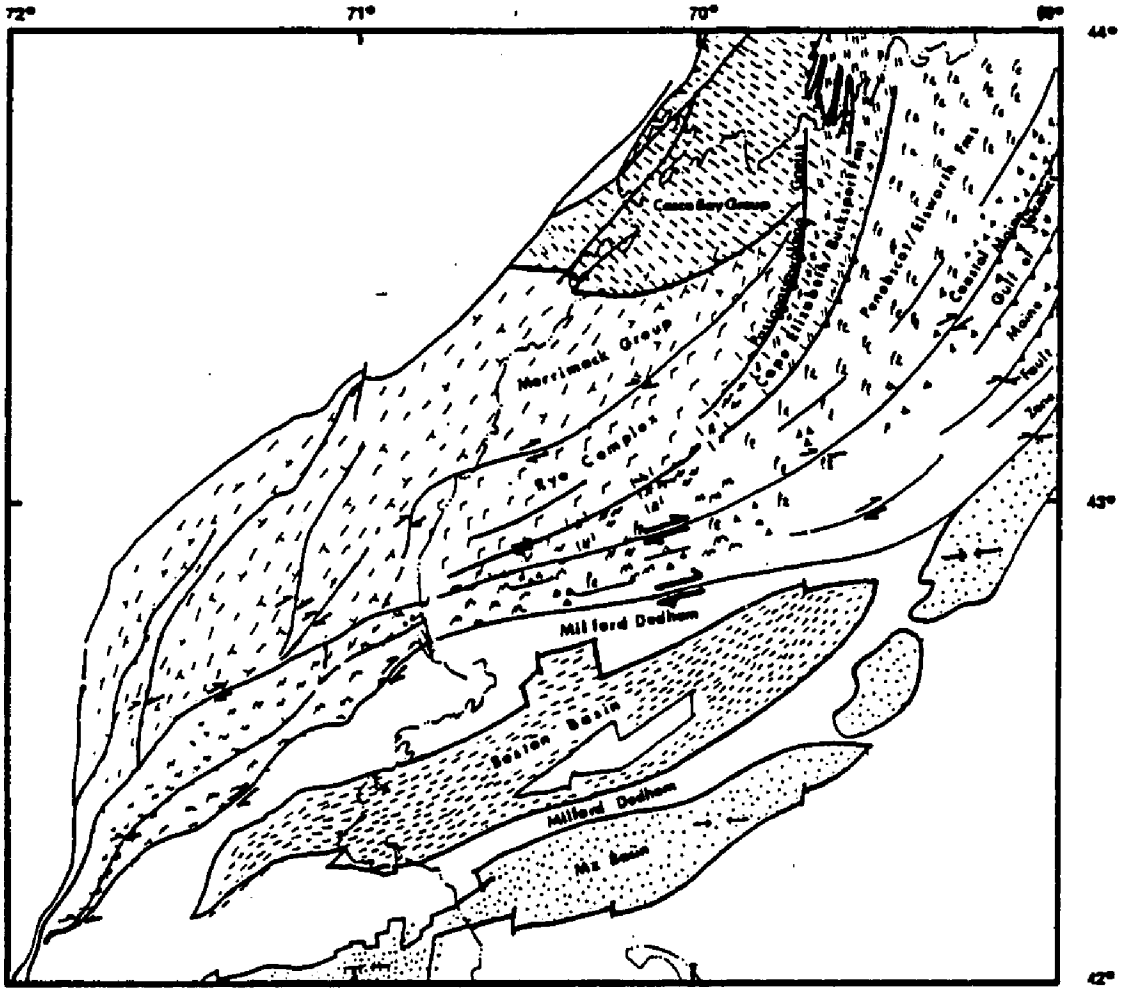

Fig. 2.8 Interpretation of fault motion within the Gulf of Maine dextral transpressional zone and adjacent regions.

zones within the Gulf of Maine Fault Zone. Lithotectonic zones located to the north of the Bloody Bluff Fault Zone were transposed and attenuated by strike-slip motion along the fault's offshore extensions. Onshore this juxtaposition is preserved as the Newbury Volcanics inlier, for example, within the Nashoba-Marlboro zone but offshore may include lithologies belonging to any of the zones that bound the BBFZ.

The role of the Carboniferous basins and the Cashes Ledge Granite during this collision is unclear. Imbrication of the leading edge of the Milford Dedham Zone within the Gulf of Maine fault zone may have progressed from west to east until the sole fault of the Carboniferous basin was reactivated. Subsequent thrusting may have been accommodated by closure of the Carboniferous basin resulting in unimbricated Esmond-Dedham rocks to the southeast. Undoubtedly the Narragansett Basin and its offshore extension played a similar cushioning role west of the Cashes Ledge Granite. Sinistral and subsequent dextral strike-slip deformation within the Narragansett Basin noted by Mahlaer and Mosher (1988) could be related to the transpressional deformation described here. The occurrence of the Cashes Ledge Granite at the point of flexure of the Gulf of Maine fault zone may not be purely fortuitous. This large pluton may have caused the change from thrusting within the Gulf of Maine to strike-slip motion to the west as observed for plutonic bodies in the Najd shear zone in Egypt (Sultan et al., 1988). Alternatively, collision of the Cashes Ledge pluton may have mitigated transpression within this portion of the Gulf of Maine.

Within the MMR, the anastomizing patterns of aeromagnetic linears associated with the Calef Member and the Portsmouth Fault zone against the Clinton-Newbury Fault Zone suggest that they may have also developed during this Alleghanian transpression. However, evidence for Alleghanian deformation within the MMR zones is sparse. The 473 Ma Exeter diorite places a minimum age on the development of the penetrative structures observed within the eastern portion of the Merrimack Zone. Motion along the Calef phyllonite is constrained by the intrusion of the Devonian Biddeford Pluton and probably the Ordovician Exeter Pluton. Therefore, if Alleghanian thrusting did occur along the Calef phyllonite, it would have occurred to the south of the Exeter Pluton requiring a scissor-like fault motion. This interpretation is compatible with the proposal that deformation increases towards the Bloody-Bluff Fault Zone.

However, Permian monazite ages for both the Massabesic Gneiss (270 Ma) and high-grade Berwick Formation (250 Ma) in western MMR are interpreted as peak metamorphism and place a maximum age on uplift of the western MMR basement relative to the Kearsarge-Central Maine Synclinorium basement (Barreiro and Eusden, 1988); ages here supported by $^{40}Ar/^{39}Ar$ hornblende ages (Lux, 1989, written comm.). A similar, but opposite, dichotomy of hornblende and biotite ages occurs across the Flying Point Fault Zone (Hussey, 1989) in the Casco Bay Region (West et al., 1988). West et al. (1988) suggest that the difference in ages can be explained by juxtaposition along a strike-slip or normal (east side down) fault. Alleghanian normal faulting (west down) has also been proposed for

the Lake Char - Clinton-Newbury Fault system (Goldstein, 1988, 1989) and the adjacent Merrimack Trough. The development of the Calef Fault and the late-brittle features of the Portsmouth Fault Zone could therefore be related to the late Permian extension suggested by the above data. This extension might be explained in terms of a releasing bend during the final episodes of the dextral transpressional collision of the Boston-Avalon with the terranes to the west of the Hope Valley - Bloody-Bluff Fault System. Alternatively the later Permian ages (250 Ma) could reflect the earliest stages of extension related to the opening of the Atlantic Ocean during the Mesozoic Era (McHone and Butler, 1984). Eusden (1988) suggests that the exposed basement complexes within the coastal region may be metamorphic core complexes exposed during Mesozoic extension. Recent seismic interpretations by Stewart (1989) and Heck (1989) also emphasize the important role Mesozoic extension, along listric faults, played in the final juxtaposition of terranes within the Appalachian orogenic belt.

Implications for Mesozoic Igneous Activity

Analysis of the potential field maps support the presence (Weston Geophysics, 1976; Shih et al., 1988) of circular to oval positive aeromagnetic and, in several instances, circular positive gravity anomalies associated with the Jurassic and Cretaceous mantle-related anorogenic complexes in southwestern Maine and adjacent New Hampshire. The lack of such anomalies associated with the Triassic complexes in southwestern Maine suggests that a mafic component was absent in their evolution. Alternatively, such

a mafic component has remained at lower crustal levels beyond the resolution of the currently available potential field data.

Analysis of the aeromagnetic data has also enabled the addition of several more complexes to the Mesozoic anorogenic magmatic province. An aeromagnetic high overprinting the Biddeford granite suggests that this pluton is underlain by a Mesozoic complex. The effect of this complex on radiogenic ages (Gaudette et al., 1982) obtained for the Biddeford granite must be considered. Two positive aeromagnetic anomalies within the Gulf of Maine are in line with and are correlated to the NW/SE-trending Mesozoic magmatic corridor. However, because Ordovician anorogenic complexes within the Esmond-Dedham terrane are also associated with positive aeromagnetic anomalies, this correlation must be tested by obtaining radiogenic ages for the rocks.

Unfortunately, the findings of this study do not contribute significantly to the present understanding of the deep crustal structure within coastal New Hampshire and Maine. The tectonic interpretation suggests that the coastal region is comprised of a number of lozenge shaped lithotectonic packages bounded by regional fault systems. The aeromagnetic and gravity data emphasize these important regional lithotectonic fault boundaries (The Campbell Hill - Nonesuch River and Portsmouth Fault Zones) and intrazonal faults (i.e., the Calef Phyllonite or Silver Lake Fault) within this region. Thompson et al. (in press) and Lyons et al., 1986) suggest that these faults are sub-vertical and penetrate only the upper crust. The confluence of these faults, and those from the Casco Bay Block, in the region of the Agamenticus Complex likely facilitated the rise of

these magmas from lower crustal levels. NW-trending regional linears or other anomalous potential field patterns that might help constrain the nature of the crustal structure responsible for the NW regional trend of the Mesozoic complexes are absent in the potential field data.

An important feature of the gravity map is the high plateau that overprints the Casco Bay, eastern Merrimack Block, and western Rye Block. As noted previously, the lack of high density rocks at the surface suggests that these regions are underlain by a different, possibly more mafic, crust than other regions of the Merrimack Trough. These rocks could provide a unique source for crustally derived anatectic rocks or provide a distinct signature in assimilation processes.

CHAPTER 3

PETROGENESIS OF THE AGAMENTICUS COMPLEX: SOUTHWESTERN MAINE

INTRODUCTION

The opening of the Atlantic Ocean during the Mesozoic was accompanied by the intrusion of subalkalic to alkalic, epizonal plutons and stocks in New England and Quebec (Billings, 1956; Eby, 1987; DeBoer et al., 1988). These rocks form the Triassic Coastal New England Province, the Jurassic White Mountain Magma Series (WMS), the Cretaceous New England-Quebec Province (NEQ) and the Cretaceous New England Seamounts (McHone and Butler, 1985). Petrogenetic models of this rift-related magmatism include magmatism related to a hotspot trace (Morgan, 1981; Crough, 1981; Foland et al., 1985, 1988; Foland et al, 1989), to a leaky transform fault (Uchupi et al., 1970), or to doming and/or passive rifting (McHone and Butler, 1984; Bedard, 1985). Although a number of petrologic studies have been conducted on the WMS and the NEQ (Eby, 1987 and references therein; DeBoer et al., 1988 and references therein), little is known about the geochemistry and petrology of the Coastal New England Province. This petrologic province is important as it was the earliest know pulse of rift-related magmatism in the New England region.

The largest and most diverse pluton in the CNE is the Agamenticus Complex. A petrogenetic study of the Agamenticus Complex, York Maine, was undertaken to investigate the nature of the magmatism in this province. Field mapping and petrographic analysis augment work by Woodard (1957) and Hussey (1962). Geochemical data which include new major and trace element analyses provide a basis for understanding the petrogenetic relationships of the rocks exposed through the development of quantitative petrologic models.

Previous Work

The Agamenticus Complex was originally mapped by Wandke (1922) and later remapped in reconnaissance studies by Woodard (1957) and Hussey (1962, 1985). Hussey (1962) divided the complex into four major rock types (Fig. 3.1): alkalic syenite, alkalic granite, porphyritic biotite granite, and "contaminated alkalic granite" (later renamed quartz syenite; Hussey, 1985). From the oldest to the youngest, the relative ages of the phases, established by cross-cutting relationships and textural arguments, are alkalic syenite, alkalic granite, and porphyritic biotite granite (Hussey, 1962;1985).

Using the composition and distribution of xenoliths and internal chemical gradients within individual xenoliths, Woodard (1957) suggested that the Agamenticus Complex evolved through the interaction of a quartz syenite to syenite magma with the surrounding country rock. In this interpretation, the quartz content of the granites reflects the amount of assimilation of country rock

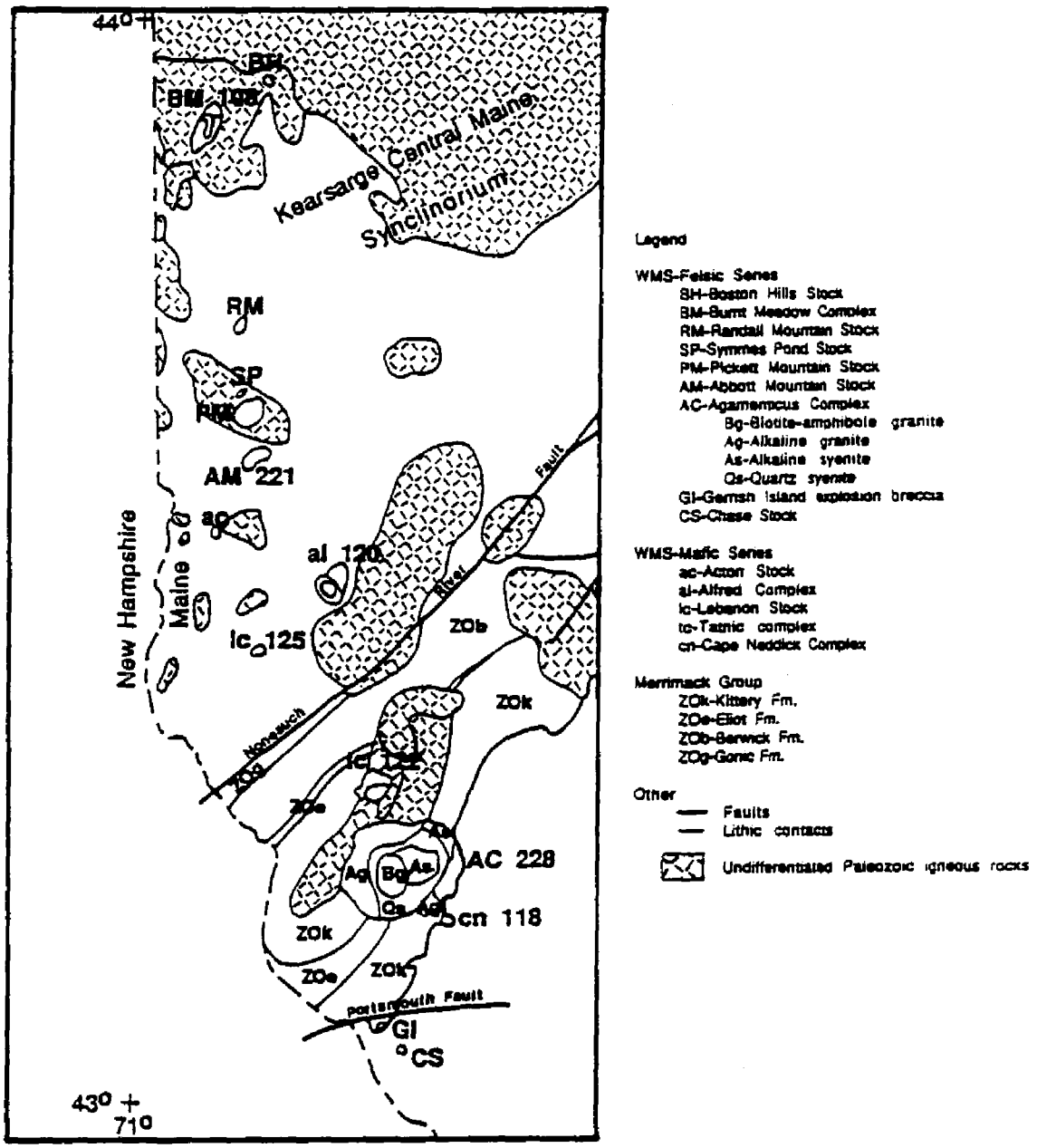

Fig. 3.1 Simplified geology of southwestern Maine. Adapted from Hussey 1985. Ages (Ma) indicated where known (Foland and Faul, 1977; Foland et al., 1977; Hoefs, 1967). Except for the Merrimack Group the metamorphic rocks are undifferentiated.

by the syenite magma. Blocks of quartz syenite in the "contaminant" zone were interpreted as the products of extensive potassium metasomatism of metasedimentary xenoliths by the magma. An alternative interpretation, proposed by Hussey (1962), is that the quartz syenite blocks of the "contaminant" zone were products of variable degrees of assimilation of the alkalic syenite by the intruding, cogenetic alkalic granite.

Isotopic analyses of the Agamenticus Complex are limited. Hoefs (1967) obtained a whole rock Rb-Sr age of 227 ± 3 Ma and an initial Sr^{87}/Sr^{86} value of 0.710 using representative samples from all of the rocks except for the syenite to quartz syenite zone (SQSZ). The samples cluster in three regions of Rb^{87}/Sr^{86} values; 6.42 to 28.4- biotite granite, alkalic syenite, and quartz syenite, from the western lobe of the alkalic granite, 104.0 to 109.8 - an alkalic and aegirine granite, and 194.0 - alkalic granite. The age determined by Hoefs (1967) was later substantiated by Foland and Faul (228 ± 5 Ma; 1977) and Foland et al. (216 ± 4 Ma; 1971) using K-Ar systematics (biotite ages). A 172 Ma fission track age determined for the alkalic syenite was interpreted as a possible time of solidification (Christopher, 1969) but more likely reflects uplift of the Agamenticus Complex through the 150°C isotherm. Christopher (1969) suggested that a 166 Ma apatite fission track age for the biotite granite is due to annealing associated with a younger thermal event. Zimmerman et al. (1975) attributed a 84 ± 5 Ma apatite fission track age for the biotite granite to regional uplift past the 150°C isotherm or to a regional heating event.

Paleomagnetic data have been obtained by Fang Wu and Van Der Voo (1988) for the Agamenticus Complex, Abbott Complex, and the Litchfield Pluton. A paleopole of 48°N,99°E was determined for the Agamenticus Complex. Pole reversals that occurred during the emplacement of the Agamenticus Complex do not appear to correlate to the emplacement of a particular unit. However, such details are hard to interpret because their map of the Agamenticus Complex does not correlate to known geology and sample locations are not specified. Fang Wu and Van Der Voo (1988) note that the paleopole estimated from the Agamenticus Complex falls approximately 10° southeast of those previously published for the Triassic. This disagreement is attributed to smaller displacements for the North American craton then previously calculated or to polar wander.

Geologic Setting

The Agamenticus Complex intrudes the Precambrian to Ordovician Kittery and Eliot Formations of the Merrimack Group and the Devonian Webhannet Pluton (Hussey, 1962, 1985; Osberg et al., 1985; Gaudette et al., 1982) (Fig. 3.1). The Kittery Formation is comprised of thin- to thick-bedded feldspathic and calcareous quartzites, quartzites, siliceous phyllites, and subordinate interlayered marble beds. The Eliot Formation contains calc-silicate and thin interbedded phyllite and quartzose phyllite. Rock types within the Webhannet Pluton range from quartz diorite to biotite granite.

The Kittery and Eliot Formations were deformed and metamorphosed to regional greenschist facies prior to the emplacement of the Ordovician Exeter Diorite (Hussey, 1985; Gaudette et al.,1982). Contact metamorphism of these formations to pyroxene hornfels is apparent in close proximity to the Agamenticus Complex and in foundered blocks within the complex (Woodard, 1957) as evidenced by abundant epidote and diopside in calcareous quartzites of the Kittery Formation.

The region into which the Agamenticus Complex intruded is cut by of a number of major anastomosing transpressional faults that separate rocks with different lithotectonic characteristics (Hussey, 1985; Bothner et al., 1984). These faults have experienced a complex history of motion from Paleozoic initiation to Mesozoic reactivation (Hussey, 1985; Carrigan, 1984; Brooks, 1986; Eusden, 1988). The most significant of these are the Nonesuch River Fault, the Portsmouth Fault Zone, and the Calef Fault (Fig. 3.1). The Nonesuch River Fault separates the rocks of the Kearsarge Central Maine Synclinorium to the north from the Merrimack Trough (Hussey, 1985). The Portsmouth Fault Zone is the boundary between the latter and the more southerly block that consists of the Rye Formation (Hussey, 1985; Carrigan, 1984; Brooks, 1986). The intraterrane Calef Fault separates the Eliot and Berwick Formations of the Merrimack Group.

Models for the petrogenesis of A-type magmas

The petrogenesis of syenite to alkalic granite complexes, such as the Agamenticus Complex, is a multi-faceted problem. Models used to explain similar felsic alkalic, or A-type (Loiselle and Wones, 1979) granitoids call upon large amounts of fractionation from an alkali olivine basalt parent derived from partial melting of the mantle (Eby, 1987; Nelson et al., 1987; Loiselle, 1978; Foland and Friedman, 1977) or the partial melting of dehydrated, granulite facies, lower crust (Collins et al., 1982 ; Barker et al. 1975). In the latter model, melting of the lower crust is initiated by: 1) Heat provided through the emplacement of mantle derived basalt magmas (Barker et al. 1975; Hildreth, 1981), 2) Isothermal decompression associated with rifting (Bailey, 1974; Bedard, 1985), and/or 3) Lowering of the solidus by the introduction of volatiles (Bailey, 1974).

Mixing of magmas, which have undergone varying degrees of evolution, is often evoked to produce intermediate alkalic rocks (Loiselle, 1978; Whalen and Currie, 1984; Nelson et al., 1987). Heat provided by the passage of the felsic and/or mafic alkalic magmas through the middle crust and/or latent heat provided by cooling of a magma chamber at upper crustal levels may result in the generation of anatectic, subalkalic melts that may accompany and sometimes mix with the alkalic magmas (Barker et al., 1975; Henderson et al., 1989; Fowler, 1988).

The final evolution of the alkalic magmas occurs in shallow level magma chambers by variable degrees of fractional

crystallization, assimilation, volatile complexing, Soret diffusion, deuteric alteration and recrystallization (Parsons and Becker, 1986; Mahood, 1981; Hildreth, 1981; Macdonald, 1987; Bowden et al., 1987). In addition to these processes, the effect of the inefficient separation of fractionating crystals and evolved liquids in granitoid systems (McCarthy and Hasty, 1976; Lee and Christiansen, 1983; Tindle and Pearce, 1981) must be considered in the development of petrologic models.

As in the White Mountain Magma Series and the New England-Quebec Province (Eby, 1987), some of these processes occurred during the development of the Agamenticus Complex. After a brief review of methods used in this research, the results from field, petrographic, and geochemical analyses are presented. These findings are discussed in light of the general model presented above and quantitative geochemical modeling conducted in this study. A petrogenetic model for the Agamenticus Complex is introduced which incorporates the information gained from this research.

ANALYTICAL TECHNIQUES

The Agamenticus Complex was mapped at a scale of 1:24000 over portions of two field seasons. Standard petrographic techniques were used for detailed microscopic analysis of mineral and textural relationships.

Four samples from the Agamenticus Complex and representative samples from the other felsic Mesozoic plutons in southwestern Maine were analyzed for major and trace element

abundances by X-Ray Energy Dispersive Spectrometry at the University of Rhode Island using the techniques described by Hamidzada (1988) (Appendix III.I). Major and trace element analyses for other rocks were obtained from the University of Florida and the University of Michigan (X-Ray Fluorescence analysis) and the USGS, Denver (Induced Coupled Plasma Spectrometry) (Appendix III.I). FeO/Fe_2O_3 ratios were determined by standard titration techniques for the samples analyzed at the University of Rhode Island and the USGS (Appendix III.II). REE abundances were analyzed by Instrumental Neutron Activation (Boston College, Department of Geology and Geophysics) or Induced Coupled Plasma technique (USGS, Denver (Appendix III.I).

Chemical analysis of selected minerals were obtained using a JOEL 733 Super Probe (Massachusetts Institute of Technology, Department of Earth and Planetary Sciences; Appendix III.I). Data reduction for the electron microprobe follows that of Bence and Albee (1978) and Albee and Ray (1970). All mineral analyses determined by electron microprobe analysis and mineral normalizations are presented in Appendix III.III. EXCEL spreadsheet Macros, used to normalized the mineral data and to recast the major and trace element data (PrbMac and PetMac, respectively), are presented in Appendix III.IV. Mineral compositions stated in the text as end members (i.e., An_{50}) are calculated from electron microprobe analyses and are presented in mol % units. Amphibole and pyroxene classifications follow that of Leake and Winchell (1978) and Morimoto et al. (1988), respectively.

Least squares mixing models are calculated using Mix n' Mac V2.4 least squares modeling software developed by Mason (1987). The minerals used as input to the models are those interpreted, on the basis of petrographic observations, to be the earliest minerals to crystallize in the parent rocks. Mineral compositions used are from electron microprobe analyses, or those given in Cox, Bell, and Pankhurst (Appendix 5, 1979). Although apatite was present in the rocks as an early crystal, it was not included in all of the models because the addition of this mineral does not balance P_2O_5.

Trace element calculations for fractional crystallization follows the approach of MacCarthy and Hasty, 1976 and Tindle and Pierce, 1981. Liquid and solid (cumulate) trends for equilibrium and Rayleigh fractional crystallization are calculated using the mineral assemblages from least squares mixing models as input. The involvement of zircon in the petrologic models was estimated from petrographic observations and by fitting Zr and/or Hf concentrations within the models. Trace element-trace element diagrams showing the results of these models differ from those presented by MacCarthy and Hasty (1976) or Tindle and Pierce (1981) because the fractionating mineral assemblage is not kept constant and several types of liquid and cumulate trends are calculated.

RESULTS

The general map pattern of the Agamenticus Complex published by Hussey (1962) (Fig. 3.1, Plate 3.1) is confirmed by this study (Plate 3.2). It is apparent that Hussey's map is a simplification of

more complex features. Detailed mapping has defined broad regions of textural and mineralogical variability within and between rock units (Plate 3.2). In this respect, several rock units have been renamed or subdivided. The eastern lobe of the alkalic granite is renamed aegirine alkalic granite. The "contaminant zone" (Hussey, 1962) or quartz syenite (Hussey, 1985) is subdivided into an aenigmatite-bearing syenite and an undifferentiated syenite to quartz syenite zone (SQSZ). The aenigmatite syenite and the SQSZ are both intimately intruded by one or more granites.

Petrography and Mineral Chemistry

Biotite Granite

The central portion of the complex is underlain by a gray to pink, fine- to medium-grained, porphyritic, subsolvus biotite granite (Fig. 3.2 and Plate 3.2; Table 3.1). Plagioclase phenocrysts within the biotite granite are continuously zoned from cores of An_{50-16} to rims of $An_{13-0.8}$ and potassium feldspar phenocrysts are nearly pure orthoclase (Or_{93}). Albite, orthoclase, quartz, biotite ($Fe^T/(Fe^T+Mg)=0.5-0.47$; where Fe^T = total iron), and subordinate olive-green to green hastingsite amphibole compose a finer-grained matrix. Apatite, ilmenite, and multiply zoned, rusty-colored allanite occur as accessory phases within the matrix. Magnetite is present as inclusions within the amphiboles.

Fig. 3.2 - Photomicrograph of biotite granite showing porphyritic, zoned plagioclase (plg) biotite (bio), and zoned allanite (al) inclusion in plagioclase. a) Plane polarized light B) Crossed polarized light. 27.2X


a
b
a
b

Table 3.1 - Point counts of representative samples

Rock type	Bio-amb gran	Aegirine granite			Alkalic granite		Aenigmatite syenite		Alkalic syenite		Aug sye
Sample#	MAG 4	MAG 122a	MAG 49	MAG 91-4	MAG 5	MAG 20	MAG 155	MAG 139	MAG 3	MAG 84b	MAG 91-1
Minerals											
ksp-undiff	27.96			39.50	70.58	61.72	61.74	69.51	85.88	79.00	70.46
micro		9.27	33.61								
perth		33.93	11.76								
plg	31.65	13.51	13.83	10.63	1.40	4.17	4.19	5.30	4.86	1.45	8.68
qtz	31.65	32.63	29.02	39.12	12.07	31.86	3.79	6.16	1.38	0.87	1.52
amb	2.99				15.37	2.00	8.14	6.34		2.89	5.74
aenig							10.43	5.49			
bio	5.52					0.08				0.30	
cpx		10.66	11.76	10.77			11.70	6.63	4.60	9.21	11.72
olv									3.09	6.20	1.41
other*	0.23			0.10	0.58	0.17	0.40	0.57	0.20	0.50	0.47
# pts	796	1229	1547	1381	1210	1199	1265	1056	1523	1727	853
*	Zr,Ap,Op,Al	CC,Op	CC,Op,Sp	CC,Op	Zr,Ap,Op,Al	Op,Fl	Ap, Op	Ap, Op	Op,Ap	Op,Ap	Op,Ap

Abbrv.: ksp-undiff - undifferentiated alkali feldspar, micro-microcline,perth-perthite,plg-plagioclase,qtz-quartz amb-amphibole,aenig-aenigmatite,bio-biotite, cpx-clinopyroxene,olv-olivine, Zr-zircon,Ap-apatite,Op-opaque,Fl-fluorite,Al-allanite,CC-calcite,Sp-sphene

A variation in modal proportion of the plagioclase and potassium feldspar phenocrysts, from approximately 10 to 60 %, results in a distinctive change in the appearance of the rock within and between outcrops. Rare xenoliths are comprised of calcareous quartzites (Kittery Fm.) and biotite clots with euhedral plagioclase crystals. This unit is cut by sinuous, pink, rhyolitic dikes that are associated with pyrite and chalcopyrite mineralization.

Alkalic Granite to Quartz Syenite

A significant amount of leucocratic quartz syenite is present within the eastern portion of the alkalic granite lobe defined by Hussey (1962; 1985) (Plate 3.2). Both the quartz syenite and the alkalic granite are medium-grained, medium to light gray, and weather light-tan to white. The mineralogy is dominated by turbid, highly exsolved, euhedral to subhedral perthitic orthoclase and anorthoclase (Fig. 3.3). Exsolution lamellae have nearly pure albite and orthoclase compositions (Or_{01} and Or_{96-98}, respectively). Fine-grained albite and microcline are commonly present as late, fine-grained, euhedral to anhedral grains and as replacement intergrowths within the perthitic phenocrysts. Myrmekite occurs in several samples near the western contact of the alkalic granite with the Webhannet biotite granite (Plate 3.1; MAG 16). Rocks in the western portion of the alkalic granite (Plate 3.1; MAG 23) are subsolvus and contain strongly zoned, medium-grained, euhedral to subhedral perthite and plagioclase. Both feldspars have highly serrate grain boundaries suggesting late subsolidus recrystallization.

Fig. 3.3 - Photomicrograph of alkalic granite. Note the microcline perthite lamellae and the fine-grained potassium feldspar overgrowths on the feldspars. Crossed polarized light. 24.5X


kps
s
qtz

Medium- to fine-grained, subophitic to anhedral quartz grains contain trails of fluid inclusions. Quartz also forms interconnected curvilinear veins that separate and enclose perthite phenocrysts.

Subophitic to interstitial amphibole is the dominant mafic mineral of the western lobe. It is compositionally zoned with green to brown pleochroic barroisite to katophorite-richterite cores and rims of blue-green to green pleochroic richterite to arfvedsonite and riebeckite (Fig. 3.4; MAG 26 and 193). Fine-grained, blue-green and blue, acicular riebeckite or arfvedsonite fringes also occur as overgrowths on the amphiboles.

Lime-green hedenbergite rims fayalitic olivine and both are included within amphiboles. Orange-red amorphous cores within a few of the amphiboles are interpreted as highly altered olivine grains. Biotite forms thin overgrowths on the other mafic minerals or is intergrown with the late interstitial amphiboles. Minor euhedral apatite and zircon are usually associated with clots of amphibole ± plagioclase, opaques, and quartz (Fig. 3.5). Many of the zircon grains are zoned with dark, anhedral cores and clear euhedral rims. Fluorite and calcite occur as interstitial grains.

Aegirine Alkalic Granite

The eastern lobe of the alkalic granite (Hussey, 1962;1985) is renamed the aegirine granite. Although the offshore extension of this rock has not been mapped, the numerous miarolitic cavities and xenoliths of Kittery Formation located in outcrops along the coastline suggest that these rocks are in close proximity to the contact with the country rock. The western contact of this portion

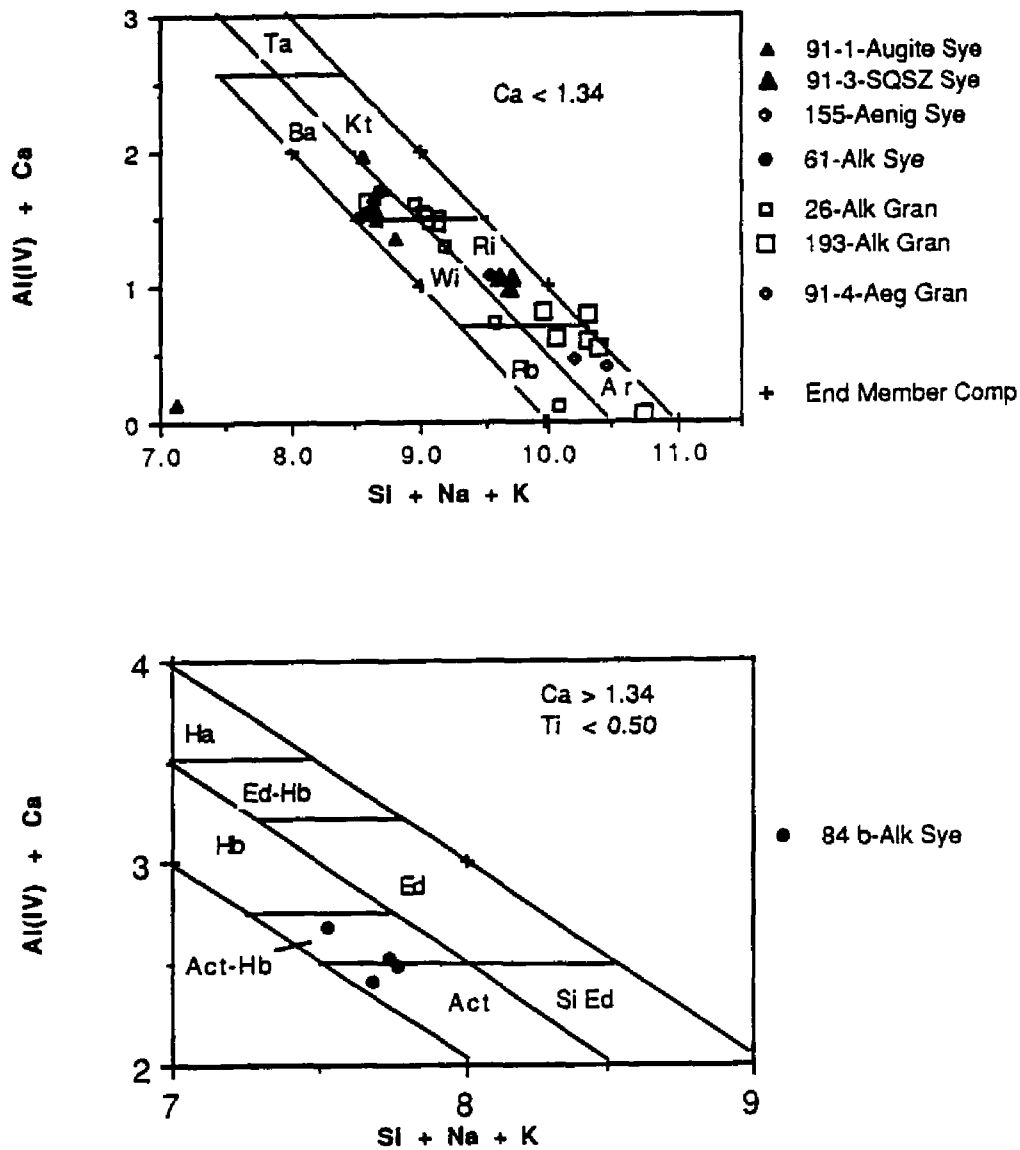

Fig. 3.4 - Representative amphibole compositions. (After Giret et al. 1980). Abbrev. Ha - ferro - and magnesiohastingsite, Ed - edenite, Ta - taramite, Kt - katophorite, Ri - richterite, Ar - arfvedsonite, Hb - fe- and Mg-hornblende, Ba - barroisite, Wi - winchite, Rb - riebeckite, Act - actinolite.

Fig. 3.5 - Backscatter image of alkalic granite showing interstitial amphibole with inclusions of magnetite. Scale bar in mm.


amb
Mt

of the aegirine granite with the aenigmatite syenite is well exposed along Rt 1 (Plates 3.2).

Along the coast the aegirine alkalic granite contains medium-grained, euhedral to subhedral perthite, antiperthite, microcline, and quartz. Aegirine occurs as individual, euhedral to subhedral grains and in mineral clumps associated with arfvedsonite, fluorite, calcite, and an amorphous red-brown alteration product (hematite or iron hydroxides) (Fig. 3.6). The calcite occurs as poorly defined cores within the clumps. Alteration of the feldspars and the aegirine is enhanced in close proximity to quartz- and calcite-bearing veins 1 to 2 mm in thickness. These veins cross-cut the medium-grained quartz indicating that the medium-grained quartz predates vein formation.

In addition to the aegirine granite of the eastern lobe, several fine to medium-grained, aegirine, alkalic granites intrude the SQSZ (Plate 3.1; MAG 122a, 11c, 91-4 (hyphenated sample numbers and letters after the numbers refer to sample sites where more than one sample was obtained)). Medium-grained, perthite within these rocks is highly exsolved with string and braid lamellae. Subordinate, finer grained, highly zoned plagioclase also occurs in these rocks. Euhedral to subhedral needles of aegirine (Fig. 3.7, MAG 91-4) have colorless and light yellow to blue-green to light green pleochroic colors. Most of the needles are highly corroded, altered to calcite and opaques, and exhibit complex intergrowth with arfvedsonite (Fig. 3.4, MAG 91-4). Fluorite and calcite are late interstitial minerals. One of the aegirine granites within the SQSZ,

Fig. 3.6 - Photomicrograph of aegirine granite showing calcite (cc) replacement of aegirine (aeg). Plane polarized light. 7.5X


kps
zib

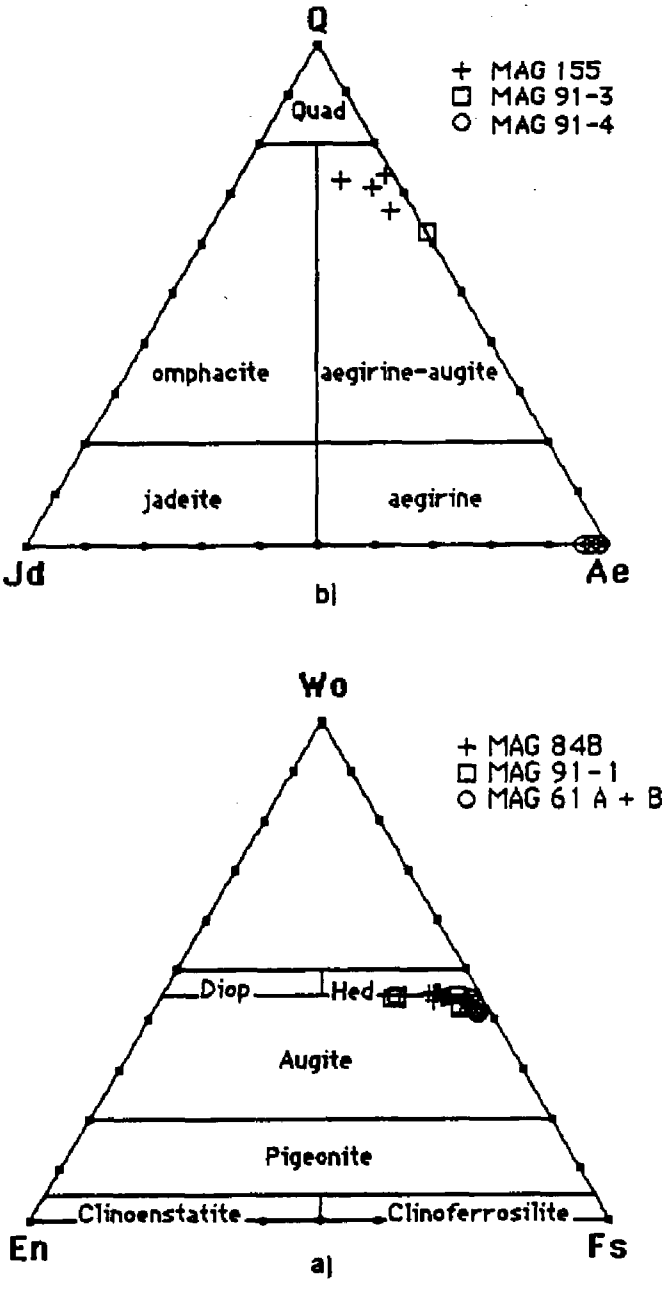

Fig. 3.7 - Representative clinopyroxene compositions (after Morimoto et al., 1988). The increase in the ferrosilite component observed in plot a) is due to Na substitution. Clinopyroxenes from 91-1 are augites to ferrian, sodian augites and those from 84b are hedenbergites. Abbrev. Dio - diopside, Hed - hedenbergite, Quad - Wo+En+Fs clinopyroxenes.

MAG 11c, is a dike which contains abundant angular to rounded xenoliths of Kittery Formation and autoliths of syenites.

Alkalic Syenite

The alkalic syenite varies considerably in texture and mineralogy. It is generally a medium-to coarse-grained, dark blue-green to tan-green rock containing perthite, ferrian sodian augite to augite to hedenbergite, fayalite (Fa_{98}), actinolite to barroisite, quartz, albite, apatite, biotite, and ilmenite (Figs. 3.4, 3.7, 3.8 (MAG 61a+b)). The perthites contain euhedral apatite inclusions, and have fine-grained albite rims. The mafic silicate minerals are subhedral to anhedral. Olivine is rimmed by either clinopyroxene or amphibole, and clinopyroxene is rimmed by amphibole. In some cases these reaction rims are abrupt and the olivine appears to be resorbed (Fig. 3.9). Many olivine grains are altered to a orange-brown amorphous material (iddingsite?). Quartz is a late interstitial mineral that occurs in contact with fayalite and magnetite.

In several localities, the alkalic syenite is fine- to medium-grained and nearly amphibole-free (Table 3.1). Medium-grained varieties are texturally similar to the amphibole-bearing alkalic syenites described above, but the fine-grained alkalic syenites have a trachytic texture. The mafic minerals are more abundant and more euhedral in the finer-grained alkalic syenites. In these rocks euhedral augite, and to a lesser extent euhedral fayalite, are included within the potassium feldspar phenocrysts and also occur as euhedral to subhedral minerals within the matrix (Fig. 3.8; MAG 61a). Hedenbergite in the matrix is essentially homogeneous

Fig. 3.8 - Photomicrograph of alkalic syenite. The sample is from the contact between the fine-grained alkalic syenite and the coarse-grained amphibole-bearing alkalic syenite at MAG 61 (Plate 1). Plane polarized light. 8.9X

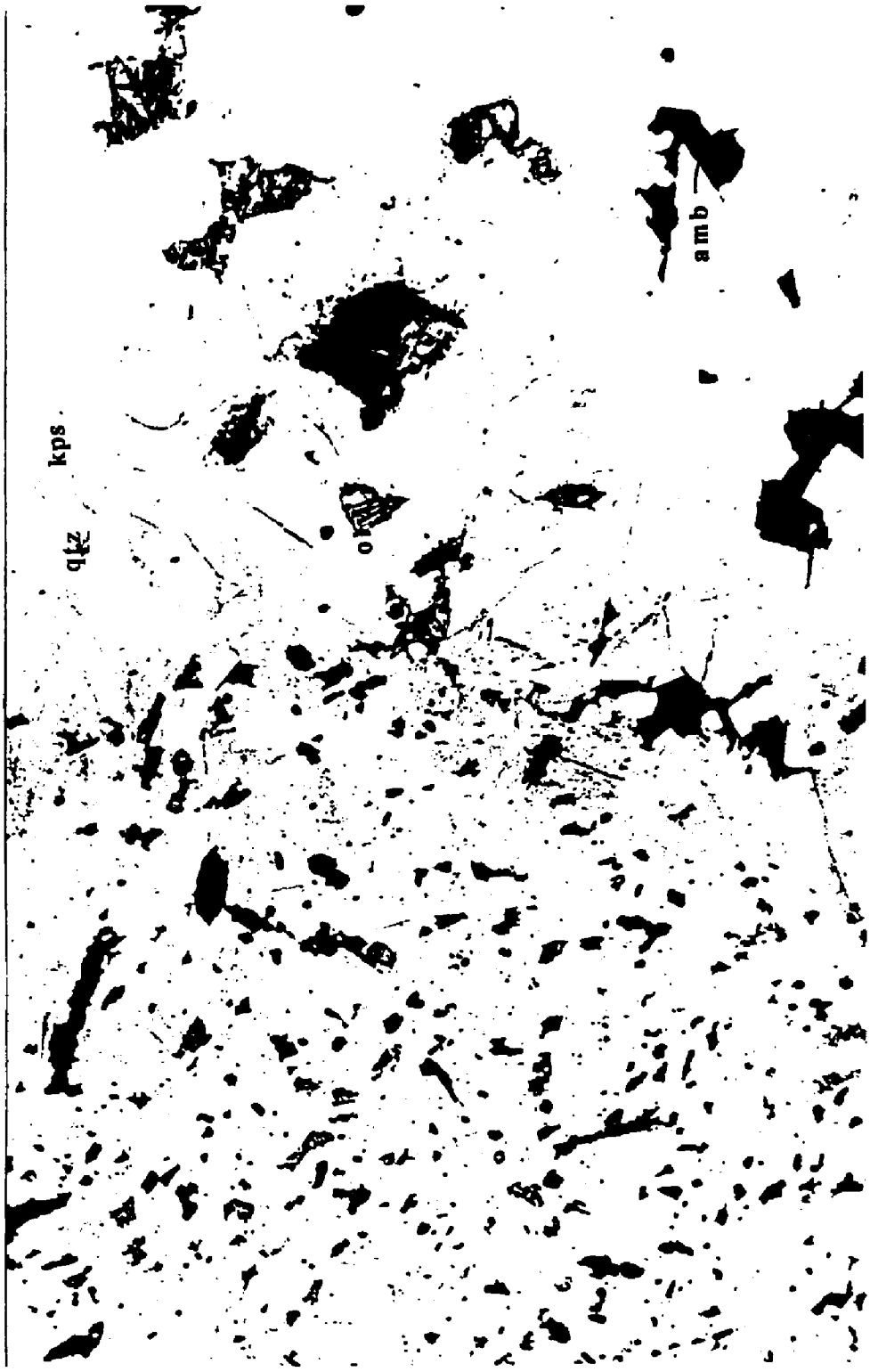
amb
kps
qtz
o

Fig. 3.9 - Photomicrograph of disequilibrium textures from the alkalic syenite MAG 84b. Note the irregular shape of the olivine and the amphibole overgrowth. Plane polarized light.


amb

(Ac_{14-16}) and differs slightly from those included in the potassium feldspar phenocrysts (Ac_9) (Fig. 3.7).

Porphyritic Aenigmatite Syenite

The porphyritic aenigmatite syenite occurs along the southeastern border of the complex in contact with the aegirine granite and within the southcentral portions of the complex (Plate 3.2). Contact relationships within the southcentral portion of the complex are poorly defined. The aenigmatite syenite comprises varying portions of the outcrops and in places appears to be transitional with SQSZ rocks. A block of the aenigmatite syenite is also present within the aegirine granite near MAG 49 at York Beach (Plate 3.1).

The porphyritic aenigmatite syenite is a dark to medium-green rock with euhedral to subhedral, perthitic, potassium feldspar phenocrysts. The matrix consists of fine-medium-to fine-grained, euhedral to subhedral aenigmatite, aegirine-augite (Ae_{17-29}, Fig. 3.7; MAG 155), and perthite with subhedral to anhedral richterite (Fig. 3.4, MAG 155), quartz, plagioclase, microcline, ilmenite, and magnetite (Fig. 3.10). The potassium feldspar phenocrysts have perthitic cores with coarse exsolution lamellae and inclusions of apatite. The perthite phenocrysts also have rims of perthite with fine lamellae. Aegirine-augite and richterite commonly concentrate at the phenocryst-rim boundary. Lamellae compositions in the core and rim of the phenocryst and matrix potassium feldspar are all similar to those observed in the alkalic granite; nearly pure albite and orthoclase. Arfvedsonite overgrowths of the aegirine-augite and richterite are associated with late brittle fractures.

Fig. 3.10 - Photomicrograph of the aenigmatite syenite. Note the concentration of fine-grained aenigmatite, aegirine-augite, and richterite at the edge of the inclusion-free potassium feldspar phenocryst. The richterite also occurs as late interstitial crystals. Plane polarized light. 32.5X

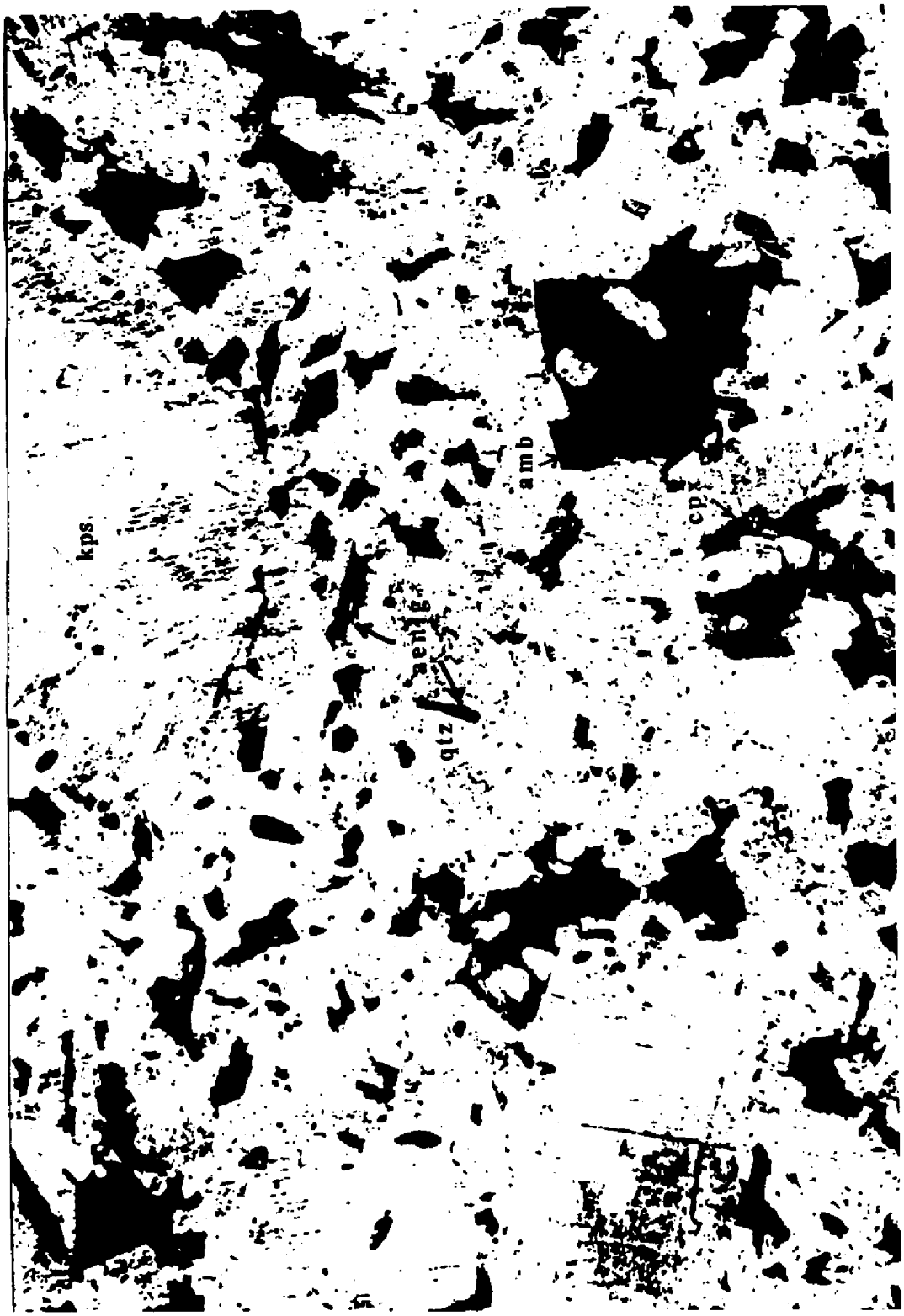
kps
amb
cpx
qtz

Syenite to Quartz Syenite Zone (SQSZ)

This zone occurs within the south-central portion of the complex and is part of the unit assigned by Hussey (1985) as a quartz syenite. The relationships of the different syenites within this zone are unclear. Mapping is complicated by the similar appearance of the rocks in outcrop and/or transitional nature of many of the syenites. The pervasive intrusion by later granites further masks the intrusive relationships of the syenites.

The most mafic syenite located in this zone is the sub-solvus augite syenite. This medium-grained, dark green syenite was observed at only one locality within the syenite to quartz syenite zone (Plate 3.1; MAG 91). Unlike the majority of the rocks within the complex, this syenite contains early, coarse-grained, coexisting potassium feldspar and plagioclase (Fig. 3.11). Both feldspars have continuously zoned, inclusion-free cores and perthitic potassium feldspar rims. Core to rim composition of the plagioclase varies from An_{19} to An_{05}. Subordinate plagioclase occurs with fine-grained perthite in the matrix. Contacts between the matrix feldspars are highly irregular and convolute. Clinopyroxene occurs as euhedral to subhedral grains in the perthitic rims and within the matrix. Augite to ferrian sodian augite ($Wo_{44}En_{15}Fs_{41}$) occurs as individual crystals and as cores to augite to ferrian sodian augite ($Wo_{44}En_5Fs_{51}$) with higher ferrosilite component (MAG 91-1; Fig. 3.7). Barroisite to barroisite-winchite (MAG 91-1; Fig. 3.4) rims the clinopyroxenes and is present as subophitic to interstitial grains. Ilmenite occurs as inclusions in the amphibole and within the matrix in association with sparse pyrite.

Fig. 3.11 - Photomicrograph of subsolvus augite syenite. Plane polarized light. 6X

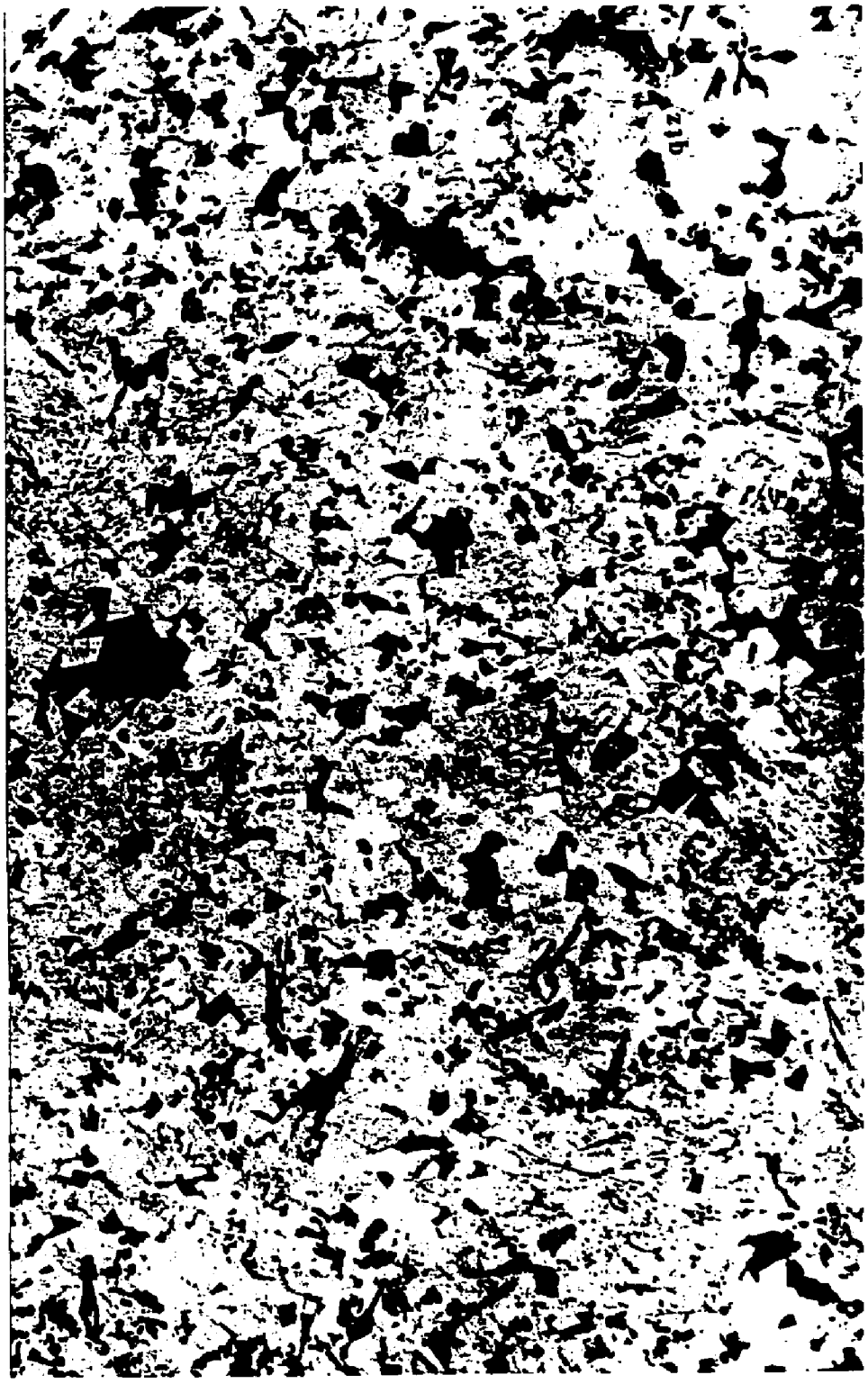

The quartz syenites in the SQSZ are medium-grained, mesocratic rocks containing feldspars with subhedral cores of untwinned plagioclase and perthitic potassium feldspar and discontinuous rims of perthitic orthoclase. Fine-grained amphibole often occurs at the core-rim contact of the perthites. Intergranular boundaries of the perthitic rims are irregular to serrate. Quartz occurs as subhedral to interstitial grains. Barroisitic amphibole displays an ophitic to subophitic intergrowth with fine-grained perthitic potassium feldspar and has narrow rims of blue-green arfvedsonite. Altered cores within the amphibole are interpreted as remnant olivine or aegirine-augite. Aenigmatite is present as subophitic grains and often forms complex intergrowths with amphibole and aegirine-augite (Fig. 3.7). Apatite is a ubiquitous accessory phase.

Dikes

Trachyte Dikes - Three centimeter to two meter wide trachytic dikes occur within all rock types but the aegirine granite and the porphyritic biotite granite. Most of these dikes are steeply dipping and have strikes that either overlap those of the basalt dikes or strike approximately E/W (Plate 2). Trachyte dikes on Middle Pond are on the order of two to three meters and are parallel to the basalt dikes described above. These have not been observed in association with the basalt dikes on Boulter Pond.

Mafic Syenite Dikes - The east-central portion of the alkalic syenite is intruded by shallowly to steeply dipping mafic syenite dikes (Plate 3.1 and 3.2; MAG 41, 57, 85). One of these dikes and the alkalic syenite host are both cross-cut by granitic pegmatite

stringers containing sodic amphiboles (arfvedsonite?). The mafic syenite dikes have a phenocryst assemblage comprised of euhedral to subhedral plagioclase and potassium feldspar and ophitic to subophitic hedenbergite. These minerals are also found in the matrix as subhedral to anhedral grains with apatite and zircon. The dikes contain distinctive, round, green, glomerocrysts of hedenbergite, biotite, and barroisite. Amphibole also occurs as inclusions within plagioclase phenocrysts and as rims on clinopyroxene.

Mafic Dikes - A number of dolerite and lamprophyre dikes cross-cut the various rocks within the complex (Plate 2) (see also; McHone and Trygstad, 1982). These 0.5 to 1.5 meters wide dikes are steeply dipping and strike dominantly to the NE. Within the southwestern portion of the complex a number of parallel, approximately 3 to 6 meter wide basalt dikes crop out along the shores of Boulter and Middle Pond and on the access road to Folly Pond (Plate 2). Although they have not been mapped between these localities, the similarity of rock type, orientation, size, and position along strike suggest that they are part of a dike swarm. Similar dikes were not observed along strike on the shore of Chases Pond within the biotite granite.

Geochemistry

Major Elements

Most of the rocks in the Agamenticus Complex contain low abundances of CaO, MgO, MnO, and TiO_2 and moderate to high abundances of K_2O and Na_2O (Fig. 3.12, Table 3.2). The least siliceous SQSZ is enriched in CaO, TiO_2, and P_2O_5 relative to the

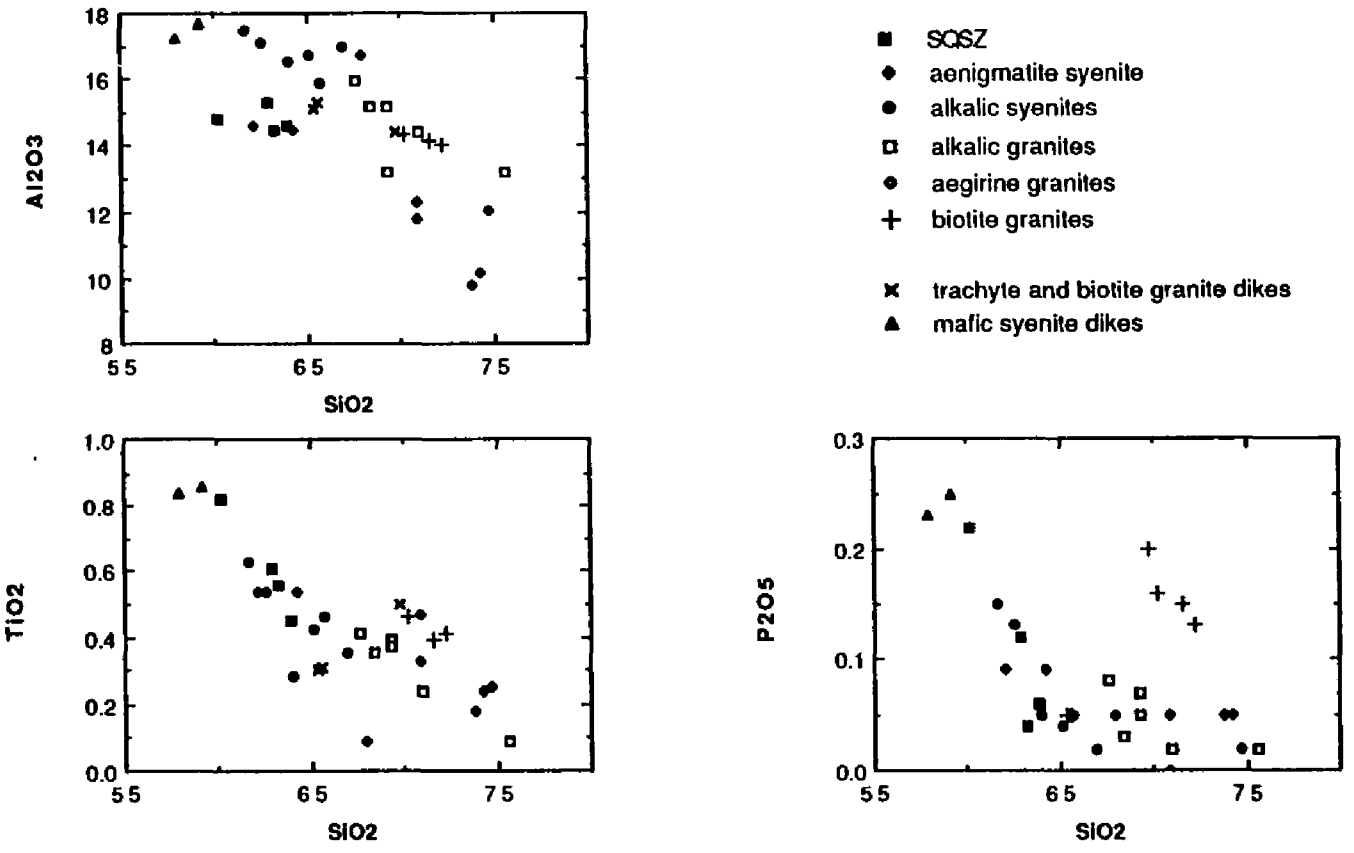

Fig. 3.12 - Major element-SiO_2 plots. The alkalic syenite, SQSZ, alkalic granites, and aenigmatite syenites form separate trends on the Al_2O_3, Fe_2O_3, K_2O, and MnO diagrams. Flexures between these trends occur at approximately 65 weight percent SiO_2. Also note the separation of the biotite granite from the other rocks on a number of the plots. Numbers on diagrams refer to samples discussed in text.

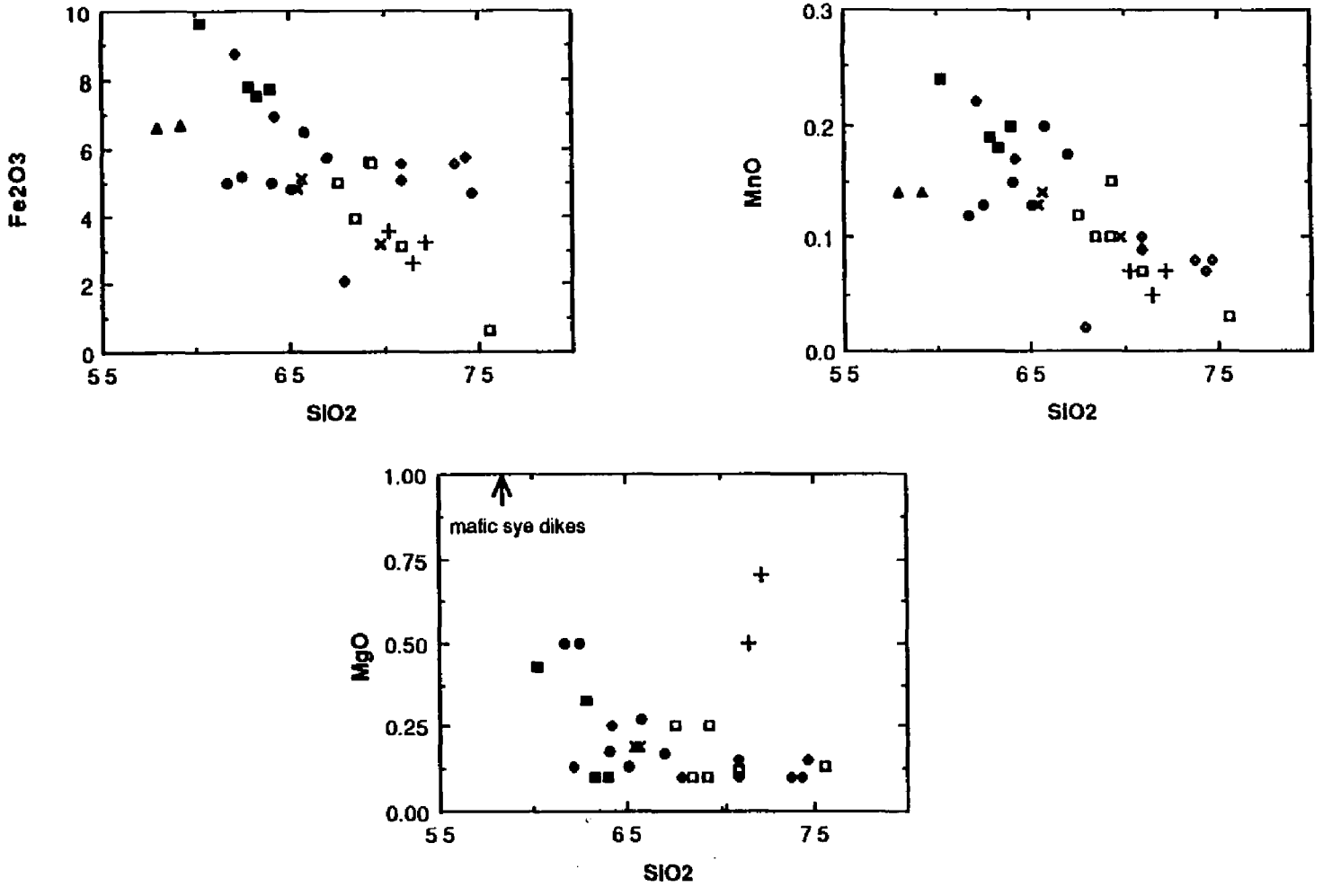

Fig. 3.12 continued - Major element-SiO_2 plots.

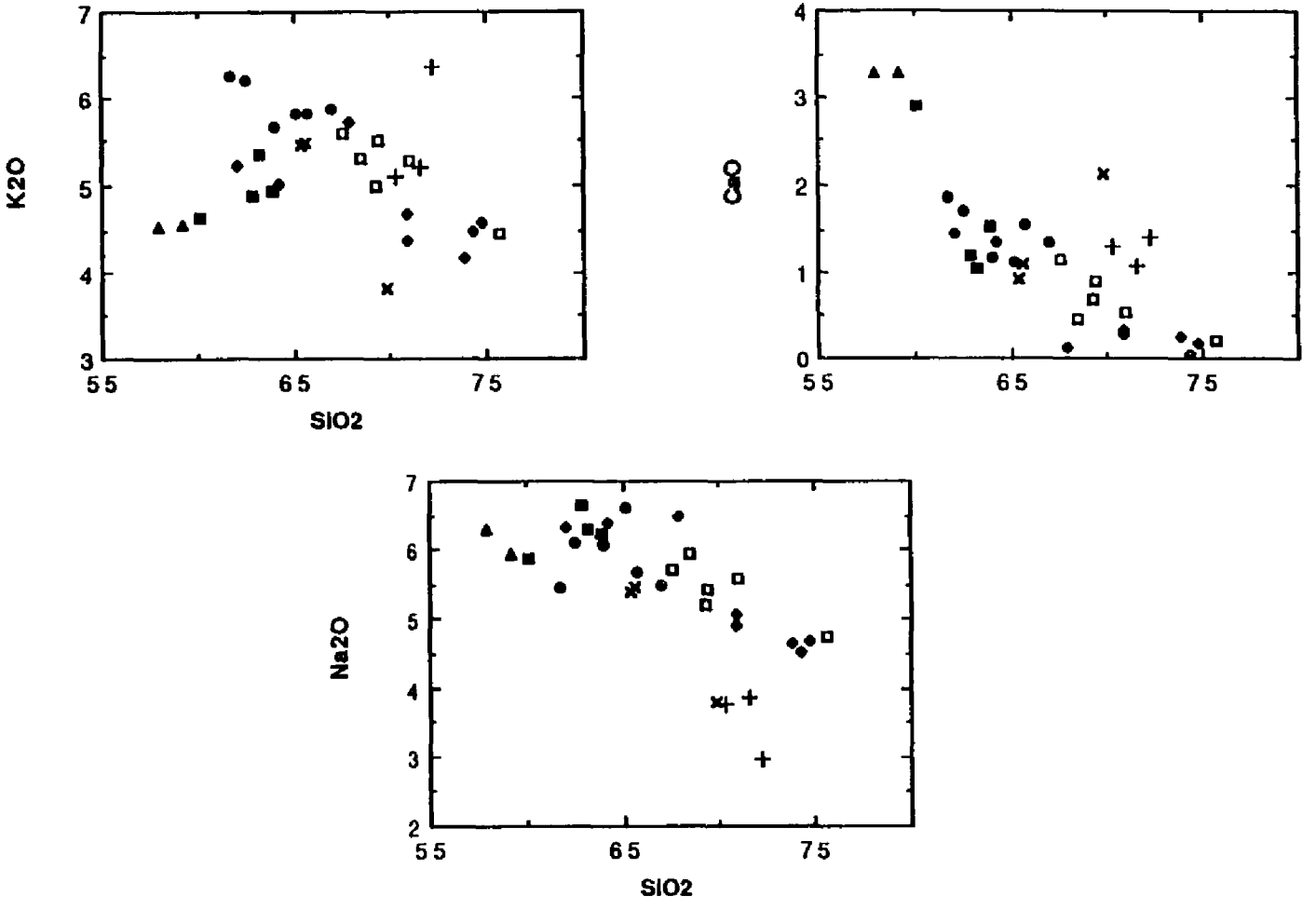

Fig. 3.12 continued - Major element-SiO_2 plots.

	BIOTITE GRANITES			ALKALIC GRANITE-WEST LOBE						AEGIRINE GRANITES					
SAMPLE #	MAG-4	MAG-177	MAG-179	MAG-5	MAG-17	MAG-23	MAG-26	MAG-120	MAG-135	MAG-47	MAG-48	MAG-49	MAG-122A	MAG-11c	MAG- 91-4
SiO2	72.24	70.25	71.5	69.34	69.3	75.64	70.95	67.58	68.43	74.3	73.6	70.9	70.92	67.9	74.72
TiO2	0.41	0.46	0.39	0.37	0.39	0.09	0.24	0.41	0.35	0.24	0.16	0.33	0.465	0.09	0.25
Al2O3	14	14.34	14.14	15.17	13.2	13.2	14.43	16.97	15.2	10.2	9.79	11.6	12.29	16.7	12.06
RbO	0	0	0	0	0	0	0	0	0	0	0	0	0	0	0
Fe2O3	3.23	3.55	2.62	5.59	5.61	0.83	3.12	4.87	3.92	5.74	5.6	5.08	5.58	2.12	4.71
MnO	0.07	0.07	0.05	0.15	0.1	0.03	0.07	0.12	0.1	0.07	0.08	0.09	0.1	0.02	0.08
MgO	0.7	0.58	0.5	0.25	0.1	0.13	0.12	0.25	0.1	0.1	0.1	0.1	0.15	0.1	0.15
CaO	1.4	1.32	1.08	0.91	0.88	0.21	0.53	1.15	0.47	0.08	0.26	0.34	0.275	0.13	0.17
Na2O	2.95	3.76	3.87	5.42	5.22	4.77	5.6	5.73	5.93	4.54	4.67	4.93	5.08	6.48	4.7
K2O	5.36	5.11	5.2	5.5	4.99	4.47	5.27	5.58	5.32	4.5	4.17	4.39	4.7	5.71	4.58
P2O5	0.13	0.16	0.15	0.07	0.05	0.02	0.02	0.08	0.03	0.05	0.05	0.05	0.01	0.05	0.02
LOI		0.72	0.56		0.27	0.33	0.23	0.45	0.34	0.17	0.43	1.16	1.16	0.39	1.23
SUM	101.49	99.8	99.5	102.77	99.64	99.19	100.35	101.84	99.85	99.8	98.7	98.01	99.57	99.3	101.44
CIPW Norm															
AP	0.34	0.383	0.339	0.18	0.1135	0.04	0.04	0.179	0.088	0.12	0.118	0.118	0.0228	0.07	0.045
Il	0.93	0.904	0.761	0.91	0.805	0.17	0.47	0.795	0.69	0.46	0.307	0.672	0.931	0.2	0.49
Mt	0.69	0.799	0.585	1.22		0.14		1.1	0.145						
Or	31.41	31.16	31.48	33.78	30.14	26.74	31.82	33.6	32.53	28.14	26.37	27.76	29.76	35.15	27.87
Ab	31.99	32.84	33.56	46.61	38.16	40.86	45.68	49.41	50.27	28.02	28.05	38.6	38.61	56.14	37.58
An	5.12	5.66	4.49	3.14		0.92		1.1		-0.03					
Di				0.96	2.47		2.01	3.07	1.74		0.809	1.14	1.06	0.36	0.657
Hy	2.7	2.97	2.27	3.42	3.38	0.57	1.73	2.82	2.25	4.06	3.87	3.33	3.66	1.37	3.15
Cl															
Ns															
Ac					2.6		1.39		1.47	2.64	2.8	2.36	2.57	0.88	2.1
C	0.58	1.25	1.11			0.37				0.02					
Q	24.93	24.04	25.42	9.78	14.12	30.18	16.43	7.82	10.83	33.33	34.41	25.08	22.49	4.48	28
Ns					2.22		0.29			2.02	2.4	0.738	0.87433	1.34	0.112
total	99.7	100.008	100.014	100	100.0085	99.89	100	99.694	99.893	99.8	99.894	99.998	99.99823	99.99	100.004

	SiO2				AENIGMATITE SYENITE		SYENITE DIKES		MAFIC SYENITES		ALKALIC SYENITES					
SAMPLE #	MAG-11a	MAG-51D	MAG-91-1	MAG- 91-2	MAG-44-a	MAG-139	MAG-40-2	MAG-40-4	MAG-57D	MAG-125CR	MAG-2	MAG-3	MAG-37b	MAG-39	MAG-61B	MAG-72B
SiO2	63.9	62.86	60.18	63.25	64.2	62.11	65.4	65.9	57.03	59.22	65.7	66.99	64	61.7	65.11	62.48
TiO2	0.45	0.61	0.82	0.56	0.54	0.84	0.3	0.31	0.84	0.86	0.46	0.351	0.28	0.63	0.42	0.84
Al2O3	14.6	15.28	14.78	14.5	14.5	14.58	15.1	15.3	17.22	17.65	15.88	16.98	16.5	17.5	16.69	17.09
RbO	0	0	0	0	0	0	0	0	0	0	0	0	0	0	0	0
Fe2O3	7.69	7.8	9.59	7.52	8.98	8.78	4.84	5.12	8.65	6.73	5.52	5.75	5	5	4.78	5.2
MnO	0.2	0.19	0.24	0.18	0.17	0.22	0.13	0.14	0.14	0.14	0.2	0.174	0.15	0.12	0.13	0.13
MgO	0.1	0.33	0.43	0.1	0.25	0.13	0.19	0.19	1.95	1.97	0.27	0.17	0.18	0.5	0.13	0.5
CaO	1.54	1.21	2.89	1.05	1.37	1.46	0.92	1.11	3.27	3.26	1.56	1.36	1.17	1.87	1.14	1.71
Na2O	6.22	6.64	5.87	6.29	6.4	6.34	5.39	5.47	5.29	5.84	5.68	5.5	6.08	5.45	6.62	6.08
K2O	4.94	4.91	4.64	5.36	5.02	5.24	5.47	5.48	4.53	4.56	5.82	5.88	5.67	6.28	5.81	6.2
P2O5	0.08	0.12	0.22	0.04	0.09	0.09	0.05	0.05	0.23	0.25	0.05	0.02	0.05	0.18	0.04	0.13
LOI	0.2	0.54	0.15	1.05	0.15	0.3	0.8	0.55	0.27	0.46			0.3	0.6	0.42	0.37
SUM	99.7	99.95	99.86	99.85	99.5	99.47	97.79	98.77	99.05	100.6	102.14	103.185	99.08	99.18	100.87	100.09
CIPW Norm																
AP	0.18	0.28	0.5	0.095	0.21	0.21	0.11	0.11	0.52	0.51	0.11	0.075	0.11	0.35	0.09	0.289
Il	0.93	1.23	1.61	1.15	1.09	1.11	0.59	0.61	0.32	1.64	0.9	0.695	0.51	1.24	0.822	1.04
Mt			2.16				1.1	1.16	1.46	1.45	1.46	1.25	1.13	1.13		1.14
Or	30.42	30.76	28.35	34.17	31.4	33.45	33.6	33.69	27.14	27.22	35.26	35.32	34.82	38.16	35.26	36.95
Ab	53.29	54.36	51.37	48.39	49.36	49.52	47.43	48.17	44.97	44.06	49.29	52.03	53.47	47.61	54.66	48.97
An			0.285				0.89	1.05	7.4	8.72	0.33	2.51	1.02	4.95		0.992
Di	5.75	4.57	10.32	4.18	5.18	5.64	2.78	3.42	6.06	6.83	5.48	3.26	3.68	2.89	4.36	5.37
Hy	4.22	3.77	0.777	4.31	3.84	4.68	2.45	2.48			3.11	2.84	2.56	1.48	2.26	
Cl		1.38	4.62			0.39			8.6	7.71				2.17		3.61
Ns									3.53	4.06						1.64
Ac	3.64	3.58		3.52	3.2	4.11									2.13	
C																
Q	0.21			3.08	4.18		8.64	7.87			3.74	2.36	1.74		0.0742	
Ns	1.38	0.268		1.2	1.01	0.89									0.038	
total	100	100.008	99.992	100.095	100.3	100	97.79	98.76	100	100	99.68	100.54	99.04	100	99.6952	100.001

Table 3.2 - Major element compositions and CIPW normative assemblages.

other rocks. Mafic syenite dikes have higher CaO, MgO, TiO_2 , and P_2O_5 than the other syenites. A major inflection occurs on many of the major element Harker-type variation diagrams at around 65 to 68 weight percent SiO_2 (Fig. 3.12). On these diagrams, the amphibole-bearing alkalic syenites define a separate trend from that of the SQSZ and the aenigmatite syenites (i.e. Al_2O_3, K_2O, Fe_2O_3, and MnO versus SiO_2) (Fig. 3.12). Where these separate trends exist, the mafic syenite dikes plot either between the two trends or along the SQSZ trend. On the CaO, MnO, and to a lesser extent the Fe_2O_3 versus SiO_2 Harker diagrams, MAG 2, 3, and 5, form separate trends that are slightly enriched relative to the other alkalic syenites.

The aegirine granites define separate, generally sub-parallel trends to those defined by the alkalic granite on TiO_2 , Al_2O_3, Na_2O, K_2O, Fe_2O_3, and MnO Harker diagrams. The aegirine granites plot in two separate fields that define either end of the trends on the Harker diagrams. The less siliceous (SiO_2=71%) group is comprised of the medium-grained rocks that occur in the main lobe of aegirine granite (MAG 49) and along the western edge of the SQSZ (MAG 122a). Aegirine dikes that occur in the SQSZ (MAG 91-4) and the main lobe of the aegirine granite (MAG 48 and 47) make up the other group. The alkalic granites are slightly more depleted in TiO_2, K_2O, Fe_2O_3, and MnO. MAG 26 and 23, both from the western portion of the alkalic granite, show significant SiO2 enrichment over the other samples from this zone and anchor many of the major element trends. On the P_2O_5, MgO, and Na_2O diagrams the biotite granites

plot separately from the evolutionary trends of the other rocks within the complex.

CIPW normative minerals show that the rocks are dominantly silica-saturated to silica-oversaturated (Table 3.2). Acmite and sodium-metasilicate (Na_2SiO_3; McBirney, 1984) occur as normative peralkaline minerals in the aenigmatite syenites, the aegirine alkalic granites, most of the syenite to quartz syenite zone rocks (SQSZ), and a few of the alkalic granites. The porphyritic biotite granite contains small amounts of normative corundum (0.59 to 1.25 weight %) and is slightly peraluminous. Mafic syenite dikes and one of the alkalic syenites (MAG 72b) contain three to four percent normative nepheline.

The Agamenticus Complex is composed of dominantly agpaitic rocks. They exhibit a poorly-defined, negative correlation between agpaitic (K+Na/Al) and (K+Na)/(Si/6) indexes (Fig. 3.13a) (Sorensen, 1974). Mafic syenites are within the pulmaskitic field and have a positive correlation between these two indexes. The porphyritic, biotite granites plot on the pulmaskitic-agpaitic boundary or within the pulmaskitic field at lower (K+Na)/(Si/6) values than the syenites and alkalic granites. With the exception of the peraluminous biotite granites, the rocks are metaluminous to peralkaline (Fig. 3.13b).

Trace Elements

As noted for the major elements, the biotite granites have a number of trace element characteristics that distinguish them from the other rocks in the complex. For example, they are relatively depleted in Ga (Fig. 3.14), have lower Ga/Al values (Fig. 3.15), and

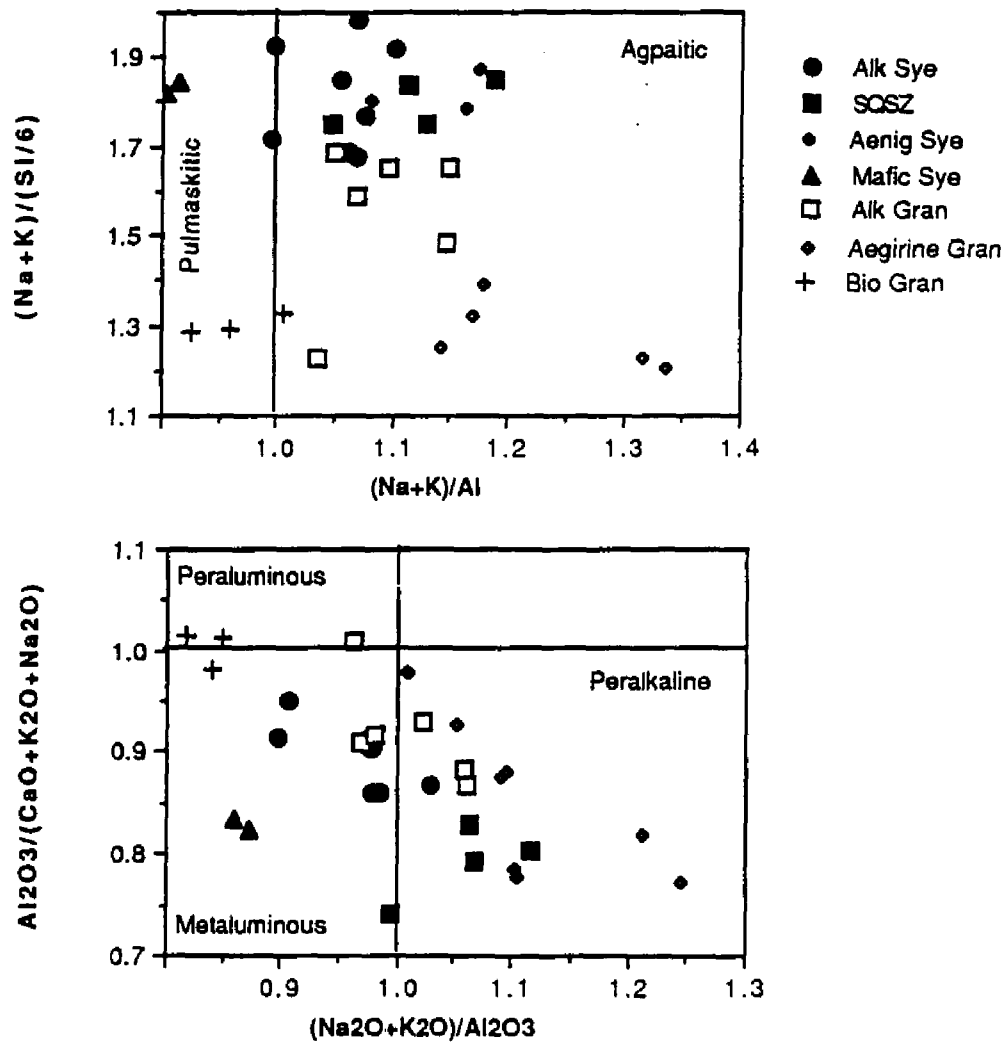

Fig. 3.13 - Compositional indexes showing the generally alkalic nature of the Agamenticus Complex. a) Cation percent. b) Mole percent. Unlike the other rocks, the biotite granite is slightly peraluminous.

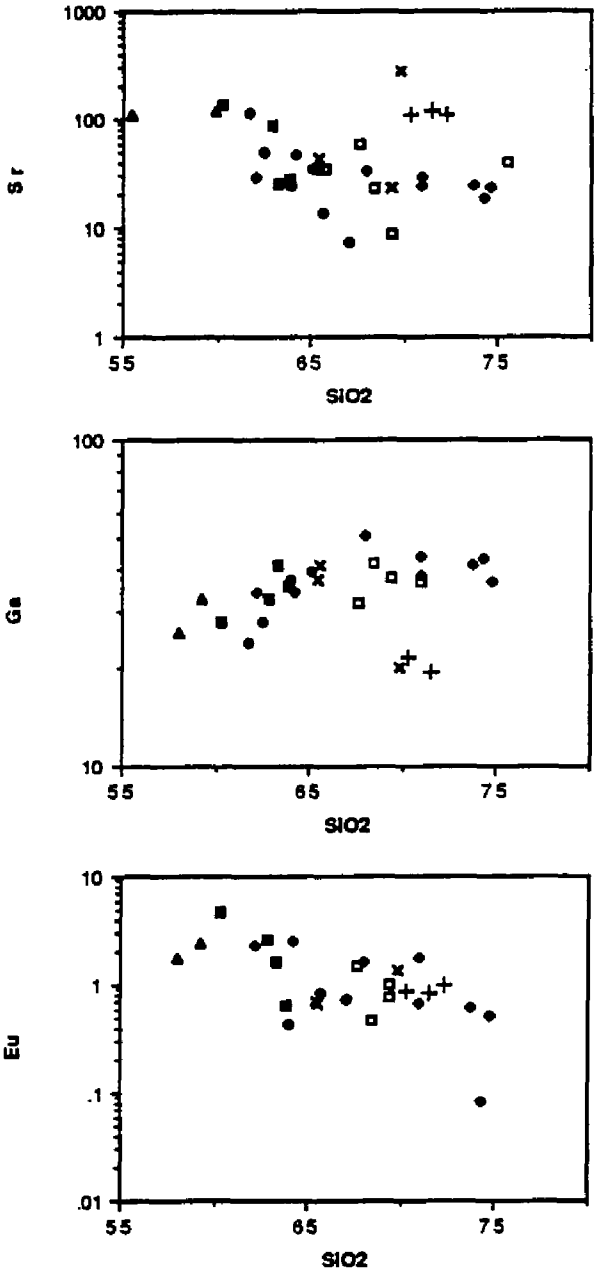

Fig. 3.14 - Selected trace element (ppm) versus SiO_2 (weight percent) plots. The flexures in these plots occurs at the same silica content (approximately 65 weight percent) as those observed on the major element-SiO_2 diagrams. The alkalic granite that is slightly Ga depleted relative to the other alkalic granites is MAG 120. Symbols as in Figure 3.12.

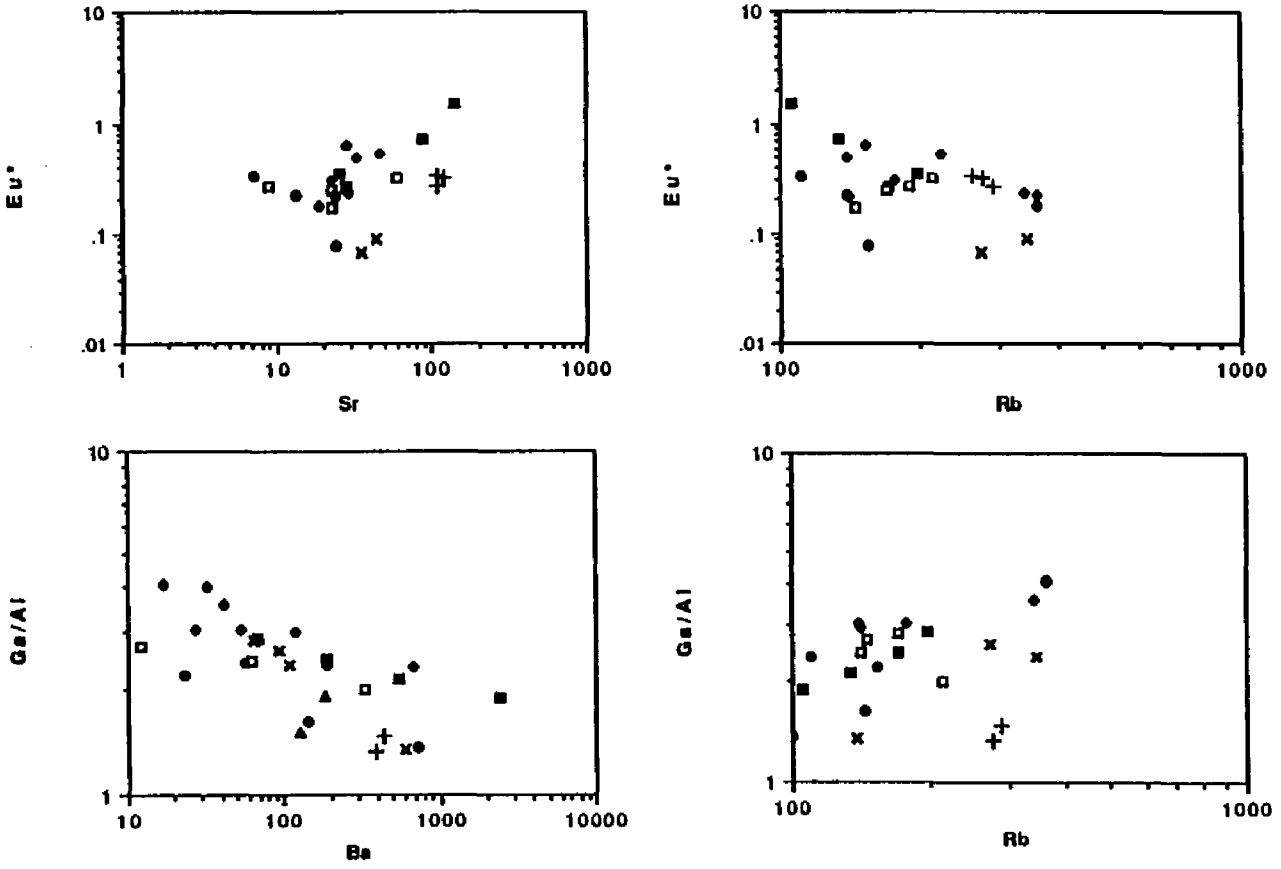

Fig. 3.15 - Eu* and Ga/Al versus Ba and Rb (Units are ppm). Note the different trends defined by the alkalic syenite relative to the other rocks within the complex and the scatter of the alkalic and aegirine granites. Numbers are for samples discussed in text. MAG 120 is the Rb enriched alkalic granite on the Ga/Al-Rb plot. Symbols as in Figure 3.12.

are enriched in Sr (Fig. 3.14) and Co. They also plot in separate fields on diagrams such as Eu* vs. Sr or Rb (Fig. 3.14; where Eu* = $Eu_{calculated}$ - $Eu_{observed}$).

Most of the trace elements for the other rocks within the complex exhibit a small to moderate variation along one or more linear trends on trace element-SiO_2 plots. A feature of such plots is the presence of inflections at approximately 65 weight percent SiO_2. On Ga, Eu, and Sr diagrams (Fig. 3.14) the inflections denote the change from increasing Ga and decreasing Eu and Sr to approximately constant values for each element at higher SiO2 content. Two of the alkalic syenites have Sr abundances that fall below the pattern defined by the other rocks. In addition, the alkalic syenite forms a separate trend, at lower Ga values, that is sub-parallel to the trend defined by the SQSZ on the Ga-SiO2 plot.

Distinct subparallel trends for the alkalic syenite and SQSZ are also observed on a Ga/Al versus Ba diagram (Fig. 3.15). Alkalic granites have Ga/Al values intermediate to the alkalic syenites and SQSZ for a set Ba abundance, and the aegirine granites branch off the Ga/Al enriched end of the SQSZ trend. On a Ga/Al versus Rb diagram the SQSZ and a portion of the aegirine granites (MAG 49,47,48) define a positive linear which divides the alkalic granites and syenites. The rest of the aegirine granites plot near to the alkalic granites that are located above the SQSZ-MAG 49 trend. Considerable overlap occurs between the different rock types on a Rb-Ba-Sr diagram (Fig. 3.16). The alkalic syenites and to a lesser extent the SQSZ plot well within the field for highly differentiated granites. In addition, several alkalic granites and alkalic syenites

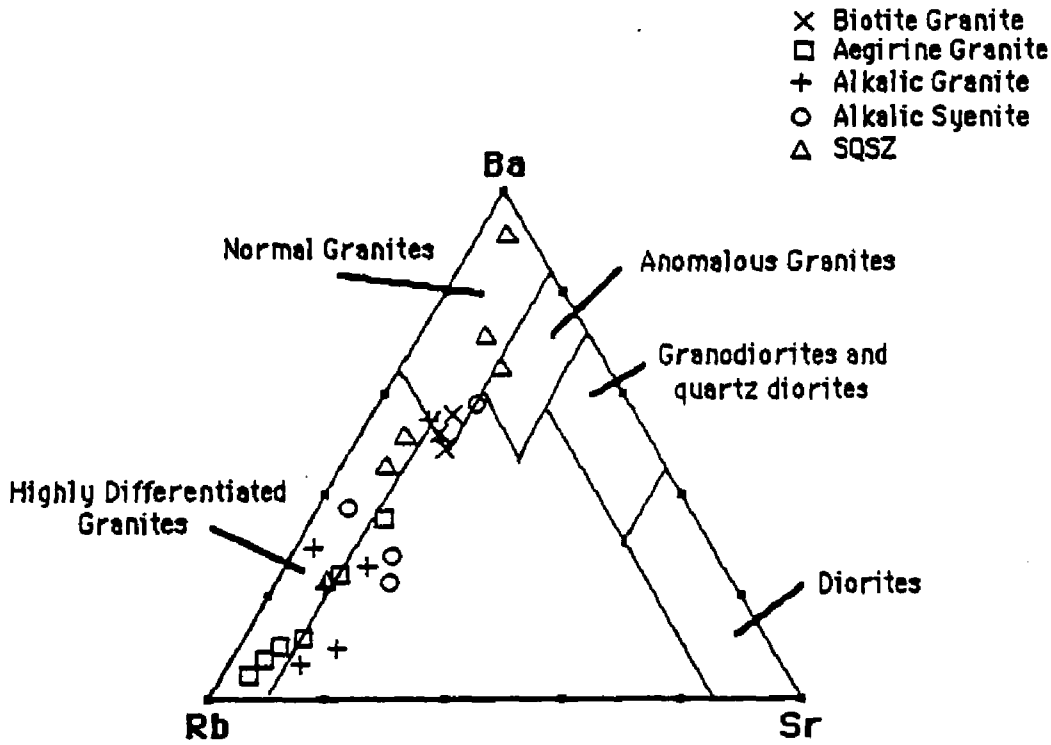

Fig. 3.16 - Rb-Sr-Ba ternary diagram showing fields for rocks which are derived by fractional crystallization from a basalt parent (after El Bouseily and El Sokkary, 1975). Syenites from this process should be located near to the Ba apex within the normal granite field. Note that most of the alkalic syenites are located within or near to the highly differentiated granite field. The alkalic granites overlap the other rocks.

are displaced towards the Sr apex outside of the fields defined for a "normal" differentiation sequence.

High field strength (HFS) element abundances also show overlap for the alkalic rocks (Table 3.3). However, a consistent pattern is present on HFS-SiO2 plots for Zr, Nb, Th, and U (Fig. 3.17). On each of these plots MAG 91-1, 91-2, and 37b, and 120 and 49 (i.e., SQSZ to alkalic syenite and alkalic granite to aegirine granite) form sub-parallel linear trends with positive slopes. A distinct jump towards reduced trace element abundances occurs on each of these plots between the syenite and granite trends (i.e., between MAG 91-2 or 37b and MAG 120). Individual rock types define linear trends with negative slopes that branch off the above trend at one or more locations (for example MAG 49 to 48 to 47 to 91-4 or 37b to 2 or 61b). The alkalic syenites less siliceous than sample 37b form a trend of lower Nb and Zr abundances relative to the 91-1 to 37 trend. Alkalic syenite dikes (40-4 and 40-2) plot above the 91-1 to 49 trend on the Th, U, and Nb plots. On trace-trace plots, such as U-Th or Zr-Y (Fig. 3.18), all of the rocks are located along linear trends with positive slopes. The different rock types exhibit considerable spread along the linear trends that correspond to the enrichment/depletion pattern described above for the HFS-SiO2 diagrams.

The rocks display a complicated pattern on plots of Zr/Hf versus Nb/Ta, Ga/Al, and Th/U (Fig. 3.19). The alkalic syenites,

Table 3.3 - Trace element concentrations.

SAMPLE #	Rb	Cs	Sr	Ba	Sc	Y	Zr	Hf	Th	U	V	Nb	Ta	La	Ce	Nd	Sm	Eu	Tb	Yb	Lu	Cr	Co	Ni	Cu	Zn	Ga
ALKALIC SYENITE																											
MAG-2	139.8	3.209	13.4	91.8	2.657	31.9	192.9	7.888	17.67	3.502		80.4	6.405	61.35	125.9	68.06	11.26	0.827	1.67	4.788	0.795	3.766	0.941	3.4	11.9	87.2	
MAG-3	111.2	1.623	7.2	25.4	1.785	16.5	126.9	4.812	8.93	1.626		34.9	3.898	39.76	87.06	42.63	7.078	0.74	0.843	3.273	0.528	2.103	0.839	2.1	10.7	92.9	
MAG-37b	155	1.092		23	2.557		833	24.07	24.39	4.699		98	9.087	119.1	234.9	84.82	15.38	0.431	1.902	7.203	1.111	2.424	0.578				37
MAG-39	100			717			0.5					41	3														24
MAG-61B	116		25.3	58.9		28.2	180				10.7	52.8											0.892	2.9	8.43	84.5	39.8
MAG-72B	145		49.5	145		30.7	188				10.8	97.1											0.825	3.2	8.77	97.4	27.5
BIOTITE GRANITES																											
MAG-4	259.5	7.328	110	472.4	5.033	37.2	231.8	8.697	37.69	9.171		34	5.06	63.56	134.1	57.65	9.892	0.992	1.128	4.155	0.567	5.907	3.82	2.1	0.9	45.5	
MAG-17T	289	6.93	109	434	3.872	44.2	396	9.387	28.44	6.077	28.7	59.4	5.369	68.73	141.9	55.86	10.05	0.89	1.786	4.314	0.683	3.804	3.586	7.26	7.32	49.1	21.7
MAG-17B	275	6.585	119	381	3.648	33.6	201	6.931	24.16	3.7	28.3	36.9	4.116	50.68	101.4	40.76	7.522	0.83	1.516	3.232	0.512	4.197	3.3	8.52	8.14	37	19.4
ALKALIC GRANITES																											
MAG-8	190	2.545	8.8	84.3	2.718	46.1	403.6	17.22	32.46	4.439		91	11.4	43.42	79.18	48.13	10.24	1.015	2.369	6.121	0.89	0.789	0.61	0.7	9.2	119.7	
MAG-17	171	1.927	22.8	53.7	0.899	42.7	449	11.88	14.16	2.93	10.8	76.8	5.31	53.55	124.8	50.93	9.89	0.762	1.33	4.97	0.817	0	0.31	4.67	6.68	104	37.6
MAG-23	148		40	22.5		14.9	118				12.3												1.84	0.079	3.33		
MAG-26	141		34	61.8		32.2	227				9.76	58.4											0.65	4.24	3.4	77.6	36.8
MAG-120	216	4.508	58.8	332	2.747	54	440	14.41	21.28	5.178	8.84	101	7.85	97.19	188.4	80.25	14.49	1.458	2.19	6.447	0.954	1.203	0.821	5.41	6.63	97.1	31.4
MAG-13B	146	1.142	23	12	0.719	34.8	226	6.379	11.21	1.84	9.37	87	5.075	49.55	93.39	45.67	8.351	0.483	1.168	3.376	0.582	0	0.809	2.93	7.82	98.5	41.9
MAG-11c	141	0.851	33.6	98	1.72	39.3	308	8.55	10.44	2.85	11.1	51.2	3.88	48.54	110	53.85	10.64	1.85	1.31	4.26	0.73	1.37	0.421	3.85	11.1	92	50.6
AEGIRINE GRANITES																											
MAG-47	362	1.88	19	17	0.327		276	9.27	8.72	1.37		40	2.85	7.98	13.89	4.31	0.915	0.083	0.488	3.03	0.598	0	0.205				43
MAG-48	362	1.22	24	32	0.218		519	28.23	10.85	3.44		73	8.11	46.09	96.13	37	8.086	0.609	1.53	5.72	0.874	0.78	0.813				41
MAG-49	340	2.32	29	41	0.401		1151	35.06	38.48	6.897		153	18.63	126.6	264.1	115	22.92	1.78	3.92	11.6	1.7	2.83	0.343				44
MAG- 91-4	140		23.1	52.7		28.4	280				11.1	48		38.44	63.18	26.35	4.706	0.508	0.98	3.206	0.535			3.24	3.84	93	38.9
MAG-122A	178	0.948	24.3	27.3	0.349	44.1	482	14.81	21.3	3.93	11.1	89.2	7.991	89.45	127.5	50.93	9.935	0.884	1.929	5.752	0.797	1.377	0.729	8.36	8.76	133	38.2
SOSZ																											
MAG-11a	172	2.32	26.3	186	0.216	33.8	317	8.96	13.52	2.81	10	80.7	4.19	82.44	88.2	38.3	7.39	0.65	0.977	2.83	0.405	2.85	0.26	3.28	4.67	0.146	35.8
MAG-61D	134	1.428	87.9	552	3.677	38.4	268	10.71	13.33	3.115	10.2	67.6	7.944	59.12	123.6	59	11.39	2.63	1.592	4.579	0.736	1.05	1199	4.75	9.04	128	32.4
MAG-91-1	109	2.77	138	2439	13.14	33.3	271	9.56	13.11	3.99	11.9	47.6	4.85	47.09	97.53	45.64	8.992	4.697	1.398	3.84	0.531	0	1.26	6.32	19.4	99.9	27.5
MAG- 91-2	198	4.584	25.9	87.2	1	47.2	430	16.59	25.97	5.46	10.3	87.6	7.072	89.88	150.1	72.16	14.89	1.66	2.327	6.914	1.047	1.315	0.436	8.49	8.67	90.1	41.4
AENIGMATITE SYENITE																											
MAG-139	154	2.109	28.7	192	2.793	43.1	397	10.34	10.77	2.835	9.29	70.3	4.992	83.97	133.3	60.93	11.38	2.282	1.521	4.837	0.803	0	0.703	5.44	10.3	129	34.2
MAG-44-a	224	5.51	47	683	3.74		885	24.02	34.8	10.05		134	13.14	81.11	189.7	72.7	14.25	2.55	2.02	7.63	1.09	1.74	0.748				34
SYENITE DIKES																											
MAG-49-2	343	2.51		107	1.738		573	32.29	57.92	14.05		171	20.03	178.5	353.4	126.2	22.2	0.716	4.291	12.32	1.748	2.472	0.92				37
MAG-49-4	273	4.73		93	1.584		855	28.47	65.18	13.91		158	17.23	223.8	443	166.8	25.93	0.658	4.738	12.52	1.912	4.377	1.048				41
MAFIC SYENITE DIKES																											
MAG-57D	125	1.917	121	454	7.331	38.2	389	10.23	10.34	2.721	54.1	96	6.193	58.25	110.1	46.43	8.725	1.796	1.22	3.85	0.617	55.54	10.94	36	18.8	94.1	25.6
MAG-125CP	182	2.145	107	842	7.03	58.6	432	14.11	9.625	3.31	58.5	115	7.076	67.45	128.9	51.93	10.53	2.408	2.124	9.938	1.642	8.145	5.565	1.7	14.1	353	32.6

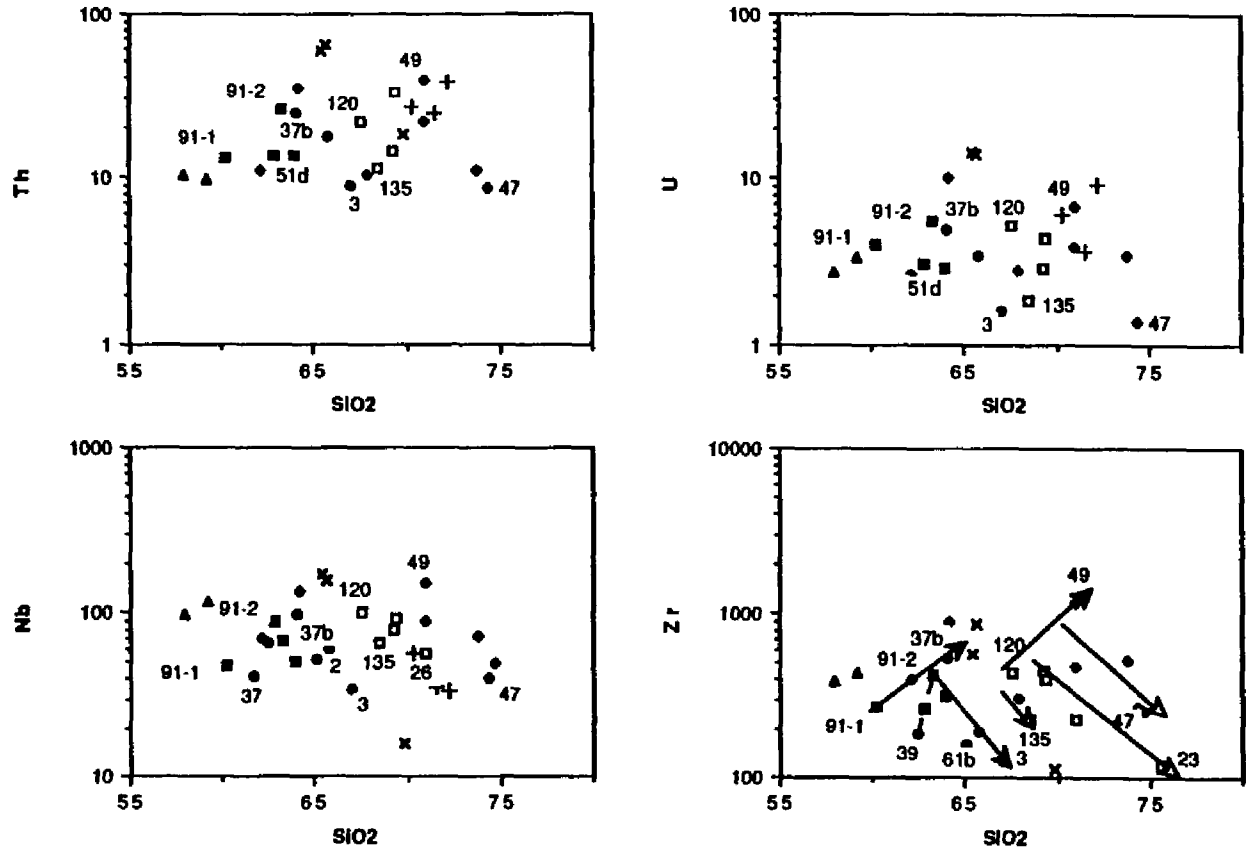

Fig. 3.17 - Plots of high field strength elements (ppm) versus SiO_2 (weight percent). Arrows on Zr-SiO2 diagram show interpreted liquid evolution trends for zircon absent (closed arrowhead) and zircon present (open arrowhead) fractional crystallization (see discussion - Controls on HFS element abundances). Similar trends exists on all of the diagrams. Numbers are sample numbers. Symbols as in Fig. 3.12: filled squares - SQSZ, filled diamonds - aenigmatite syenite, filled triangles - mafic syenite, filled circles - alkalic syenite, open squares - alkalic granite, open diamonds - aegirine granite, + - biotite granite, x - trachyte dikes.

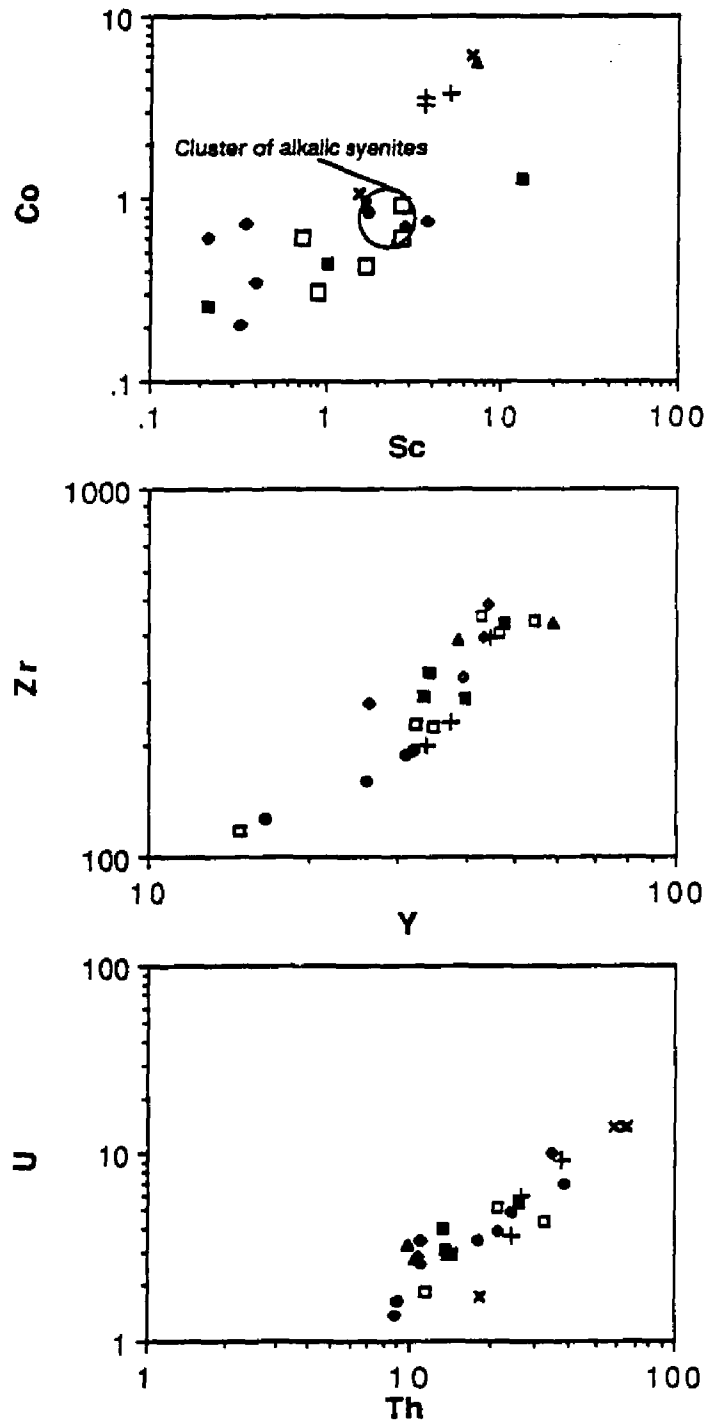

Fig. 3.18 - HFS-HFS and Sc-Co plots (ppm). The overlap on the Th-U and Zr-Y diagrams can be related, in part, to the timing of zircon stability relative to magma evolution. The decrease in Sc and Co is related to clinopyroxene fractionation. Symbols as in Figure 3.12.

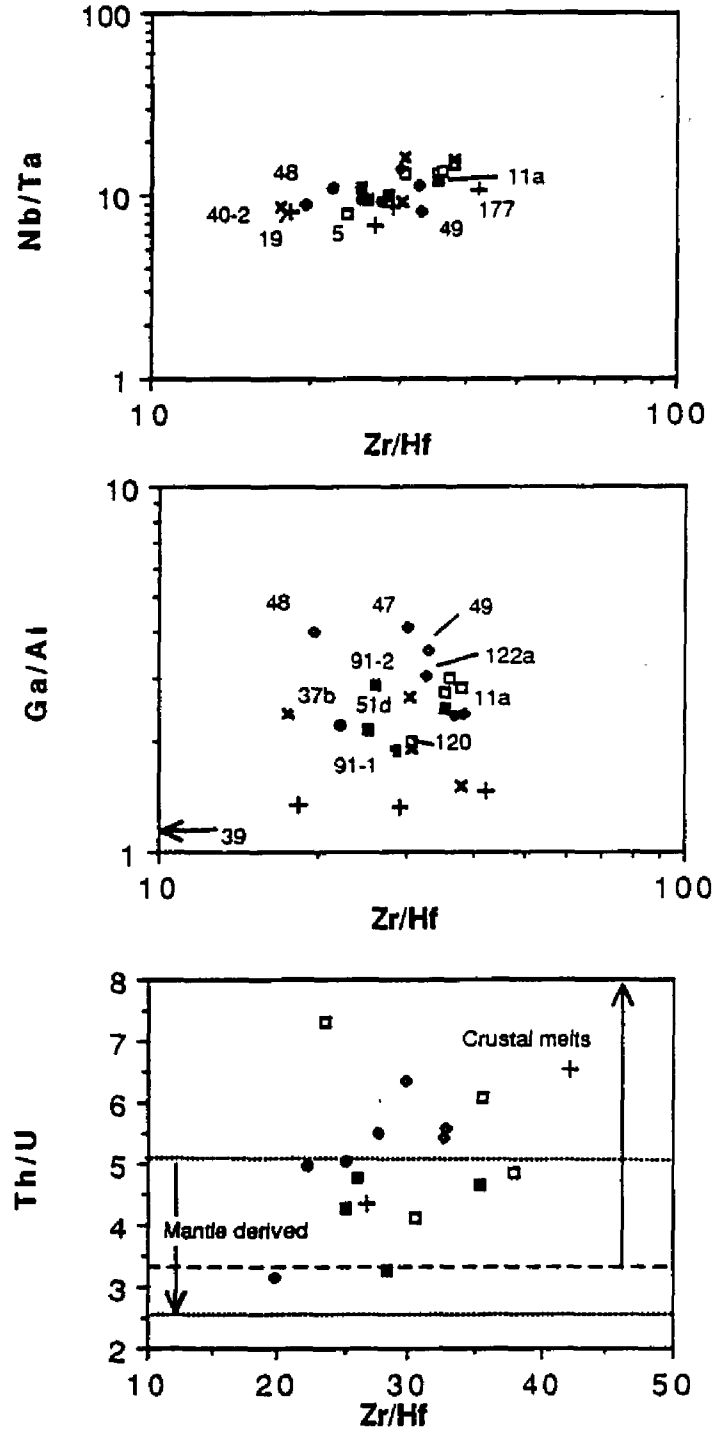

Fig. 3.19 - High field strength ratios of chemically coherent elements. These ratios are often used as indicators for magma sources. The scatter in Zr/Hf and Th/U values for the alkalic and aegirine granites reflects the influence of late magmatic deuteric fluids and/or volatiles. Fields for Th/U values after Eby (1985). Symbols as in Figure 3.12.

SQSZ, and a mafic syenite are located at a Zr/Hf ratio of approximately 28. The largest proportion of the alkalic granites, one of the SQSZ, the aenigmatite syenites, and a trachyte dike form another group at a Zr/Hf ratio of approximately 38. Nb/Ta ratios (approximately 15 versus 10) for this group are slightly elevated relative to the group comprised dominantly of syenites (Fig. 3.19b). The aegirine granites have Zr/Hf and Nb/Ta values that lie between these two groups or in the case of MAG 48 is located at Zr/Hf lower than the alkalic syenite-SQSZ cluster. Zr/Hf for the biotite granites encompasses all of the other rocks and Nb/Ta values for this rock are somewhat lower than the other rocks. Th/U ratios of the alkalic granites and the aegirine granites overlap those of the syenites (Fig. 3.19c). The alkalic syenites have slightly higher Th/U ratios than those of the SQSZ.

Rare Earth Elements

Chondrite-normalized REE patterns for all the rocks within the Agamenticus Complex overlap (Fig. 3.20; Table 3.3). There is an overall pattern of decreasing total REE (excluding Eu) with increasing SiO2 (Fig. 3.20 and 3.21). Two alkalic syenite dikes (MAG 40-4 and 40-2; Fig. 3.21) and an aegirine granite lie significantly above this trend.

The rocks are LREE enriched with La/Yb values typically in the range of 4 to 10 (Fig. 3.20 and 3.21). La/Yb ratios for each rock type exhibit a slight decrease vs. SiO2 (Fig. 3.21). One of the aegirine granites (MAG 47, Fig. 3.20) has an unusual REE pattern which is LREE depleted relative to the other rocks.

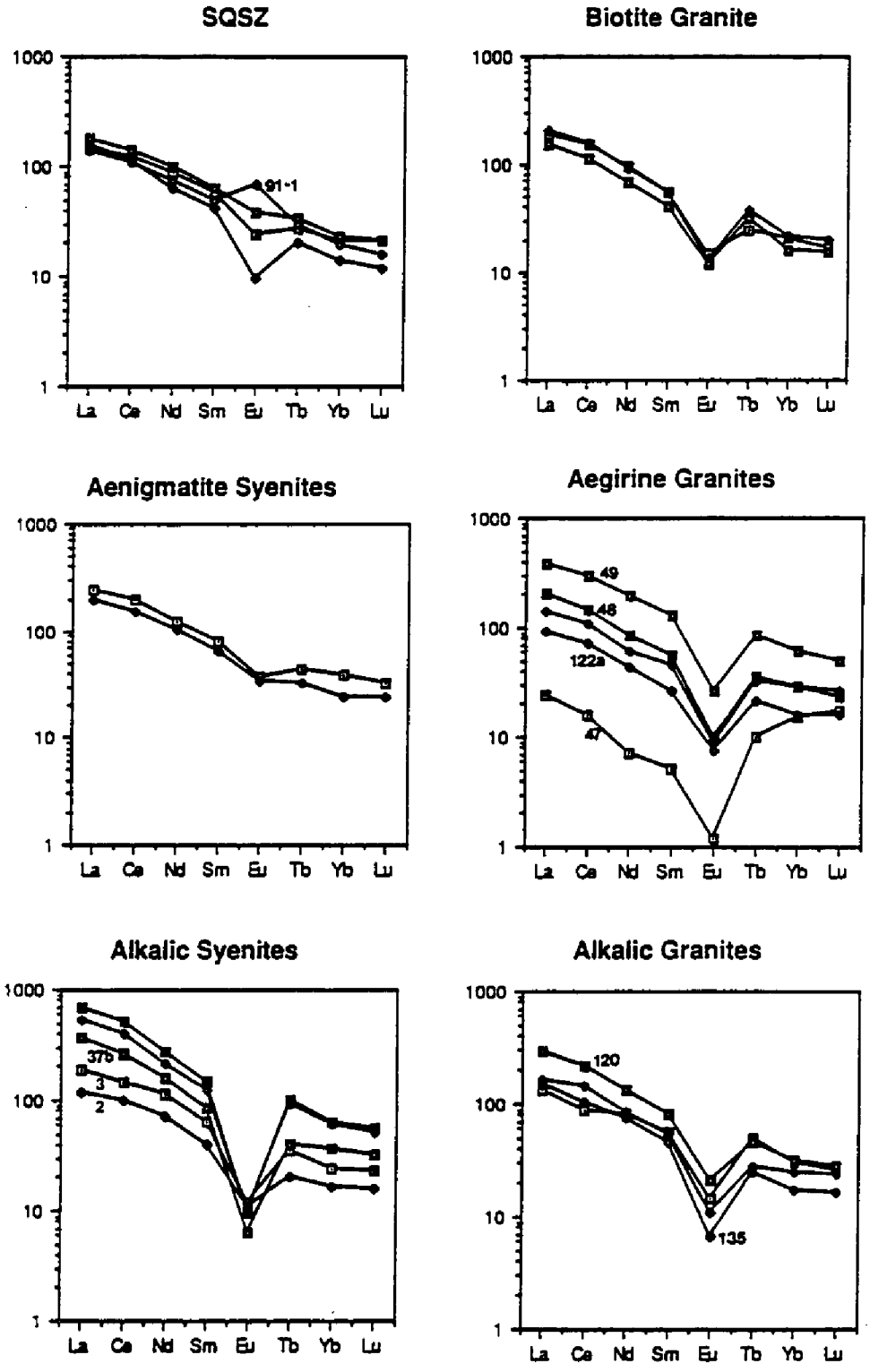

Fig. 3.20 - Rare earth elements nomalized to chondritic values (Taylor and McLennan, 1981). There is a substantial overlap of patterns between different rock types.

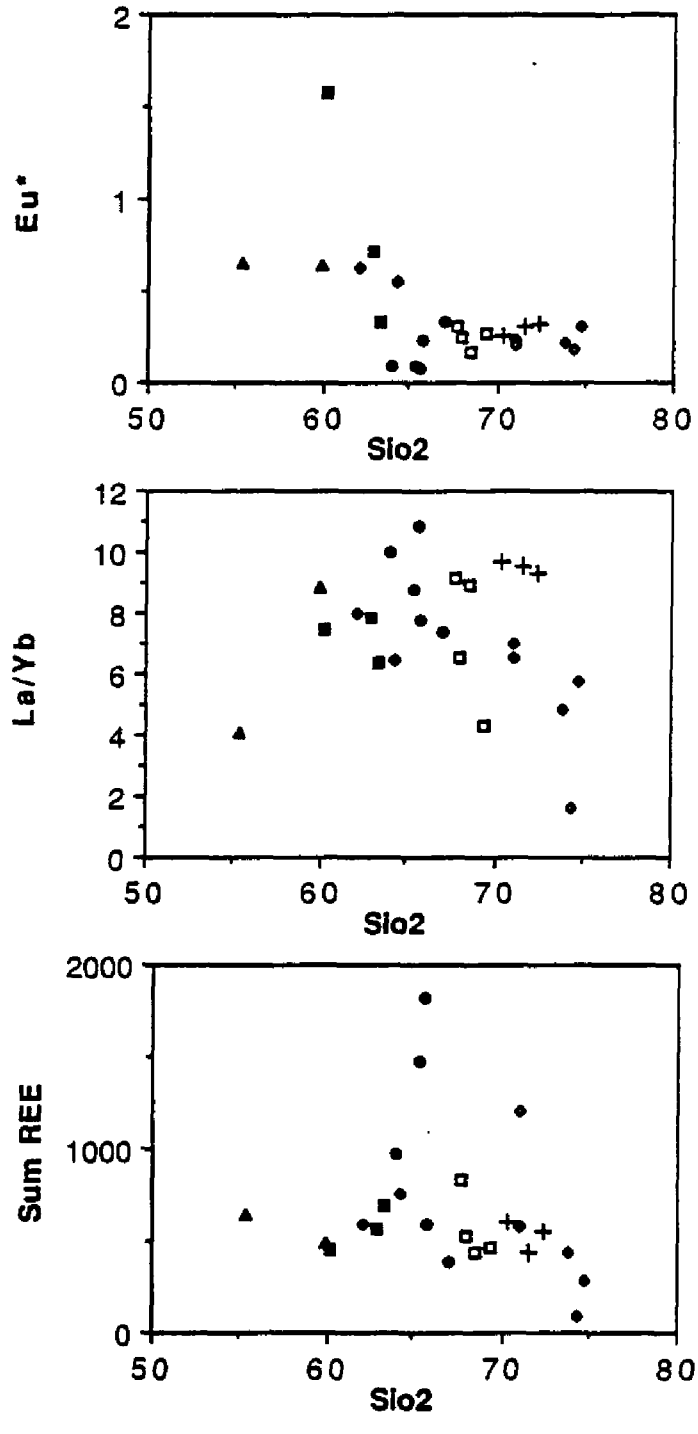

Fig. 3.21 REE factors. The overlap observed on the REE plots is apparent in the REE factors as well. The anomalously high total REE values for the alkalic syenites are for late cross-cutting trachyte dikes. Symbols as in Figure 3.12.

With one exception, the subsolvus augite syenite (Eu*=1.58), all rocks have negative europium anomalies (0.7 to 0.09) (Fig. 3.21). Eu* has several trends that merge at approximately 64 weight percent SiO2. Relative to SiO2, the SQSZ has an antithetic behavior, the alkalic syenites are positively correlated, and the granites form a level plateau. On a Eu*-Rb diagram (Fig. 3.15) the alkalic syenite plots along a trend that is parallel to, but at lower Eu* values than that defined by the SQSZ. The alkalic granites define a linear trend that is orthogonal to the syenite patterns. Aegirine granite overlaps all of these trends. On a Eu*-Sr diagram (Fig. 3.15) all of the rocks except the alkalic syenite are spread along a linear trend with a negative slope. The alkalic syenite and one alkalic granite define a pattern that is orthogonal to and at the Sr-depleted end of this linear trend.

Discrimination diagrams

On granite discrimination diagrams such as R1-R2 (Batcheldor and Bowden, 1985) or Rb vs. Y+ Nb (Pierce et al., 1984) all of the rocks plot within fields defined by anorogenic or within-plate granites (Fig. 3.22). On the Rb vs. Y+ Nb diagram the biotite granites plot separately with Rb values that are slightly enriched relative to the alkalic rocks within the complex.

DISCUSSION

Intrusive sequence

The intrusive sequence determined in this study is similar to that proposed by Hussey (1962) with syenites first, alkalic granites

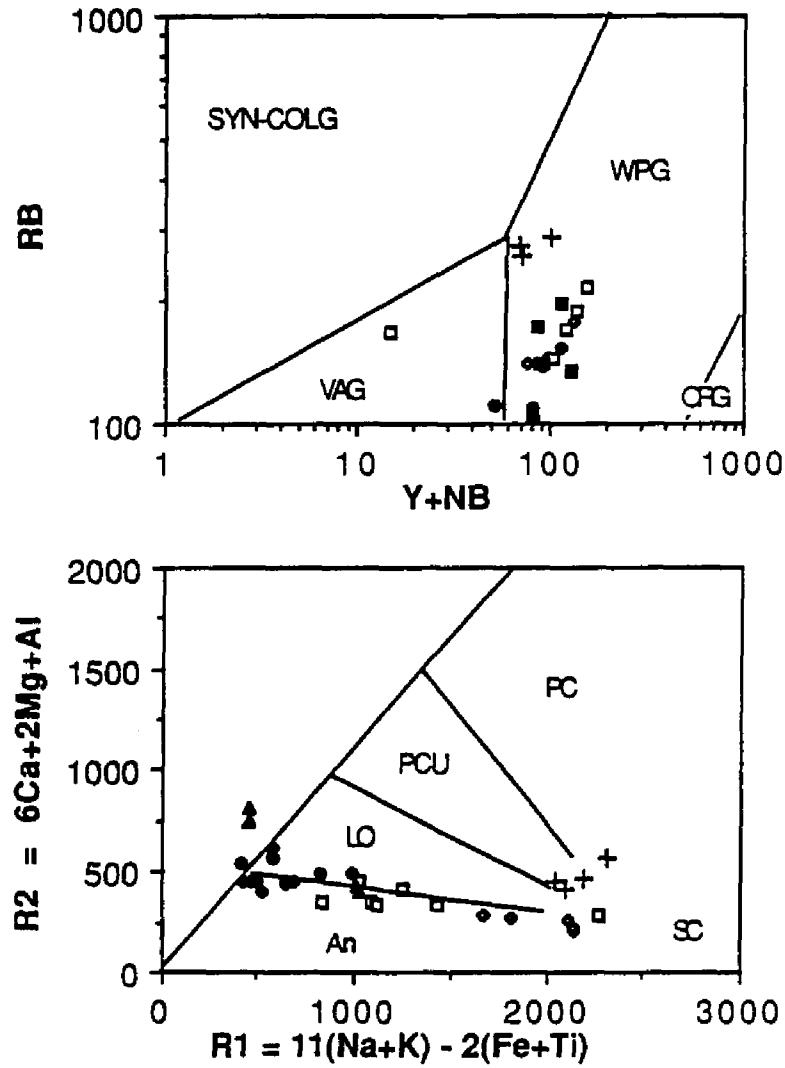

Fig. 3.22 - RI-R2 and Rb-(Y+Nb) discrimination plots (after Batchelor and Bowden (1985) and Pierce et al. (1984), respectively). The Agamenticus Complex falls within the fields for within plate and anorogenic granites. Abbrev. SYN-COLG - syn-collisional, WPG - within plate granites, VAG - volcanic arc granites, ORG - ocean ridge granites, PC - pre-plate collision, PCU - post-collision uplift, LO - late-orogenic, An - anorogenic, SC - syn-collision to post-orogenic.

next, and biotite granite last. However, the subdivision of the syenites into additional units and the recognition that the eastern lobe of the alkalic granite (Hussey, 1962) (i.e., the aegirine granite) has significant mineralogical and geochemical differences from the western lobe of the alkalic granite (Hussey, 1962), suggest the number and order of intrusive events is more complex.

The intrusive relationships between the coarse-grained alkalic syenite, SQSZ, and the aenigmatite syenites are poorly constrained due to the lack of adequate contact control caused by poor exposure and the overlapping of latter granitic rocks. The inclusion of the aenigmatite syenite as large blocks (<10 m measured along outcrop) to small clasts (several centimeters across) within the SQSZ suggests that the aenigmatite syenite is younger than the SQSZ (Fig. 3.23a, b). Gradational borders between some of the aenigmatite syenite clasts and the rocks of the SQSZ indicate that the aenigmatite has been partially assimilated by the SQSZ.

The lack of xenoliths within exposures of alkalic syenite and SQSZ closest to their mutual contact precludes a relative age assignment between the two rocks on the basis of field observations. An alternate approach for reconstructing the relative emplacement ages is to consider the possible shape of the intruding magmas. Similar complexes in the White Mountain Magma Series (Chapman and Chapman, 1940; Chapman, 1976) and the Niger-Nigerian Younger Granite Province (Turner, 1968; Bonin, 1984) developed by the intrusion of stocks or ring dikes that are often ovoid or crescent-shaped, respectively, in plan view. The overlapping of numerous magma pulses results in increasingly

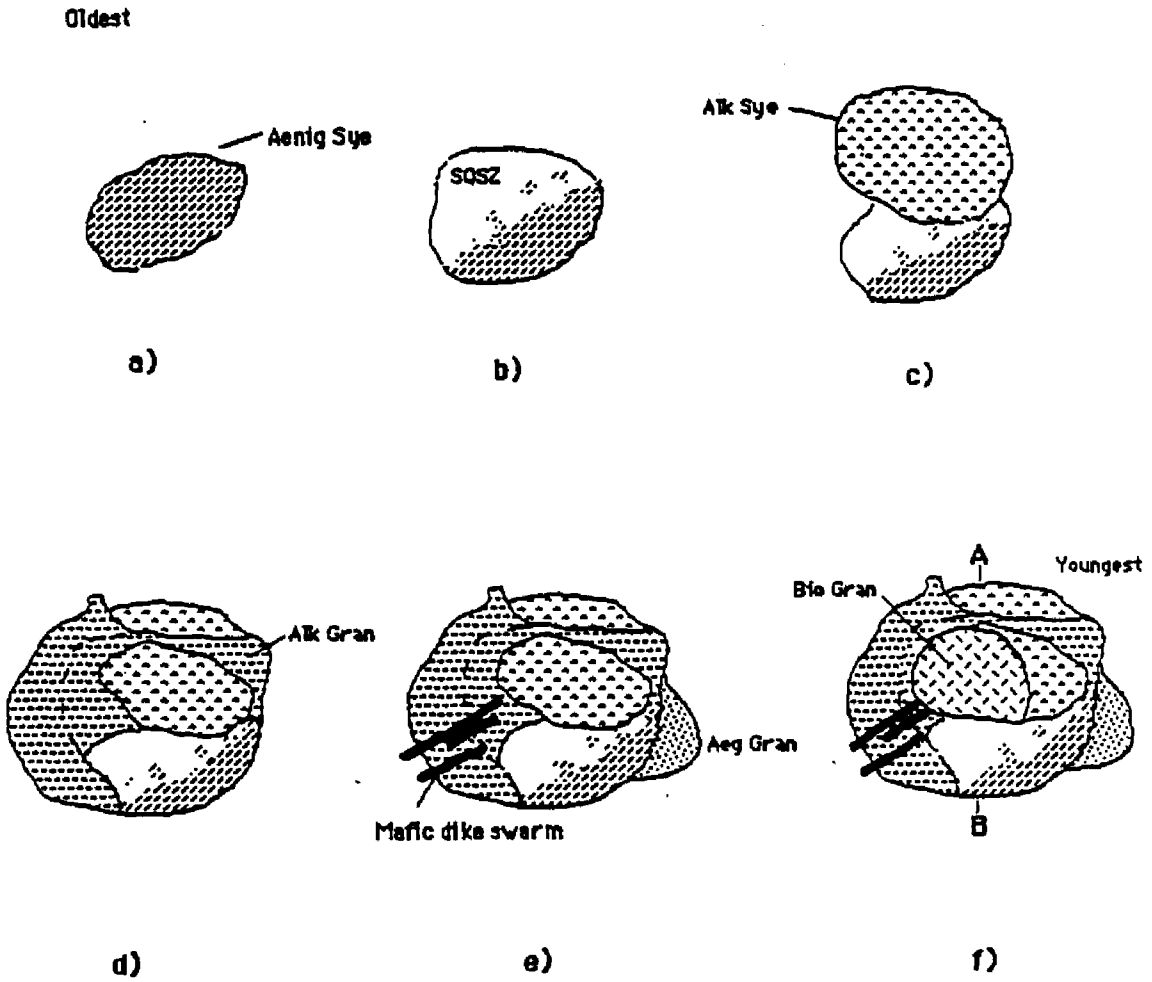

Fig. 3.23 Interpreted sequence of intrusion for the Agamenticus Complex- Plan view. Line A-B shows the orientation of cross section presented in Figure 3.42. Note that the biotite granite truncates the mafic dike swarm in the southwestern portion of the complex. Dotted line in the alkalic granite is included to indicate that this unit may be comprised of two separate pulses. Although not shown, the SQSZ is intimately intruded by the alkalic and aegirine granites.

irregular boundaries for the older units. The original shapes of earlier rocks within a complex can therefore be reconstructed after overlapping units are removed by assuming the simple shapes described above. This can be applied to the Agamenticus Complex by removing the granites and extrapolating the boundaries of the alkalic syenite (Fig. 3.23 f to c). Although the use of simple geometries for the intruding magmas makes the interpretation tentative, this process shows that the alkalic syenite overlaps, and therefore intrudes, the SQSZ (Fig. 3.23 c).

Cross-cutting relationships suggest that the fine-grained alkalic syenites are older than the coarse-grained alkalic syenite. Along the northern portion of the alkalic syenite, at MAG 61, the fine-grained alkalic syenite occurs as autoliths within the coarse-grained alkalic syenite. This suggests that the fine-grained syenite was a chill phase incorporated into the coarse-grained syenite during subsequent or continued intrusion. This interpretation is supported by the apparently gradational textural changes between the coarse- and fine-grained syenites along the southern border of the alkalic syenites (Plate 3.2).

However, trachyte dikes also intrude the coarse-grained alkalic syenite along the contact (MAG 146; Plate 3.1 and 3.2) of the fine- and coarse grained syenite in this region. If these are feeders from the fine-grained alkalic syenite, they indicate that the fine-grained alkalic syenite is younger than the coarse-grained alkalic syenite. However, the trachyte dikes in this location might be related to later trachyte dikes that cross-cut all units within the complex but the aegirine and biotite granites.

Mafic syenite dikes cross-cut the west-central portion of the alkalic syenite. The cross-cutting relationships for the mafic syenite dikes, the alkalic syenite, and alkalic granite stringers (at MAG 57d) indicate that the mafic syenite dikes and alkalic syenite are older than the alkalic granites but the mafic dikes are younger than the alkalic syenites.

Although the leucocratic quartz syenite is currently considered, on the basis of mineralogical similarities, to be transitional with the more quartz-rich portion of the quartz syenite to alkalic granite lobe, the presence of an alkalic granite pavement outcrop within the otherwise quartz syenite top of Mt. Agamenticus raises the possibility that the two rocks were separate magma pulses. In this interpretation the alkalic granite at the top of Mt. Agamenticus would be considered a cognate block enclosed within the quartz syenite. Unfortunately, the absence of exposed contacts between the two rock types prohibits a more satisfactory resolution of their relationship.

The alkalic and aegirine granites pervasively intrude and are younger than the SQSZ. The alkalic granite is assigned a younger age relative to the alkalic syenite because, in the northern portion of the complex, the alkalic granite divides the alkalic syenite into two units (Fig 3.1 and 3.23) and contains abundant xenoliths of the latter and a fine-grained alkalic granite dike occurs within the southwestern portion of the alkalic syenite at MAG 72 (Plate 3.1).

The intrusive relationships between the aegirine granite and the aenigmatite syenite are well exposed in a number of locations along the southeastern portion of the complex (MAG 139 and 155

among others). At these outcrops the aenigmatite syenite typically overlies the aegirine granite along a brittle contact. Downdropped, angular blocks of aenigmatite syenite are present within the aegirine granite below the contact. To the northwest of the aenigmatite syenite, aegirine granite occurs as a limited number of dikes and plugs within the SQSZ. The relationships observed in outcrop, aenigmatite syenite overlying aegirine granite, and the presence of aegirine granite over a large portion of the southeastern region of the complex both indicate that intrusion occurred along moderately to shallowly dipping contacts.

The aegirine granite is considered to be younger than the alkalic granite because trachyte dikes intrude into the alkalic granite but not the aegirine granite and because aegirine granite is present at the contact of the SQSZ with the alkalic granite. However, this relative age assignment cannot be substantiated because contacts between the aegirine and alkalic granites are not exposed.

Several lines of evidence indicate that the biotite granite is the youngest unit within the complex: 1) Trachyte dikes cross-cut all of the rock units except for the biotite granite and the aegirine granite. 2) A basalt dike swarm that cross-cuts the alkalic granite and SQSZ in the southwestern portion of the complex is truncated by the biotite granite (Fig. 3.23). 3) Pink rhyolite dikes, correlated with the biotite granite on the basis of early liquidus mineral assemblages, cross-cut the alkalic syenite. The general lack of xenoliths from the rocks adjacent to the biotite granite is interpreted to reflect steeply dipping contacts.

All of the rocks within the Agamenticus Complex have been cross-cut by basaltic dikes. The orientations of these dikes are consistent with that determined for early Jurassic to Cretaceous dolerite and lamprophyre dikes that intrude all of the lithologies in southwestern Maine (McHone and Trygstad, 1982; Swanson, 1982). The lack of basalt enclaves within the Agamenticus Complex and the similarity of basalt dike orientations with younger dikes in the region suggest that the basalt dikes are not cogenetic with the rocks of the Agamenticus Complex. The truncation of the basalt dike swarm in the southwestern portion of the Agamenticus Complex by the biotite granite indicates that the latter is younger, perhaps substantially, than the other rocks within the complex. This is supported by a Cretaceous apatite fission track age for the biotite granite (Christopher, 1969). A distinctly younger age for the biotite granite within the Red Hill Complex is also suggested by Henderson et al., 1989.

Depth of Emplacement

A general structural model for anorogenic ring complexes presented by Bonin (1986) provides a means to estimate the current level of erosion within a particular complex. Within ring-complexes a caldera and associated volcanic rocks at the surface are underlain at a depth of 1 of 4 km by cone sheets and ring dikes. The ring dikes are fed from a magma chamber located at depths of 7 to 32 km by foundering of the roof zone into the magma chamber (see also Chapman and Chapman, 1940; Chapman, 1976 ; Pitcher, 1978).

Estimates for the emplacement depth of the Jurassic and Cretaceous White Mountain Magma Series of New Hampshire coincide well with the mode presented above. Volcanic caldera-fill is preserved as downdropped blocks within concentric ring dikes in the Ossipee Complex (Carr, 1980). The preservation of volcanic screens and the presence of ring dikes suggests depths of emplacement from 1 to 7 km. Carr (1980) proposed a depth of emplacement of approximately 3 km. The Pliney Complex, which is exposed as numerous crescent shaped ring-dikes and stocks but lacks volcanic screens such as those exposed in the Ossipee Complex, was emplaced at approximately 2 kbars or less (Czamanski and others, 1977) or less than 7.8 km (using 2.6 kbar/10 km or 3.85 km/kbar; after Schneiderman,1989). Foland and Friedman (1977) suggest that the overlapping ring-dikes of the Red Hill Complex were emplaced at approximately 1.5 kbar or 5.7 km. A deeper emplacement, 5.8 to 14.5 km , was estimated for the ring dikes and stocks of the Ascutney Complex, Vermont, by Schneiderman (1989).

The absence of volcanic rocks and screens of country rock, often associated with the upper portions of ring dikes, in the Agamenticus Complex is consistent with a level of erosion below that of upper ring formation, approximately 4 km. The subhorizontal contacts inferred for the aenigmatite syenite, SQSZ, and the aegirine granite, the number of intrusive events, and variety of cogenetic rocks is compatible with intrusion at the upper regions of an underlying magma chamber or 5 to 14 km.

Normative assemblages for the alkalic rocks within the complex plot from the albite-orthoclase join to cotectics equivalent

to pressures of crystallization of 2 to 3 kbar for $P_{H2O}=P_{Total}$ (Fig. 3.24). For a geobaric gradient of 3.9 km/kbar this corresponds to depths of emplacement of 7.7 to 11.5 km. This represents a minimum estimate of ambient pressure because even a small anorthite component, such as observed for the Agamenticus Complex rocks (Table 3.2), results in a shift of the magmatic trends towards higher pressures (Fig. 3.24).

Luth et al. (1973) and Bonin (1986) suggest that subsolvus textures such as those observed in aegirine granite and the subsolvus syenite occur at water pressures of at least 2.5 and 4.5 kbar (or 8.3 and 14.9 km), respectively. Although the current juxtaposition of these two rocks might require that both crystallized at a depth greater than 14.9 km, the perthite overgrowths on early plagioclase and perthite crystals, a change from subsolvus to hypersolvus texture, suggests that P_{H2O} decreased during crystallization of the subsolvus syenite. The change in P_{H2O} could have been caused by volatile release during eruption or by a change in crustal levels at essentially constant water content within the magma. The latter suggests that the early stages of crystallization of the subsolvus syenite occurred within the magma chamber at a minimum depth of 14.5 km. The hypersolvus texture then developed following emplacement of the partially consolidated magma at a shallower upper chamber/lower ring dike horizon.

Depths for the final level of emplacement are better constrained by the aegirine granites. The minimum depth, 8.3 km, indicated by the subsolvus texture of the rocks corresponds well

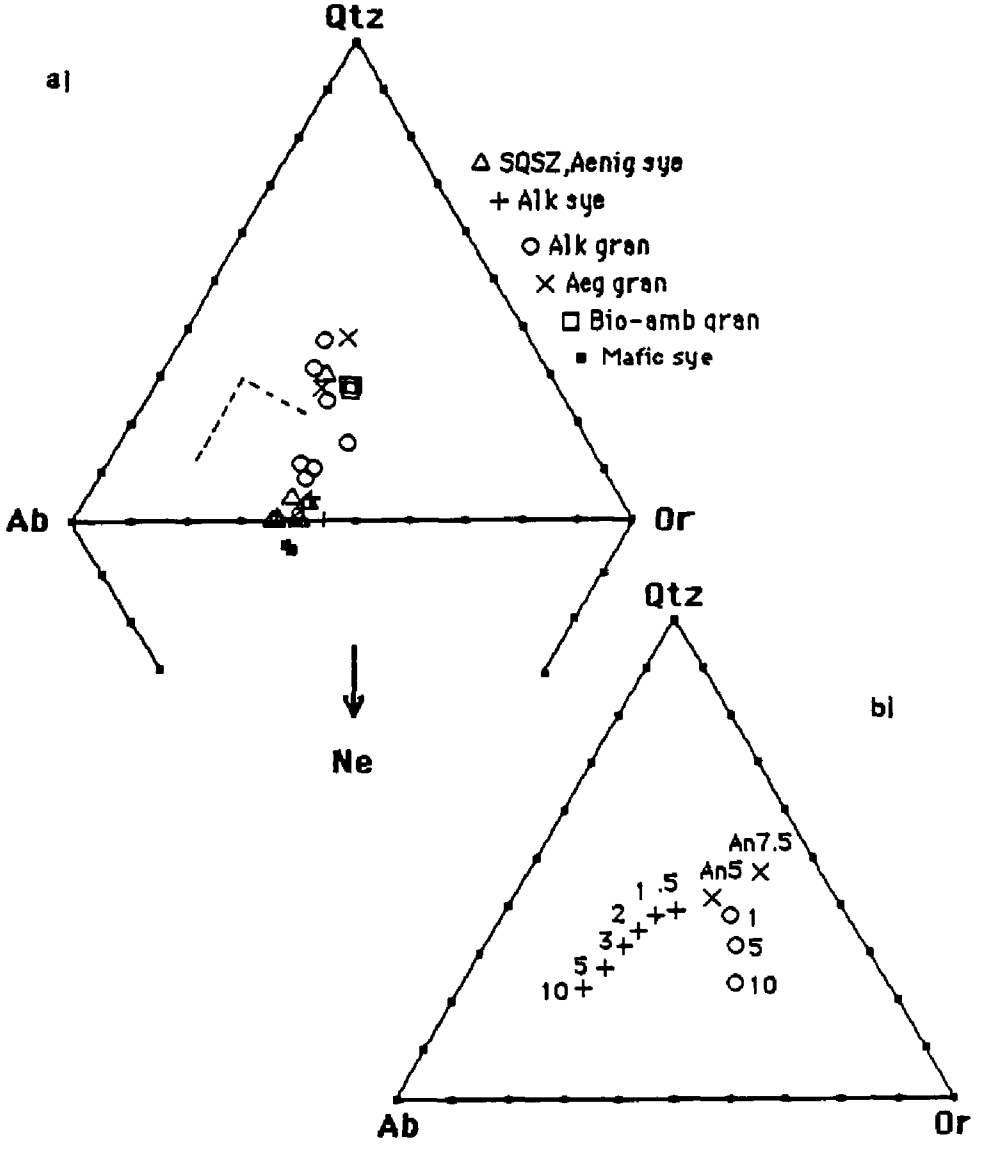

Fig. 3.24 a) CIPW norms plotted on Qtz-Alb-Or diagram. Dashed line- normative compositions of partial melts of an alkali olivine basalt (Heltz, 1975) b) Ternary minima (+) for $P_{H2O} = P_{Total}$ (Tuttle and Bowen, 1958; Luth et al., 1964), (X) minima in An-bearing systems and $P_{H2O} - P_{Total} = 1kb$ (James and Hamilton, 1969), and (o) anhydrous conditions (Luth, 1969).

with the depth estimated by comparison of the normative assemblage of the granite to experimental data (7 to 10 km, Fig. 3.24), and falls within the range, approximately 5 to 10 km, indicated by comparison of the postulated structural level (upper chamber/lower ring dike) to other alkalic complexes.

Apatite fission track data from the alkalic syenite indicates that the rocks had cooled past the 150°C isotherm required for fission track retention by 172 Ma (Christopher, 1969). This suggests that the rocks of the Agamenticus Complex were at or below 3.8 to 5 km (using 40°C/km and 30°C/km, respectively) before 172 Ma. On the basis of apatite closure ages and heat flow considerations, Doherty and Lyons (1980) calculate an emplacement depth of 5.3 to 7.6 km for the Jurassic White Mountain Plutonic Series to the northwest of the Agamenticus Complex. Using their post Jurassic erosional rate (0.031 mm/yr) and the differences in ages between the Jurassic Belknap and Triassic Agamenticus Complexes (67 million years), the depth of emplacement for the Agamenticus Complex can be estimated to be 7.38 to 9.68 km. This is in agreement with the estimates of depth derived above.

Petrology of the Agamenticus Complex

The petrogenesis of felsic alkalic rocks is complex and involves melting of mantle or crustal sources followed by varying amounts of fractional crystallization (Eby, 1987; Collins et al., 1982). The emplacement of mid- to upper-crustal melts, derived from heat provided by the passage of the alkalic magmas (Barker et

al. 1975), often results in the juxtaposition of magmas with different parents within the same complex. Evolution of the magmas can include assimilation of crustal rocks and mixing of cogenetic alkalic rocks (Loiselle, 1978; Whalen and Currie, 1984). Late magmatic and hydrothermal fluids can redistribute the trace element patterns of the lithophile elements, mobile major elements, and isotopic signatures (Macdonald, 1987; Bowden et al., 1987).

This very general model provides the basic framework against which the petrogenesis of the Agamenticus Complex can be considered. The roles of magma mixing, assimilation, and fractional crystallization in the development of the complex are evaluated through a qualitative analysis of available geochemical and field data. The petrogenesis of the different rock types within the complex will be discussed in light of the results from this qualitative analysis and quantitative numeric modeling of major and trace element abundances. Sources for proposed parental magmas are considered in relation to available geochemical and isotopic data and experimental findings. A petrogenetic model for the Agamenticus Complex that incorporates these findings is considered. Although this model is not unique, it provides a basis for testing proposed petrologic precesses and lays the foundation for future research. More complex models that can test the geochemical nature of assimilation, source rocks, and/or hydrothermal interaction require additional major and trace element analyses and radiogenic and stable isotopic data.

Magma Mixing

Rock trends on major element Harker diagrams (Fig. 3.12) indicate that magma mixing was not an important magmatic process in the Agamenticus Complex. If rocks with compositions intermediate to syenites and granites formed by wholesale magma-mixing, then the compositions for these hybrid magmas would be located along a linear between the two parents. Such compositions do not occur between the alkalic syenite and alkalic granite or the SQSZ and aegirine granite on Al_2O_3, Fe_2O_3, or K_2O Harker diagrams. By a similar argument, products that would result from the mixing of SQSZ and aegirine granite do not appear on the K_2O Harker diagram. These diagrams do not preclude mixing of rocks that lie along the individual linear segments (Holm and Praegel, 1988) nor the mixing of the alkalic syenite and the aegirine granite. However, the latter is considered unlikely due to the lack of field evidence for interaction between the two and the lack of xenocrysts that would be expected of magmas (McConough and Nelson, 1984) which were evolving below the liquidus at the time of mixing.

Support for limited magma mixing along major element geochemical trends is observed within aegirine-arfvedsonite granite dikes that occur in the aegirine granite at York Beach (near to MAG 48, Plate 3.1). Internal contacts in these fine-grained compound dikes are usually highly undulose and lobate suggesting that multiple intrusion of the dikes occurred over a short interval and that magma comingling occurred. However, this magma interaction appears to be restricted to the interior of the dikes. Shear fabric (alignment of minerals and folding of internal layers)

observed within one dike does not extend into the host aegirine granite. The lack of shearing in the host rock adjacent to the deformed dike and the sharp host-dike contact suggest that the main body of aegirine granite was relatively solid prior to the intrusion and deformation of the dikes.

Mixing of the late aegirine granite magmas would have no effect on the overall geochemical evolution of the other rocks within the complex. Two important observations that argue against mixing between the syenites and granites must be stressed: 1) Contacts between all syenites and granites are brittle and 2) Magma pillows and convolute contacts commonly cited as evidence for mixing in other complexes (Bloomfield and Arculus, 1989; Whittemore and Hannah, 1988; Frost and Mahood, 1987; Whalen 1985; Whalen and Currie, 1984) are absent from the Agamenticus Complex. These observations preclude mixing of syenites and granites at the current level of exposure to produce intermediate magma compositions and suggests that it did not occur at depth. Disequilibrium textures do occur in the some of the rocks, such as reaction oscilli of sodic amphibole over olivine and clinopyroxene (Fig. 3.9) in the alkalic syenite or mineral reactions (amphibole overgrowths on clinopyroxene and earlier amphibole) and convolute crystal boundaries in the matrix of the subsolvus augite syenite, could be interpreted as evidence for magma mixing prior to intrusion. However, these textures are interpreted here as manifestations of late magmatic to subsolidus interactions with deuteric fluids.

Assimilation

Contrary to the findings of Woodard (1957), assimilation of the country rock at the current level of exposure did not have an important impact of the evolution of the complex. Woodard considered all blocks or ghosts within the complex to be xenoliths of country rock. The degree of chemical similarity between xenoliths and host as well as the quartz content of the syenites and granites was ascribed to varying amounts of metasomatism and/or assimilation.

An important corner stone of this hypothesis was that the southern portion of the complex is simply a xenolith-rich portion of the alkalic syenite. The mesocratic to melanocratic blocks within this region were considered to represent the end product of metasomatic alteration of country rocks. The work of Hussey (1962) and the findings of this study have demonstrated that the southern portion of the complex (the SQSZ) is a distinct unit from the alkalic syenite and that the melanocratic to mesocratic ghosts within this zone are partially assimilated syenites rather than metasomatized country rock.

As suggested by Woodard (1957), calcareous quartzite xenoliths from the Kittery Formation are preserved throughout the alkalic granite and within other units close to the perimeter of the complex. The presence of amphibole reaction rims around these xenoliths supports the metasomatic processes proposed by Woodard (1957), but the angular outline of these xenoliths indicate that wholesale assimilation has not occurred. Sample localities and geochemical analyses from this study are insufficient to fully test

Woodard's contention that the quartz content of the alkalic granite is proportional to the xenolith abundance. However, the fact that sample MAG 17 is within a xenolith-rich zone of the alkalic granite but is less siliceous than a sample in a xenolith-free zone (Mag 23, Plates 1 and 2) suggests that the quartz content is not directly related to the amount of assimilation. It is therefore, suggested that the assimilation/metasomatism demonstrated by Woodard (1957) to have occurred in close proximity to the xenoliths, including both Kittery Fm. xenoliths in the alkalic granite and syenite xenoliths in the SQSZ, did not appreciably alter the chemical evolution of the magmas of the Agamenticus Complex.

The current data base is insufficient to test if assimilation was more significant at a lower depth in the magma chamber or at some deeper level within the crust during the upward migration of the magma. Quantitative modeling of radiogenic and stable isotope data (Eby, 1985; Foland and Friedman, 1977; Pankhurst et al. 1976) and trace element data (Fowler, 1988) obtained from both rocks that may represent magmas and potential contaminants has shown that variable amounts of assimilation has occurred within other alkalic complexes.

The use of a limited number of major element analyses available for the Kittery Formation (Woodard, 1957) in assessing the effects of assimilation must be approached with caution for a number of reasons. Bowen (1928) noted that the liquid line of descent is not affected by assimilation but rather the proportion of end product is altered. Therefore, the major element trends would remain the same even if assimilation has occurred. In addition,

unless wholesale assimilation has occurred, the assimilation process is better modeled using a contaminant composition that represents a partial melt of the country rock rather than bulk rock composition (Fowler,1988). Even if wholesale assimilation (i.e., two component mixing) of the country rocks is considered a viable alternative, the large scatter (Fig. 3.25) in the major element data for the Kittery Formation would make any model developed capricious.

Fractional Crystallization

A qualitative vector analysis of compositional trends versus mineral compositions on major element-SiO_2 diagrams (Fig. 3.26) indicates that fractional crystallization could have controlled the evolution of the alkalic magmas within the Agamenticus Complex. It is clearly shown on the K_2O and CaO diagrams that the flexures between the SQSZ and the granites, at approximately 65 weight percent SiO_2, can be attributed to potassium feldspar crystallization. Potassium feldspar may have been on the liquidus in the SQSZ syenites but certainly was the dominant mineral in the evolution of the granites. This interpretation is consistent with the observation that plagioclase occurs along with potassium feldspar as phenocrysts in the SQSZ and that it becomes subordinate to potassium feldspar in the matrix of these rocks and in the granites.

The location of the alkalic syenites above the trend of the SQSZ and along the trend defined by the alkalic granite on the K_2O-SiO_2 plot indicates that potassium feldspar was more important in the evolution of these rock than the mafic minerals. The relative

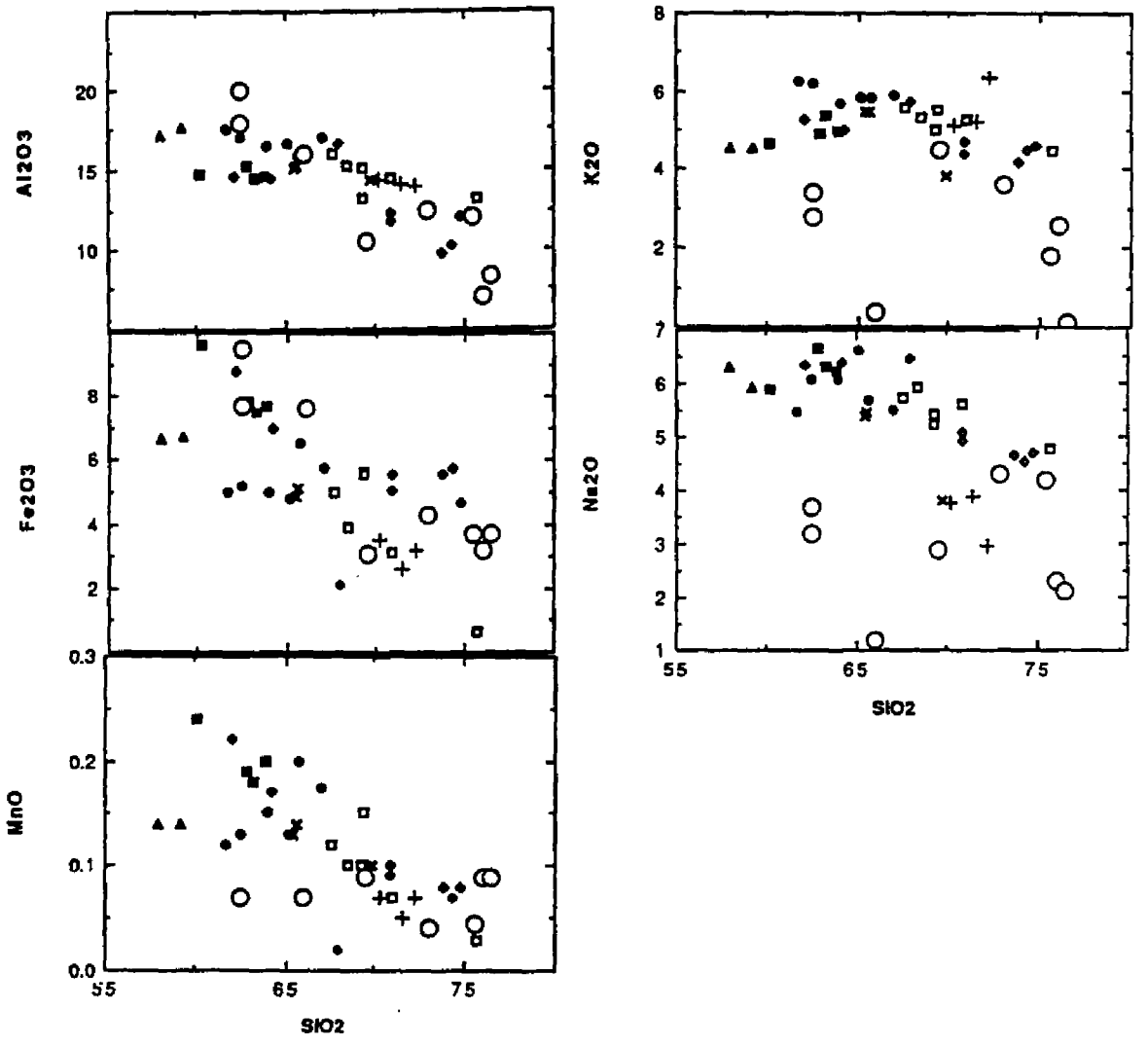

Fig. 3.25 Compositions of Kittery Formation (O) determined by Woodard (1957) compared to major element-SiO_2 plots for Agamenticus Complex. Note the large amount of variations of the Kittery Formation. Symbols as in Figure 3.12.

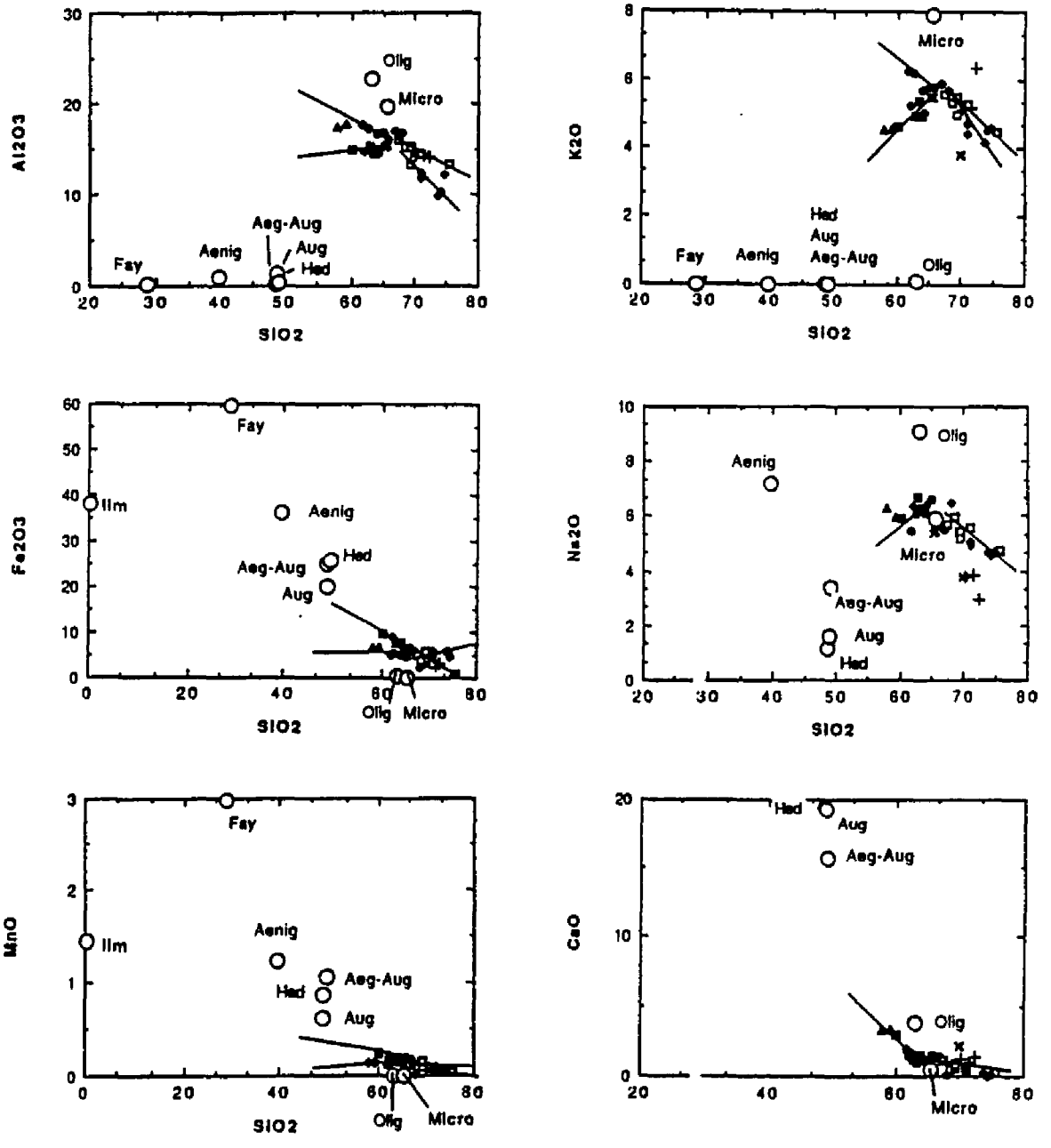

Fig. 3.26 Mineral-Harker diagrams used for qualitative vector analyses of fractionation trends observed within and between each rock type. Lines emphasize fractionation trends. Abbrev. Olig - oligoclase, Micro - microcline, Aeg-Aug - aegirine-augite, Aug - augite, Hed - hedenbergite, Aenig - aenigmatite, Fay - fayalite, Ilm - ilmenite. Symbols as in Figure 3.12.

importance of mafic silicate minerals vs. potassium feldspar in the evolution of the SQSZ and alkalic syenite is also demonstrated on the Fe_2O_3, MnO, and Al_2O_3 diagrams. The closer proximity of the mafic silicate minerals to the trend defined by the SQSZ on these plots suggests that they played a more important role in the evolution of the SQSZ than the alkalic syenite. Crystal textures, which suggests that the mafic silicates crystallized earlier in the SQSZ than the alkalic syenite, and the lower modal abundance (Table. 3.1) of these minerals in the alkalic syenites support this conclusion.

The evolution trends of the alkalic granites on the MnO, Fe_2O_3, and Al_2O_3 Harker diagrams suggest that mafic silicate minerals played a more important role, relative to orthoclase and plagioclase, in the evolution of the alkalic granites then the aegirine granites. As with the syenites this conclusion is supported by the relative modal abundance of the minerals within each rock (Table. 3.1).

P_2O_5 decreases in the alkalic syenites, the SQSZ and the aenigmatite syenites and remains essentially constant for the alkalic and aegirine granites. The changes in P_2O_5 abundance are reflected in the proportion of apatite in the rocks. These observations are consistent with apatite fractionation in the syenites and only minor involvement of apatite in the evolution of the alkalic and aegirine granites.

Quantitative models of fractional crystallization relating these magmas must be considered in several steps (Nelson et al, 1987) because these findings indicate that different cumulate

assemblages controlled the evolution of each alkalic magma. A logical step for these models is defined by the flexures within the Harker diagrams where the linear trends for the alkalic rocks merge; i.e., at 65 weight percent SiO_2. The linear trends defined by each rock type are modeled by least squares mixing and trace element fractionation models which assume the rocks can be related to the same parent by varying degrees of fractionation and varying cumulate assemblages. Some error is inherent in the approach because of the larger compositional jumps for the more evolved rocks. The interrelationship between the syenites and granites are tested by modeling the more evolved samples of the syenites and the least evolved samples of the granites. Although these models assume that the rocks can be related by fractional crystallization, it is realized that the compositions of the rocks are most likely disturbed by late deuteric fluids and volatiles. The errors associated with the fractional crystallization models should help highlight the effect of these late magmatic processes on the composition of the rocks.

SQSZ and Aenigmatite Syenite - Vector analyses of the major element trends for the SQSZ and aenigmatite syenites indicate that these rocks can be related by fractional crystallization of plagioclase, potassium feldspar, clinopyroxene, olivine, and apatite ± aenigmatite. This is compatible with textural evidence of early crystallization of plagioclase, potassium feldspar, and apatite followed by clinopyroxene and olivine crystallization. The importance of aenigmatite as a cumulate mineral is unclear. Within the SQSZ it forms as a reaction product of clinopyroxene and

amphibole suggesting that it is a late magmatic mineral. In the aenigmatite syenite it occurs as euhedral crystals that are interpreted as a primary super-solidus crystal. Amphibole is not included as a cumulate mineral for these rocks because is appears as late overgrowths on clinopyroxene and olivine and/or as late to interstitial crystals. It would therefore only effect the compositional trends of the late residual fluids within a restricted region of the sample.

The compositions of the cores of the plagioclase phenocrysts and clinopyroxene from the most mafic augite sub-solidus syenite in the SQSZ, MAG 91-1, were used as input to least squares models developed to test whether fractional crystallization controlled the chemical evolution of the rocks of the SQSZ and the aenigmatite syenite. Least squares mixing models for the SQSZ rocks and the aenigmatite syenite (MAG 139) yield acceptable results (Σr^2 = 0.45 for 91-1 to 51D, Σr^2 = 0.49 for 91-1 to 91-2, Σr^2 = 0.54 for 91-1 to 139; Table 3.4). The solutions require greater degrees of fractionation to produce more siliceous rocks (f=0.39 for 91-1 to 51d and f= 0.29 for 91-1 to 91-2; where f = liquid proportion) and larger proportions of feldspar in the cumulate assemblage.

The largest residuals for each model are associated with the underestimation of K_2O or Na_2O (Appendix III.V.I). This could be due either to an inappropriate choice of felspar composition, late deuteric alteration, and/or inaccuracies inherent in the analyses (See Appendix III.I). The first is supported by the improvement of the model that results from reducing Na_2O and increasing K_2O in potassium feldspar. The albite/orthoclase ratios from the CIPW

Table 3.4 Least Squares Models

			% Minerals							
Parent	Product	% product	KSP	CPX1*	CPX2*	CPX3*	Fay	Olig	Ilm	Σr2
SQSZ trend										
91-1	51d	39.8	29.1	5.52			13.1	16.05	1.1	0.445
"	91-2	29.47	32.35	5.08			9.38	21.27	1.23	0.49
91-1	139	48.71	19.44	6.21			7.15	17.17		0.832
SQSZ to other										
91-1	37b	200.27	-82.7	6.22			-2.5	-21.7	0.47	0.041
51d	120	43.88	27.84	-0.18			9.39	18.28	0.76	1.134
91-2	120	76.66	16.43		1.01		5.26		0.45	1.196
91-2	49	18.02	51.46		0.3		9.95	18.64	0.94	1.364
Alk Sye trend										
72b	37b	118.56	-19.2	-0.26		-0.16	-2.1		0.63	1.247
"	39	80.8	17.18	0.75		0.66	1.05		0.06	0.021
37b	3	36.53	57.66		2.93		2.48		0.27	0.023
Alk Sye to Alk Gran										
37b	120	19.12	73.05		3.75		3.57		0.37	0.105
37b	135	4.6	85.9		5.01		3.99		0.43	0.105
Alk Gran trend										
120	26	36.9	55.6		2.9		4.7		0.53	0.186
120	23	21.9	68.9		4.4		4.2		0.66	0.16
Alk Gran to Aeg Gran										
120	49	23.3	69.2	4.8			2.3		0.55	0.242
Aeg Gran trend										
49	48	73.6	24.87		1.4				0.57	0.236

*Clinopyroxene compositions used: CPX1(MAG 91-1 core),CPX2(MAG 91-1 rim),CPX3(MAG 84)

norm calculations indicate that this approach is reasonable. However, textural evidence within the matrix of MAG 91-1, such as mafic silicate reactions, late, fine-grained plagioclase and microcline, and convolute mineral contacts, indicates that the SQSZ has experienced some degree of fluid interaction. These fluids could relate to autometasomatism of the rocks or to the later intrusion of the alkalic or aegirine granites. In either case, the fluid interaction was most likely accompanied by some changes in major and trace element chemistry (Bowden and Kinnard, 1984). For example, if the deuteric or hydrothermal fluids results in the subsolidus growth of microcline, this would lead to a preferential enrichment of K_2O in MAG 91-1 and the underestimation of this oxide in the least squares models.

Changes in large ion lithophile (LIL) element (i.e., Rb, Sr, and Ba) abundances within the SQSZ and aenigmatite syenites are satisfactorily modeled using Rayleigh fractionation equations (Fig. 3.27; Appendix III.V.I). One of the SQSZ samples, MAG 91-1, and the aenigmatite syenite plot within the field calculated for liquids on Ba-Rb, Sr-Rb, and Sr-Ba plots (Fig. 3.27). The less siliceous SQSZ, MAG 51D, plots within the region of residua compositions on these diagrams. These results are consistent with fractional crystallization dominated by plagioclase and potassium feldspar. The incorporation of Sr and Ba by both of these minerals leads to a reduction of these elements in the liquid. The incompatibility of Rb in plagioclase (Kd = 0.02) and potassium feldspar (Kd = 0.9) produces the observed increase of this element in the liquid. The fit of the data to Rayleigh fractionation trends is reasonable in

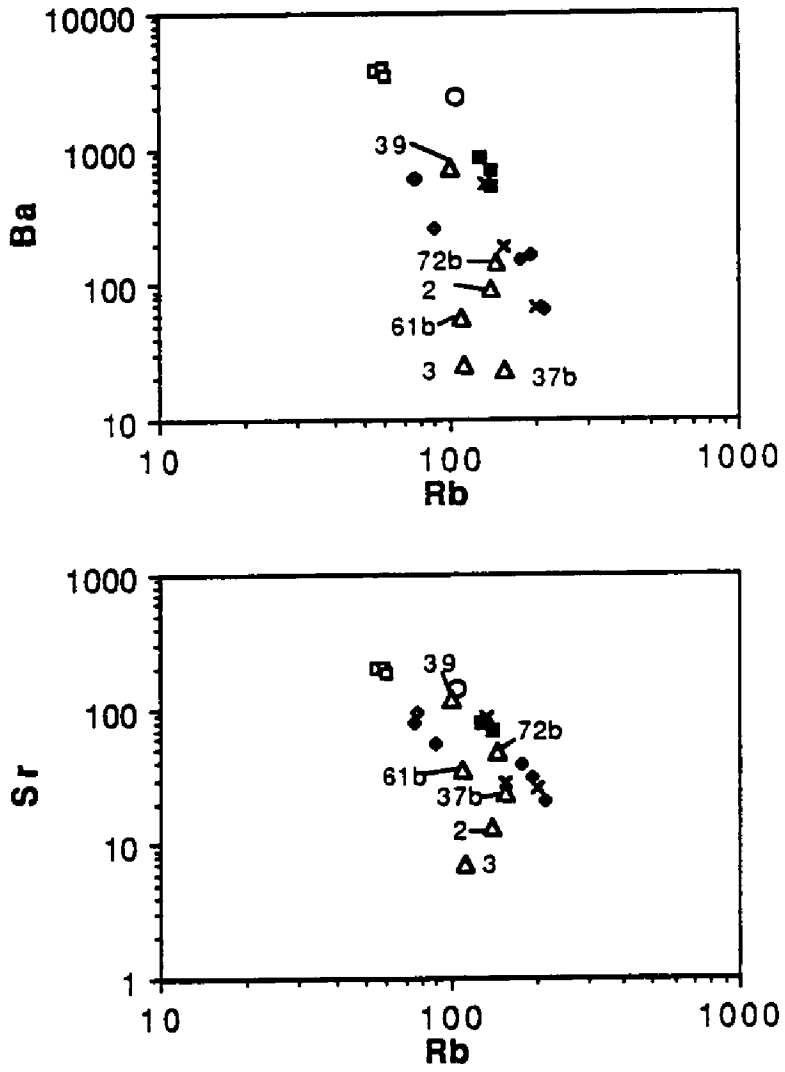

Fig. 3.27 Calculated trace element trends for the SQSZ and rocks used as parents and products of these calculations. The SQSZ can be modeled acceptably as a liquid derived from the augite syenite by fractionation of oligoclase, potassium feldspar, augite, and fayalite. Alkalic syenites are shown in relation to this model to demonstrate that they are not related to the SQSZ. Symbols for model compositions; Filled squares-residual liquid, filled diamonds-liquid from Rayleigh fractionation, open diamonds-instantaneous cumulate, open squares-average cumulate (see Appendix V for formulas used to calculate these compositions). Other symbols; open circle-parent (MAG 91-1), x-SQSZ compositions used as input for product of fractionation, open triangles-alkalic syenites.

light of the compositional zoning observed in the mineral from these rocks (see below).

Decreases in Co and Sc (Fig 3.18) are explained by clinopyroxene and, to a lesser extent, olivine fractionation. Although these models require high Sc distribution coefficients (Kd (Sc = 30) for clinopyroxene, this value is realistic in light of similar coefficients determined for hedenbergite in the Chaine de Puys trachyte (Lemarchand et al., 1987).

Changes in REE abundances are predicted less successfully than changes in the other elements (Appendix III.V.I). Similarities in the calculated bulk distribution coefficients (D*(I), Appendix III.V.I) for La, Tb, and Eu to distribution coefficients for feldspars (D*(Eu) > 1, D*(La) and D*(Tb) < 1; Lemarchand et al., 1987) suggests that the REE abundances were in part controlled by feldspar fractionation. Lower bulk distribution coefficients for La relative to Tb in two of the models could be explained by the preference of HREE in clinopyroxene, olivine, and/or zircon (Lemarchand et al., 1987).

Although quantitative models for the changes in Ga abundances are precluded by the paucity of distribution coefficients, changes in this element and Ga/Al ratios are considered because of their known petrogenetic importance (Collins et al., 1982; Gottardi et al, 1978). Ga readily substitutes for Al and Fe^{3+} (Gottardi et al, 1978; Goodman, 1971) in Al and/or Fe^{3+} bearing minerals such as plagioclase and to a lesser extent potassium feldspar, aegirine, hedenbergite, and biotite. Increases in the Ga/Al ratio, such as those observed for the SQSZ (Fig. 3.19) are compatible with feldspar

dominated fractional crystallization (Goodman, 1971). Increases in Ga, as observed for the SQSZ (Fig. 3.14), are interpreted elsewhere in terms of feldspar accumulation (Vincent and Nightingale, 1974) or as as the result of fractional crystallization in which plagioclase (Kd (Ga) = 1.7, in gabbro) is modally subordinate (Paster et al., 1974). An alternative proposal, is that Ga enrichment is due to its incompatibility in the feldspars within the SQSZ. This possibility is supported by the incompatibility of Ga in the fosterite-diopside-anorthite system (Kd(Ga) = 0.024, 0.19, 0.86, respectively; Malvin and Drake, 1987) and by the tendency for Ga abundances to be highest in sodic rather than calcic plagioclase and in plagioclase from granites with higher silica contents (Gottardi et al, 1978; Goodman, 1971).

Changes in magma composition during the evolution of the SQSZ and the aenigmatite syenites are reflected in the chemistry of minerals from these rocks. The changes in clinopyroxene composition as the liquids evolved from the SQSZ (Mag 91-1) to the aenigmatite syenite (Fig. 3.28; iron enrichment followed by sodium enrichment) is compatible with that observed in other oversaturated, alkalic complexes (Holm and Praegel, 1988; Stephenson and Upton, 1982 and references therein). Core-rim compositions in MAG 91-1 (CPX samples 5 and 6, Appendix III.III) indicate that Fe enrichment is accompanied by a decrease in Mg, Al, and Ti, enrichment in Mn, and nearly constant Si, Ca, and Na. The increase in Na in clinopyroxenes from the aenigmatite syenite relative to those in the SQSZ is associated with an increase in Si,

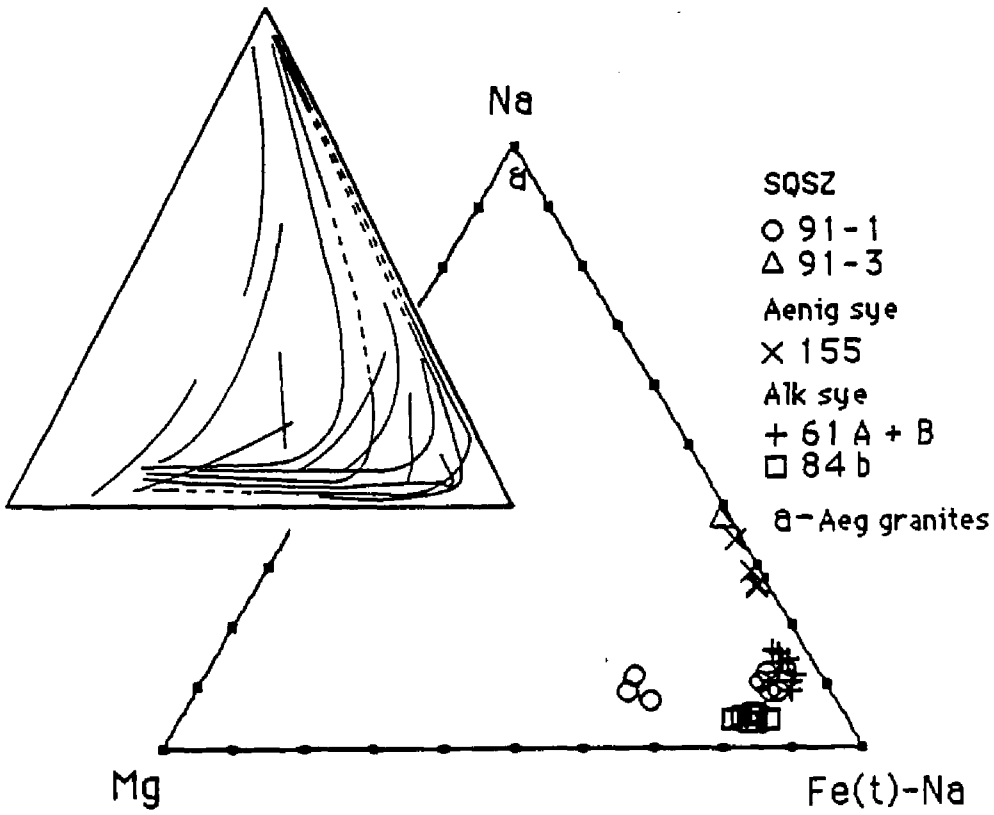

Fig. 3.28 Mg-(Fe-Na)-Na ternary plot of clinopyroxene compositions. Sodium enrichment of the SQSZ and aenigmatite syenites, compositional gap between the SQSZ trend and aegirine granite, and sodium poor alkalic syenites are shown. Inset of clinopyroxene trends from other under- and over-saturated alkalic complexes (After Mitchell and Platt, 1977).

Al, Mn, and Fe^{3+} and a decrease in Ca and Mg (MAG 155, Appendix III.III).

The sodium enrichment of these clinopyroxenes can be attributed to several factors. Stephenson and Upton (1982) and Mitchell and Platt (1977) suggest that Na enrichment in clinopyroxenes in alkalic rocks is a function of magma peralkalinity and is not coupled to silica activity. This is supported by the presence of aegirine-rich clinopyroxenes in the undersaturated rocks of the Tenerife Complex (Scott, 1976). The higher Ac component and lower SiO2 content of MAG 139 relative to 91-2 (Table 3.2) coupled with the high sodium content of the aenigmatite syenites from MAG 155 suggest a similar relationship between peralkalinity, SiO2, and Na content for the clinopyroxenes from the SQSZ and aenigmatite syenite.

Scott (1976) suggests that the major control for Na enrichment in clinopyroxenes is fO_2 and secondly the availability of Na. Scott (1976) and Nash and Wilkenson (1970) suggest that slowly falling fO_2 promotes Fe^{3+} and hence Na enrichment in clinopyroxenes. Therefore, the increased acmite component in clinopyroxene is dependant on the rate of change of fO_2 rather than the absolute fO_2. Mitchell and Platt (1977) reach similar conclusions for acmite enrichment in clinopyroxenes from the syenites in the Coldwell Complex, Canada.

In the Kungnat Fjeld Complex clinopyroxene evolution occurred parallel to the diopside-hedenbergite join at fO_2 set by the FMQ buffer (Stephenson and Upton,1982). Na enrichment was accompanied by increased fO_2 and the instability of olivine. The

absence of olivine from the aenigmatite sample suggests that a similar mechanism operated in the SQSZ. However, the FMQ buffer could not have controlled fO_2 in the SQSZ because ilmenite rather than magnetite was stable throughout the early to middle crystallization history of the SQSZ.

Oxygen fugacity was more likely controlled by a peralkaline analogue to the FMQ buffer similar to those proposed for other alkalic complexes (Nicholls and Carmichael, 1969; Marsh, 1975; Larsen, 1977; Grapes et al., 1979). The association of aenigmatite with aegirine-augite, richterite and opaques in MAG 91-3 and the aenigmatite syenite is similar to the common association of aenigmatite with aegirine (Ac>80) and/or arfvedsonite in other complexes (Grapes et al. 1979). The late magmatic aenigmatite in these complexes is considered to be a reaction product of ilmenite and arfvedsonite and/or ilmenite and aegirine (Grapes et al., 1979). These reactions can act as oxygen buffers in a "no-oxide" zone where the FMQ buffer is unstable (Nicholls and Carmichael, 1969; Marsh, 1975; Larsen, 1977; Grapes et al., 1979). Although poorly constrained, the aenigmatite - Ti magnetite - aegirine buffer,

$$3/2\ Na_2Fe^{2+}{}_5TiSi_6O_{20} + O_2 =$$
$$4\ NaFe^{3+}Si_2O_6 + 3\ SiO_2 + 3/2\ Fe_2TiO_4 + 1/2\ Fe_3O_4$$

lies at fO_2 and T within the normal range expected for trachytes and phonolites (Nash et al, 1969; Mitchell and Platt, 1977) (Fig. 3.29) and the aenigmatite - ilmenite - aegirine buffer,

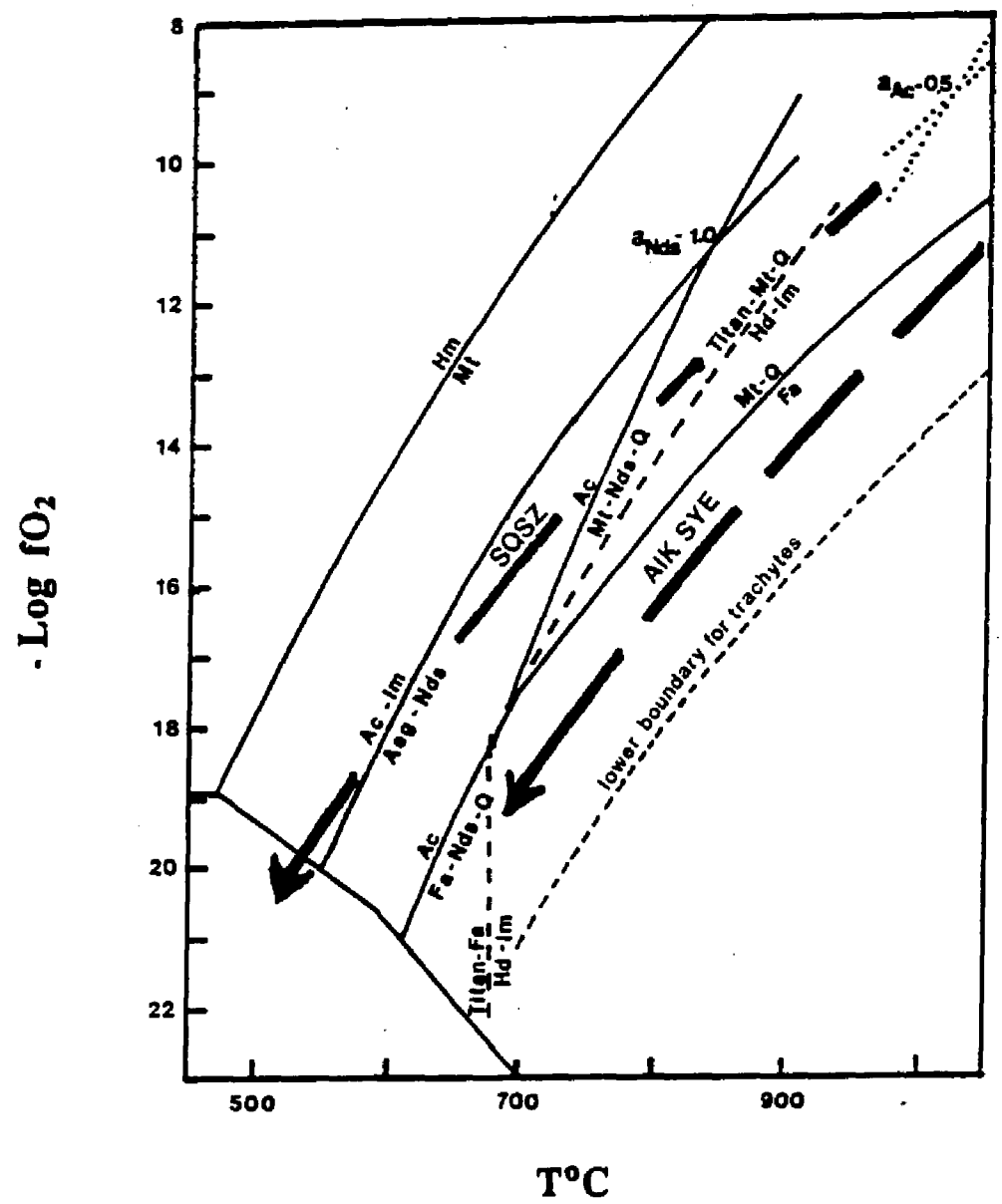

Fig. 3.29 fO_2-T diagram showing proposed peralkaline buffers that likely controlled fO_2 during the evolution of the SQSZ, aenigmatite syenite, and aegirine granite. Buffers from Wones (1989), and Nicholls and Carmichael (1969). Lower boundary for trachyte field from Nash et al. (1969).

$$Na_2Fe^{2+}{}_5TiSi_6O_{20} + Na_2Si_2O_5 \text{ (liquid)} + O_2 =$$
$$4\ NaFe^{3+}Si_2O_6 + Fe^{2+}TiO_3,$$

lies slightly above the FMQ buffer (Marsh, 1975). T-fO2 estimates suggested by these buffers are compatible with the proposed stability range for aenigmatite proposed by others; between the NNO ("ideal" aenigmatite) and WI and MW (Ti free aenigmatite) buffers (Grapes et al., 1979, Ernst, 1962).

The presence of aegirine-augite instead of aegirine would move the buffer towards lower fO_2 and higher temperatures than the aenigmatite - ilmenite - aegirine buffer (Nicholls and Carmichael, 1969) (Fig. 3.29). Aenigmatite formed in reaction with clinopyroxene and/or amphibole in the SQSZ rocks but occurs as individual crystals in equilibrium with these minerals in the aenigmatite syenite. The greater stability of aenigmatite in the aenigmatite syenite relative to the SQSZ suggested by these textures implies that magma evolution from the SQSZ to the aenigmatite syenite has been accompanied by reaction progress along the aenigmatite - ilmenite - aegirine-augite buffer and decreasing fO_2 and temperature.

The aenigmatites have rims that are enriched, relative to the cores, in Na, Si, Fe^{2+}, Cr, and K and depleted in Ca, Al, Mn, and Fe^{3+} (Appendix III.III). These changes reflect the substitutions listed in Table 3.5 and $CrFe^{2+}{}_{-1}$. The increase in Na and Si towards the rims reflects increased activity of these components in the magma (Larsen, 1977) and the decrease in Fe^{3+} implies falling fO_2. Slightly higher Fe^{3+}-Al, 'Fe^{3+}-Tsch', and Ferri-aenigmatite

Table 3.5- Analyses of aenigmatite expressed as end member compositions** (following Larsen, 1977)

	Rhonite	Fe^{3+}-Al-aen.	Fe^{3+}-Tsch' aen.	Ferri -aen.	Ideal aen.
MAG 155					
core	6.43	4.03	8.86	10.70	69.98
rim	2.48	0	0	15.49	81.67
MAG 91-3					
	2.51	1.80	4.68	9.01	82
	2.4	1.75	5.28	8.01	83

**Component	Formula	Substitution
Rhonite	$Ca_2Fe_5^{2+}TiAl_2Si_4O_{20}$	$Na_xSi_z<>Ca_xAl_z$
Fe^{3+}-Al-aen.	$Na_2Fe_4^{2+}Fe^{3+}TiAlSi_5O_{20}$	$Fe^{2+}_ySi_z<>Fe^{3+}_yAl_z$
'Fe^{3+}-Tsch' aen.	$Na_2Fe_4^{2+}Fe^{3+}TiFe^{3+}Si_5O_{20}$	$Fe^{2+}_ySi_z<>Fe^{3+}_yFe^{3+}_z$
Ferri -aen.	$Na_2Fe_4^{2+}Fe_2^{3+}Si_6O_{20}$	$Fe^{2+}_yTi<>2Fe^{3+}_y$
Ideal aen.	$Na_2Fe_5^{2+}TiSi_6O_{20}$	Base composition

components in the cores of aenigmatite from the aenigmatite syenite compared to those in the SQSZ (91-3) most likely reflect higher fO_2 (Larsen, 1977) of the magma. Lower fO_2 within the more evolved SQSZ (MAG 91-3) could result from continued differentiation along the aenigmatite - ilmenite - aegirine-augite buffer or the SQSZ and the aenigmatite syenite were buffered along two different fO_2-T paths.

The change of amphibole in the SQSZ and aenigmatite syenite from winchitic barroisite (MAG 91-1) to richterite (MAG 91-3 to 155) (Fig. 3.4) reflects decreases of Ca and Al and increases of Si and Na in magma composition. The linear trend defined by 91-1 and 91-3 on the Al(IV)-Si plot (Fig. 3.30) suggests that changes in the amphibole composition are due to the plagioclase ($NaSiCa_{-1}Al^{(IV)}_{-1}$) coupled substitution. Because the interstitial textures of the amphibole indicate that this mineral is not cumulate, the amphibole compositions monitor the composition of residual fluids within the rocks. This is consistent with the findings of Giret et al. (1980) who suggest that sodic amphiboles (Ca < 1.34) such as those found in the SQSZ, as well as a majority of the other rocks of the Agamenticus Complex, are typical of late magmatic to deuteric crystallization.

These findings indicate that the rocks of the SQSZ can be related by moderate amounts of fractional crystallization of oligoclase, potassium feldspar, augite, fayalite, and ilmenite. The aenigmatite syenite can be derived from the SQSZ parent magma by moderate amounts of fractionation of these minerals (FC = 52%; where FC is the proportion of cumulate to liquid). Following the

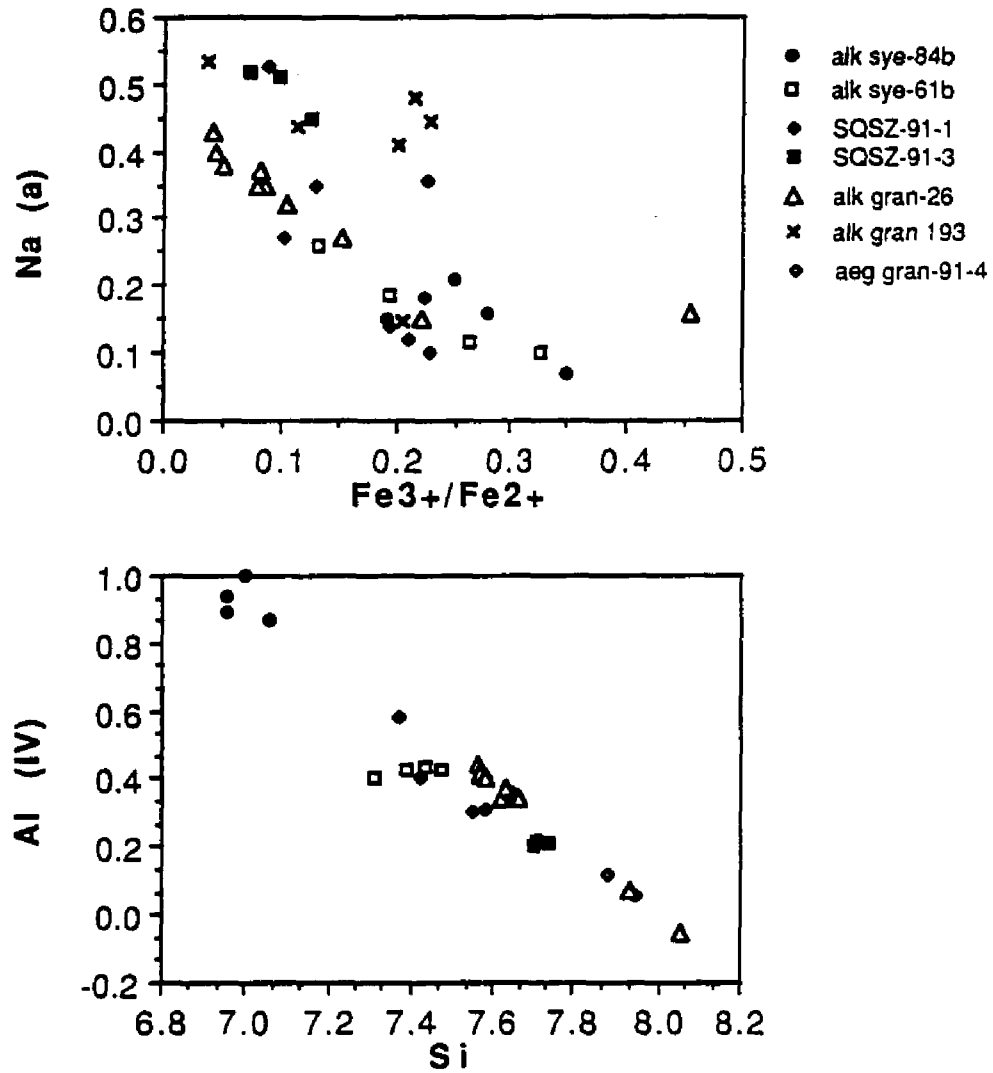

Fig. 3.30 Amphibole cation plots. The coherence of Na(A) with Fe^{3+}/Fe^{2+} and Si with Al(IV) reflect the coupled substitutions - arfvedsonite and plagioclase, respectively. Symbols as in Figure 3.12.

removal of the aenigmatite syenite the SQSZ continued to fractionate to produce more evolved liquids (i.e., 91-2, FC=71%) containing more sodic clinopyroxene compositions (Fig. 3.28). Oxygen fugacity was in part controlled by the aenigmatite - ilmenite - aegirine-augite peralkaline buffer.

Alkalic Syenite - The interrelationship of the alkalic syenites is problematic. Major and trace element variations suggest that several geochemical groups can be defined within the alkalic syenites. For example, a well defined trend that incorporates all of the alkalic syenites samples, occurs on the Al_2O_3-SiO_2 diagrams (Fig. 3.12). On the K_2O-SiO_2 and MnO-SiO_2 diagrams (Fig. 3.12) however somewhat separate fields occur for the relatively mafic, coarse-grained (MAG 39 and 72b) and relatively siliceous fine-grained alkalic syenites (MAG 2 and 3), respectively. On a number of trace element plots (for example: Ga/Al-Rb (Fig. 3.15), HFS-SiO_2 (Fig. 3.17), and Sr/Ba-Ga/Al plots; Fig. 3.31) MAG 2 and 3 and the coarse-grained alkalic syenite, MAG 61b, form a distinct trend from that defined by MAG 39 and 72b. MAG 37b occurs at the flexure between these trends on a number of the trace element diagrams (for example: HFS-SiO2, Fig. 3.17). Therefore, MAG 37b is used as a parent in least squares and trace element models developed for the alkalic syenites

The least squares models indicate that the alkalic syenites more siliceous than 37b (MAG 61b, 2, 3) can be derived as liquids by fractional crystallization of potassium feldspar, hedenbergite, fayalite, and ilmenite (Table 3.4, Σr^2 = 0.02 - 0.13; Appendix III.V.II). The alkalic syenites less siliceous 37b (MAG 72b, 39) can

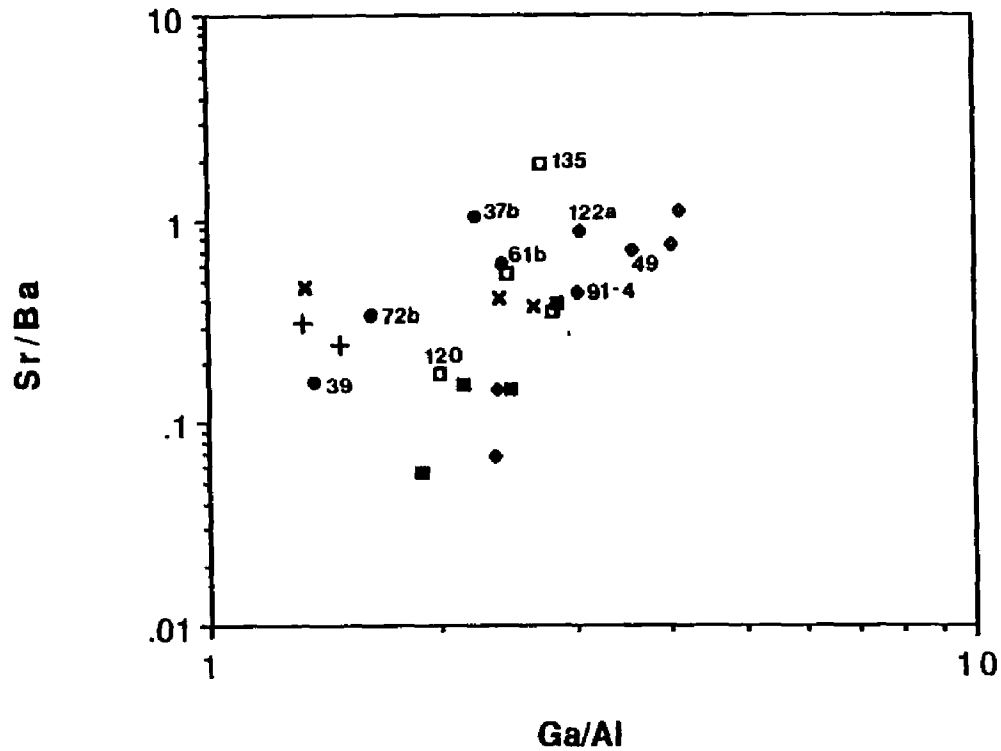

Fig. 3.31 Sr/Ba versus Ga/Al plot. This diagram emphasizes the chemical differences between the SQSZ and the alkalic syenites, the compositional continuity of the SQSZ and the aegirine granites, and the scatter of alkalic granite data. Symbols as in Figure 3.12.

be modelled as cumulates (Table 3.4, Σr^2 = 0.097 - 0.099, Appendix III.V.II) of potassium feldspar dominated fractional crystallization.

However, trace element trends calculated for MAG 2, 3, and 61b, using distribution coefficients from the SQSZ, are not compatible with this simple model (Fig. 3.32). Although the behavior of Rb and Sr in the fine-grained alkalic syenites relative to MAG 37b suggests a liquid evolution for the rocks, the incompatibility of Ba and Eu ($D^*(l)$ = -0.5 to 0.9 and 1.073, respectively; Appendix III.V.II) and the compatibility of LA and Tb (D^* (l) = 1.72 to 2.09 and 1.14 to 1.7, respectively; Appendix III.V.II) supports a cumulate relationship of the fine-grained alkalic syenites to MAG 37b. The latter is considered to be unlikely because of the sub-porphyritic to fine-grained texture of the fine-grained alkalic syenites. The trace element behavior of MAG 72b and 39 relative to MAG 37b, enrichment of Ba and Sr, the depletion of Rb, and a decrease in Ga/Al ratios (Figs. 3.15 + 3.32), support the cumulate origin for these rocks suggested by the least squares modeling. However, the amount of Ba enrichment required to produce the abundances observed in MAG 39 (2 orders of magnitudes) indicates that MAG 37b is not an appropriate parental magma for this fractionation event (Fig. 3.19; See also Cs-inst and Cs-avg for 37 b to 2, 3, and 135 models, Appendix III.V.II). Unless their trace element abundances have been significantly disturbed by fluid interaction, these results suggest that either the alkalic syenites are derived by fractionation from the different parents or that they are related to the same parent by some other petrologic process such as partial melting.

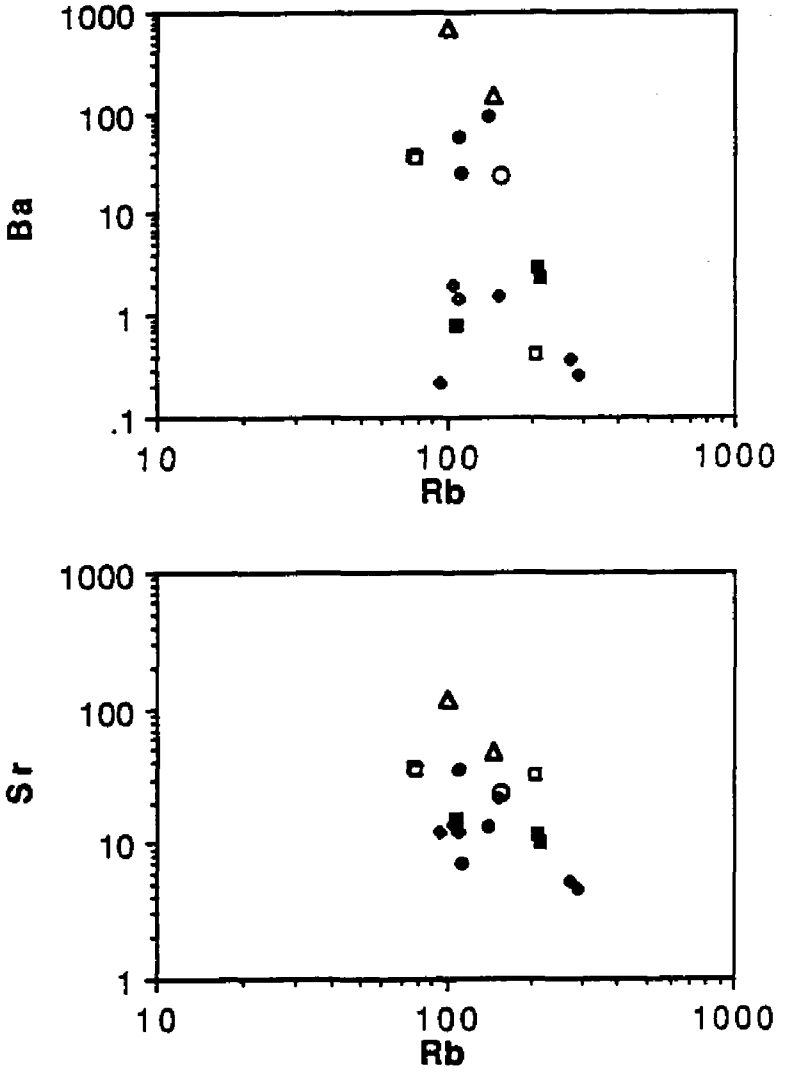

Fig. 3.32 Calculated trace element trends for the alkalic syenite using MAG 37b as a parent and the same distribution coefficients as in the SQSZ trace element model. The trace element calculations contradict the conclusions made from the least squares mixing

The presence of late magmatic fluids within the coarse-grained alkalic syenites is supported by late actinolite overgrowths on hedenbergite and fayalite and by the alteration of the fayalite. However, the linearity of the separate trends defined on the trace element diagrams by the two groups of alkalic syenites (For example; Zr-SiO2 or Nb-SiO2, Fig. 3.17) suggests that either these late magmatic fluids had little effect on the trace elements or that the effect was systematic. The latter is considered unlikely in light of the scatter in the trace elements caused by late magmatic fluids in the alkalic granites and aegirine granites and similar rocks elsewhere (Mcdonald, 1987).

The possibility that partial melting may have played a role in the development of the alkalic syenite can be tested by the use of trace elements which can distinguish between partial melting and fractional crystallization processes (Allegre and Minster, 1978). For example, variable degrees of partial melting will result in a cluster of data on a plot of compatible elements whereas fractional crystallization will develop a linear trend. The cluster observed for the alkalic syenites (MAG 37b, 2, and 3) in a Sc-Co plot (Fig. 18) suggests that they are related by partial melting from a parent in which Sc and Co are compatible elements.

Trace elements that are dominantly controlled by feldspar; i.e., Sr, Ba, and Ga can also shed light on the relative role of partial melting and fractional crystallization in these rocks. On a Sr/Ba-Ga/Al diagram (Fig. 3.31) the fractionation of potassium feldspar would result in the enrichment in both the Sr/Ba and Ga/Al ratios and the accumulation of feldspar would have the opposite effect.

Such changes are demonstrated by the positive, linear trend defined by the potassium and plagioclase feldspar controlled fractionation of the SQSZ.

The alkalic syenites form several trends on this diagram. The fractionation trend suggested by the alignment of MAG 37b, 72b, and 39 is considered unlikely due to the least squares models and trace element considerations presented above. However, this does not preclude the possibility that MAG 39 is derived as a cumulate from MAG 72b.

If MAG 37 is grouped with MAG 61b they form a trend on the Sr/Ba-Ga/Al diagram (Fig. 3.31) that is orthogonal to that of the SQSZ. Although any two points can define a trend, including these two samples in one trend is supported by linear trends define by 61b, 2, 3 and 37b on other trace element diagrams (Fig. 3.17). The orientation of this trend indicates that they can not be related by fractionation of a potassium feldspar dominated assemblage but can be derived by partial melting of a source rock in which D (Sr) < D (Ba) < 1 and D (Ga) $\leq$ 1; where D = bulk distribution coefficient. Increasing amounts of partial melting under these conditions would result in Sr becoming depleted faster in the liquid than Ba and a consequent decrease in Sr/Ba ratios. Although highly speculative due to the small number of data points that define the observed trend, this model is supported by the partial melting signature for these rocks on the Sc-Co diagram.

The incompatible behavior of Ba and Sr and compatible behavior of Sc and Co required by this model indicate that the bulk distribution coefficients were not controlled by plagioclase and/or

potassium feldspar. However, the large amount of scatter observed for the granites on the Sr/Ba-Ga/Al diagram suggest that this diagram is sensitive to non-liquid -solid equilibrium processes. Therefore, it is obvious that additional analyses of the alkalic syenite are required to determine which, if any, of the observed trends defined by the alkalic syenites are petrologically meaningful.

Clinopyroxene compositions are available from a restricted number of alkalic syenite samples in the north central portion of the complex. Within the fine-grained alkalic syenite at MAG 61 (Plate 1), augite occurs within potassium feldspar phenocrysts and ferrian-sodian augite is present within the matrix. The change in clinopyroxene compositions (Fig. 3.28) indicates that the magma became enriched in sodium and ferric iron and depleted in magnesium as crystallization progressed (see analyses for MAG 61-cpx 1 or 2 and cpx 4-8; Appendix III.V.III).

The composition of the clinopyroxenes in the coarse-grained alkalic syenite from the same locality, MAG 61b, are nearly identical to those in the matrix of the fine-grained alkalic syenite (See analysis MAG 61-cpx 14; Appendix III.V.II). If these two rocks are related, the coarse-grained alkalic syenite is more chemically evolved than the fine-grained alkalic syenite. The inclusion of fine-grained alkalic syenite clasts within the coarse-grained alkalic syenite at this locality is consistent with this interpretation. Hedenbergites from a coarse-grained alkalic syenite at the alkalic syenite-alkalic granite contact, MAG 84b, contain slightly less sodium than the augites present in MAG 61b (Fig. 3.28; Appendix III.V.II). The compositional zoning in these hedenbergites, slightly

more sodium- enriched and magnesium-depleted rims, is similar to that in the augites from MAG 61a. Together, the hedenbergites and augites form a compositional trend that is similar to, but less sodium enriched than, a portion of the SQSZ trend. This suggests the augite alkalic syenites at MAG 61 can be related to the hedenbergite alkalic syenites by fractional crystallization.

The inability to interrelate the alkalic syenites by petrologic modeling suggests that the alkalic syenite is composite. Further, the location of MAG 39 and 37 relative to the partial melting trend defined by the other alkalic syenites suggests that they are derived from a separate parent.

In addition, many of the geochemical and mineralogical features of the alkalic syenites indicate that the evolution of all of the alkalic syenites is separate from the other alkalic rocks within the complex: 1) Significant differences are observed in major element parameters. For example, these rocks are metaluminous (Fig. 3.22), generally have higher (Na+K)/(Si/6) values (Fig. 3.22), and define separate enrichment trends on a number of major element Harker diagrams (Fig. 3.12). The separate major element trends indicate that they are not part of a fractionation series related to the SQSZ, and mass-balance calculations indicate that they are not cumulates from alkalic granite fractionation (Fig. 3.33). 2) The alkalic syenites define separate trends on a number of trace element diagrams (For example; Ga/Al vs. Rb or Ba, Eu* vs. Rb or Sr, Ga or Sr vs. SiO_2). Trace element calculations support the conclusions that the alkalic syenites can not be derived as cumulates from the fractional crystallization of alkalic granites

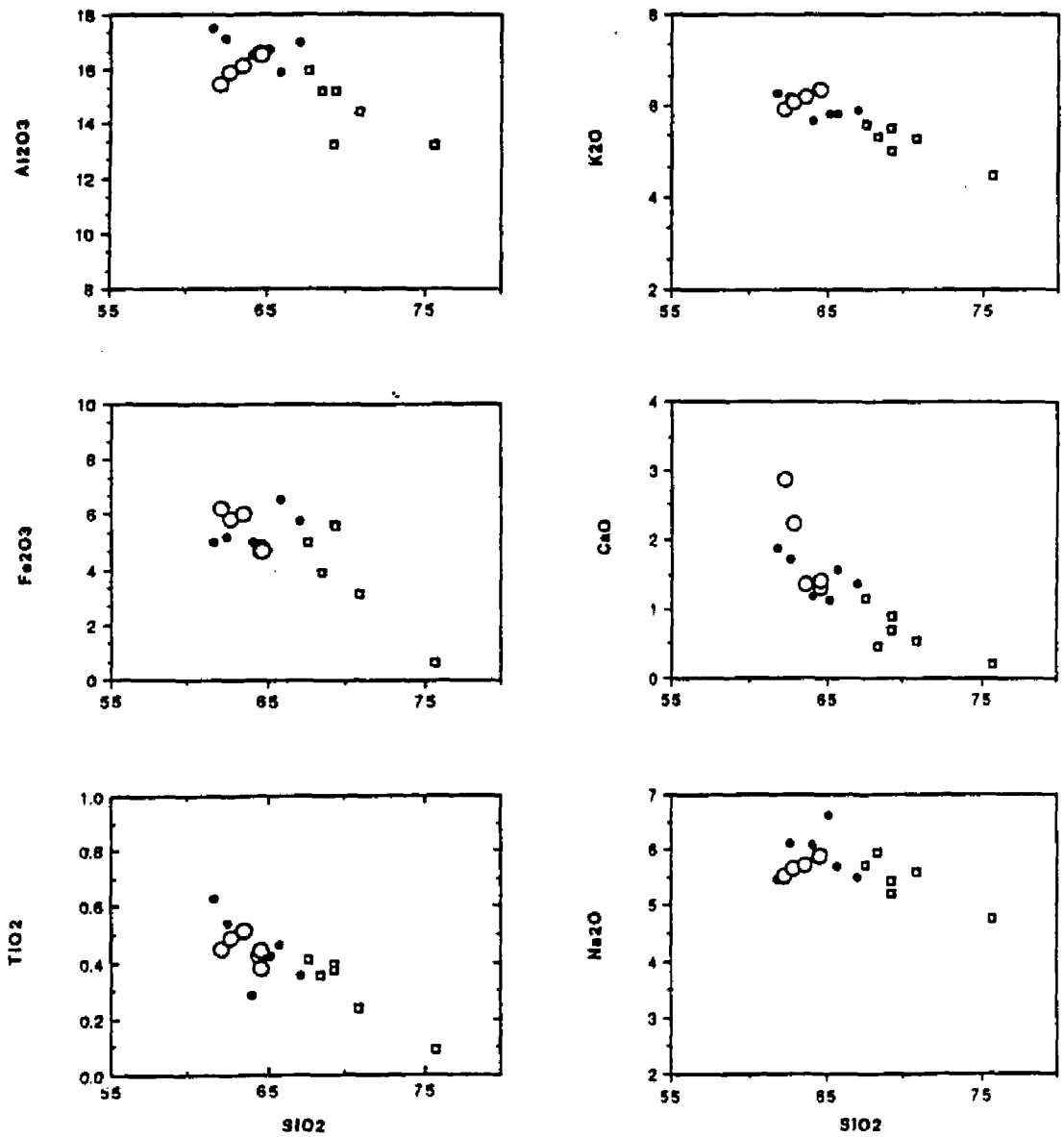

Fig. 3.33 Calculated cumulate compositions (O) from the fractionation of the alkalic granites. Comparison of the cumulate compositions to the alkalic syenites supports the conclusion that the alkalic syenites (•) are not cumulates of an alkalic granite (□) fractionation.

3) The less siliceous alkalic syenites (MAG 39, 72b, and 84b) contain greater proportions of olivine (Table 3.1) and less sodic clinopyroxene (Fig. 3.28) and amphibole (Fig. 3.4) than SQSZ rocks with corresponding amounts of SiO_2. These modal and composition differences support the conclusions that the alkalic syenites can not be derived by feldspar dominated fractional crystallization, either as cumulates or liquids, from any of the other rocks within the complex. 4) Differences in P_{H2O} are implied by hypersolvus textures in the alkalic syenite versus subsolvus textures in the SQSZ.

Quartz Syenite to Alkalic Granite - Least squares mixing models were calculated that relate the quartz syenite, MAG 120, to the most siliceous alkalic granites, MAG 26 and 23. MAG 120 was selected as a parent because it was located nearest to a larger number of the major element flexures on the Harker diagrams than the other rocks. This places MAG 120 at the mafic end of the linear trend defined by the alkalic granites.

Although MAG 23 is subsolvus and contains plagioclase, the fractionation models do not use plagioclase as a fractionating phase for several reasons: 1) The other alkalic granites and quartz syenites that are potential parents from this zone are hypersolvus. 2) The subsolvus texture of MAG 23 is interpreted to be due to increased volatile concentration in the fractionating liquids. Therefore, the plagioclase was a late magmatic mineral that was incapable of changing the composition of the magma. 3) The low normative An content ($An_{0.9}$, Table 3.2) of this rock indicates that

fractionation of plagioclase would have little affect on the CaO content of the rocks.

As in the SQSZ, the compositions and textural features of the amphiboles from this zone indicate that they crystallized late in the magmas history. Therefore, amphibole was not included in the petrogenetic models because it likely effected only the most evolved alkalic granites and their residual fluids.

The least squares mixing models accurately reproduce the data (Σr^2 = 0.19 - 0.12, Table 3.4; Appendix III.V.III) and indicate proportionally increasing amounts of potassium feldspar fractionation with only small changes in the amount of clinopyroxene and olivine required. The large scatter of the trace elements controlled by potassium feldspar crystallization (i.e., Rb, Sr, Ba; Fig. 3.14, 3.15) made trace element modeling ambiguous. Using the distribution coefficients from the SQSZ model, trace element models calculations suggest that the alkalic granite products are cumulates (Fig. 3.34 a) or liquid-cumulate mixtures (Fig. 3.34 b). This obviously contradicts the least squares models which indicate that these rocks are related by liquid evolution.

If the calculated liquid trend is fit to the observed Rb abundances by increasing the distribution coefficients, it can be shown that the depletion of Rb (Fig. 3.35) is consistent with fractional crystallization of potassium feldspar with a distribution coefficient greater than 1 (Maximum Kd (Rb) = 1.9; Appendix III.V.III). Although the required distribution coefficient is higher than typical values for intermediate compositions (Lemarchand et al., 1987; Long 1978), similar distribution coefficients for Rb have

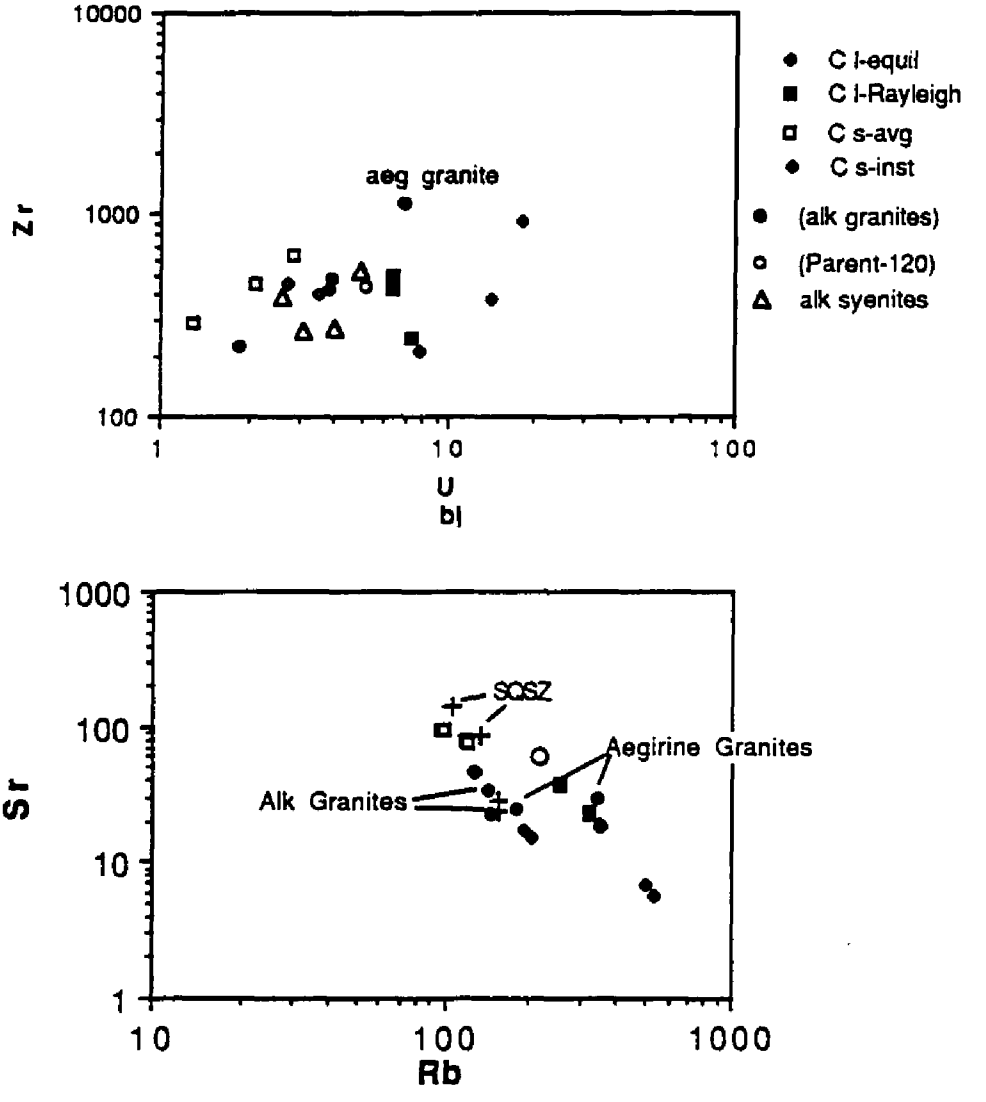

Fig. 3.34 Trace element fractionation trends calculated for the alkalic granites using the distributions from the SQSZ model. This model suggests that alkalic granites are cumulates and/or cumulate-liquid mixtures it is not accepted. This trace element model is not accepted because it contradicts the model derived from least squares mixing calculations. Symbols for model compositions; Filled squares-residual liquid, filled diamonds-liquid from Rayleigh fractionation, open diamonds-instantaneous cumulate, open squares-average cumulate (see Appendix V for formulas used to calculate these compositions). Other symbols; open circle-parent (MAG 120), • - alkalic granite compositions used as input for product of fractionation.

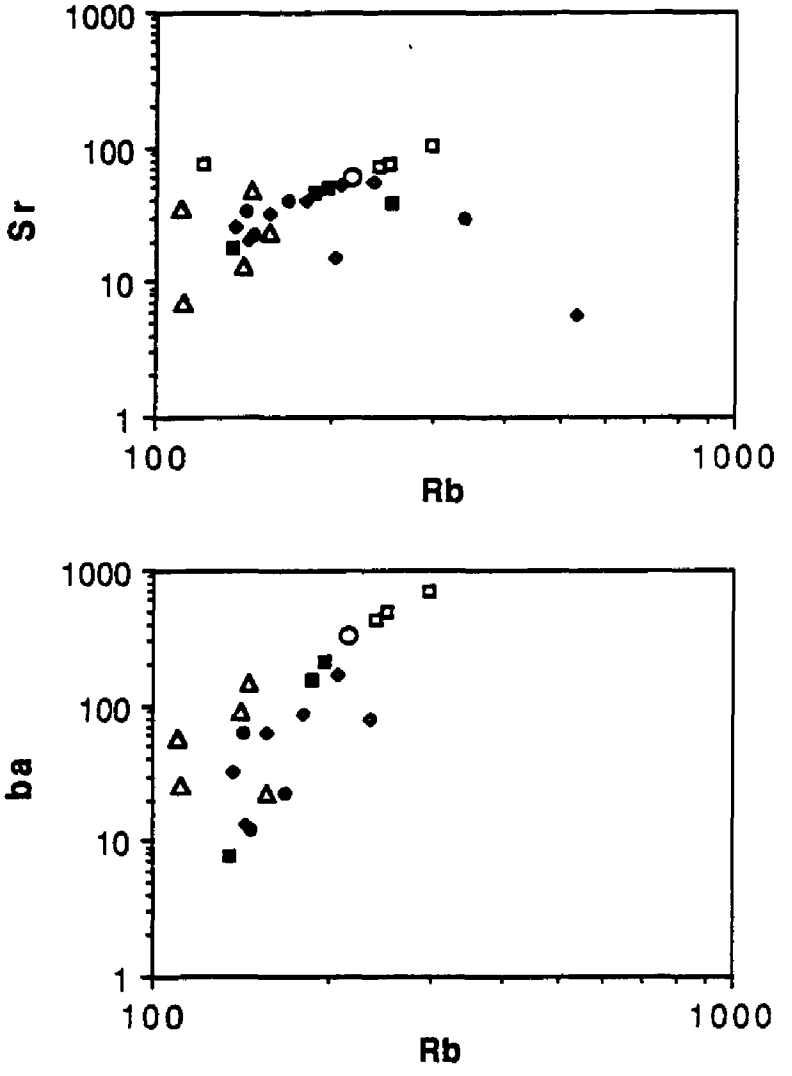

Fig. 3.35 Trace element fractionation trends calculated by adjusting the distribution coefficients and assuming that the alkalic granites are liquids. The overlay of data from the alkalic syenites (filled circles and open triangles) supports the conclusion that the alkalic syenites are not derived as cumulates from the fractionation of the alkalic granites. Symbols as in Fig. 3.34

been determined for high-silica rhyolites from Twin Peaks, Utah (Nash and Crecraft, 1985). Ba and Sr distribution coefficients (Appendix III.V.III) required to balance these elements in the MAG 120 to 135 (Kd (Ba) = 7 and Kd (Sr = 3) and MAG 120 to 23 (Kd (Ba) = 3 and Kd (Sr = 1.8) models vary significantly.

Nash and Crecraft (1985) and Mahood and Hildreth (1983) suggest that although distribution coefficients correlate positively with the degree of melt polymerization, the volatiles within the magma become the dominant control on trace element partitioning during late crystallization of siliceous magmas. The late crystallization of acicular riebeckite and arfvedsonite, the presence of interstitial fluorite and calcite, and the change from hypersolvus to subsolvus textures all suggest that volatiles also played a role during the late magmatic development of the more evolved alkalic granites. These volatiles are the likely cause of anomalous trace element behavior for the alkalic granites; i.e., Ba depletion in MAG 135, Ga depletion in MAG 120, and possibly Rb enrichment in MAG 120 (Fig. 3.14 + 3.36).

On the basis of the distribution coefficients used in the petrogenetic model relating the quartz syenite to the alkalic granite, feldspar dominated fractionation would result in a decrease of Eu*, an enrichment of total REE and a depletion of Rb, Sr, and Ba (Appendix III.V.III, see calculated bulk Kd). These changes are observed on a plot of Eu* vs. Rb but are inconsistent with the relationships for the alkalic granites on the Eu* vs. Sr plot (Fig. 3.15) and with the observed change in total REE abundances (Figs. 3.20 + 3.21). Total REE abundances cluster around the abundances

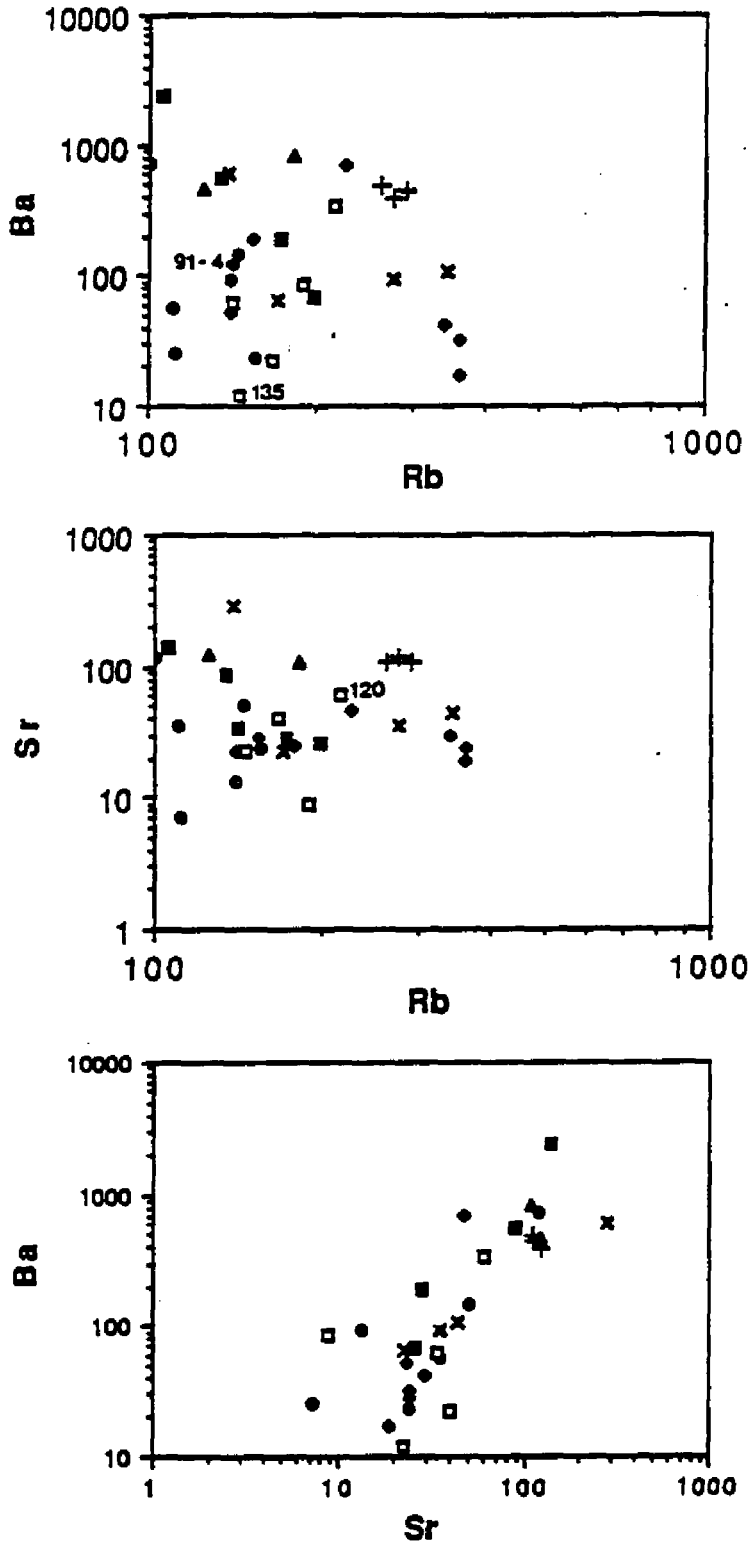

Fig. 3.36 LIL-LIL plots. Note the scatter for the alkalic granites, aegirine granites, and alkalic syenites. Symbols as in Figure 3.12.

for MAG 5 and 17 (Fig 3.20). Relative to MAG 5 or 17, MAG 120 is LREE-enriched and MAG 135 is HREE-enriched. If MAG 5 or MAG17 are parental rocks, then zircon fractionation could produce the REE pattern of MAG 135 by slightly lowering total REE and depleting HREE relative to LREE. Conversely, LREE enrichment in MAG 120 would be produced by zircon accumulation. The relative Zr abundances of the rocks is compatible with this suggestion (Fig. 3.17). However, zircon accumulation implies that MAG 120 and 135 are cumulates rather than parents for MAG 5 and 17. The contrasting behaviors of Eu*, Rb, and Ba in MAG 120 ad 135 (Fig. 3.15) indicate that a common cumulate origin for the two is not possible.

An alternative suggestion is that volatiles and/or late magmatic fluids that disturbed the other trace elements also effected the REE patterns. Mahood and Hildreth (1983) and Nash and Crecraft (1985) suggest that increasing volatile content results in an overall decrease in REE partition coefficients and a larger decrease for HREE than LREE. This would result in HREE enrichment in the liquids and LREE enrichment in the cumulates during fractionation. Bowden and Whitley (1974) note that the REE patterns for alkalic granites from Nigeria that have experienced albitization associated with late magmatic autometasomatism by alkali- and fluorine-rich fluids exhibit HREE enrichment and a decrease in Eu*. Similar processes could have effected the alkalic granites. However, the effect of these processes would be difficult to assess because of the variable nature (Parsons and Becker, 1986) of fluid and/or volatile interaction

The small change in Ga abundances on the Ga-SiO2 diagram (Fig. 3.14) indicate that Ga has a distribution coefficient closer to one in the alkalic granite, and the aegirine granites, than in the SQSZ and other syenites. This could reflect a larger distribution coefficient for Ga in potassium feldspar than for plagioclase and/or the affinity of Ga for Fe^{3+} (Gottardi et al, 1978). Ferric iron enrichment in the clinopyroxenes during fractionation, such as that demonstrated for the SQSZ, would result in the enhanced incorporation of Ga into these minerals. The fractionation of ferric iron rich clinopyroxenes from the early alkalic granites would therefore result in the depletion of Ga in the liquid.

Because amphibole is the only mafic silicate mineral present in all of the alkalic granites, it provides the sole mineral monitor for changes in magma compositions for these rocks. As discussed above, the amphiboles are thought to have had only minor influence on magma evolution and reflect late magmatic or subsolidus fluid composition.

Amphibole compositions were determined for two alkalic granites (MAG 26 and 193, Plate 1) from the southwestern portion of the quartz syenite to alkalic granite lobe. The most sodic amphiboles in these rocks, riebeckite and arfvedsonite, crystallized as rims or acicular overgrowths on barroisite and katophorite cores, respectively. In other alkalic granites petrographic evidence indicates that the sodic amphiboles formed as late interstitial grains. The arfvedsonite and riebeckite trends (Fig. 3.4; MAG193 and 26, respectively) and calculated Fe^{3+}/Fe^{2+} (Fig. 3.30) for the

two sets of amphiboles analyzed suggest that fO_2 was variable within the alkalic granite.

These changes in amphibole compositions partially overlap the amphibole compositions of the SQSZ and the aenigmatite syenite. This suggests that either the alkalic granite is derived from another parent than the SQSZ or that amphibole crystallized earlier in the alkalic granite than in the SQSZ. The latter can not be attributed to higher P_{H2O} because the alkalic granites are hypersolvus whereas the SQSZ is subsolvus.

The amount of scatter in the trace element data from the alkalic granites makes it difficult to test least squares models relating these rocks to the other alkalic rocks within the complex. The results from least squares models relating the SQSZ to the alkalic granites are unacceptable (Table 3.4; Σr^2 = 1.33 to 1.13, for MAG 51-d or 91-2 to 120, respectively; Appendix III.V.III). Although the large sodium residuals in these models may in part be inherited from the sodium errors already discussed for the SQSZ, they could also indicate a separate evolution for the two groups of rocks.

This is supported by the hypersolvus versus subsolvus textures of the alkalic granites and SQSZ, respectively. If the alkalic granites are derived from the SQSZ rocks, then the textures indicate that P_{H2O} changed during the magma evolution. If $P_{H2O} = P_{Total}$ the change in P_{H2O} could simply reflect a difference in emplacement level or depth within the magma chamber; i.e., shallower levels, $P_{H2O} \leq$ 2.5 kbar (Luth et al., 1973) and Bonin, 1986), for the alkalic granite relative to the SQSZ. Both of these would require somewhat fortuitous circumstances. Assuming that

the alkalic granites and the SQSZ both evolved at nearly the same level in the crust (i.e., same total pressure), then both would have crystallized two feldspars. The lack of two feldspars within the alkalic granite, as observed within the SQSZ, would therefore require the unlikely condition that it was emplaced entirely as a liquid.

Alternatively, if $P_{H2O} < P_{Total}$ then the lower P_{H2O} of the alkalic granites may reflect changes in magmatic conditions, such as volatile release associated with volcanic eruption. Volatile release during and following eruption has been shown to have a large effect on the chemical and rheologic evolution of trachytic volanoes in Kenya (Mcdonald, 1987). The association of geochemical and volatile gradients within magma chambers (Mcdonald ,1987; Hildreth, 1981) could also help explain the large scatter of trace element abundances observed in the alkalic granite. For example, the Ba depletion in MAG 135 or Rb enrichment of MAG 120 noted above could reflect the lower and upper levels (after Mcdonald, 1987), respectively, of the magmas within the magma chamber prior to the emplacement at the current levels. The decrease in HFS elements between the SQSZ and alkalic granite on the HFS-SiO2 diagrams (Fig. 3.17) might also represent a "resetting" due to the removal of these elements in the volatile enriched eruptive rocks. This resetting could also help explain the overlap of the alkalic granites and the SQSZ on the Zr-Y and Th-U diagrams (Fig. 3.18).

A third explanation for the differences in implied P_{H2O} is that the alkalic granites are not related to the SQSZ but rather to another alkalic rock within the complex or a separate parent

altogether. The hypersolvus textures observed in the alkalic granites and syenites, the coherence of MAG 135 with alkalic syenite trends on several of the trace element diagrams (i.e., Ga/Al-Ba (Fig. 3.15) or Sr/Ba-Ga/Al (Fig. 3.31)), and the good results from least squares mixing models (MAG 37b to 120), all support a genetic relationship between the alkalic granite and syenite. However, trace elements for alkalic granites other than MAG 135 show no systematic relationship to the alkalic syenite and MAG 135 is not associated with the alkalic syenites on all trace element plots. This suggests that large scatter of trace elements in the alkalic granite may have resulted in the fortuitous juxtaposition of MAG 135 and the alkalic syenites on the trace element plots cited above.

If the alkalic granites are related to a separate parent from the other rocks within the complex, the scatter observed within the trace element diagrams could reflect inhomogeneities within the source rock. The horizontal scatter of trace elements on the Sr-Rb plot is suggestive of trace element behavior expected during partial melting (Cocherie, 1986)

Aegirine Granites - The aegirine granites can be separated into two groups on the basis of silica content (Fig. 3.12), texture, and intrusive style. Group one is composed of aegirine granites with the lower silica content, that are medium-grained, and that occur as large stocks or plugs (MAG 49 and 122a). High silica, medium to fine-grained dikes (MAG 48, 47, and 91-4) make up the other group. As noted previously, several of the dikes (MAG 47 and 48) intrude the medium-grained aegirine granite (MAG 49) along the eastern

border of the complex. This cross-cutting relationship and a higher silica content suggests that the dikes are fractionates derived from the medium-grained alkalic syenite.

A least squares model relating representative samples from these groups (MAG 49 to 48, Appendix III.V.IV) yields good results using a fractionating assemblage of potassium feldspar, Ti-magnetite and either hedenbergite or aegirine (Table 3.4; Appendix III.V.IV; MAG 49 to 48). Although the textural relationships within the aegirine granites indicate that quartz was in equilibrium with the other minerals, the inclusion of quartz as a cumulate mineral does not improve the residuals from the model.

Trace element calculations for the model calculated using hedenbergite (Appendix III.V.IV) indicate that Rb is slightly incompatible ($D^* = 0.8$) and Sr and Ba are equally compatible ($D^* = 1.58$ and 1.76, respectively). Because potassium feldspar dominates the cumulate assemblage (Table 3.4), this mineral controls the bulk distribution coefficients. The calculated bulk distribution coefficients for Ba and Sr are significantly lower than those of sanidines from other rhyolites (Lemarchand et al., 1987; Mahood and Hildreth, 1983; Nash and Crecraft, 1985) and indicate that they were not controlled by crystal-liquid equilibrium.

Rb and Ba abundances for the two aegirine granites that intrude the SQSZ are not consistent with derivation by fractional crystallization. Both are significantly depleted in Rb and MAG 91-4 is slightly enriched in Ba (Fig. 3.15 + 3.36). The coincidence of these disturbed trace element signatures in the aegirine granites and the intrusion of these granites into the SQSZ suggests a genetic

relationship. However, because the Rb values of the disturbed aegirine granites are lower than the trend defined by the SQSZ (Fig. 3.36), the assimilation of the SQSZ would not produce the observed Rb of the aegirine granites. The similarity of the aegirine granite Rb values to those of the most evolved alkalic granites and portions of the alkalic syenite (Figs. 3.15, 3.31 and 3.36) indicate that interaction with either of these rocks at a deeper level could help explain the observed variations.

Although such assimilation can not be ruled out, volatile and/or fluid interaction, such as observed in the alkalic granites, could also cause the scatter observed in the trace elements. Fluid interaction in the aegirine granites is supported by calcite alteration of the aegirine, the presence of interstitial fluorite, and cross-cutting quartz and calcite micro-veins.

The effects of these fluids can also be seen in the REE elements (Fig. 3.20). For example, the REE pattern of MAG 47 exhibits LREE depletion that is incompatible with any reasonable model of fractional crystallization. In addition, the relative total REE abundances of the other aegirine granites suggest either that MAG 49 is not an appropriate parent for the fractionation model or that the abundances are not controlled by potassium feldspar fractionation. The observed change in REE patterns, not including MAG 47, is more compatible with a fractionation model in which MAG 122a is a parent and MAG 49 is more evolved than MAG 48. However, the latter contradicts the major and trace element trends for these rocks which suggest that MAG 49 is less evolved than MAG 47. These data suggests that the volatile or fluid interaction

resulted in the REE enrichment of MAG 49 and the LREE depletion of MAG 47.

Additional evidence for the interaction with fluids is the large degree of scatter observed within the aegirine granites on the Nb/Ta-Zr/Hf plot (Fig. 3.19). The decreases of Zr/Hf observed for the aegirine granites may reflect the higher stability (Wedepohl et al. 1987) of zirconium fluoride complexes relative to those formed by hafnium. The differences in stability could allow the preferential leaching of Zr from zircons during autometasomatic events (Bayer et al., 1978).

Because all of the clinopyroxenes analyzed from the aegirine granite are essentially pure aegirine, they provide little insight into magma evolution. However, clinopyroxene compositional trends from other alkalic complexes are similar to those defined by the clinopyroxenes from the SQSZ and the aegirine granite (Fig. 3.28). Within these complexes aegirine stability results from the complex interplay of Na enrichment and amphibole stability (Ferguson, 1978; Nicholls and Carmicael, 1969). Increasing sodium content within the magma can lead to the instability of sodic amphiboles and a subsequent reaction to from aegirine. The compositional gap that is observed within suite of rocks from the same complex therefore results from the greater stability of amphibole than aegirine at lower magmatic sodium contents. The size of the clinopyroxene compositional gap depends on the stability range of the amphibole, which in turn is dependant on $P_{volatiles}$ and magma composition (Ferguson, 1978). The amphibole to clinopyroxene transition can be seen within the northeastern portion of the aegirine granite where

aegirine has formed at the expense of riebeckite-arfvedsonite. The subsolvus texture of the aegirine granite suggests aegirine stability was promoted by increasing sodium content rather than decreasing P_{H2O}.

The colinearity of portions of the aegirine granite and the SQSZ on Ga/Al versus Ba (Fig. 3.14) and Sr/Ba-Ga/Al (Fig. 3.31) diagrams suggests that they are related by fractional crystallization. However, this is unsupported by least squares mixing models relating the two (Σr^2 = 1.364, for MAG 91-2 to 49, Table 3.4; Appendix III.V.IV). Better results can be obtained from least squares mixing models relating the alkalic granite to the aegirine granite. These findings suggest that the aegirine granite could have evolved from either the alkalic granite and/or the SQSZ. For example, the trace element scatter, such as observed on Ga/Al-Rb, Sr/Ba-Ga/Al, or REE plots, could reflect differing liquid evolution paths instead of volatile/fluid interactions. The Ga/Al-Rb diagram suggests that the aegirine granites located along the eastern border of the complex (MAG 47,48,49) are derived from the SQSZ and that the aegirine granites that intrude the SQSZ and the SQSZ-alkalic granite contact are related to the alkalic granite. These models can only be assessed after the degree of volatile and/or deuteric interaction within the rocks is further investigated.

Biotite granite - The small amount of variation observed for the biotite granites on major element and a majority of the trace element diagrams indicates that the biotite granite is fairly homogeneous and precludes a comprehensive analysis of the petrologic evolution of these rocks. Compositionally zoned

plagioclase phenocrysts and negative Eu* anomalies (Fig. 3.20 and 3.21) suggest that, prior to emplacement, these rocks evolved towards more sodic compositions by disequilibrium fractional crystallization. Inclusion free phenocrysts of plagioclase and potassium feldspar indicate that the early fractionation was dominated by both feldspars. Euhedral biotite and amphibole textures indicate that these minerals likely played an important role as cumulate phases as fractionation progressed. The removal of zircon and apatite from the rocks during their evolution is suggested by observed variations in Th, U, Zr, Nb, and Y (Figs. 3.17 + 3.18) and P_2O_5 (Fig 3.12), respectively.

As noted previously, the textures, mineralogy, and chemistry of this rock indicate that it evolved from a different parent than the other rocks within the complex. In addition, the separate fields defined by these rocks on a number of major and trace element diagrams (i.e., P_2O_5, Na_2O, and MgO (Fig. 3.12) or Ga and Sr (Fig. 3.14) indicates that these rocks did not experience significant, if any, interaction with the alkalic rocks in the complex thru assimilation and/or mixing processes.

Controls on HFS element abundances

As noted previously, the changes in Zr, Th, U, and Nb abundances follow consistent enrichment and depletion trends on trace-SiO2 diagrams; enrichment occurs between the alkalic rocks and depletion occurs within the individual alkalic rocks. The enrichment trend is offset towards lower trace element abundances between the syenites and granites.

These trends are considered to reflect magmatic processes, more specifically zircon stability, with some degree of deuteric overprinting. On a Zr-M diagram (Fig. 3.37; where M = (Na+K+2Ca)/(Al+Si), units in cation proportions) the samples that define the enrichment pattern on the Zr-SiO2 diagram, MAG 91-1, 91-2, 37, and 49, define the upper limit a Zr-M field that encompasses all of the other samples. MAG 120, which is located at the offset of the enrichment trend on the HFS-SiO2 diagrams, is located slightly below the boundary of the Zr-M field.

It is important to note that some of the samples have M values greater than the maximum limit (Watson and Harrison, 1983) for which the zircon saturation curves on this diagram are valid . These samples are therefore, considered to be projected onto the Zr-M surface from within an undetermined Zr-M-Zircon saturation volume. In addition, caution must be used when applying the saturation temperatures determined from Figure 3.37 as indicators of magmatic conditions because they do not take into account other magmatic variables that affect zircon stability such as fluorine content. Dietrich (1968) has demonstrated that zircon stability is decreased in the presence of fluorine because of the preferential complexing of zirconium with fluorine (i.e., Na_2ZrF_6). The presence of fluorite in the alkalic and aegirine granites indicates that fluorine was involved in the evolution of the Agamenticus Complex. Therefore, the zircon saturation curves presented on Figure 3.37 are not strictly applicable to rocks from the Agamenticus Complex and the temperatures suggested below provide only a crude approximation of magmatic temperatures.

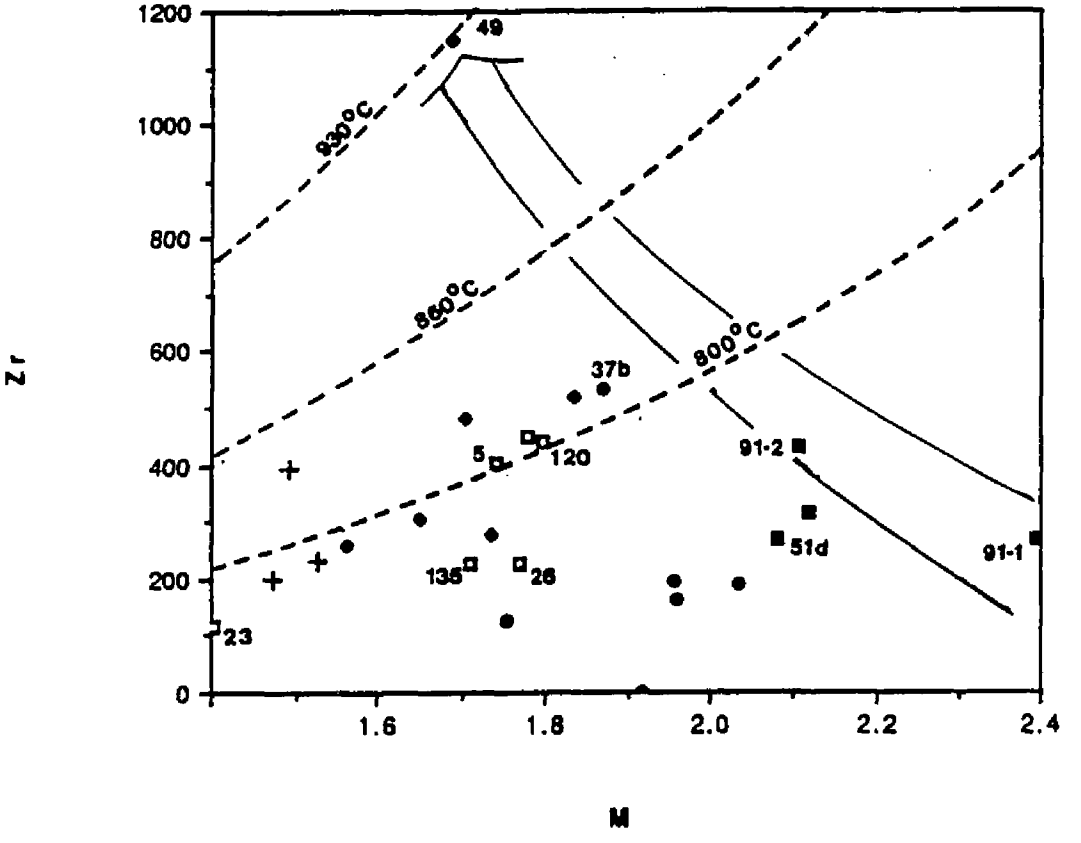

Fig. 3.37 Zr-M diagram after Watson and Harrison (1983). The trend from MAG 91-1 to 49 defines a liquidus trend before zircon stability. Zircon saturation curves help define liquidus temperatures for the other rocks. Symbols as in Figure 3.12.

With these qualifiers in mind, the rocks that define the upper limit of the Zr-M field on the Zr-M plot are interpreted to from a continuous "liquid line of descent" under zircon absent conditions. As fractionation progresses from MAG 91-1 to 91-2 to 49, Zr abundances increase and temperature decreases until zircon saturation occurs at approximately 930°C.

The abundance of Zr in the alkalic rocks within the Zr-M field are determined by several processes. Separation of magmas from the evolving primary liquid described above would result in separate magma batches with new initial Zr values. This stage could reflect the tapping of an underlying magma chamber and emplacement of the magma at higher crustal levels. Fractional crystallization of these separated magmas under zircon absent conditions would lead to a Zr increase and M decrease in the liquids. As in the SQSZ, initial zircon saturation is reached in the evolving magma as temperature decreases and Zr increases.

Following zircon saturation the magma can either evolve at constant temperature, i.e., buffered on the saturation curve or fractionate zircon as temperature continues to decrease. The first would result in Zr-M paths parallel to the zircon saturation curves and the latter would result in the preferential decrease in Zr relative to M; for example MAG 120 or 17 to MAG 5 to MAG 23 and MAG 5 to MAG 135 and 23 respectively. Based on the discussion of the behavior of Zr relative to Hf in the aegirine granite, the large decreases in Zr observed in the aegirine granites on the Zr-M plot are in part due to late fluid interaction.

This diagram therefore helps place several important constraints on the evolution of the Agamenticus Complex. Textural evidence, such as the occurrence of zircon within amphibole and as late intercrystalline crystals, suggests that zircon crystallized late in the cooling history of the alkalic rocks. Therefore, the zircon saturation temperatures estimated using the Zr-M saturation curves represent late magmatic conditions. It can be seen that a majority of the granites, and one alkalic syenite (MAG 37b), fall within a fairly restrictive range near to the 800°C Zr saturation curve. Several rock trends are sub-parallel to saturation curves defined by true isothermal buffering (i.e., MAG 120 to 23). This suggests that cooling within the portions of the complex was slow enough to allow partial buffering of Zr to occur. The sub-solidus zircon saturation temperatures estimated for the alkalic syenite and the lack of zircons in these rocks indicate that they did not reach zircon saturation. In contrast, the SQSZ rocks have sub-solidus estimated temperatures for zircon saturation but contain zircon as a late magmatic mineral. This suggests that zircon saturation is more accurately predicted for the alkalic syenites than for the SQSZ on the Zr-M diagram and provides additional evidence for the disparity between the two magmas.

Source considerations

The petrologic models presented above suggest that the SQSZ, the alkalic syenite, and, possibly, the alkalic granites were derived from separate parents. As noted previously, syenite and granite magmas in other alkalic complexes are considered to be the products of fractional crystallization of alkalic olivine basalt or derived by

partial melting of basalts or mafic to felsic granulites (Eby, 1987; Collins et al, 1982; Bailey and Schairer, 1966 ; Clemens et al. 1986).

Geochemical signatures, such as REE patterns (see Nelson et al., 1987; Fig. 6) , trace element abundances (Fig. 3.38), or major element trends (Fig. 3.38), of the most mafic SQSZ are similar to syenites observed in other alkalic complexes where an alkalic olivine basalt lineage is supported by field evidence put. However, the mafic enclaves, xenocrysts, or large amounts of mafic cumulates that are indicative of such complexes are absent in the Agamenticus Complex. Therefore, if the SQSZ is derived from a basalt parent, separation of the SQSZ fractionates from the basalt parent occurred deep within the crust. In addition, the fractionates did not comingle with the basalt parents following separation.

Although there is no geophysical evidence to support the presence of mafic rocks within the upper crust, as observed for several of the WMS bodies, a gravity high occurs beneath the Agamenticus on low frequency residual maps (Brooks, 1989). This could represent a basalt component of the Agamenticus Complex located at lower crustal levels or, just as likely, be a continuation of a gravity plateau associated with mafic lithologies underlying the Casco Bay region to the north (Brooks, 1989).

Melting of such mafic lithologies at amphibolite to granulite facies is capable of providing a source for syenites to quartz syenites (Bailey and Schairer, 1966; Helz, 1973, 1976; Peterson and Newton, 1989; Clemens and Vielzeuf, 1987). Melting of mafic source rocks with varying compositions would provide a mechanism for

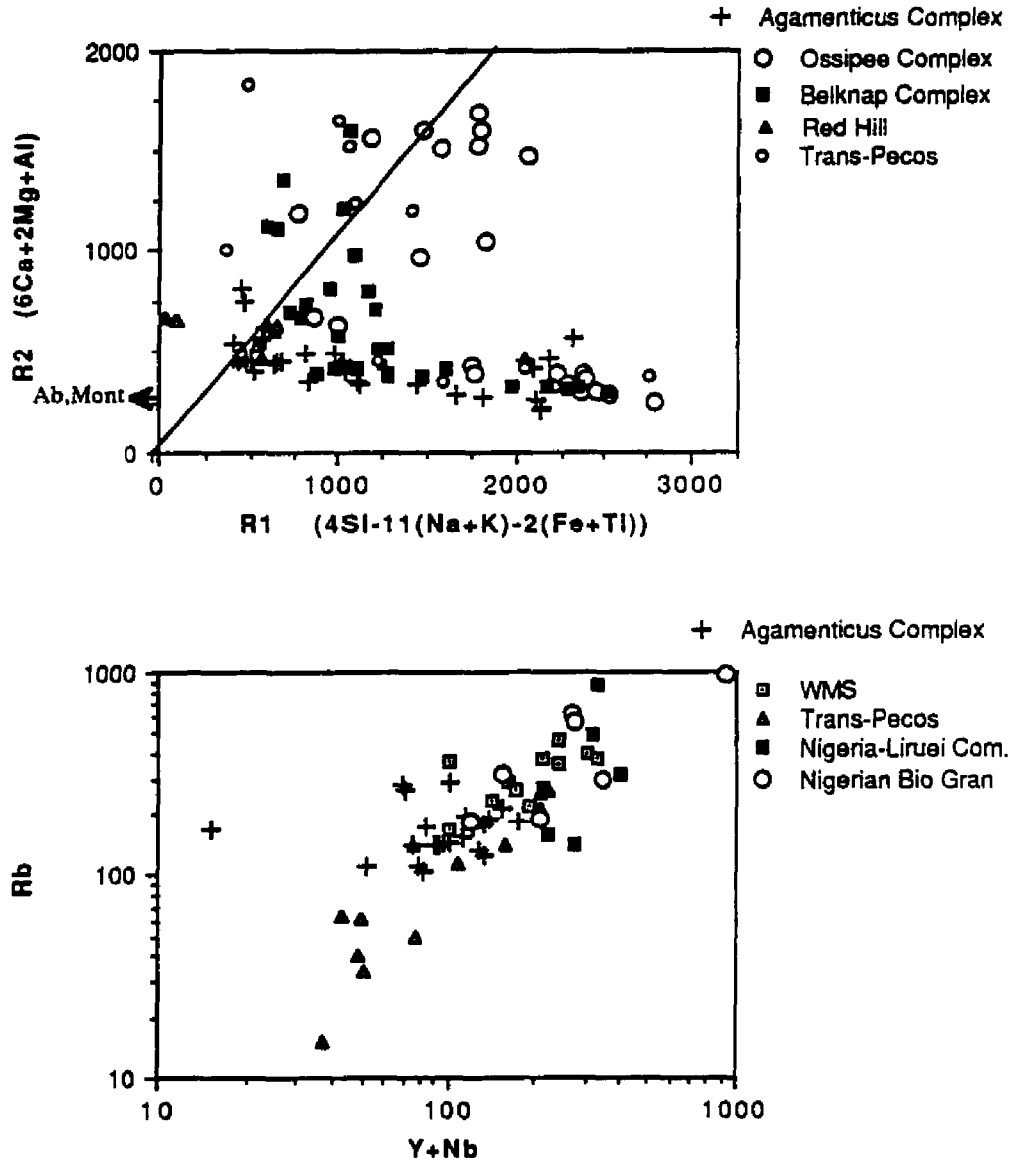

Fig. 3.38 Comparison of geochemical data from the Agamenticus Complex to other alkalic complexes. The Ossipee Complex, Belknap Complex, and Trans Pecos alkalic rocks are derived from basalts by fractional crystallization. Symbols as in Figure 3.12.

generating magma compositions capable of evolving to form the SQSZ and the alkalic syenites.

The high $Sr^{87/86}$ initial ratio for the rocks of the Agamenticus complex (0.710; Hoefs, 1967) would appear to be incompatible with syenites derived by fractionation from mantle melts or from basalt anatexis (Eby, 1985a,b). However, because the geochemical data indicates the biotite granite and alkalic syenite can not be derived from the other rocks within the complex, the use of data from these rocks to calculate the Rb/Sr isochron of Hoefs (1967) is inappropriate. The exclusion of these data from the isochron changes the age and initial $Sr^{87/86}$ initial ratio of the alkalic granites to 221 Ma and 0.716, respectively (Fig. 3.39).

If the Rb/Sr systematics represent primary magmatic signatures, then the abnormally high (Eby, 1985 a, b; Foland and Faul, 1985) $Sr^{87/86}$ initial ratios for the syenites indicate that; 1) the isochron is a mixing line, 2) basaltic sources for the rocks were old enough to have allowed the accumulation of sufficient radiogenic Sr to create high $Sr^{87/86}$ initial ratios, 3) the biotite granite and alkalic syenite are older than and have lower initial $Sr^{87/86}$ than the alkalic granite and/or 4) the syenites and granites where derived from an isotopically homogeneous crust. The first option is rejected on the basis of geochemical evidence already presented. The second is unlikely because the different compositions (i.e., different original $Rb87/Sr^{86}$) of the sources for the granites and syenites would require a remarkable coincidence of radiogenic Sr maturation times for the data to fit the isochron. Because intrusive relationships indicate that the biotite granite is younger than the

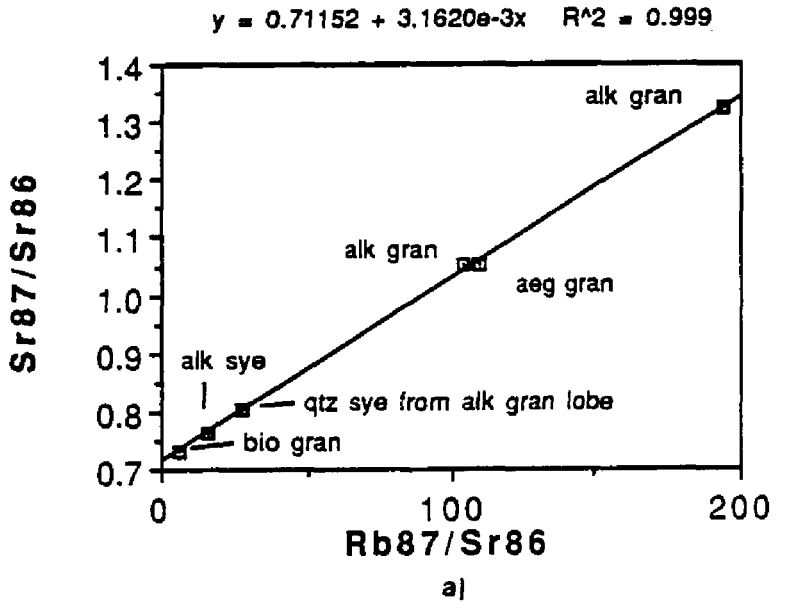

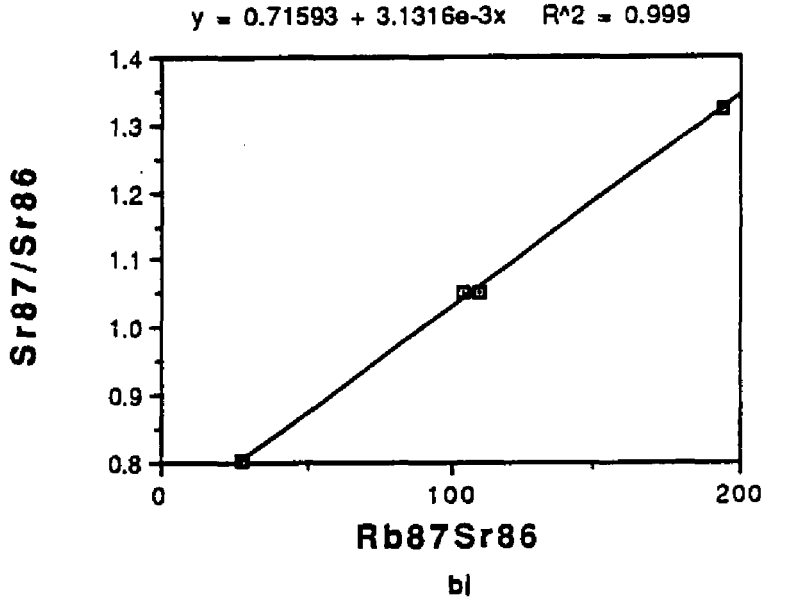

Fig. 3.39 a) Rb/Sr isochron of Hoefs (1967). Because the biotite granite and alkalic syenite are not comagmatic with the alkalic granites, they should not be used to calculate the isochron. b) Excluding these rocks results in slightly higher $Sr^{87/86}$ initial ratio (0.715) and a younger age (221 Ma) for the alkalic granites.

alkalic granite, the third option is not possible for this rock. A model age calculated for the alkalic syenite (239.8 Ma), assuming a $Sr^{87/86}$ initial ratio of 0.704 (after Eby, 1985a (value for crustal derived nordmarkite) and Gaudette et al., 1982), suggests that this magma could have been emplaced approximately 10 million years before the alkalic granite. Such prolonged time spans for the emplacement of magmas with different parents have been demonstrated for the Red Hill Complex (Henderson et al., 1989) but additional isotopic data is required before this can be stated for the Agamenticus Complex. Isotopic homogeneity of the crust beneath the Agamenticus Complex is considered to be highly improbable in light of the findings of Gaudette et al. (1982) who demonstrated a range of $Sr^{87/86}$ initial ratios (from 0.7045-0.7067) for nearby Paleozoic diorites to granites.

Foland et al. 1985 and Van Breeman et al. (1975) have demonstrated that the assimilation of radiogenic country rock or late deuteric metasomatic processes are capable of raising the measured $Sr^{87/86}$ of the magmas to typical crustal levels. Wholesale assimilation is unsupported by textural, field, or geochemical evidence within the Agamenticus Complex but the deuteric textures present in rocks of the Agamenticus Complex suggest that a metasomatic enrichment of $Sr^{87/86}$ needs to be considered. The lack of the abundant late-stage mineralization (see also Fig. 3.38, Rb vs. Y+Nb) and fennitization of the country rocks that is associated with the Nigerian Complexes (Bowden et al., 1987), where this process was active, suggests that fluid resetting

of Sr systematics most likely played a smaller role in the Agamenticus Complex.

A number of key trace element ratios of chemically coherent elements (i.e., Zr-Hf, U-Th, Nb-Ta) have proven to be useful tools elsewhere for devining source characteristics in the absence of isotopic data (Eby, 1985b; Paige, 1988). The use of these ratios as source tracers is dependant on the absence of accessory minerals (for example zircon) or processes (such as weathering or deuteric alteration) that are capable of fractionating the elements. Although the changes in the trace element ratios that would result from such fractionation can often be difficult to predict (Bayer et al., 1978), changes in the ratios of these elements for the Agamenticus Complex indicate that primary magmatic signatures have been at least partially preserved.

The distinct fields formed by the syenites, exclusive of the aenigmatite syenites, and the alkalic granites on the Nb/Ta-Zr/Hf diagram (Fig. 3.19) are considered significant because zircon fractionation and deuteric/hydrothermal processes would both act to reduce the Zr/Hf ratio. The proposed behavior of Zr/Hf during fractionation is supported by the fractionation trends observed for the rocks of the SQSZ on the Ga/Al-Zr/Hf plot. The decrease in the Zr/Hf ratios of MAG 51d relative to 91-1 and 91-2 corresponds to the zircon saturation trend proposed on the basis of the Zr-M and Zr-SiO2 diagrams. The Zr/Hf ratios for the syenites and alkalic granites (high twenties and high thirties, respectively) are considered by Paige and Hon (1988, 1989) to be representative of

rocks derived by partial melting of a crustal source and by mixing of crustal and mantle melts, respectively.

The occurrence of the aenigmatite syenite with the alkalic granites on the Nb/Ta-Zr/Hf diagram (Fig. 3.19) suggests that this rock is related to the alkalic granites by variable degrees of partial melting of the same source rocks or that substantial mixing between the SQSZ and alkalic granites occurred to produce the aenigmatite syenites. Neither of these interpretations is consistent with the trace element data and least squares models relating the aenigmatite syenite to the SQSZ by fractionation and the lack of field and petrographic evidence for mixing between the alkalic granites and the aenigmatite syenite. Zircon accumulation could effectively raise the Zr/Hf ratios (See Cs-avg, Appendix III.V) which then predicts that the aenigmatite is a cumulate of the SQSZ and contradicts the findings of the trace element and least squares mixing models. An alternative is that Zr/Hf enriched volatiles derived from underlying alkalic or aegirine granites infiltrated the aenigmatite syenites. This interpretation is consistent with the occurrence of arfvedsonite growth in late brittle fractures within the aenigmatite syenite. However, unless the contaminating fluids had a Zr/Hf ratio greater than those of the alkalic granites, an unreasonable amount of contamination is required to produce the observed Zr/Hf ratios in the aenigmatite syenite.

The alkalic syenites have Th/U ratios that fall well within the field defined for crustal melts defined by Eby (1985b) for the Monteregian Hill and WMS (Fig. 3.19). Most of the SQSZ rocks have slightly lower Th/U ratios and plot within fields of both crustal and

mantle affinities. Eby (1985b) attributes increases in the Th/U ratios of the Monteregian Hills and the WMS to the assimilation of Th/U enriched contaminants such as pelitic rocks. The fact that the alkalic syenites have a greater Th/U than the SQSZ but similar Nb/Ta ratios might indicate that assimilation has occurred within the alkalic syenites. As discussed previously, assimilation at crustal levels below the current level of exposure can not be completely ruled out. However, the scatter of Th/U ratios for the granites and the low Th/U ratio of 91-1 from the SQSZ indicates that the assignment of source rocks on the basis of Th/U ratios should be treated with caution.

The presence of fluorite and the hypersolvus textures within the alkalic granites and trace element abundances (HFS, Ga, Rb, and Sr) are suggestive of fluorine- and HFS- enriched, anhydrous granitic melts thought to be generated by the partial melting of felsic granulites elsewhere (Collins et al., 1982; Clemens et al., 1986). However, the alkalic granites contain greater abundances of HFS and Ga relative to the Australian A-type granites described by Collins et al. (1982) (Fig. 3.40). This could reflect the greater availability of sodium and potassium to form alkali-HFS-silicates (Collins et al., 1982) in the alkalic granites relative to the metaluminous A-type granites of Australia. In addition to differences in HFS abundances, many of the mineralogic features of the alkalic granite are incompatible with the phase relationships determined by Clemens et al. (1986) for the Watergums A-type granite (i.e., early zircon crystallization, annite crystallizing before sodic amphibole, magnetite, allanite, and plagioclase (An_{30-5})). This suggests that

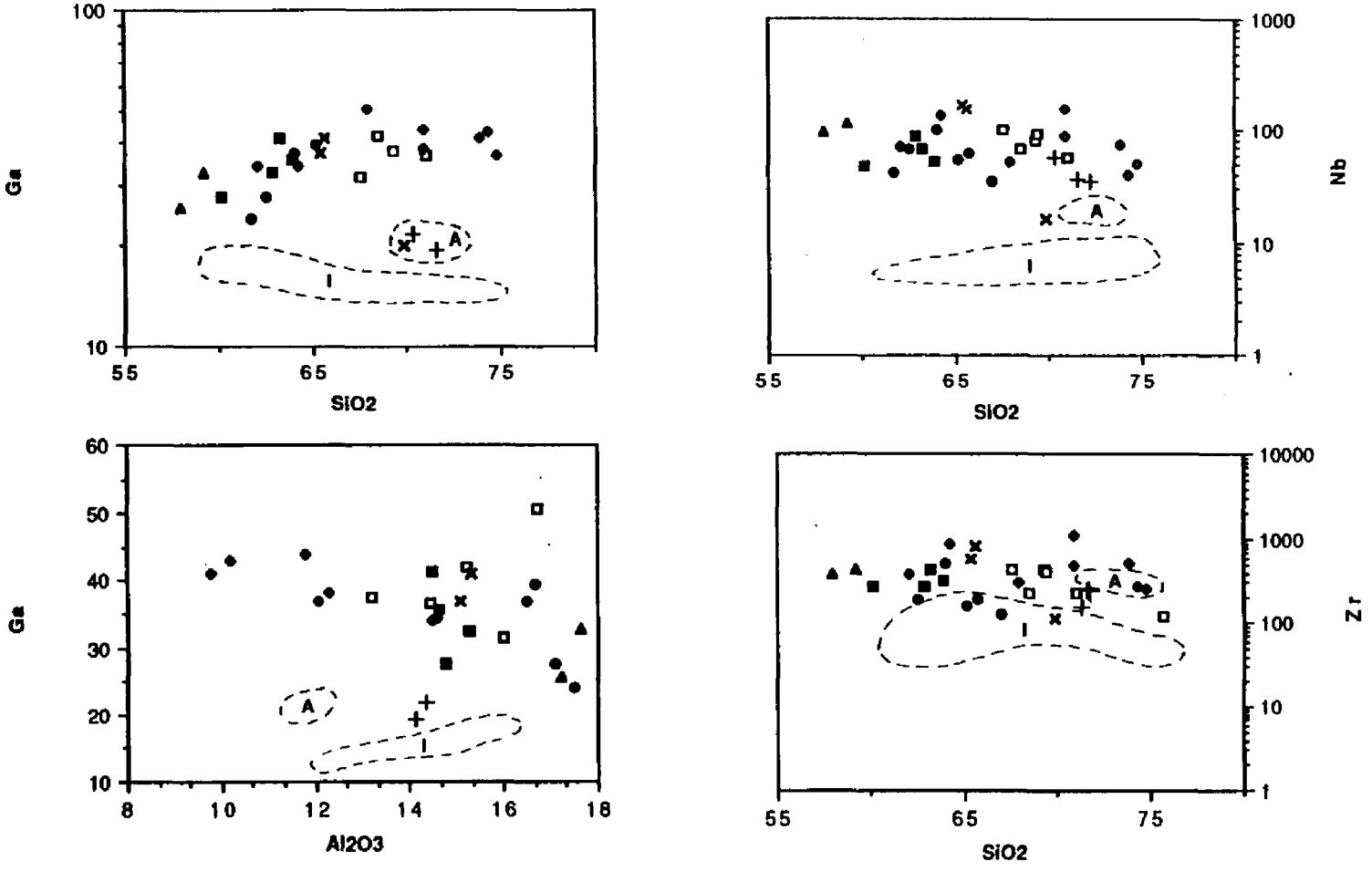

Fig. 3.40 Selected trace element compared to A- and I-type granites from Australia. The A-type granites are interpreted as partial melts of a felsic granulite lower crust (Collins et al., 1982).

the source rocks or conditions of formation for the alkalic granites was significantly different than that described by Collins et al. (1982) and Clemens et al. (1986). Although the Zr/Hf ratios of the alkalic granites suggests mixing of crustal and mantle sources (Paige, 1989), they might also reflect the preferential removal of Hf from the source rock during the initial anatectic event that resulted in the production of a felsic granulite source.

The mineralogy and Ga abundances of the biotite granite are more typical of the Australian A-type granites (See mineralogy described for the Watergums granite described above, petrography of biotite granite, and Fig. 3.40; Collins et al., 1982; Clemens et al. 1986). Collins et al. (1982) suggests that the generation of A-type magmas are preceded by a partial melting of the crust to produce I or S type granites. Within the Merrimack Trough, the biotite granite from the Agamenticus Complex was preceded by the intrusion of Paleozoic biotite and two-mica granites (Hussey, 1962; Gaudette et al. 1982). Therefore, crustal conditions underlying the Merrimack Trough during the Mesozoic were likely similar to those present during the production of the Australian A-type granites. This suggests that the biotite granite of the Agamenticus Complex may have been derived from the granulitic residuum from an anatectic event responsible for the Paleozoic granites.

Petrogenesis of the Agamenticus Complex

The development of the Agamenticus Complex is associated with the early Mesozoic taphrogenic events that led to the opening of the Atlantic Ocean. Extension along preexisting Paleozoic faults, such as the Nonesuch River Fault bordering the Merrimack Trough,

likely resulted in focussed decompression melting of the athenosphere to produce alkalic basalts (Bedard, 1985). Heat and volatiles provided by the ponding of these melts in the lower crust/upper mantle could in turn have resulted in the production of syenite melts (Barker et al., 1975) by partial melting of a heterogeneous basaltic source (Bailey and Schairer, 1966; Helz 1976).

The augite syenite is interpreted to be the product of limited fractional crystallization of one such syenite partial melt (Fig. 3.41). Fractionation likely occurred during transit from the lower crust and/or within a magma chamber at mid-crustal levels (approximately 10 to 15 km). Additional fractional crystallization of the subsolvus augite syenite, by accumulation of potassium feldspar, plagioclase, augite, fayalite, apatite, and possibly ilmenite, drove the liquids towards more peralkaline residues and compositions equivalent to the aenigmatite syenite (Fig. 3.41). Oxygen fugacity during this crystal fractionation was controlled in part by an aenigmatite - ilmenite - aegirine-augite buffer.

The hypersolvus, porphyritic texture of the aenigmatite syenite indicates that it solidified at lower P_{H2O} and temperatures than those present in the magma chamber. This suggests that the aenigmatite crystallized in the upper levels of or was emplaced at a higher crustal level than the augite syenite magma chamber (Fig. 3.42 a).

Following the partial solidification of the aenigmatite syenite, this rock was intruded by the SQSZ along a subhorizontal contact (Fig. 3.42 b). Chemical bracketing of the aenigmatite syenite by

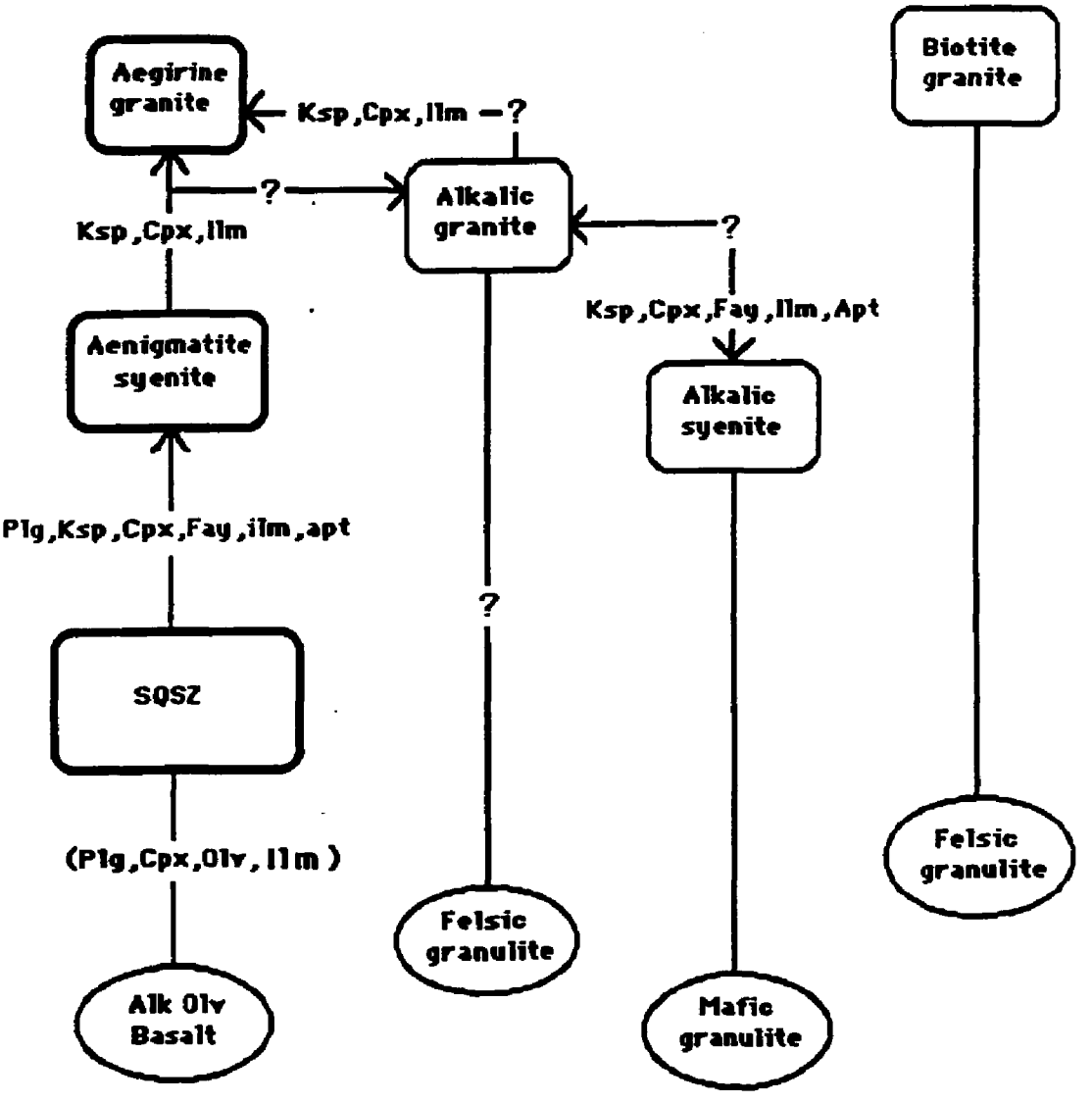

Fig. 3.41 Flow diagram for the evolution of the Agamenticus Complex. Arrows point towards the direction that liquids evolve during fractional crystallization. Minerals along these trends are proposed cumulate assemblages. Possible partial melting relationships are indicated by the connection of source rocks (oval shape) and melts (rectangles).

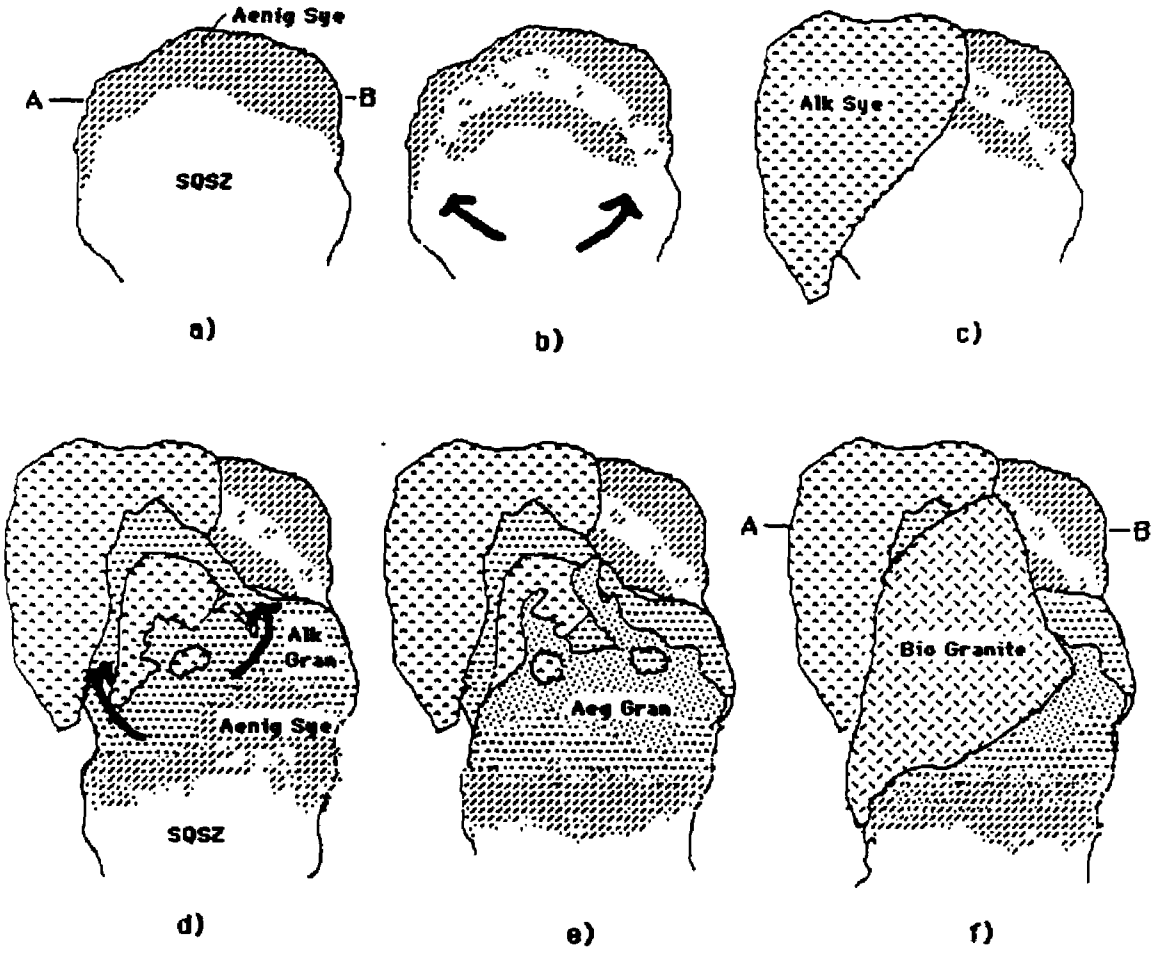

Fig. 3.42 - Cross sectional view of emplacement of the rocks within the Agamenticus Complex. Profile is along line A-B in Fig. 3.23. In this figure line A-B also represents the present level of erosion. Note the stratification within the magma chamber through time to produce the aenigmatite syenite and the alkalic and aegirine granites. The alkalic syenite and biotite granite are considered to be separate from this fractionation sequence. Arrows denote intrusion of magma.

magmas of the SQSZ (Figs. 3.12, 3.14, 3.15) suggests that the sub-solvus augite syenite had continued to fractionate after the removal of the aenigmatite syenite. This fractionation likely produced a stratified magma chamber as proposed for other alkalic complexes (Hildreth, 1981; Macdonald, 1987). The juxtaposition of varying SQSZ magmas suggests that emplacement of this zone was accompanied by the comingling of several layers of this stratified magma chamber.

As the upper crustal SQSZ magma chamber was evolving, continued melting of a heterogeneous lower crust tapped a source rock capable of producing the alkalic syenites (Fig. 3.41). Major element compositions indicate that the source for the alkalic syenites, relative to that of the SQSZ, was enriched in Al2O3 and K2O, and depleted in Fe2O3. Geochemical variations within the alkalic syenite suggests that this rock is composite. Temperature of crystallization for the alkalic syenites, calculated using the clinopyroxene-olivine geothermometer of Powell and Powell (1974), is 971 ^{o}C-998 ^{o}C at 1 kbar and 977 ^{o}C-1003 ^{o}C at 2 kbar. Although these may be minimum temperature estimates because the geothermometer does not account for Na substitution in clinopyroxene (Wood, 1976 and Parsons,1981), the calculated temperatures are in rough agreement (higher by 100-200 ^{o}C) with those predicted by experimentally determined phase relationships in syenites of the Kungnat Complex, Greenland (McDowell and Wyllie, 1971). The occurrence of fayalite, hedenbergite, and ilmenite in the alkalic syenites suggests that fO2 was lower than in the SQSZ; below the magnetite-titanite-quartz-hedenbergite-

ilmenite (Wones and Gilbert,1982) or fayalite-magnetite-quartz (Wones,1989) buffers (Fig. 3.29)

Chemical evidence indicates that the alkalic syenite and SQSZ magmas did not interact either at the current level of exposure or at the level of the SQSZ magma chamber. The fine-grained alkalic syenite along the alkalic syenite-SQSZ contact, a possible chill margin, indicates that the SQSZ had cooled before the intrusion of the alkalic syenite. The lack of geochemical and field evidence of interaction between the two syenite magmas suggests that the SQSZ magma chamber was completely solidified before the introduction of the alkalic syenite. However, the aegirine granite, which is interpreted to be derived from the SQSZ magmas, was emplaced latter than the alkalic syenites. This requires that the SQSZ magma chamber was still partially liquid at the time of the alkalic syenite intrusion. Therefore, the intrusion of the alkalic syenite is tentatively interpreted to have occurred along a steeply dipping contact at the periphery of the SQSZ magma chamber (Fig. 3.42 c).

The intrusion of the alkalic syenite was followed by the emplacement of the alkalic granite. The mineralogical and geochemical evidence suggest that the rocks have been effected by late deuteric and/or volatile interaction. Because of the resulting trace element scatter, relating the alkalic granites to the other rocks within the complex is problematic (Fig. 3.41).

If the alkalic granite is related to the SQSZ, then the overlap of the trace element data and the SQSZ suggests that the SQSZ magma chamber devolatilized, leading to the reduction of

peralkalinity, P_{H2O}, and mobile trace elements (such as the LIL), prior to evolving to the alkalic granite. Major element least squares mixing models relating the alkalic granite and alkalic syenite are largely unsupported by trace element abundances but can not be completely ruled out. If this relationship is correct, then it suggests that a currently unexposed alkalic syenite magma chamber fractionated to produce the alkalic granites. The hypersolvus textures of the alkalic syenite suggests that this magma chamber was at a higher crustal level than or was less hydrous than the SQSZ magma chamber. Alternatively, the alkalic granites are derived by the partial melting of a felsic granulitic source in the lower crust and are thus not comagmatic to either the SQSZ or the alkalic syenites. The current data set does not differentiate between these three models. The alkalic granites are shown tentatively as differentiates of the SQSZ in Figure 3.42d.

Trace element abundances and mineral chemistry indicates that the aegirine granites are derived by extreme fractionation of the SQSZ magma and/or the alkalic granite magma (Fig. 3.41). This rock was most certainly emplaced after the SQSZ rocks and most likely after the alkalic granites and alkalic syenites (Fig. 3.42e). The stability of aegirine within the rocks is related to increasing the Na content and fO2 of the magma as fractionation progressed. As the result of these magmatic changes arfvedsonite became unstable in the late residua and reacted to form aegirine. Trace element scatter observed in these rocks, such as a wide range of Zr/Hf ratios, indicates that these rocks also were affected by late magmatic fluids.

Sometime between the intrusion of the alkalic granite and biotite granite the southwestern portion of the Agamenticus Complex was intruded by a basalt dike swarm. The intrusion of these basalts late in the development of the Agamenticus Complex is similar to intrusive relationships observed in other alkalic complexes (Bowden and Turner, 1974). The lack of any field or petrographic evidence for basalt interaction suggests that basalts were not involved in the chemical evolution of the Agamenticus Complex rocks. However, they may be related to the basalts that initiated melting in the lower crust/upper mantle to produce syenite melts, see above. The orientations of the dikes suggests that they were intruded under the same stress field that was present during the late Triassic to Jurassic intrusion of basalt dikes elsewhere in the seacoast region.

The biotite granite and related rhyolite dikes were the last magmas to intrude the Agamenticus Complex. The biotite granite is interpreted to be a partial melt of a felsic granulite within the lower to middle crust (Fig. 3.41). The truncation of the basalt dike swarm by the biotite granite and a Cretaceous apatite fission track age for the biotite granite suggest that significant time may have elapsed between the intrusion of the alkalic rocks within the complex and the biotite granite.

In conclusion, the evolution of the Agamenticus Complex contains many facets of the petrogenetic model described by Barker et al. (1980) for the Pikes Peaks Complex. The syenites and biotite granite, and possibly the alkalic granite, are interpreted to be the products of partial melting of a heterogeneous lower crust. Heat

required for this anatectic event was likely supplied by underplating of mantle derived basalts during the early stages of Mesozoic taphrogenesis. Further modification of these magmas occurred by fractional crystallization of a potassium feldspar, plagioclase, augite to hedenbergite, fayalite, apatite, and ilmenite cumulate assemblage. The aegirine granites are interpreted to be the residual liquid of this fractionation. Late interaction with deuteric fluids resulted in the growth of riebeckite and arfvedsonite and the redistribution of trace element abundances within the alkalic and aegirine granites. Field, petrographic, and geochemical evidence suggests that little, if any, interaction occurred between the crustal derived melts and the underplating mafic magmas.

CHAPTER 4

SUMMARY

Comparison of Triassic and Cretaceous Complexes

In addition to the Triassic Agamenticus and Abbot Complexes, southwestern Maine is intruded by a number of Cretaceous, and undated, felsic and mafic complexes and stocks (Fig. 4.1). These anorogenic bodies were studied to investigate magmatism during early rifting, changes that can occur in magma petrogenesis at the beginning and end of a rifting cycle, the effect of crustal variation across proposed terrane boundaries on magma compositions, and the effect of preexisting crustal fabrics on the emplacement of these magmas.

The Triassic and Cretaceous anorogenic complexes and stocks can be distinguished on the basis of field, geophysical, and geochemical data. These differences are emphasized by comparison with nearby Cretaceous complexes in New Hampshire (Fig. 4.1)

Although the dominant rock types, syenite and quartz syenite, of the Burnt Meadow Complex are similar to those found of the Agamenticus Complex, several lines of evidence indicate that mafic rocks were important components in the development of the Burnt Meadow Complex. Gilman (1979) suggests that andesite porphyry exposed within the complex is cogenetic to and predates the intrusion of the subvolcanic syenite. Abundant mafic enclaves

Fig. 4.1 Simplified geology of the southeastern New England.

LEGEND

Mesozoic plutons

MR- Randall Mt. Stock
Mp- Pickett Mt. Stock
Ko- Ossipee Complex
Kg- Green Mt. Stock
Kb- Burnt Meadow Stock
Km- Merrymeeting Complex
Kp- Pawtuckaway Mt. Complex
Ka- Alfred Complex
Kt- Tatnic Complex
Jr- Red Hill Complex
Trag- Agamenticus Complex
Tra- Abbott Complex

Paleozoic Plutons

Cb- Biddeford Pluton
Cl- Lyman Pluton
Cs- Sebago Pluton
Dw- Webhannet Pluton
Oe- Exeter Pluton
Od- Dracut Diorite
On- Newburyport Complex
Oca- Cape Ann Complex
Zs- Salem Diorite/Gabbro

Metamorphic rocks

Casco Bay Area

DOb- Bucksport Fm.
OZsc- Scarboro Fm.
OZce- Cape Elizabeth Fm.

MMR Zones

ZOk- Kittery Fm.
ZOe- Eliot Fm.
ZOec- Calef Member
ZOb- Berwick Fm.
ZOmg- Massabesic Gneiss
ZOr- Rye Fm.

Esmond-Dedham Zone

DSv- Newbury Volcanics
ZOn- Nashoba Fm.
ZOnb- Boxford Member
ZOm- Marlboro Fm.

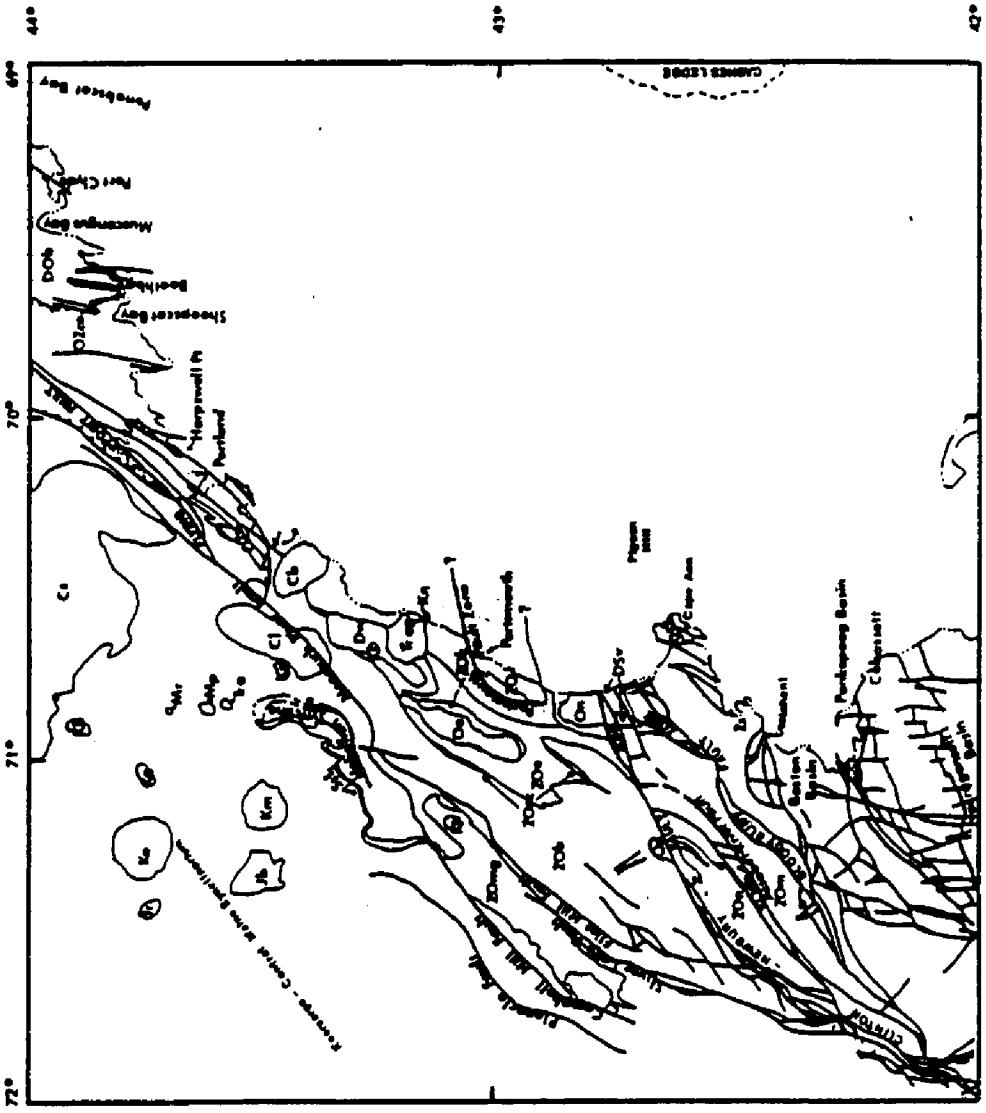

within the southern portion of the alkalic quartz syenite suggests that comingling of the andesite and quartz syenite magmas occurred. In addition, the presence of an aeromagnetic high overlying the complex, similar in shape and magnitude to those over the Cretaceous complexes in New Hampshire, suggests that the complex is underlain by a substantial mafic body.

Another characteristic common to the Cretaceous complexes is the presence of volcanic rocks. In addition to the andesite porphyries trachyte porphyries and fragmental gray porphyries are also exposed in the Burnt Meadow Complex (Gilman, 1979). Andesite and "light and dark aphanites" are found within the mafic, Cretaceous Acton and Tatnic Complexes, respectively (Hussey, 1985). Basalt and rhyolite porphyries form an important part of the Cretaceous Ossipee Complex (Carr, 1980; Billings; 1956).

The geochemistry of the Burnt Meadow Complex is also different from the Triassic Complexes (Table 4.1). For example, relative to the Agamenticus and Abbot Complexes, the Burnt Meadow Complex is depleted in Ga, Zn, and Rb/Sr and enriched in Sr and Ba (Figs. 4.2 and 4.3). The Burnt Meadow Complex and portions of the SQSZ rocks and aegirine granites from the Agamenticus Complex overlap the field defined by the more evolved members of the Ossipee, Belknap, Pliny, and Moat Mountain Complexes on a number of geochemical diagrams (For example: K/Rb and Ba-Rb diagrams, Fig. 4.3).

Several of the undated Mesozoic rocks within southwestern Maine are considered to be coeval to the Cretaceous rocks on the basis of similarities in the above characteristics. Trachyte

	LOCATION	SAMPLE #	REF.	SiO2	TiO2	Al2O3	FeO	Fe2O3	MnO	MgO	CaO	Na2O	K2O	P2O5	LOI	H2O+	H2O-	CO2	SUM	Rb	Cs	Sr	Ba	Sc	V
1	Abott Mt	AB-2	BROOKS(UH)	63.75	0.39	16.25	0	6.52	0.24	0.3	1.74	4.48	5.23	0.06				-	99.97	121.7	2	33.3	173.2	3.28	35.4
2	Abott Mt	AB-5	BROOKS(UH)	64.7	0.336	16.02	0	6.23	0.191	0.31	1.14	5.01	5.44	0.06					103.04	169.1	0.381	7.2	43.6	3.101	33.9
3	Abott Mt	AB-8	BROOKS(UH)	61.74	0.37	16.84	0	6.25	0.24	0.37	1.78	5.4	5.97	0.07					99.03	81.4	1.1	62.3	408.3	7.28	14
4	Boston Hills	BH-B2	BROOKS(UH)	65.29	0.39	17.01	0	3.95	0.1	0.4	1.26	4.76	5.63	0.1					98.95	130.4	3.445	168.4	1142	4.651	21.8
5	Burnt Mt	BMC-1	BROOKS(UH)	63.96	0.797	17.7	0	4.93	0.172	1.1	1.28	4.81	5.61	0.21					100.77	142.3	4.97	283.9	843.6	3.399	24.6
7	Burnt Mt	BMC-5	Perlit(UF)	59.8	1.36	17.3	0	5.69	0.23	1.47	2.47	6.28	5.06	0.4	0.12				99.34	186	1.172	348	1289	3.695	26.1
8	Burnt Mt	BMC-6A	Perlit(UF)	66.6	0.68	16.1	0	3.32	0.17	0.84	1.9	5.3	5.22	0.18	0.31				100.16	282	1.943	308	568	2.636	25.8
9	Burnt Mt	BMC-6B	Perlit(UF)	66.1	2	16.1	0	5.68	0.21	4.81	5.84	4.84	3.1	0.48	0.35				101.26	168	2.535	556	978	14.89	28.8
10	Chase St	ea1	Perlit(UF)	69.2	0.8	17.6	0	4.75	0.1	0.54	1.46	5.66	5.38	0.16	0.51					218		178	887		24.3
11	Chase St	ea1a	Perlit(UF)	69.2	0.81	16.8	0	7.48	0.13	1.41	2.13	5.69	2.42	0.26	0.87					307		138	154		64.6
12	Chase St	ea1b	Perlit(UF)	68.6	1.28	12.9	0	8.34	0.19	3.38	3.83	3.38	2.73	0.32	1.84					388		257	255		31.8
13	Chase St	ea1c	Perlit(UF)	71.4	0.34	15.4	0	2.87	0.05	0.48	0.82	4.87	4.88	0.12	0.72					335		198	228		24.2
14	Chase St	ea2	Perlit(UF)	64.5	0.64	17.6	0	4.71	0.1	0.81	1.88	5.8	5.78	0.28	0.8					184		259	493		24.5
15	Chase St	ea-1	Perlit(UF)	70.1	0.68	12.8	0	0.84	0.01	0.1	0.18	3.88	4.69	0.02	0.85					301		33.6	57.7		30.6
16	Chase St	ea-9	Perlit(UF)	61.3	2.78	14.8	0	11.2	0.14	7.06	5.78	3.62	2.8	0.58	3.11					98.1		648	838		28.5
17	Chase St	ea-11	Perlit(UF)	68.8	1.36	16.2	0	5.66	0.14	1.46	2.22	5.67	4.17	0.44	0.64					166		566	832		33
18	Chase St	CS-1	BROOKS(UH)	62.87	0.673	17.63	0	4.8	0.11	0.8	2.12	5.66	5.08	0.255					100.3	182.7	2.299	297.5	600.5	2.282	21.6
19	Pickett Mt	PM-5	BROOKS(UH)	73.91	0.29	14.81	0	1.96	0.055	0.32	0.76	3.67	5.2	0.03					100.81	319.1	5.05	123.1	261.9	1.49	27
20	Pickett Mt	PM-6	BROOKS(UH)	74.86	0.07	13.22	0	1.17	0.02	0.31	0.45	4.35	4.78	0.05					99.28	271.4	1.986	40.7	95.2	0.6431	18.9
21	Pickett Mt	PM-7	BROOKS(UH)	73.9	0.179	14.63	0	2	0.051	0.33	0.64	4.63	5.18	0.04					101.58	347.9	5.74	111.2	286.2	1.16	32.7
22	Pickett Mt	PM-8	BROOKS(UH)	71.8	0.23	14.49	0	2.42	0.06	0.39	0.87	4.66	5.14	0.06					99.92	331.7	8.01	140.1	318.3	1.37	33.1
23	Randall Mt	RM-6C	BROOKS(UH)	62.13	0.99	18.61	0	2.84	0.16	0.67	1.52	6.29	5.89	0.1					99.2	117.1	2.971	290.1	2106.6	0.5437	26.2
24	Randall Mt	RM-6D	BROOKS(UH)	64.04	0.28	19.01	0	2.04	0.11	0.19	0.8	6.84	7.91	0.01					99.93	174.1	1.24	120.8	215.9	0.282	22.2
25	Randall Mt	RM-9	BROOKS(UH)	62.33	0.48	18.6	0	2.46	0.17	0.44	1.59	6.26	6.36	0.07					97.89	161.6	1.847	424.8	788.1	0.8857	25
26	mafic dikes-york	mag 12	Perlit(UF)																	53.6		440.7	251.5		18.2
27	mafic dikes-york	mag60b1	Perlit(UF)																	55.9		376.4	236.1		21.9
28	mafic dikes-york	mag60b2	Perlit(UF)																	61.9		327.1	402.1		24
29	mafic dikes-york	mag60d	Perlit(UF)																	49.8		506.1	333.2		24.6
30	mafic dikes-york	mag60b	Perlit(UF)																	145.2		660.4	613.1		20.5
31	mafic dikes-york	mag60d	Perlit(UF)																	79.4		31.9	913.5		27.6
32	mafic dikes-york	mag60c	Perlit(UF)																	74.6		385.7	439.8		19.4

	Zr	Hf	V	Nb	Ta	La	Ce	Nd	Sm	Eu	Tb	Yb	Lu	Th	U	Cr	Co	Ni	Cu	Zn	Ga	Pb
1	527.9	10.66		68.9	5.63	38.69	87.09	41.32	8.43	1.299	1.03	4	0.633	8.798	3.58	3.08	0.633	5.7	37.2	104	28.92	7.72
2	392.2	13.11		79.8	7	61.79	164.1	70.69	12.62	1.104	1.476	5.357	0.841	11.26	2.363	3.03	0.455	2.7	0	135.3	24.63	6.71
3	284.6	8.44		32.6	2.65	25.78	47.66	19.66	3.85	2.34	0.603	1.6	0.268	5.26	1.83	0	1.15	5.7	2.8	78.7		
4	257.6	8.464		41	5.184	30.91	65.02	35.66	7.303	3.657	0.908	2.689	0.39	10.14	1.888	1.849	1.843	1.4	4.7	103.5		
5	456.2	14.62		76.3	6.764	173.6	253.5	97.23	8.721	2.334	0.886	3.014	0.478	20.25	4.101			0.7	35.4	92.9		
7	234	6.329	43.6	83	5.848	71.93	137.6	55.1	8.417	2.628	1.065	2.212	0.348	13.46	2.747	2.166	3.387	2.18	6.4	92.2	17.6	
8	388	10.09	39.3	169	10.43	73.87	132.9	43.81	6.619	1.387	0.813	2.832	0.451	35.54	4.793	3.813	4.406	5.68	9.77	48.7	16.2	
9	264	6.952	173	81.8	7.083	63.71	102.6	45.13	7.584	1.953	1.324	2.388	0.414	20.88	3.949	124.5	21.08	46	14	338	17.8	
10	467		11.5	91.3		48.8										18.1	2.15	8.5	16.7	61.6		
11	288		56	168		51.6										56	7.6	12.2	16.9	94.5		
12	283		123	68.3		58.2										143	17.3	72.6	22.2	139		
13	282		22.1	63.4		39.1										33.2	3.3	3.2	16.2	38.2		
14	424		26.7	76.3		46.1										23.8	4.3	4	16.6	57.6		
15	148		12.9	83.4		43.2										28.6	2.1	1.5	22.2	63.5		
16	255		198	64.1		42.9										256	41	143	41.3	94.9		
17	328		20.7	91.1		56.7										21.8	6.2	3.6	39.7	63.1		
18	303.9	11.3	16.86	67	7.777	51.03	94.46	35.37	6.119	1.22	0.724	2.76	0.389	28.09	9.024	5.674	5.125	2.1		57.8	23.24	1.88
19	247.6	7.57		55.2	8.38	75.41	141.86	56.81	7.7	0.646	0.679	2.67	0.365	54.65	8.598	4.91	1.46	5.7	6.2	46.2		
20	183.6	5.5985		108.6	24.23	10.881	51.801	14.812	3.9	0.189	2.514	2.732	0.414	62.037	19.702	1.92	0.5969	5.7	19.4	18.2	25.69	
21	226.6	7.25	1.88	69.6	8.17	67.11	114.49	43.26	7.59	0.979	2.22	2.49	0.406	51.84	9.18	1.45	1.095	4.1	9.2	42.3	24.98	2.69
22	268.9	9.14	7.52	74.3	9.02	80.68	147.07	51.01	7.51	0.716	0.613	2.9	0.417	65.38	5.39	3.91	1.58	5.4	10.4	57.1	21.39	2.06
23	295.2	8.742	16.26	98.6	14.245	85.917	183.04	75.623	10.388	2.557	1.104	3.185	0.397	7.934	1.063	2.47	1.18	0.7	12.2	48.5	18.15	19.76
24	758.2	14.63	9.69	108.6	4.585	71.68	89.08	17.29	1.81	0.251	0.188	2.56	0.44	20.77	4.87	4.89	0.497	1.4	5.1	69.6	13.76	72.26
25	559.9	14.348	8.91	103.4	9.636	87.736	185.83	75.718	8.434	1.844	0.709	2.772	0.436	19.057	3.9895	0.759	0.0874	0.7	3.2	49.7	19.84	12.76
26	163.8		236.9	28.7		15.5										97.7	41.5	52.6	43.6	120.6		
27	130		236.6	20.9		18.6										175.1	43.3	77.2	65.7	128.8		
28	198		200.1	26.3		24.8										49.9	39.4	105.4	37.3	132.9		
29	191.5		191.6	40.6		25.5										274.9	32.9	32.9	18.6	173.8		
30	198.7		188.9	40.6		29.5										95.9	28.7	43.4	32.3	98.1		
31	181.4		9.8	27		33.2										29.8	1.2	0.6	16.1	62.2		
32	198.1		220.8	33.8		22.5										202.4	38	63.5	32.6	89.7		

Table 4.1 Major and Trace Elem

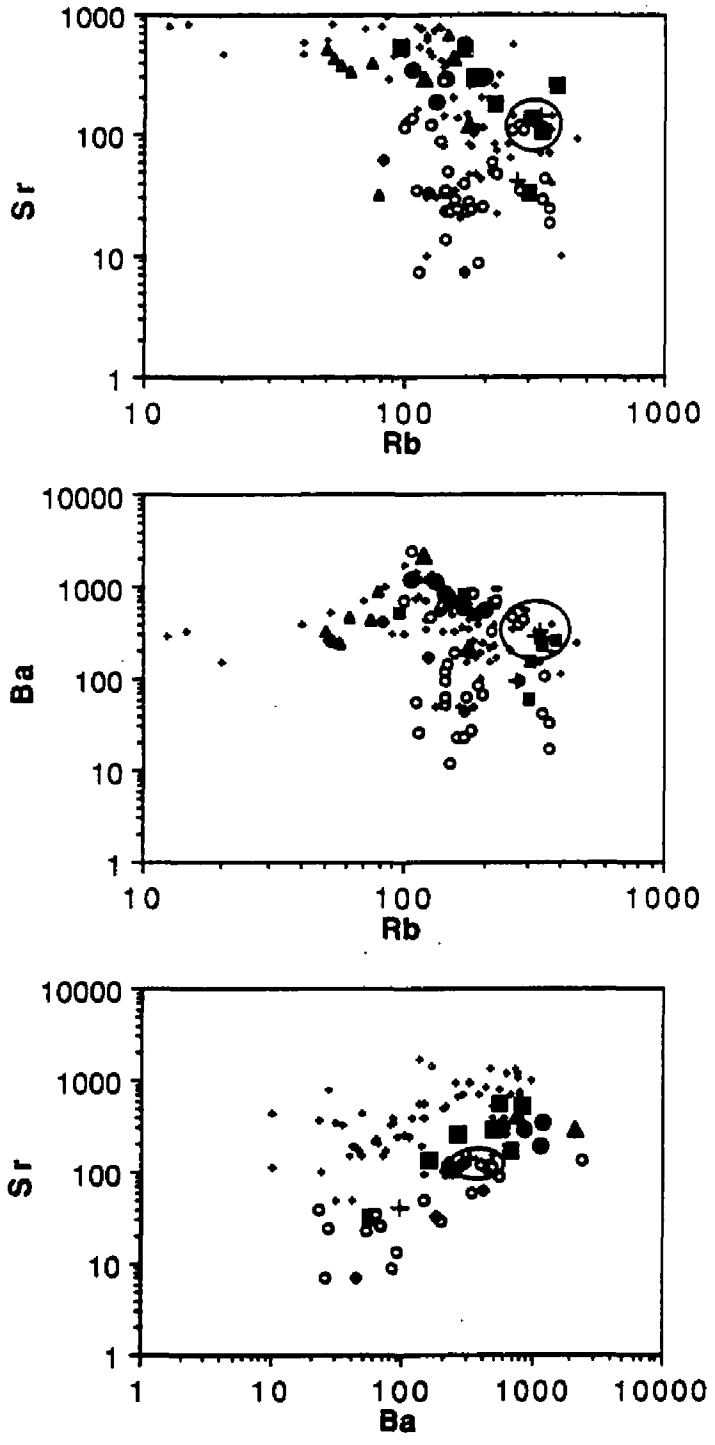

Fig. 4.2 LIL-LIL trace element diagrams showing comparison of Triassic and Cretaceous Complexes. Open triangles are for basalts that cross-cut the Agamenticus Complex.

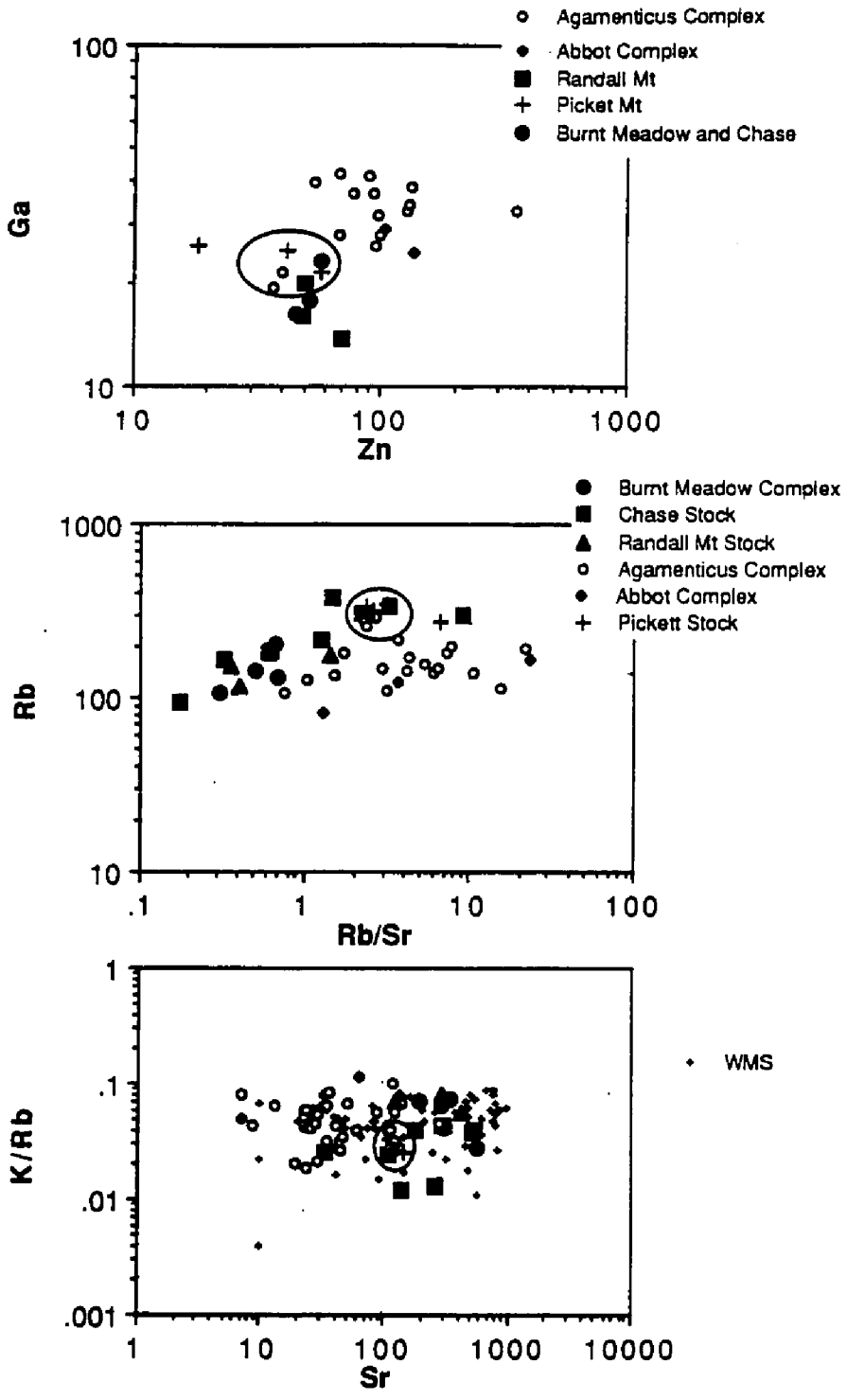

Fig. 4.3 Comparison of LIL ratio-LIL and Ga-Zn for Triassic and Cretaceous Complexes.

porphyries within the Randall Mountain Stock and mafic enclaves within the Chase Stock are suggestive of the volcanic and mafic characteristics, respectively, of the Cretaceous Complexes. In addition, both of these stocks are overlain by aeromagnetic highs and are chemically similar to the Burnt Meadow Complex (Figs. 4.2 + 4.3).

The data for biotite granites from the Agamenticus Complex, Pickett Mountain Stock, and a rhyolite from the Chase Stock form tight clusters on each of the geochemical diagrams in figures 4.2 and 4.3. Chemically similar biotite granites in New Hampshire ("Conway Granites") are not unique to complexes of a particular age (Billings, 1956; Eby, 1987). Therefore, the geochemical similarity of the biotite granites in southwestern Maine can not be used to assess the age of the undated Pickett Mountain and Chase Stocks.

The geochemical similarity of the Cretaceous felsic Burnt Meadow Complex and likely coeval Randall and Chase Stocks to that of the Belknap and Ossipee Complexes in New Hampshire implies a similar petrogenesis for the complexes. The rocks of the Belknap and Ossipee Complexes are interpreted to be fractionates from a mantle derived partial melt which have been modified by a number of secondary processes (Loiselle, 1978; Carr, 1980; Foland et al., 1989). The mafic enclaves and aeromagnetic highs over the Cretaceous bodies in southwestern Maine support the presence of a similar mafic precursor for the syenites within these complexes. The importance of mantle derived melts for the Cretaceous magmatism in southern Maine is also emphasized by the nearby

intrusion of nearly coeval mafic, gabbro to granodiorite complexes (Gilman, 1972,1979; Hussey, 1985).

In contrast, evidence of a mafic component in the geochemical development of the Triassic complexes in southwestern Maine is lacking. The Abbott and Agamenticus Complexes, comprised of alkalic syenites and granites, are devoid of mafic enclaves and lack aeromagnetic highs that support a mafic component in the Cretaceous Complexes . On the basis of major and trace element geochemistry, the rocks of the Agamenticus Complex are interpreted to be fractionates of crustally derived partial melts. The geochemical similarities of the Abbot and Agamenticus Complexes suggests a crustal origin for the Abbot Complex parental magmas. Eby (1987) makes the same basic argument for alkalic syenite-quartz syenite-granite complexes in New Hampshire.

Implications for the petrogenesis of Mesozoic magmatism in southwestern Maine

The differences summarized above for the Triassic and Cretaceous Complexes indicate different petrogeneses; early rifting was accompanied by magmas generated in the lower crust and late rifting involved the emplacement of mantle derived magmas. This fundamental conclusion can be synthesized in the following working hypothesis. Ponding of mantle derived melts under relatively cold Triassic lower crust resulted in the partial melting of mafic and felsic granulite sources and the production of alkalic syenite and

granite magmas; i.e. primary magmas of the Agamenticus and Abbot Complexes. Progressive heating of the crust due to the continued supply of mantle derived magmas during more advanced stages of taphrogenesis facilitated the rise of the mantle melts and their fractionates to higher crustal levels during the Cretaceous. This thermal effect on the rise of mafic magmas within the crust was compounded by progressive extension and thinning of the crust along preexisting Paleozoic faults (Bedard, 1985) during the Mesozoic.

The absence of Jurassic anorogenic igneous rocks in southwestern Maine is unexplained. Bedard (1985) suggests that favorably oriented Paleozoic faults were activated as melt/intrusion zones at different times in response to dextral shearing generated by the rotation of the North American plate during Mesozoic rifting. Rotation could have resulted in a temporary constriction within southwestern Maine during the Jurassic preventing the egress of magmas to the upper crust (See also Manning and deBoer, 1989).

The presence of volcanic rocks within the Cretaceous Complexes implies that they are exposed at higher structural levels than the Triassic Complexes. This suggests that approximately 2 to 4 kilometers of erosion occurred between the emplacement of the Triassic and Jurassic Complexes. The cause of the uplift suggested by this erosion can not be identified. Undoubtably, crustal adjustments during this time reflected a complex interplay of doming in response to magma underplating in the lower crust and upwelling mantle and subsidence due to extension along listric faults (Bedard, 1985).

The current data set yields little information about the crustal structure underlying southwestern Maine. A crustal signature in the major and trace geochemistry of the Cretaceous Complexes is difficult to assess because the primary geochemical signature of these rocks reflects their mantle related origin. The higher peralkalinity of some of the syenites and granites within the Agamenticus Complex suggests that the source rocks for these magmas were different than those of the Abbot Complex. However, the petrographic similarity of the syenites within the Abbot Complex (Gilman, in press) to the alkalic syenites within the Agamenticus Complex implies a similar source. In the absence of isotopic data, assessing the nature of the source rocks is fraught with complications because the final composition of the magmas derived from these rocks can represent the combined influence of a number of petrologic processes.

The emplacement of the southernmost Mesozoic magmas in southwestern Maine were likely controlled by reactivation of the Paleozoic structural fabrics and by underlying terrane boundaries. For example, the Agamenticus Complex is located within a region of the Merrimack Block cut by a number of within terrane faults in a narrow zone between the Central Maine Terrane and Rye Block. In addition to Agamenticus Complex, the mafic Cretaceous Complexes, including the Pawtuckaway Complex in New Hampshire, are near to the Massabesic-Merrimack Block and Central Maine Terrane suture.

Geologic and geophysical analyses of the east-central coastal region of New England and the Gulf of Maine have shown that these Paleozoic faults and sutures are the consequence of extended and

perhaps episodic dextral transpression. Within southeastern New England this transpression culminated with the docking of the Boston-Avalon Terrane during the Alleghanian. Late-Permian to Triassic extension resulted in the reactivation of favorably oriented sutures and faults within the coastal region setting the stage for subsequent Mesozoic rifting and magmatism.

REFERENCES

Abu-Moustafa A and Skehan JW (1976) Petrography and geochemistry of the Nashoba Formation, East-central Massachusetts. in; Lyons PC and Brownlow AH (eds) Contributions to New England Geology. GSA Mem 146: 31-70.

Albee AL and Ray L (1970) Correction Factors for Electron Probe Microanalysis of Silicates, Oxides, Carbonates, Phosphates, and Sulfates. Anal Chem 42(12):1408-1414.

Aleinikoff JN, Zartman RE, and Lyons JB (1979) U-Th-Pb geochronology of the Massabesic Gneiss and the granite near Milford, south-central New Hampshire; new evidence for Avalonian basement and Taconic and Alleghanian disturbances in eastern New England. Cont Mineral and Petrol 71:1-11.

Allegre CJ and Minster JF (1978) Quantitative models of trace element behavior in magmatic processes. Earth Planet Sci Lett 38:1-25.

Bailey DK (1974) Continental rifting and alkaline magmatism. *in*: H. Sorensen ed., The Alkaline Rocks. Wiley, London, pp 148-159.

Bailey DK and Schairer JF (1966) The System Na_2O-Al_2O_3-Fe_2O_3-SiO_2 at 1 Atmosphere, and the Petrogenesis of Alkaline Rocks. J Petrol 7(1):114-170.

Ballard RD (1974) Summary of the geologic dives conducted in the Gulf of Maine during 1971 and 1972 by the research submersible Alvin. Wood Hole Oceanographic Institution Technical Report WHOI-74-29, 73 p.

_____ (1974) The nature of Triassic continental rift structures in the Gulf of Maine. Wood Hole Oceanographic Institution Technical Report WHOI-74-71, 96 p.

_____ and _____ (1972) Carboniferous and Triassic rifting: A preliminary outline of the tectonic history of the Gulf of Maine. Geol Soc Amer Bull 83: 285-2303.

_____ and Uchupi E (1975) Triassic rift structure in Gulf of Maine. Amer Assoc Petrol Geol Bull 59(7): 1041-1072.

Barker F, Wones DR, Sharp WN, Desborough GA (1975) The Pikes Peak Batholith, Colorado Front Range, and a model for the origin of the Gabbro-Anorthosite-Syenite-Potassic Granite suite. Prec Res 2:97-160

Barreiro B and Eusden JD (1988) Monazite U-Pb ages of schists and migmatites in the Kearsarge-Central Maine synclinorium. Geol Soc Amer: Abstr With Prog 20(1):9.

Batchelor RA and Bowden P (1985) Petrogenetic interpretation of granitoid rock series using multicationic parameters. Chem Geol 48:43-55.

Bayer G, Ahrens LH, and Erlank AJ (1978) Hafnium. *in* Wedepohl KH Correns CW, Shaw DM, Turekian KK Zemann J eds. Handbook of Geochemistry. II-5 Chapter 72.

Bedard JH (1985) The opening of the Atlantic, the Mesozoic New England igneous province, and mechanisms of continental breakup. Tectonophys113: 209-323.

Bence and Albee (1968) Empirical Correction Factors for the Electron Microanalysis of Silicates and Oxides. J Geol 76(4):382-403.

Besancon JR , Gaudette HE and Naylor RS (1977) Age of the Massabesic Gneiss, southeastern New Hampshire. Geol Soc Amer: Abstr With Prog 1 3:122.

Billings MP (1956) The geology of New Hampshire: Part II, Bedrock geology. NH Planning and Development Commission, Concord NH 203 p.

Birch FS (1984) Geophysical survey of bedrock on the inner continental shelf of New Hampshire. Northeastern Geology 6(2):92-101.

Bloomshield AL and Arculus RJ (1989) Magma mixing in the San Francisco Volcanic Field, AZ: Petrogenesis of the O'Leary Peak and Strawberry Crater Volcanics. Contrib Mineral Petrol 102:429-453.

Bonin B (1986) Ring complex Granites and Anorogenic Magmatism. Elsevier, New York NY 188 p.

Bothner WA, Boudette EL, Fagan TJ, Gaudette HE, Laird J, Olszweski WJ (1984) Geologic framework of the Massabesic anticlinorium and the Merrimack trough, southeastern New Hampshire. in Geology of the Coastal Lowlands Boston, MA to Kennebunk, ME (Hanson, LS, editor): 76th Annual New England Intercollegiate Geological Conference, 186-206.

_____, Brooks JA, and Eusden JD (1988) Geology and Geophysics of the Massabesic, Merrimack, and Rye "Zones" in central coastal New England. Geol Soc Amer: Abstr With Prog 20(1):9

_____, Simpson RW, and Diment WH (1980) Bouguer gravity map of the northeastern United States and adjacent Canada. US Geol Surv Open-File Report 80-2012, 13 p.

_____, Simpson W, Eskeresy D, Shride AF, Oldale RF, and Gage TB (1983) Preliminary interpretation of marine reflection profiles offshore from Cape Ann, Massachusetts to Hampton, New Hampshire: US Geol Surv Open-File Report 83-460. 28 p, 2 plates.

Bowden P and Kinnard JA (1984) Geology and Mineralization of the Nigerian Anorogenic Ring Complexes. Geologisches Jahrbuch, Reiche B, 68 pp.

_____, Black R, Martin RF, Ike EC, Kinnaird JA and Batchelor RA (1987) Niger-Nigerian alkaline ring complexes: a classic example of African Phanerozoic anorogenic mid-plate magmatism. in Alkaline Igneous Rocks. Fitton JG and Upton GJ (eds) pp 357-380.

_____ and Turner CD (1974) Peralkaline and associated ring-complexes in the Nigerian-Niger Province, West Africa. *in*: H. Sorensen ed., The Alkaline Rocks. Wiley, London, pp 330-354.

_____ and Whitley JE (1974) Rare-earth patterns in peralkaline and associated granites. Lithos 7:15-21.

Bowen NL (1928) The evolution of the igneous rocks. Princeton University Press.

Brooks JA (1986) Bedrock geology of New Hampshire's inner continental shelf. Master thesis, University of New Hampshire, 127 p.

_____ and Bothner WA(1988) Late (?) Alleghanian Dextral Transpression and Terrane Accretion within Coastal New England and Western Gulf of Maine as Interpreted from Regional Aeromagnetic and Gravity Maps. AGU EOS Trans 70(15):462.

Cameron B (ed) (1976) Geology of southeastern New England: 68th Annual New England Intercollegiate Geological Conference, 513 p.

Carr RS III (1980) Geology and Petrology of the Ossipee Ring-Complex Carroll County, New Hampshire. MS Thesis Dartmouth College. 174 pp.

Carrigan JA (1984) Geology of the Rye Formation: New Castle Island and adjacent areas of Portsmouth Harbor, New Hampshire and Maine. MS Thesis, University of New Hampshire, 128 p.

Castle RO, Dixon HR, Grew ES, Grimson A, and Zietz I (1976) Structural dislocations in eastern Massachusetts: USGS Survey Bull 1410, 39 p.

Caudill MR and Nance RD (1986) Variscan tectonostratigraphy of the Mispec Group, southern new Brunswick: stratigraphy and depositional setting. Geol Survey Canada Paper 86-1a: 343-392.

Chandler VW and Southwick DL (1990) Aeromagnetic Minnesota. EOS Trans AGU 71(11):1.

Chapman CA (1976) Structural evolution of the White Mountain magma series. In Lyons PC and Brownlow AH eds Studies in New England Geology. Geol Soc Amer memoir 146. pp 281-300

Chapman CA (1968) A comparison of the Maine Coastal Plutons and the magmatic Central Complexes of New Hampshire. *in* Studies of Appalachian Geology : Northern and Maritime. Zen E-An, White WS, Handley JB, and Thompson JB eds. pp 385-398.

Chapman RW and Chapman CA (1940) Cauldron subsidence at Ascutney Mountain, Vermont. Geol Soc Amer Bull 51:191-212.

Christopher PA (1969) Fission Track ages of younger intrusions in southern Maine. Geol Soc Amer Bull 80: 1809-1814.

Clemens JD, Holloway JR, and White AJR (1986) Origin of an A-type granite: Experimental constraints. Amer Mineral 71:317-324.

_____ and Vielzeuf D (1987) Constraints on melting and magma production in the crust. Earth Planet Sci Lett 86:287-306.

Cocherie A (1986) Systematic use of trace element distribution patterns in log-log diagrams for plutonic suites. Geochim Cosmochim Acta 50:2517-2522.

Collins WJ, Beans SD, White AJR, Chappell BW (1982) Nature and Origin of A-type granites with Particular Reference to Southeastern Australia. Contrib Mineral Petrol 80:189-200

Cox KG, Bell JD and Pankhurst RJ (1979) The Interpretation of Igneous rocks. George Allen & Unwin, publs. 450 pp.

Crough ST (1981) Mesozoic hotspot epeirogeny in eastern North America. Geology 9: 2-6.

Czamanske GK, Wones DR, Eichelberger JC (1977) Mineralogy and petrology of the intrusive complex of the Pliny Range, NH. Am J Sci 277:1073-1123

de Boer JZ, McHone JG, Puffer JH, Rafland PC, and Whittington D (1988) Mesozoic and Cenozoic Magmatism. in Sheridan RE and Grow JA eds. The Geology of North America, Vol I-2, The Atlantic Continental Margin, US: Geol Soc Amer. pp 217-241.

Dietrich RV (1968) The behavior of ziconium in certain artificial magmas under diverse P-T conditions. Lithos 1:20.

Doherty JT and Lyons JB (1980) Mesozoic erosion rates in northern New England. Geol Soc Amer Bull 91(1):16-20.

Eby GN (1987) The Monteregian Hills and White Mountain alkaline igneous provinces, eastern North America. in Fitton JG and Upton BGJ (eds.) Alkaline Igneous rocks Geol Soc Spec Publ No. 30 pp 313-333.

_____ (1985) Monteregian Hills II. Petrography, major and trace element geochemistry, and strontium isotopic chemistry of the eastern intrusions: Mounts Shefford, Brome, and Megantic. J Petrol. 26:418-448.

_____ (1985) Sr and Pb isotopes, U and Th chemistry of the alkaline Monteregian and White Mountain igneous provinces, eastern North America. Geochim Cosmochim Acta 49:1143-1153.

Ernst WG (1962) Synthesis, stability relations, and occurrence of riebeckite and riebeckite-arfvedsonite solid solutions. J Geol 70:689-836.

Eusden, JD and Barreiro B (1989) The timing of peak high-grade metamorphism in Central Eastern New England. Maritime Sed and Atlantic Geol 24:241-255.

Eusden, JD (1988) The bedrock geology of the Gilmanton 15-minute quadrangle, New Hampshire: PhD Thesis, Dartmouth College, Hanover, NH 245p.

Eusden, JD, Bothner, WA, and Hussey, AM (I987) The Kearsarge-Central Maine synclinorium of southeastern New Hampshire and southwestern Maine: Stratigraphic and structural relations of an inverted section: Am. Jour. Sci., 287, 242-264.

_____,(1984) The bedrock geology of part of the Alton, New Hampshire and Berwick, Maine 15' quadrangles. MS Thesis, University of New Hampshire, 114 p.

Fagan TJ (1985) Metamorphic petrology and structure of a transect from the Berwick Formation into the Massabesic Gneiss complex, southeastern New Hampshire. MS Thesis, University of New Hampshire.

Foland KA, Jiang-feng C, Gilbert LA, and Hofmann AW (1989) Nd and Sr isotopic signatures of Mesozoic plutons in northeastern North America. Geology 16:684-687.

_____, Henderson CMB, and Gleason J (1985) Petrogenesis of the magmatic complex at Mount Ascutney Vermont, USA. Contrib Mineral Petrol 90:331-345.

_____ and Faul H (1977) Ages of the White Mountain intrusives-New Hampshire, Vermont, and Maine, USA. Am J Sci 277: 888- 904.

_____ and Friedman I (1977) Application of Sr and O isotope relations to the petrogenesis of the alkaline rocks of the Red hill complex, New Hampshire, USA. Contrib Mineral Petrol 65: 213-225.

_____, Quinn AW, Giletti BJ (1971) K-Ar and Rb-Sr Jurassic and Cretaceous ages for intrusives of the White Mountain Magma Series, northern New England. Am J Sci 270:321-330

Fowler MB (1988) Elemental evidence for crustal contamination of mantle-derived Caledonian syenite by metasediment anatexis and magma mixing. Chem Geol 69: 1-16.

_____ and Doig R (1988) The significance of europium anomalies in the REE spectra of granites and pegmatites, Mont Laurier, Quebec. Geochim Cosmochim Acta 47(6):1131-1137.

Frost TP and Mahood GA (1987) Field, chemical, and physical constraints on mafic-felsic magma interaction in the Lamarck Granodiorite, Sierra Nevada, California. Geol Soc Amer Gull 99:272-291.

Fung Wu and Van Der Voo R (1988) Paleomagnetism of Middle-Late Triassic plutons in southern Maine. Tectonophysics 156:51-58.

Gaudette, HE, Kovack A, Hussey AM II (1982) Ages of some intrusive rocks of southwestern Maine, USA. Can J Earth Sci 19: 1350-1357.

Getty SR and Gromet LP (1988) Alleghanian polyphase deformation of the Hope Valley shear zone southeastern New England. Tectonics 7(6):1325-1338.

Giret A, Bonin B, and Leger JM (1980) Amphibole compositional trends in oversaturated and undersaturated alkaline plutonic ring-complexes. Can Mineral 18:481-495.

Goldstein AG, Vyhnal C and Hopper J (1988) Structrural analysis of the eastern Merrimack block, Eastern Massachusetts. Geol Soc Amer Abstr 20(1): 23.

Goldstein (1989) Nature of the Alleghanian Orogen in eastern Massachusetts. Geol Soc Amer Abstr 21(2):18.

Goodman RJ (1972) The distribution of Ga and Rb in coexisting groundmass and phenocryst phases of some basic volcanic rocks. *Geochim Cosmochim Acta* 36:303-317.

Gottardi G, Burton JD, and Culkin F (1978) Gallium. *in* Handbook of Geochemistry Wedepohl KH Correns CW, Shaw DM, Turekian KK Zemann J eds. Vol II-3 Chapter 31.

Grapes R, Yagi K, and Okumura K (1979) Aenigmatite, Sodic Pyroxene, Arfvedsonite, and Associate minerals in Syenites From Moroty, Sakhalin. Contrib Mineral Petrol 69:97-103.

Hamidzada N (1988) Geochemistry and structure of the northeastern part of the Scituate Pluton, Rhode Island: Kingston; unpub. MS Thesis 294 p.

Hanson LS (ed.) (1984) Geology of the Coastal Lowlands Boston, MA to Kennebunk, ME: 76th Annual New England Intercollegiate Geological Conference.

Harwood DS and Zietz I (1977) Geologic interpretation of an aeromagnetic map of southern a New England. US Geol Survey Geophys Investigations Map GP-906, 11 P.

Haskin LA, Haskin MA, Frey FA, and Wildeman TR (1968) Relative and absolute terrestrial abundances of the rare earths. In Origin and Distribution of the Elements (ed. LH Ahrens) pp 889-912.

Hatcher , Williams, H, and Zietz, I (eds.) (1983) Contributions to the Tectonics and Geophysics of Mountain Chains, Geological Society of America Memoir 158, 223 p.

Haworth and Jacobi RD (1983) Geophysical correlation between the geological zonation of Newfoundland and the British Isles. in Hatcher RD, Williams H, and Zietz I (eds.) Contributions to the tectonics and geophysics of mountain chains. Geological Society of America Memoir 158: 25-32.

Heck FR (1989) Mesozoic extension in the southern Appalachians. Geology 17:711-714.

Helz RT (1976) Phase Relations of Basalts in their Melting Ranges at PH2O = 5 kb. Part II. Melt Compositions. J Petrol 17(2):139-193.

_____ (1973) Phase Relations of Basalts in their Melting Ranges at PH2O = 5 kb as a function of Oxygen Fugacity. Part I. Mafic Phases. J Petrol 14(2):249-302.

Henderson CMB, Pendlebury K and Foland KA (1989) Mineralogy and Petrology of the Red Hill Alkaline Igneous Complex, New Hampshire, USA. J Petrol 30(3): 627-666.

Hermes OD and Zartman RE (1985) Late Proterozoic and Devonian plutonic terrane within the Avalon zone of Rhode Island. Geol Soc Amer Bull 96(2): 272-282.

_____, Ballard RD and Banks PO (1978) Upper Ordovician peralkaline granites from the Gulf of Maine. Geol Soc Amer Bull 96:272-282.

Hildreth W (1981) Gradients in silicic magma chambers: Implications for lithospheric magmatism. J Geophys Res 86(B11): 10153-10192.

Hoefs J (1967) A Rb-Sr investigation in the southern York County area, Maine: Variations in isotopic abundances of Sr, Ca, and Ar and related topics. MIT Cambridge, Mass, 15th Annual Report: 127-129.

Hoffman PF (1987) Continental transform tectonics: Great Slave Lake shear zone (ca. 1.9 Ga), northwest Canada. Geology 15:785-788.

Hogan JP, Jurinski JB, Sinha AK, and Eriksson SR (1988) Space-Time-Compositional relationships of plutonism in the coastal Maine Magmatic Province: Constraints on tectonic settings. Geol Soc Abstr 20(10):27.

Holm PM and Praegel NO (1988) The Tertiary Kaerven Syenite Complex, Kangerdlugssuaq, East Greenland: Mineral chemistry and Geochemistry. Mineral Mag 52: 433-450.

Hussey AM II (1988) Lithotectonic Stratigraphy, Deformation, Plutonism, and Metamorphism, Greater Casco Bay Region,

Southwestern Maine. *in* Tucker RD and Marvinney RG Eds, Maine Geol Survey, Studies in Maine Geol: Vol I, pp 17-34.

_____ (1985) The bedrock geology of the Bath and Portland 2° sheets, Maine. Maine Geol Surv Open-File No 85.87: 82 p.Hussey AM (1980) Gerrish Island, revisited, the Rye Formation of Gerrish Island, Kittery, Maine- a reinterpretation. The Maine Geologist 7:2-3.

_____, Rickerich S, and Bothner WA (1984) Sedimentololgy and multiple deformation of the Kittery Formation in southwestern Maine and southeastern New Hampshire. in Geology of the Coastal Lowlands Boston, MA to Kennebunk, ME (Hanson, LS, editor): 76th Annual New England Intercollegiate Geological Conference, p 47-60.

_____ (1962) The geology of southern York County area, Maine. Maine Geol Surv, Spec Geol Studies Series no 4: 67 p.

Hutchinson, DR, Klitgord KD, Lee MW, and Trehu AM (1988) US Geological Survey deep seismic reflection profile across the Gulf of Maine. Geol Soc Amer Bull 100(2):172-184.

James RS and Hamilton DL (1969) Phase relations in the system NaAlSi3O8-KAlSi3O8- CaAl2Si2O8-SiO2 at 1 kilobar water vapor pressure. Contrib Mineral Pet 21: 111- 141.

Kane MF (1968) Gravity anomalies in Maine. in Zen E-an, White WS, Hadley JB, and Thompson JB Jr (eds) Studies of Appalachian geology-northern and maritime: New York, Intersci Publ 415-423.

_____, Yellin MJ, Bell KG, and Zietz I (1972) Gravity and magnetic evidence of lithology and structure in the Gulf of Maine region. US Geol Surv Prof Paper 726-B, 22 p.

King LH (1976) Cruise Report No. 76-016- C.S.S. Hudson. Atlantic Geoscience Center, Bedford Institute of Oceanography, Dartmouth Nova, Scotia 5 p.

_____ and MacLean B (1976) Geology of the Scotian shelf. Geol Surv of Can Paper 74-31, 31 p.

Koteff C and Cotton JE (1962) Preliminary results of recent deep drilling on Cape Cod, Massachusetts. Science 137(3523): 34.

Larsen LM (1977) Aenigmatites from the Ilimaussaq intrusion, south Greenland: Chemistry and petrological implications. Lithos 10:257-270.

Leake BE and Winchell H (1978) Nomenclature of amphiboles. Amer Mineral 63:1023-1052.

Lee DE and Christiansen EH (1983) The granite problem as exposed in the southern Snake Range, Nevada. Contrib Mineral Petrol 83:99-116.

Lemarchand F, Villemant B, and Clas G (1987) Trace element distribution coefficients in alkaline series. Geochim Cosmochim Acta 51:1071-1081.

Loiselle MC (1978) Geochemistry and petrogenesis of the Belknap Mountains complex and Pliny Range, White Mountain series, NH. PhD Thesis, MIT, Boston, Ma 302p

Loiselle MC and Wones DR (1979) Characteristics and origin of anorogenic granites. Geol Soc Amer Abstr Progs 11:468.

Long PE (1978) Experimental determination of partition coefficients for Rb, Sr and Ba between alkali feldspar and silicate liquid. Geochim Cosmochim Acta 42:833-846.

Luth WC (1969) The systems NaAlSi3O8-SiO2 and KAlSi3O8-SiO2 to 20 Kb and the relationship between H2O content, PH2O, and Ptotal in granitic magmas. Am J Sci Schairer Vol: 325-341.

_____, Jahns RH, and Tuttle OF, (1964) The granite system at pressures of 4 to 10 kilobars. J Geophys Res 69:759-773.

Lyons JB, Bothner WA, Moench RH, and Thompson JB (eds.) (1986) Interim geologic map of New Hampshire: NH Dept of Environmental Services Map OF-86-1, scale 1:250,000.

Lyons JB, Boudette, EL and Aleinikoff JN (1982) The Avalonian and Gander zones in central eastern New England. in St-Julien P and Beland J (eds.) (1982) Major structural zones and faults of the northern Appalachians. Geol Soc Canada Spec Paper 24: 43-66

Lyons PC and Brownlow AH (eds) (1976) Studies in New England Geology. GSA Mem 146.

Mahood GA (1981) A Summary of the Geology and Petrology of the Sierra La Primavera, Jalisco, Mexico. J Geophys Res 86(B11):10137-10152.

_____ and Hildreth EW (1983) Large partition coefficients for trace elements in high-silica rhyolites. Geochim Cosmochim Acta 47:11-30.

Malvin DJ and Drake MJ (1987) Experimental determination of crystal/melt partitioning of Ga and Ge in the system forsterite-anorthite-diopside. Geochim Cosmochim Acta 51:2117-2128.

Manning AH and de Boar JZ (1989) Deformation of Mesozoic dikes in New England. Geology 17(11):969-1064.

Marsh JS (1975) Aenigmatite stability in silica-undersaturated ricks. Contrib Mineral Petrol 50:135-144.

McCarthy TS and Hasty RA (1976) Trace element distribution patterns and their relationship to the crystallization of granitic melts. Geochim Cosmochim Acta 40:1351-1358

McConough WF and Nelson DO (1984) Geochemical constraints on magma processes in a peralkaline system: The Paisano volcano, west Texas. Geochim Cosmochim Acta 48:2443-2455.

Mcdonald R (1987) Quaternary peralkaline silicic rocks and caldera volcanoes of Kenya in Fitton JG and Upton BGJ (eds.) Alkaline Igneous rocks Geol Soc Spec Publ No. 30 pp 313-333.

McDowell SD and Wyllie PJ (1971) Experimental studies of igneous rocks series: The Kungnat Syenite Complex of southwest Greenland. J Geol 79:173-194.

McHone JG and Butler JR (1985) Mesozoic igneous provinces of New England and the opening of the North Atlantic Ocean. Geol Soc Am Bull 95: 757-765.

_____ JG and Trygstad JC (1982) Mesozoic mafic dikes of southern Maine. in eds Hussey, AM II and Westerman DS, Maine Geology; Geol Soc Maine Bull 2: 16-32.

Miller HG (1988) Geophysical interpretation of the geology of the northeast Gander Terrane, Newfoundland. Can J Earth Sci 25:1161-1174.

Miranda JM, Galdeano A, Rossignol JC, and Mendes Victor LA (1989) Aeromagnetic anomalies in mainland Portugal and their tectonic implications. Earth Planet Sci Letters 95:161-172.

Mitchell RH and Platt RG (1978) Mafic mineralogy of ferroaugite syenite from the Coldwell Alkaline Complex, Ontario, Can J Petrol 19(4): 627-651.

Morency RE (1986) The geophysical expression of structures between the Clinton-Newbury and Bloody Bluff fault zones near Newbury, Ma. MS Thesis, University of New Hampshire, 96p.

Morgan WJ (1981) Hotspot tracks and the opening of the Atlantic and Indian Oceans. in Emiliani C ed., The Ocean Lithosphere: The Sea, Volumn 7, New York, NY, 447-487.

Morimoto N, Fabries J, Ferguson AK, Ginzburg IV, Ross M, Seifert FA, Zussman J, Aoki K, and Gottardi G (1988) Nomenclature of pyroxenes. Amer Mineral 73:1123-1133.

Nash WP and Crecraft HR (1985) Partition coefficients for trace elements in silicic magmas. Geochim Cosmochim Acta 49:2309-2322.

_____ and Wilkinson JFG (1970) Shonkin Sag Laccolith, Montana. 1. Mafic minerals and estimates of temperature, pressure, oxygen fugacity, and silica activity. Contr Miner Petrol 25:241-269.

_____, Carmichael ISE, and Johnson RW (1969) The mineralogy and petrology of Mount Suswa, Kenya. J Petrol 10(3):409-439.

Nelson DO, Kerri LN, Keith DR, and Mattison GD (1987) Geochemistry of Tertiary alkaline rocks of the Eastern Trans-Pecos Magmatic Province, Texas. Contrib Mineral Petrol 97: 72-92.

Nicholls J and Carmichael ISE (1969) Peralkaline acid liquid; a petrological study. Contrib Mineral Petrol 20:268-294.

Novotny RF (1969) The geology of the Seacoast Region of New Hampshire. New Hampshire Department of Resources and Economic Development, Concord, NH 46 p.

O'Hara K and Gromet (1985) Two distinct late Precambrian (Avalonian) terranes in southwestern New England and their late Paleozoic juxtaposition. Amer J Sci 285: 637-709.

Olszewski WJ and Gaudette HE (1988) Early Paleozoic thermotectonic history of eastern New England: Cambro-Ordovician metamorphism and plutonism- A distinctive feature of the "Casco" terrane. Geol Soc Amer: Abstr With Prog 20(1):60.

_____, Gaudette HE, Bothner WA, Laird J, Cheatam MM (1984) The Precambrian(?) rocks of southeastern New Hampshire-- A forgotten land. Geol Soc Amer: Abstr 16(10):54.

Osberg PH, Hussey AM, and Boone GM (eds.) (1985) Bedrock geologic map of Maine. Maine Geol Surv.

Paige M and Hon R (1988) The Petrological Implications for the Mafic Phases of the Cape Ann Complex, an Acadian A-type Suite Located in Northeastern Massachusetts. AGU EOS Trans 69(16):513.

Paige M and Hon R (1989) Zr/Hf systematics in alkaline granites: Case study of the Cape Ann Complex, Northeastern Massachusetts. Geol soc amer Abstr 21(2):57.

Pankhurst RJ, Beckinsale RD, and Brooks CK (1976) Strontium and Oxygen Isotope Evidence Relating to the Petrogenesis of the Kangerdlugssuaq Alkaline Intrusion, East Greenland. Contrib Mineral Petrol 54:17-42.

Parsons I (1981) The Klokken Gabbro-Syenite Complex, South Greenland: Quantitative Interpretation of Mineral Chemistry. J Petrol 22(2):233-260.

_____ and Becker SM (1986) High -temperature fluid-rock interactions in a layered syenite pluton. Nature 321:764-766.

Paster TP, Schauwecker DS, and Haskie LA (1974) The behavior of some trace elements during solidification of the Skaergaard layered series. Geochim Cosmochim Acta 38:1549-1577.

Pe-Piper G and Loncarevic BD (1988) Offshore continuation of Meguma Terrane, southwest Nova Scotia. Can J E Sci

Pearce JA, Nigel BWH, and Tindle AG (1984) Trace element discrimination diagrams for the tectonic interpretation of granitic rocks. J Petrol 25: 956-983.

Peterson JW and Newton RC (1989) Reversed experiments on biotite-quartz-feldspar melting in the system KMASH: Implications for crustal anatexis. J Geol 97: 465-485.

Powell M and Powell R (1974) An olivine-clinopyroxene geothermometer. Contrib Mineral Petrol 48:249-263.

Public Service Co of New Hampshire (1981) Seabrook Station, Final safety analysis report Vol 2.

Rast, N and Grant, R (l973) Transatlantic correlation of the Variscan-Appalachian orogeny: Am. Jour. Sci, 273, 572-579.

Rast N, O'Brian BH, and Wardle RJ (1976) Relationships between Precambrian and Lower Paleozoic rocks of the "Avalon Platform' in New Brunswick, the northeast Appalachians and the British Isles. Tectonophysics 30:315-338.

Rast N and Skehan JW (1983) The evolution of the Avalonian plate. Tectonophysics 100:257-286

Rickerich SF (1983) Sedimentology, stratigraphy and Structure of the Kittery formation in the Portsmouth, New Hampshire Area. MS Thesis, University of New Hampshire, 115 p.

Rivers T, Marignole, Gower CF, and Davidson A (1989) New Tectonic Divisions of the Grenville Province, Southeast Canadian Shield. Tectonics 8(1):51-62.

Schneiderman JS (1989) The Ascutney Mountain Breccia: Field and Petrologic Evidence for an Overlapping Relationship Between

Vermont Sequence and New Hampshire Sequence Rocks. Amer J Sci 289:771-811.

Scholle PA and Wenkam CR (eds.) (1982) Geological studies of the COST Nos. G-1 and G-2 wells, United States of north Atlantic outer continental shelf. US Dept of the Interior, Geol Surv Circ 861, 293 p.

Scott PW (1976) Crystallization trends of pyroxenes from the alkaline volcanic rocks of Tenerife, Canary Islands. Mineral Mag 40(316):805-816.

Stettler EH, DeBeer JH, and Blom MP (1989) Crustal Domains in the Northern Kaapvaal Craton as Defined by Magnetic Lineaments. Precamb Res 45:263-276.

Shih KG, Klitgord KD, Macnab R, and Bothner WA (1988) New Tectonic and Magnetic maps for the Gulf of Maine. EOS Trans AGU 69(16):479.

Simpson RW, Hassemer, JH, and Linton, JR (l980), Digitized aeromagnetic map of part of the Boston 1° x 2° quadrangle, Massachusetts, New Hampshire, Connecticut, Rhode Island, and Maine: U. S. Geological Survey Open File Report 80-243,

_____, Shride AF, and Bothner WA (1980) Offshore extension of the Clinton-Newbury and Bloody Bluff fault systems, of northeastern Massachusetts. in Wones Dr (ed.) The Caledonides in the USA, Virginia Polytechnical Institute and State University Department of Geological Science Memoir 2:229-233.

Sorensen H (1974) Introduction in The Alkaline Rocks, Sorensen H (ed) John Wiley and Sons pp 1-14.

Spector A (1971) Aeromagnetic map interpretation with the aid of the digital computer. Can Mining and Metallurgical (CIM) Bull 64(711):27-33.

_____ and Parker W (1979) Computer compilation and interpretation of geophysical data. in Hood PJ (ed.) Geophysics and geochemistry in the search for metallic ores. Geol Surv Can Econ Geol Report 31:527-544.

Stephenson D and Upton BGJ (1982) Ferromagnesian silicates in a differentiated alkaline complex: Kungnat Fjeld, South Greenland. Mineral Mag 46:283-300.

Stewart DB, Unger JD, Philips JD Goldsmith R, Poole WH, Spencer CP, Green AG, Loiselle MC and St-Julien P (1985) The Quebec-Western Maine seismic reflection profile: Setting and first year results. in Barazangi M and Brown LD (eds.) Amer Geophys Union, Geodynamics Series Volumn on International Symposium on deep structure of continental crust: Results from reflection seismology.

_____, Unger JD, Wright BE, Philips JD, Liberty LM, Spencer CP, Charlesworth P, Hutchinson DR, Klitgord KD, Luetgert JH, and Bothner WA (1989) Geological processes shown by digitized Quebec-Maine-Gulf of Maine Global Geosciences Transect. Abstr Proceedings 28th International Geol Cong, Wash, USA p 3-182.

Sultan M, Arvidson RE, Duncan IJ,Stern RJ, Kaliouby BE (1988) Extension of the Najd shear system form Saudi Arabia to the central eastern desert of Egypt based on integrated field and landsat observations. Tectonics 7(6):1291-1306.

Swanson MT (1982) The structure and tectonics of Mesozoic dike swarms in eastern New England. PhD Thesis SUNY-Albany.

_____ and Carrigan JA (1984) Ductile and brittle structures within the Rye Formation of coastal Maine and New Hampshire. in Geology of the Coastal Lowlands Boston, MA to Kennebunk, ME (Hanson, LS, editor): 76th Annual New England Intercollegiate Geological Conference, 165-185.

Taylor Sr and McLennan SM (1981) The composition and evolution of the continental crust: rare earth element evidence from sedimentary rocks. Phil Trans Roy Soc 301: 381-399.

Tindle AG and Pearce JA (1981) Petrogenetic modelling of in-situ fractional crystallization in the zoned Loch Doon pluton, Scotland. Contrib Mineral Petrol 78:196-207.

Turner DC (1968) Volcanic and intrusive structures of the Kila-Warji ring-complexes, northern Nigeria. Q J Geol Soc Lond 124:81-89.

Tuttle OF and Bowen NL Origin of granite in the light of experimental studies in the system NaAlSi3O8-KAlSi3O8-SiO2-H2O. Geol Soc Am Mem 74:153 pp.

Uchupi E (1966) Structural framework of the Gulf of Maine. Jour Geophys Research 71: 3014-3028.

_____, Phillips JD, and Prada KE (1970) Origin and structure of the New England Seamount chain. Deep-Sea Res 17: 483-494.

Van Breeman O, Hutchinson J, and Bowden P (1975) Age and origin of the Nigerian Mesozoic Granites: A Rb-Sr isotopic study. Contrib Mineral Petrol 50:157-172.

Vincent Ea and Nightingale G (1974) Gallium in rocks and minerals of the Skaergaard Intrusion. Chemical Geol 14:63-73.

Wandke A (1922) Intrusive rocks of the Portsmouth Basin, Maine and New Hampshire. Amer J Sci 4: 139-158.

Watson EB and Green TH (1981) Apatite/liquid partition coefficients for the rare earth elements and strontium. Earth Planet Sci Lett 56:405-421.

_____ and Harrison TM (1983) Zircon saturation revisited: temperature and composition effects in a variety of crustal magma types. Earth planet Sci Lett 64:295-304.

Webring M (1986) SAKI: A FORTRAN program for generalized linear inversion of gravity and magnetic profiles. USGS Surv Open File Report.

West DP, Lux Dr, and Hussey AM III (1988) $^{40}Ar/Ar^{39}$ ages from the Casco Bay Group, southwestern Maine. Geol Soc Amer Abstr 20(1):78.

Weston Geophysics Research, Inc (1976) Geological investigations for the Pilgrim II Station (5 Vols). BP-SG 7603.

Whalen JB (1985) The McGerrigle Plutonic Complex, Gaspe, Quebec: Evidence of magma mixing and hybridization. in Current Research, Part A, Geological Survey of Canada, Paper 85-1A, p. 795-800.

_____ and Currie KL (1984) The Topsails igneous terrane, Western Newfoundland: evidence for magma mixing. Contrib Mineral Petrol 87:319-327.

Whittemore AS III and Hannah JL (1988) Comingling of contrasting magmas in the Belknap Mountains Complex, New Hampshire. Geol Soc Amer Abstr 29(1):79.

Williams H and Hatcher RD (1983) Appalachian suspect terranes. in Hatcher RD, Williams, H, and Zietz, I (eds.) Contributions to the tectonics and geophysics of mountain chains Geological Society of America Memoir 158: 33-54.

Wones DR (1989) Significance of the assemblage titanite + magnetite + quartz in granitic rocks. Amer Mineral 74:744-749.

_____ and Gilbert MC (1982) Amphiboles in the igneous environment. in Amphiboles: Petrology and Experimental Phase Relations. Veblen, DR and Ribbe PH (eds.) Rev Miner 9B:355-390.

Wood BJ (1976) An Olivine-Clinopyroxene Geothermometer; A Discussion. Contrib Mineral Petrol 56:297-303.

Woodard HH (1957) Diffusion of chemical elements in some naturally occurring silicate inclusions. J Geol 65: 481-495.

Zartman RE (1988) Three decades of geochronologic studies in the New England Appalachians Geol Soc Amer Bull 100(8):1283-1290.

_____ and Naylor RS (1984) Structural implications of some radiometric ages of igneous rocks in southeastern New England. Geol Soc Amer Bull 95(5): 594-598.

Zen, E-an (I989) Tectonostratigraphic terranes in the Northern Appalachians: Their distribution, origin, and age: Evidence for their existence: Guidebook for Excursion T359, 28th Int Geo. Congress, Washington, DC (in press)

_____, Stewart DB, and Fyffe LR (1986) Paleozoic tectonostratigraphic terranes and their boundaries in the mainland northern Appalachians. Geol Soc Amer: Abstr With Prog 18:800.

_____ (1983) Exotic terranes in the New England Appalachians-limits, candidates, and ages; A speculative essay. in Hatcher RD, Williams, H, and Zietz, I (eds.) Contributions to the tectonics and geophysics of mountain chains. Geological Society of America Memoir 158: 55-82.

Zietz I, Haworth RT, Williams H, and Daniels DL (1980) Magnetic anomaly map of the Appalachian orogen. United States-Canada contribution no. 15 Coledonides orogen Map no. 2a.

Zimmerman RA, Reimer GM, Foland KA, and Faul H (1975) Cretaceous fission track dates of apatites from northern New England. Earth Planet Sci Lett 28:181-188.

APPENDIX II.I

Location of gravity measurements and flight lines for aeromagnetic data.

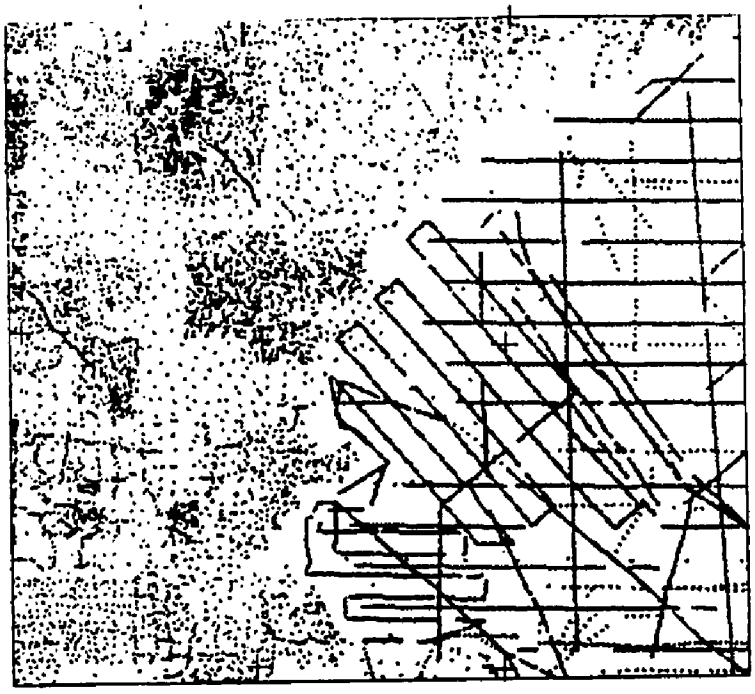
45°
71°

APPENDIX II.II

Power spectra of aeromagnetic and gravity data and filter responses

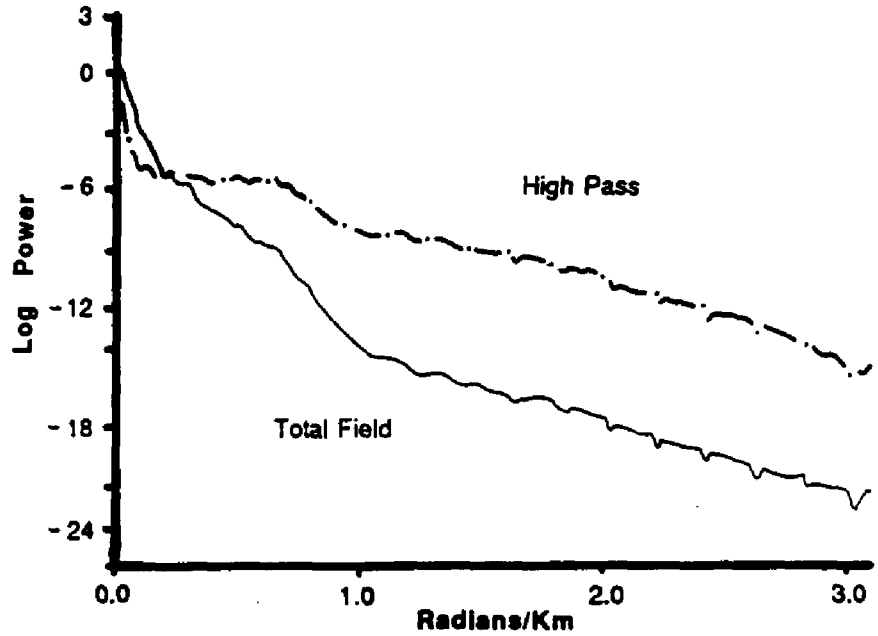

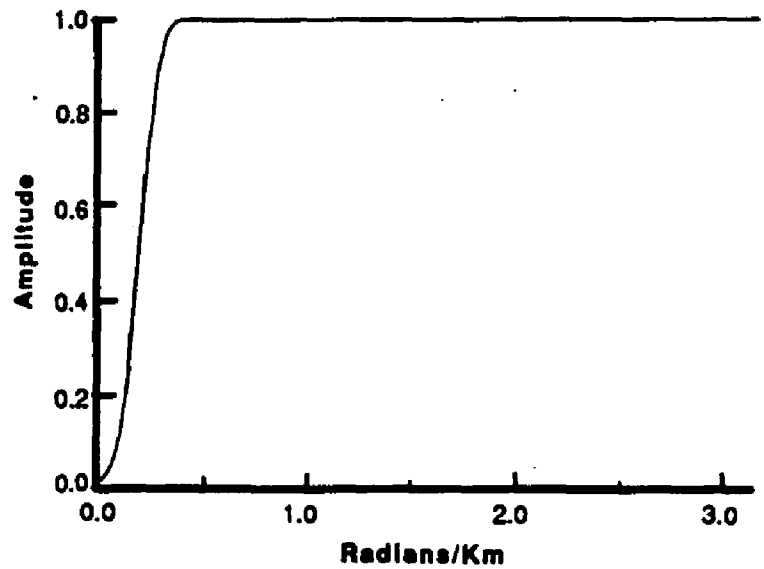

Aeromagnetic Power Spectra (a) and High Pass Filter Response (b)

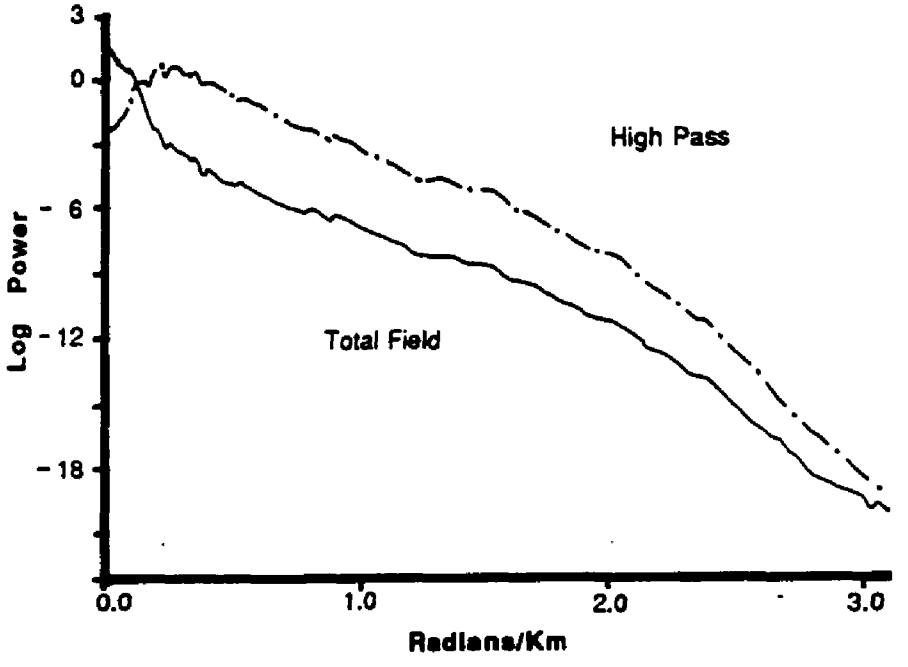

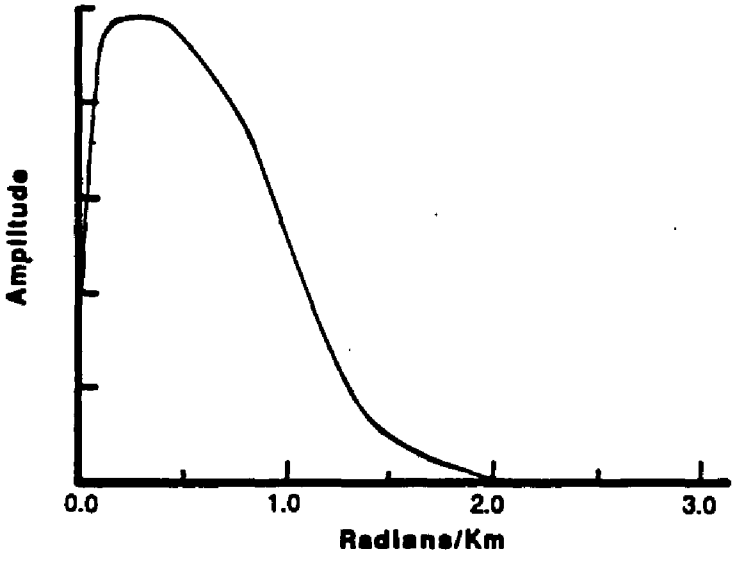

Gravity Power Spectra (a) and High Pass Filter Response (b)

APPENDIX II.III

Information about matched filters.
Excerpt from Spector and Parker (1979)

APPENDIX II.IV

PLOTTING AND DIGITIZING PROGRAMS

```
!       program to plot vector output from USGS programs
!
!
!*************************************************************************
!declarations
!*************************************************************************

        parameter       max_size=300000         ! max size of array

        integer*2       array(max_size)         ! array of points
        integer*4       array_end               ! index to end of array
        integer*4       element                 ! index to array element
        character*20    infile                  ! vector input file
        integer*4       ios                     ! ios status
        logical         newline_found           ! newline found flag
        integer*4       offset                  ! offset into array
        real*4          x                       ! x-coordinate
        real*4          y                       ! y-coordinate
        integer*4       record                  !counter
        integer*4       index                   !counter
        integer*4       pens                    !pen identifier
        real*4          maxx                    !max x- output by contour
        real*4          addx                    !adjustment for x axis
        real*4          prevx,prevy
        real*4          xtemp,xtemp1,xtemp2,xtemp3      !temp values used to
        real*4          ytemp,ytemp1,ytemp2,ytemp3      !calc transposed x,y
        real*4          maxw                    !form width
        real*4          tx(max_size),ty(max_size)       !temp values for splice
        integer*4       i                       !counter
        integer*4       overtype                !overlay type

!declarations for variables associated with plotting geology

        integer*4       tnpts,tgnpts            !number of data in temp file
        character*20    geofil                  !geology input file
        character*1     overlay                 !decision for overlay of data
        integer*4       iunit,tunit             !input and temp files
        real*4          gxmin,gymin             !x,y min for geo plot
        real*4          gxmax,gymax             !x,y max for geo plot
        integer*2       giunit,tgiunit          !geol input and splice file
        integer*2       k                       !file counter
        integer*2       j                       !geol data counter
        character*6     id(max_size),tid(max_size)!geol feature id
        real*4          gx(max_size),gy(max_size)!projected inches for geology
        real*4          tgx(max_size),tgy(max_size)!temp inches for splice
        integer*4       iscale                  !map scale
        real*4          mscale                  !km to inches conversion factor
        real*4          xt,yt,xo,yo             !plot origins

!*************************************************************************
!initialize parameters
!*************************************************************************

!initialize counters

        i=1
        k=1
```

```
!initialize plotter

        call plots (0.,0.,1)

        call newpen(1)

!assign maxx and maxw

        print *, 'input max x value from contour (real): '
        read(*,12)maxx
12      format(f5.2)

        addx=maxx + 4.0

        print *, ' enter plotter width: 33.0 or 13.0 '
        read (*,14) maxw
14      format(f4.1)

!initialize file unit numbers

        iunit=20
        tunit=30
        giunit=40
        tgiunit=50
!initialize maximum geol inches from geophysical plot

!       gxmax=0.0
!       gymax=0.0

!input vector file created in contour.for

13      print *, ' input vector grd name: '
        read(*,11)infile
11      format(a20)


        open (
     .          status='old',
     .          form='unformatted',
     .          unit=iunit,
     .          access='sequential',
     .          recl=128,
     .          recordtype='fixed',
     .          organization='sequential',
     .          file=infile
     .                          )


! open temp file for splice

        open (unit=tunit,form='unformatted',file='plot.tmp',status='scratch')

!*******************************************************************************
! input geophysical plot vectors
********************************************************************************

        record = 1                              ! initialize record counter
        ios = 0                                 ! init io status symbol
        do while (ios .eq.0)                    ! while not eof or error...

10              offset = ((record-1) * 256) + 1 ! compute offset into array
```

```
                read (iunit,err=40,iostat=ios)  ! read a 256 word record
     .                  (array(element),        ! store in ARRAY at OFFSET
     .                          element=offset,(offset+255))
                record = record + 1             ! increment record counter
        end do                                  ! go back for another record

40      close (iunit)                           ! close input file
        if (ios .gt. 0)                         ! if an error occurred...
     .  then                                    ! then signal
                call lib$signal (%val(ios))
                .
        else if (ios .eq. -1 .or.               ! else if end of file...
     .                  ios .eq. 0)             ! or no error at all...
     .  then
                continue                        ! simply continue
        end if
!
!
! find number of array points (array_end)

        array_end=0                             ! init index to end of array

        do 50 index=1,((record-1)*256)
                if(array(index) .ne. 0) array_end = array_end + 1 !increment
                                                                  !array_end
50      continue


!find start of first line

        index=1                                 !initialize array index
        newline_found = .false.                 !clear new line flag

        do while(.not. newline_found .and.      !test flag for found
     .          index .le. array_end)           !and for array end

                newline_found = (array(index) .lt. 0)

                                                !set flag if lt 0
                index = index + 1               !increment array

        end do

                index = index -1                !reset index to flag index

!warning if start of 1st line not found

        if (.not. newline_found) print *, ' start of line not found'

!*************************************************************************
!if new line found read rest of line and plot points
!*************************************************************************

!assign min/max values for plotting geol data within geophys plot border
!assumes that geophys has a border plotted!!!!

        gymin=array(3)*.01
        gxmin=array(2)*.01
        gymax=array(7) *.01
        gxmax=array(4)*.01
```

```
      do while (index .le. array_end)          !while points remain...

            if (newline_found) then            !if start of newline

                  x = array(index + 1)         !read x and y value for
                  y = array(index + 2)         !start pt of newline

                  x = 0.01 * x                 ! scale down
                  y = 0.01 * y

!test for max values
!                 if (x .gt. gxmax) gxmax=x
!                 if (y .gt. gymax) gymax=y
!continue plot
                  if (y .le. maxw) then

                        call plot(x,y,3)

                  else

                        i=i+2
                        tx(i-2)=-999.0
                        ty(i-2)=0.0
                        write (tunit) tx(i-2),tx(i-2)

                        ty(i-1)=(y- maxw)
                        tx(i-1)=(x + addx)
                        write (tunit) tx(i-1),ty(i-1)

                  endif

                  prevy=y
                  prevx=x

                  newline_found =          !test for newline
                        (array(index+3) .lt. 0)
                  index = index + 3        !increment index
            else                           !if not newline

                  x = array(index)         !assign x,y values
                  y = array(index + 1)

                  x = 0.01 * x             ! scale down
                  y = 0.01 * y


!compare pt to previous pt and make corrections for plotting purposes

                  if ((y .le. maxw) .and. (prevy .le. maxw)) then
                        call plot (x,y,2)

                  else
                        if ((y .gt. maxw) .and. (prevy .gt. maxw)) then
                              tx(i)=x+addx
                              ty(i)=y-maxw
                              write(tunit) tx(i),ty(i)
                              i = i+1

                  else
```

```
                        if ((y .gt. maxw) .and. (prevy .le. maxw)) then
                                ytemp2=y - prevy
                                xtemp2=x - prevx
                                ytemp= maxw - prevy
                                xtemp= (xtemp2/ytemp2) * ytemp
                                xtemp3= prevx + xtemp

                                call plot (xtemp3,maxw,2)

                                i=i+3

                                tx(i-3)=-999.0
                                ty(i-3)=0.0
                                write (tunit) tx(i-3),ty(i-3)

                                tx(i-2)=xtemp3 + addx
                                ty(i-2)=0.0
                                write (tunit) tx(i-2),ty(i-2)

                                tx(i-1)= x + addx
                                ty(i-1)= y - maxw
                                write (tunit) tx(i-1),ty(i-1)

                        else

                                if ((y .le. maxw) .and. (prevy .gt. maxw)) then
                                ytemp= prevy - maxw
                                ytemp2= prevy - y
                                xtemp2= x - prevx
                                xtemp= (xtemp2/ytemp2) * ytemp
                                xtemp3 = prevx + xtemp

                                i= i+1

                                tx(i-1) = xtemp3 + addx
                                ty(i-1) = 0.0
                                write (tunit) tx(i-1),ty(i-1)

                                call plot (xtemp3,maxw,3)
                                call plot (x,y,2)
                                endif
                                endif
                                endif
                        endif

                        newline_found =         !test next datum for newline
                                (array(index + 2) .lt. 0)
                        index = index +2        !increment index

                        prevy=y
                        prevx=x

                end if

        end do

! read and plot data in temp file

        tnpts = i - 2
```

```
        if (tnpts .eq. 0) then
                close (tunit)
                go to 132
        endif

                read (tunit,end=130) tx(i),ty(i)
130     continue

        close (tunit)

        do 135 i = 1,tnpts
                if (tx(i) .eq. -999.0) then
                        call plot (tx(i+1),ty(i+1),3)
                else
                        call plot (tx(i),ty(i),2)
                endif
135     continue

!*************************************************************************
!choose additional overlays
!*************************************************************************

132     print *, ' do you wish an overlay ? (y or n)'
        read (*,136) overlay
136     format(a1)

!choose pen color

        if (overlay .eq. 'n') go to 140
                print *, ' choose pen color:1=black,2=red,3=blue,4=green)'
                read (*,137) pens
137             format(i1)
                call newpen(pens)

!reset unit numbers

                iunit=iunit+1
                tunit=tunit+1

!choose type of overlay

        print*, ' type of data: geologic=1,geophysical=2'
        read (*,155) overtype
155     format(i2)

        if (overtype .eq. 2) go to 13

!*************************************************************************
!plot geologic data
!*************************************************************************

!set constants and file names

61              print *, ' enter projected geologic data filename? '
                read (*,65) geofil
65              format (a20)


!set file number and open file

                j=1
```

```
                giunit = giunit + k

                open (unit=giunit,file=geofil,form='formatted',status='old')
                open (unit=tgiunit,file='geo.tmp',form='unformatted',status='scratch')

!if second geology file; do not reset constants

                if (k .gt. 1 ) go to 79

                print *, ' map scale: (1/scale) '
                read (*,70) iscale
70              format (i8)

                mscale = (.393701*100000.0)/real(iscale)        ! km to inches

                print *, ' enter xo,yo: (projected km,neg w + e of cm + baslat) '
                read (*,75) xo,yo
75              format(2f9.4)

!adjust so that origin is assigned to corner of border as plotted
!
!               xt=xo-gxmin
!               yt=yo-gymin
!
!read data from input file

79              print *, ' reading geol data, unit= ',giunit

                i=1

80              read (giunit,85,end=90) gx(i),gy(i),id(i)
85              format(2f9.3,1x,a5)

!scale projected km to plotter inches

                gx(i)=((gx(i) - xo) * mscale) + gxmin   !adjust to origin of
                gy(i)=((gy(i) - yo) * mscale) + gymin   !geophysical data

                i= i + 1
                go to 80


90              npts = i - 1

                close (giunit)

!plot geologic data, splice to temp file if x>maxx

                print *, ' ***plotting geol data, file # ', k
    c                   ,' filename: ',geofil

!start plot and put data for splice in temp file
                do 120 i= 1,npts

!check to see if geol will plot outside of gephysical data

                        if ((gy(i) .gt. gymax) .or. (gx(i) .gt. gxmax)
    c                           .or. (gy(i) .lt. gymin) .or. (gx(i) .lt. gxmin))
    c                   then
                                id(i)='xxx'
```

```
                        go to 120
                    endif

!compare id to indicate new line

                    if ((id(i) .ne. id(i-1)) .or. (i .eq. 1)) then


!if newline then
                        if (gy(i) .le. maxw) then

                            call plot(gx(i),gy(i),3)

                        else

                            tid(j)='txxx'
                            tgy(j)=(gy(i)- maxw)
                            tgx(j)=(gx(i) + addx)
                            write (tgiunit)tgx(j),tgy(j),tid(j)
                            j=j+1
                        end if
                    else
!if not newline
                    if ((gy(i) .le. maxw) .and. (gy(i-1) .le. maxw)) then
                        call plot (gx(i),gy(i),2)

                    else
                        if ((gy(i) .gt. maxw) .and.
    c                       (gy(i-1) .gt. maxw)) then

                            tgx(j)=gx(i)+addx
                            tgy(j)=gy(i)-maxw
                            tid(j)=id(i)
                            write (tgiunit)tgx(j),tgy(j),tid(j)
                            j=j+1

                    else

                        if ((gy(i) .gt. maxw) .and. (gy(i-1) .le.
    c                       maxw)) then
                            ytemp2=gy(i) - gy(i-1)
                            xtemp2=gx(i) - gx(i-1)
                            ytemp= maxw - gy(i-1)
                            xtemp= (xtemp2/ytemp2) * ytemp
                            xtemp3= gx(i-1) + xtemp

                            call plot (xtemp3,maxw,2)

                            j=j+1
                            tgx(j-1)=xtemp3+addx
                            tgy(j-1)=0.0
                            tid(j-1)='txxx'

                        write (tgiunit)tgx(j-1),tgy(j-1),tid(j-1)

                            tgx(j)=gx(i)+addx
                            tgy(j)=gy(i)-maxw
                            tid(j)=id(i)

                        write (tgiunit)tgx(j),tgy(j),tid(j)
                        j=j+1
```

```
                        else

                                if ((gy(i) .le. maxw) .and. (gy(i-1) .gt.
     c                                  maxw)) then
                                ytemp= gy(i-1) - maxw
                                ytemp2= gy(i-1) - gy(i)
                                xtemp2= gx(i) - gx(i-1)
                                xtemp= (xtemp2/ytemp2) * ytemp
                                xtemp3 = gx(i-1) + xtemp

                                tgx(j)=xtemp3+addx
                                tgy(j)=0.0
                                tid(j)=id(i)

                                write (tgiunit)tgx(j),tgy(j),tid(j)

                                call plot (xtemp3,maxw,3)
                                call plot (gx(i),gy(i),2)

                                j=j+1
                                endif
                                endif
                                endif
                                endif
                        endif

120     continue

        k=k+1

!read temp file and plot

        tgnpts= j-1

        if (tgnpts .eq. 0) go to 138

                read (tgiunit,end=150) tgx(j),tgy(j),tid(j)

150     continue

        do 165 j=1,tgnpts

                if ((j .eq. 1)
     c          .or. (tid(j) .ne. tid(j-1))
     c          .or. (tid(j) .eq. 'txxx')) then

                        call plot (tgx(j),tgy(j),3)

                else

                        call plot (tgx(j),tgy(j),2)

                endif

165     continue

138     close (tgiunit)
        tgiunit=tgiunit + 1

139     go to 132
```

```
140     call plot (0.,0.,999)
        stop
        end
```

```
      GEODIG.FOR desinged to digitized from maps
       real xbl,ybl                    !x,y-bottom left corner
       real xbr,ybr                    !x,y-bottom right corner
       real xul,yul                    !x,y-upper left corner
       real xur,yur                    !x,y-upper right corner
       character*20 outfil,outfil2     !name of output file
       parameter maxnum=100000         !max number of points
       real x(maxnum),y(maxnum)        !digitized data points
       character*5 id(maxnum)          !identifier for geologic features
       character*5 index               !temporary identifier
       character*2 delim               !button deliminator
       integer i,npts                  !counter,number of data points
       integer j,k                     !file counters
       real baselat                    !base latitude
       real cm                         !central meridian
       real maxlat,maxlon              !max lat,lon of map digitized
       real minlat,minlon              !min lat,lon of map digitized
       real lon(maxnum),lat(maxnum)    !corrected lat/lon
       real xscale,yscale              !scaling values used to calc lat/lon


!set file counters
       j=20
       k=30

!define boundaries so that digitized inhes can be converted to lat/lon

       print *, ' digitize lower left hand corner: '
       read (*,10) xll,yll
10     format (2x,2f5.3)
            PRINT *,XLL,YLL

       print *, ' digitize upper left hand corner: '
       read (*,10) xul,yul

       print *, ' digitize upper right hand corner: '
       read (*,10) xur,yur

       print *, ' digitize lower right hand corner: '
       read (*,10) xlr,ylr

       print *, ' enter maxlat, minlat (decimal degrees xx.xx,xx.xx) '
       read (*,12) maxlat,minlat
12     format(2f6.2)

       print *, ' enter maxlon,minlon (decimal degrees) '

       read (*,12) maxlon,minlon

!open output file

130    print *, ' enter output filename: ; print stop for program exit '
       read (*,5) outfil
5      format(a20)

       if(outfil .eq. 'stop') go to 95

       open(file=outfil,unit=j,status='new',form='unformatted')

!write to outfil
```

```
      write (j) maxlon,maxlat,minlon,minlat,xll,yll,xul,yul,xur,yur,xlr,ylr

!enter data points- end when id=ex

      i=0

25    print *, ' enter id then digitize line: ; id=ex for newfile
     c         or program exit'

      read (*,15) index
15    format (a5)


      if (index .eq. 'ex') go to 100

      print *, 'digitize line; use button 3 for end of line'

30                  i=i+1
                    read (*,35)delim, x(i),y(i)
35                  format(a2,2f5.3)

                    id(i)=index

                    if (delim .eq. 'p3Z')  then
                                      i=i-1
                     go to 25
                endif

                    write(j) x(i),y(i),id(i)

      go to 30

100   npts=i-1

      close (j)

!convert data to lat/lon and put in separate data file

      print *, ' enter filename of lat/lon output file: '
      read (*,5) outfil2

      open(unit=k,status='new',form='formatted',file=outfil2)

      xscale=(maxlon-minlon)/(((xur-xul)+(xlr-xll))/2)
      yscale=(maxlat-minlat)/(((yul-yll)+(yur-ylr))/2)
           write (*,185) xscale,yscale
185     format(2f8.3)

      do 120 i=1,npts

            lon(i)=maxlon - (xscale * (x(i)-xll))
            lat(i)=minlat + (yscale * (y(i)-yll))

            write (k,50) lon(i),lat(i),id(i)
50          format(2f9.3,1x,a5)

120   continue

      close (k)

!increment file counters
```

```
        j=j+1
        k=K+1

        go to 130

95      continue
      stop

        end
```

APPENDIX III.I

Information about labs from which mineral analyses were obtained.
Comparison of analyses from different geochemical labs.

Appendix I

X-Ray Energy Spectrometry

Laboratory facilities- University of Rhode Island, Dr. OD Hermes

Elements analysed
Majors- SiO2,TiO2,Al2O3,Fe2O3,MnO,MgO,CaO,Na2O,K2O,P2O5
Trace- Rb,Sr,Ba,Y,Zr,Nb,La,Ce,Cu,Zn,Ni

% Error-Majors- 1

Standards- BCR 11, AGV 11, GSP-12, URI internal

X-Ray Fluoresence

Laboratory facilities- University of Florida, Dr M Perfit

Elements analysed
Majors- SiO2,TiO2,Al2O3,Fe2O3,MnO,MgO,CaO,Na2O,K2O,P2O5
Trace- Rb,Sr,Ba,Y,Zr,Nb,La,Ce,Cu,Zn,Ni,Cr,V,Co,Ga (Ti and K also determined from pressed powders)

% Error-Majors- 1.65

Standards- AGV 1, G-2

Laboratory facilities- University of Michigan, Dr. RJ Arculus

Elements analysed
Majors- SiO2,TiO2,Al2O3,Fe2O3,MnO,MgO,CaO,Na2O,K2O,P2O5
Trace- Rb,Sr,Ba,Y,Zr,Nb,La,Ce,Nd,Cu,Zn,Ni,Cr,V,Co,Ga,Th,U,Pb,Sc

Induced Coupled Plasma

Laboratory facilities- United States Geologic Survey- Reston.

Elements analysed
Majors- SiO2,TiO2,Al2O3,Fe2O3,MnO,MgO,CaO,Na2O,K2O,P2O5
Trace-
Rb,Sr,Ba,Y,Zr,REE,Cu,Zn,Ni,Cr,Co,Th,U,Pb,Sc,Ta,Li,Cs,Sc,Be,Bi,Bo

Electron Microprobe Analyses

Laboratory facilities- Massachusetts Institute of Technology

Filament current- 15 kV
Beam current of 10 nA.
Beam diameter- Biotite 10 microns. Other minerals- 1 to 2 microns.
Count times- Dependent on mineral being analysed.
Elements analysed
SiO2,TiO2,Al2O3,Fe2O3,MnO,MgO,CaO,Na2O,K2O, CrO, Cl, F (Cl and F only for a limited number of amphibole and biotite analyses)

Standard deviation- range of 0.2% to 25.0% depending on element and run
Mineral Normalization- To the number of cations.
Amphibole normalized to 13 cations excluding Na, K, and Ca. Fe3+ calculated by balancing charges of cations vs anions. See PRBMAC macro spread sheet below for calculations.
End member compositions
Plagioclase-
Olivine- Fayalite=Fe2+, Fosterite=Mg.
Clinopyroxene: Wollastonite= Ca/2, Enstatite=Mg/2, Ferrosilite=(Fe(total)-Na)/2, Acmite=Na or as Diopside=Mg, Hedenbergite=Fe(total)-Na, Acmite=Na. As can be seen the Wo-En-Fs-Ac plot below the mineral analyses all lie close to the Di-Hd-Ac plane.
Ilmenite-Geikerlite=Mg, Ilmenite=Ti,Hematite=Fe3+.
Rehomogenenization of potassium feispar compositions from perthite grains accomplished by using the scanning integration facility on the JOEL 733 SUPER PROBE and by calculating a weighted average composition using visual estimates of lamellae proportion.

Standard analyses from Univ of Florida

	AGV-1	AGV-1	AGV-1	AVG	STD	avg-min	% error
SiO2	59.44	60.06	60.31	59.94	0.45	0.50	0.83
TiO2	1.08	1.08	1.08	1.08	0.00	0.00	0.00
Al2O3	17.1	17.33	17.48	17.30	0.19	0.20	1.18
Fe2O3	6.95	6.97	6.97	6.96	0.01	0.01	0.19
MnO	0.1	0.1	0.1	0.10	0.00	0.00	0.00
MgO	1.59	1.56	1.58	1.58	0.02	0.02	1.06
CaO	5	5.02	5.02	5.01	0.01	0.01	0.27
Na2O	4.47	4.42	4.64	4.51	0.12	0.09	2.00
K2O	2.93	2.94	2.75	2.87	0.11	0.12	4.29
P2O5	0.51	0.51	0.52	0.51	0.01	0.00	0.65

Comparison of Univ of Florida and USGS analyses

	MAG 11a UF	MAG 11a USGS	Avg	STD	avg-min	% error
SiO2	63.66	63.9	63.78	0.17	0.12	0.19
TiO2	0.46	0.45	0.46	0.01	0.01	1.10
Al2O3	15.07	14.6	14.84	0.33	0.24	1.58
Fe2O3	7.92	7.69	7.81	0.16	0.12	1.47
MnO	0.19	0.2	0.20	0.01	0.01	2.56
MgO	0.12	0.1	0.11	0.01	0.01	9.09
CaO	1.49	1.54	1.52	0.04	0.03	1.65
Na2O	7.08	6.22	6.65	0.61	0.43	6.47
K2O	4.87	4.94	4.91	0.05	0.04	0.71
P2O5	0.07	0.06	0.07	0.01	0.01	7.69

	MAG 11c UF	MAG 11c USGS	Avg	STD	avg-min	% error
SiO2	66.8	67.9	67.35	0.78	0.55	0.82
TiO2	0.1	0.09	0.10	0.01	0.01	5.26
Al2O3	16.86	16.7	16.78	0.11	0.08	0.48
Fe2O3	1.97	2.12	2.05	0.11	0.08	3.67
MnO	0.03	0.02	0.03	0.01	0.01	20.00
MgO	0.1	0.1	0.10	0.00	0.00	0.00
CaO	0.13	0.13	0.13	0.00	0.00	0.00
Na2O	7.22	6.48	6.85	0.52	0.37	5.40
K2O	5.78	5.71	5.75	0.05	0.04	0.61
P2O5	0.03	0.15	0.09	0.08	0.06	66.67

Comparison of Na2O from UF (XRF), BC (INAA),USGS (ICP)

	UF	USGS	BC	Avg	STD	avg-min	% error
MAG 11a	7.08	6.22	5.81	6.37	0.65	0.56	8.79
MAG 11c	7.22	6.48	6.79	6.83	0.37	0.35	5.12

APPENDIX III.II

Ferric-Ferrous Iron Analyses

SAMPLE #	Fe2O3	FeO	Fe2O3*	FeO/Fe2O3*	FeO/FeOt
alk sye					
MAG-2	6.52	3.67	2.43	1.51	0.60
MAG-3	5.75	4.12	1.16	3.54	0.78
MAG-37b	5.00	3.19	1.45	2.20	0.69
MAG-39	5.00	3.12	1.53	2.04	0.67
MAG-61B	4.78	n.a.			
MAG-72B	5.20	n.a.			
dikes					
MAG-19	3.17	1.98	0.97	2.05	0.67
MAG-40-2	4.84	2.84	1.68	1.69	0.63
MAG-40-4	5.12	2.95	1.84	1.61	0.62
bio gran					
MAG-4	3.23	2.48	0.47	5.22	0.84
MAG-177	3.55	n.a.			
MAG-179	2.62	n.a.			
Alk gran					
MAG-5	5.59	3.60	1.58	2.27	0.69
MAG-17	5.61	2.57	2.75	0.93	0.48
MAG-23	0.63	n.a.			
MAG-26	3.12	n.a.			
MAG-120	4.97	n.a.			
MAG-135	3.92	n.a.			
Aeg gran					
MAG-47	5.74	2.07	3.44	0.60	0.38
MAG-48	5.60	0.16	5.42	0.03	0.03
MAG-49	5.08	2.09	2.75	0.76	0.43
MAG- 91-4	4.71	n.a.			
MAG-122A	5.58	n.a.			
SQSZ					
MAG-11a	7.69	4.64	2.53	1.84	0.65
MAG-11c	2.12	0.36	1.72	0.21	0.17
MAG-51D	7.80	n.a.			
MAG-91-1	9.59	n.a.			
MAG- 91-2	7.52	n.a.			
aenig sye					
MAG-44-a	6.96	3.84	2.69	1.43	0.59
MAG-139	8.76	n.a.			
mafic sye					
MAG-57D	6.65	n.a.			
MAG-125CP	6.73	n.a.			

Fe2O3*=Fe2O3-(feO*1.113)

Source Code

2.45 -URI

2.45 -USGS

APPENDIX III.III

Mineral Microprobe Analyses

15-Jun-89 h+b gran?			2-4 from mafic clot			5 and up from bio-hm gran			
Mag-4	7	1	2(1)	3	4(3)	5	6(5)	7	7
	bio-c	bio-r	bio-c	bio-r	bio-c	bio-c	bio-r	bio	bio
MGO	5.455	5.541	5.388	5.465	5.578	5.48	5.327	5.178	5.236
AL203	13.189	12.347	12.577	12.269	12.695	12.641	12.915	13.352	13.227
SIO2	35.756	35.898	35.902	35.212	35.605	35.718	36.103	35.493	35.778
CO	0.018	0	0.021	0	0.054	0.041	0	0.054	0.025
TIO2	4.126	3.86	3.788	3.841	3.702	3.788	4.127	3.466	3.386
CR2O3	0.42	0.484	0.423	0.441	0.432	0.493	0.516	0.554	0.529
NIO	28.367	28.377	28.411	28.975	28.122	28.634	28.261	27.975	27.882
MNO	0.035	0.033	0.056	0.027	0.044	0.05	0.05	0.038	0.032
FEO	9.022	9.009	9.18	9.022	8.998	9.188	9.151	9.331	9.578
NA2O	0.378	0.372	0.348	0.414	0.396	0.38	0.38	0.28	0.331
K2O	0.317	0.321	0.642	0.813	0.902	0.569	0.695	0.078	0
F									
CL									
SUM=	97.082	96.762	96.746	96.579	96.928	97.3	97.525	95.799	96.005
SI	3.02879	3.04979	3.05396	3.00178	3.02788	3.02206	3.04561	3.05179	3.06874
Al(tot)	1.31729	1.23641	1.26103	1.23281	1.28534	1.26087	1.28418	1.3532	1.33724
Al([illegible] IV	-0.0298	-0.0498	-0.054	-0.0018	-0.0278	-0.0221	-0.0456	-0.0518	-0.0687
Al([illegible]) VI	1.34707	1.28821	1.31499	1.23457	1.31322	1.28273	1.32979	1.40499	1.40598
TI	0.26293	0.24791	0.24233	0.25267	0.23544	0.24091	0.26183	0.22342	0.21835
Fe(tot)	0.63935	0.64011	0.65307	0.64323	0.63638	0.65015	0.64582	0.67099	0.68706
Fe +3	-1.8348	-1.7141	-1.755	-1.8145	-1.6786	-1.6937	-1.796	-1.8843	-1.8923
Fe +2	2.47418	2.35417	2.40807	2.25775	2.315	2.34382	2.44158	2.55825	2.57931
Mg	0.688	0.70157	0.68432	0.69432	0.703	0.691	0.68972	0.66352	0.66956
Mn	0.00251	0.00237	0.00404	0.00195	0.00315	0.00358	0.00367	0.00277	0.00232
NI	1.93331	1.93906	1.94361	1.9867	1.91278	1.96901	1.91753	1.93466	1.9235
Cr	0.02814	0.03251	0.02845	0.02973	0.02889	0.03298	0.03442	0.03767	0.03588
Ca	0.00183	0	0.00191	0	0.00469	0.00372	0	0.00498	0.0023
K	0.03427	0.06899	0.06967	0.06842	0.06732	0.06358	0.07372	0.00867	0
Na(tot)	0.06178	0.06128	0.0574	0.06843	0.06493	0.06234	0.06379	0.04835	0.05505
Na(M4)									
Na(A)									
SUM=	8	8	8	8	8	8	8	8	8
Fe(tot)/Fe(tot	0.48131	0.4771	0.48832	0.4809	0.47513	0.48477	0.49084	0.5028	0.50646

	19a	19b	?	11	12(11)	13(11)	14	15(14)	16(14)
	pig	pig		pig-r	pig-i	pig-c	pig-r	pig-i	pig-c
MGO	0.022	0.013	5.177	0.014	0.038	0	0	0.025	0
AL203	23.161	24.494	13.569	22.269	23.249	26.393	19.274	22.088	22.767
SIO2	62.609	66.883	35.728	64.086	63.948	58.174	68.936	64.394	63.25
CO	4.587	4.583	0.05	3.508	4.431	8.117	0.172	3.304	4.298
TIO2	0	0	0	0	0	0	0	0	0
CR2O3	0	0	0	0	0	0	0	0	0
NIO	0	0	0	0	0	0	0	0	0
MNO	0	0	0	0	0	0	0	0	0
FEO	0.167	0.106	28.535	0.036	0	0.036	0.024	0	0.036
NA2O	7.213	1.922	0.065	9.306	8.747	6.836	11.7	9.179	8.796
K2O	0.403	0.205	9.472	0.431	0.566	0.27	0.123	0.688	0.561
F									
CL									
SUM=	98.182	98.266	92.596	99.65	100.977	99.826	100.229	99.679	99.708
SI	2.85895	3.19322	1.86929	2.84224	2.80878	2.60812	3.00501	2.85729	2.81136
Al(tot)	1.24881	1.37675	0.83678	1.16413	1.20364	1.39366	0.99032	1.15523	1.19279
Al([illegible]) VI	1.14105	0.80678	0.83679	1.15776	1.19121	1.39366	0.99032	1.14271	1.18664
Al([illegible]) IV	0.10586	0.56998	0	0.00637	0.01243	0	0	0.01251	0.00415
TI	0	0	0	0	0	0	0	0	0
Fe(tot)	0.00638	0.00423	1.24889	0.00134	0	0.00135	0.00087	0	0.00134
Fe +3	-0.3024	-1.573	2.08347	-0.0239	-0.0445	0.00335	-0.0046	-0.0411	-0.0256
Fe +2	0.30875	1.57724	-0.8149	0.02528	0.04464	-0.002	0.00543	0.04106	0.02695
Mg	0.0015	0.00092	0.40367	0.00093	0.00238	0	0	0.00185	0
Mn	0	0	0	0	0	0	0	0	0
NI	0	0	0	0	0	0	0	0	0
Cr	0	0	0	0	0	0	0	0	0
Ca	0.22444	0.23468	0.0028	0.18671	0.20864	0.38983	0.00803	0.15709	0.2048
K	0.02348	0.01247	0.83228	0.02439	0.03172	0.01543	0.00884	0.039	0.03181
Na(tot)	0.63865	0.17772	0.00659	0.80028	0.74496	0.56381	0.98883	0.78874	0.75809
Na(M4)									
Na(A)									
SUM=	8	8	8	8	8	8	8	8	8
An:	0.25315	0.55238	0.00437	0.18918	0.21167	0.39007	0.008	0.15935	0.20573
Ab:	0.72037	0.41828	0.01028	0.80724	0.75614	0.56446	0.98518	0.80109	0.76228
Kp:	0.02648	0.02935	0.98535	0.0246	0.03219	0.01545	0.00681	0.03956	0.03199

6	7	8	9	10(9)
bio	bio-c	bio	bio-c	bio-r
5.377	5.312	5.208	5.599	6.052
13.763	13.723	13.569	12.717	12.943
36.565	35.754	36.052	35.178	36.429
0.062	0.033	0.058	0.021	0.033
4.854	3.396	4.888	3.452	2.775
0.437	0.571	0.456	0.512	0.455
27.499	28.163	27.454	29.092	28.301
0.056	0.05	0.062	0	0.079
8.344	8.317	8.358	8.618	8.883
0.269	0.314	0.264	0.389	0.43
0.134	0.079	0	0.378	0.195
98.16	96.712	97.183	95.954	96.575
3.06672	3.04022	3.06026	3.0137	3.06303
1.36056	1.37541	1.35963	1.26422	1.29112
-0.0867	-0.0402	-0.0603	-0.0137	-0.063
1.4273	1.41563	1.41988	1.29782	1.37415
0.29356	0.21717	0.29915	0.22242	0.17662
0.65542	0.66257	0.66419	0.6175	0.62873
-2.052	-1.8662	-2.0656	-1.8652	-1.7493
2.70744	2.53082	2.7296	2.30271	2.37799
0.67209	0.67316	0.65856	0.7149	0.76333
0.00398	0.0038	0.00446	0	0.00566
1.85502	1.92612	1.87436	2.0047	1.92644
0.02895	0.03839	0.03061	0.03468	0.03045
0.00557	0.00301	0.00528	0.00193	0.00299
0.01434	0.00857	0	0.04132	0.02105
0.04375	0.05177	0.04345	0.06462	0.07056
6	6	6	6	6
0.49372	0.49803	0.50212	0.46348	0.45166

17	18(17)	19	20	20a	20b
pig-r	pig-l	epi?	kap-r	kap	pig
0.017	0	0.07	0	0	0
21.667	23.675	26.582	18.518	18.347	19.857
65.527	62.676	37.872	65.154	64.91	66.348
2.752	4.746	22.972	0.048	0.028	0.477
0	0	0	0	0	0
0	0	0	0	0	0
0	0	0	0	0	0
0	0	0	0	0	0
0.165	0	1.145	0.109	0.129	0
9.797	8.665	0.072	0.637	0.604	11.413
0.264	0.257	0.047	15.307	15.822	0.229
100.189	100.222	90.86	99.775	100.038	100.425
2.88637	2.78207	1.94663	3.01847	2.99356	2.97873
1.12498	1.23474	1.727	1.0116	0.99734	1.02448
1.11363	1.21793	1.727	0.98053	0.99734	1.02327
0.01131	0.01681	0	0.03107	0	0.00121
0	0	0	0	0	0
0.00606	0	0.04809	0.00422	0.00498	0
-0.0461	-0.0407	0.39017	-0.0883	0.01836	-0.0014
0.05215	0.04069	-0.3411	0.0925	-0.0134	0.00142
0.00112	0	0.00535	0	0	0
0	0	0	0	0	0
0	0	0	0	0	0
0	0	0	0	0	0
0.12889	0.22501	1.2618	0.00243	0.00128	0.02228
0.01484	0.01451	0.00307	0.90503	0.93084	0.01272
0.83677	0.74367	0.00718	0.09724	0.0719	0.9635
6	6	6	6	6	6
0.13234	0.22888	0.89186	0.00252	0.00128	0.02229
0.85255	0.75639	0.00563	0.09934	0.0718	0.96497
0.01512	0.01478	0.00242	0.89814	0.92712	0.01274

mag 26	1	2	3	4(3)		5	6(5)	7(5)	8(5)	9(8)	10(7)	11(5)	12
	ksp	plg	ksp	plg-R	plgL		plgL-R	plgL-C	plgL	kspL	kspL-C	kspL	microcl
MGO	0	0	0	0.02	0.014		0	0	0	0	0	0	0
AL203	18.37	19.25	18.1	21.95	21.16		19.31	19.36	19.64	18.12	18.31	18.21	18.08
SIO2	64.86	69.36	64.94	65.38	66.63		69.07	69.74	70.16	64.58	64.51	65.26	64.66
CAO	0.049	0	0.006	0.034	0.034		0.034	0	0	0	0	0.04	0
TIO2	0	0	0	0	0		0	0	0	0	0	0	0
CR2O3	0	0	0	0	0		0	0	0	0	0	0	0
NIO	0	0	0	0	0		0	0	0	0	0	0	0
MNO	0	0	0	0	0		0	0	0	0	0	0	0
FEO	0.325	0.552	0.412	0.402	0.302		0.376	0.45	0.408	0.326	0.085	0.293	0.132
NA2O	0.366	11.86	0.718	10.61	10.78		11.73	11.68	11.78	0.245	0.22	0.437	0.541
K2O	16.48	0.108	15.75	0.109	0.054		0.102	0.072	0.069	16.54	16.68	16.2	16.14
F													
CL													
SUM=	100.5	101.1	99.93	98.51	98.97		100.8	101.3	102.1	99.82	99.81	100.4	99.55
Si	2.987	2.999	3.003	2.909	2.952		3.002	3.014	3.009	2.996	2.99	3.007	3.001
Al(tot)	0.997	0.981	0.987	1.151	1.105		0.989	0.986	0.993	0.991	1	0.989	0.989
Al(IV)	0.997	0.981	0.987	1.091	1.048		0.989	0.986	0.991	0.991	1	0.989	0.989
Al(VI)	0	0	0	0.06	0.057		0	2E-04	0.002	0	0	0	0
Ti	0	0	0	0	0		0	0	0	0	0	0	0
Fe(tot)	0.013	0.02	0.016	0.015	0.011		0.014	0.016	0.015	0.013	0.003	0.011	0.005
Fe +3	0.03	0.021	9E-04	-0.05	-0.08		0.001	-0.03	-0.03	0.019	0.026	-0.01	0.013
Fe +2	-0.02	0	0.015	0.062	0.091		0.013	0.047	0.042	-0.01	-0.02	0.022	-0.01
Mg	0	0	0	0.001	9E-04		0	0	0	0	0	0	0
Mn	0	0	0	0	0		0	0	0	0	0	0	0
Ni	0	0	0	0	0		0	0	0	0	0	0	0
Cr	0	0	0	0	0		0	0	0	0	0	0	0
Ca	0.002	0	3E-04	0.002	0.002		0.002	0	0	0	0	0.002	0
K	0.968	0.006	0.929	0.006	0.003		0.006	0.004	0.004	0.979	0.987	0.952	0.956
Na(tot)	0.033	0.994	0.064	0.916	0.926		0.988	0.98	0.98	0.022	0.02	0.039	0.049
Na(M4)													
Na(A)													
SUM=	5	5	5	5	5		5	5	5	5	5	5	5
26		2	3	4(3)		5	6(5)	7(5)	8(5)	9(8)	10(7)	11(5)	12
		plg	ksp	plg-R	plgL		plgL-R	plgL-C	plgL	kspL	kspL-C	kspL	microcl
An:	0.002	0	3E-04	0.002	0.002		0.002	0	0	0	0	0.002	0
Ab:	0.033	0.994	0.065	0.992	0.995		0.993	0.996	0.996	0.022	0.02	0.039	0.048
Or:	0.965	0.006	0.935	0.007	0.003		0.006	0.004	0.004	0.978	0.98	0.959	0.952

56	57	58(57	59(57)	60	61(60)	63	64	65	66
amb-c	amb-c	amb-r	amb-i	amb-r	amb-c	amb	amb-r	amb-c	amb-c
0.43	0.391	0.365	0.39	0.396	0.379	0.489	0.421	0.557	0.408
0.771	2.14	1.754	2.032	2.149	2.024	0.317	2.056	2.307	1.907
49.35	46.68	46.72	46.448	45.727	46.367	51.027	46.264	46.69	46.878
3.883	6.411	5.474	6.368	6.313	6.425	0.988	6.181	6.728	6.329
0.652	1.55	1.253	1.513	1.556	1.537	0.024	1.31	1.468	1.567
0.081	0.119	0.078	0.066	0.107	0.107	0.087	0.163	0.047	0.056
0	0	0	0	0	0	0	0	0	0
0.69	0.847	0.885	0.896	0.897	0.903	0.641	0.796	0.801	0.853
34.46	33.97	34.2	33.006	33.02	33.087	35.411	33.751	33.799	33.357
4.741	3.931	4.144	3.988	3.836	4.053	6.504	3.891	3.831	4.003
0.79	1.086	1.21	1.05	1.01	1.002	0.172	1.17	0.95	1.037
95.84	97.13	96.06	95.757	95.011	95.884	95.66	96.003	97.178	96.395
7.935	7.569	7.623	7.6456	7.5745	7.6305	8.0529	7.5814	7.5563	7.6582
0.146	0.409	0.337	0.3942	0.4198	0.3926	0.059	0.3971	0.4401	0.3672
0.065	0.409	0.337	0.3544	0.4198	0.3695	-0.053	0.3971	0.4401	0.3418
0.081	0	0	0.0398	0	0.0232	0.1119	0	0	0.0254
0.079	0.189	0.154	0.1873	0.1938	0.1902	0.0028	0.1614	0.1787	0.1925
4.633	4.607	4.667	4.5437	4.5744	4.5539	4.6737	4.6256	4.5747	4.5574
0.839	0.371	0.621	0.1918	0.3431	0.1823	1.4597	0.4444	0.3521	0.2242
3.794	4.236	4.046	4.3519	4.2313	4.3716	3.2141	4.1812	4.2227	4.3333
0.103	0.094	0.089	0.0957	0.0978	0.093	0.115	0.1028	0.1343	0.0993
0.094	0.116	0.12	0.1249	0.1259	0.1259	0.0857	0.1105	0.1098	0.118
0	0	0	0	0	0	0	0	0	0
0.003	0.003	0.003	0.0035	0.0035	0.0035	0.0035	0.0035	0.0035	0.0035
0.669	1.114	0.957	1.1232	1.1205	1.133	0.1671	1.0853	1.1667	1.1079
0.162	0.225	0.252	0.2205	0.2134	0.2104	0.0346	0.2446	0.1962	0.2161
1.478	1.236	1.311	1.2729	1.2321	1.2933	1.9903	1.2364	1.2022	1.268
1.331	0.886	1.043	0.8768	0.8795	0.867	1.8329	0.9147	0.8333	0.8921
0.147	0.35	0.268	0.396	0.3526	0.4263	0.1573	0.3217	0.3689	0.3759
15.3	15.56	15.51	15.611	15.555	15.626	15.185	15.549	15.563	15.588
0.022	0.02	0.019	0.0206	0.0209	0.02	0.024	0.0217	0.0285	0.0213
0.309	0.574	0.52	0.6165	0.566	0.6366	0.192	0.5663	0.5651	0.592
9.575	9.03	9.186	9.1389	9.0201	9.1342	10.078	9.0624	8.9547	9.1424
0.734	1.523	1.294	1.4776	1.5401	1.5024	0.1142	1.4825	1.6068	1.4496

mag 61	1	2	3(2)	4(2)	5	6(5)	7	8(7)	9	13	14	15
	cpx-C	cpx-R	cpx-C	cpx-R	cpx-C	cpx-R	cpx-C	cpx-R	cpx-C	cpx?	cpx	cpx?
MGO	0.92	0.95	0.954	0.729	0.812	0.74	0.62	0.559	0.771	0.509	0.82	0.406
AL203	0.232	0.272	0.202	0.141	0.124	0.122	0.027	0.096	0	2.06	0.169	1.37
SIO2	48.27	48.22	48.53	48.75	48.57	48.62	48.56	48.52	48.7	48.91	48.24	47.76
CRO	18.7	19.15	18.28	17.24	17.31	17.6	19.22	17.47	18.63	8.547	17.73	7.148
TIO2	0.367	0.472	0.261	0.202	0.095	0.201	0	0.194	0.02	1.325	0.037	0.589
CR2O3	0.035	0.057	0.051	0.117	0.073	0.095	0.105	0.104	0.106	0.09	0.114	0.08
NIO	0	0	0	0	0	0	0	0	0	0	0	0
MNO	0.914	0.885	0.761	0.786	0.754	0.884	0.913	0.847	0.903	0.697	0.893	0.677
FEO	28.54	28.81	29.19	29.29	29.56	29	28.82	29.86	29.29	35.33	29.02	36.31
NA2O	1.189	1.222	1.666	2.033	2.11	1.849	1.507	1.956	1.455	3.384	1.98	2.842
K2O	0	0	0	0	0	0	0	0	0	0	0	0
F												
CL												
SUM=	99.17	100	99.89	99.29	99.41	99.29	99.76	99.61	99.88	96.85	99.02	96.99
SI	1.986	1.986	1.975	1.993	1.991	1.99	1.982	1.983	1.988	1.978	1.976	2.026
Al(tot)	0.011	0.013	0.01	0.007	0.006	0.006	0.001	0.005	0	0.102	0.008	0.069
Al(IV)	0.011	0.013	0.01	0.007	0.006	0.006	0.001	0.005	0	0.022	0.006	-0.03
Al(VI)	0	0	0	0	0	0	0	0	0	0.08	0	0.098
TI	0.011	0.014	0.008	0.008	0.003	0.006	0	0.006	6E-04	0.042	0.001	0.019
Fe(tot)	0.982	0.983	0.993	1.002	1.008	0.993	0.984	1.02	1	1.246	0.994	1.289
Fe +3	0.067	0.12	0.155	0.152	0.19	0.146	0.15	0.17	0.135	0.132	0.192	0.053
Fe +2	0.895	0.862	0.839	0.85	0.818	0.847	0.834	0.85	0.865	1.114	0.802	1.236
Mg	0.056	0.058	0.058	0.044	0.049	0.045	0.038	0.034	0.047	0.032	0.05	0.026
Mn	0.032	0.031	0.026	0.026	0.026	0.03	0.032	0.029	0.031	0.025	0.031	0.024
NI	0	0	0	0	0	0	0	0	0	0	0	0
Cr	0.001	0.002	0.002	0.004	0.002	0.003	0.003	0.003	0.003	0.003	0.004	0.003
Ca	0.825	0.837	0.797	0.755	0.757	0.761	0.841	0.765	0.815	0.296	0.778	0.325
K	0	0	0	0	0	0	0	0	0	0	0	0
Na(tot)	0.095	0.097	0.131	0.161	0.167	0.147	0.119	0.155	0.115	0.277	0.158	0.218
Na(M4)												
Na(A)												
SUM=	4	4	4	4	4	4	4	4	4	4	4	4
Mg/(Mg+Fe(tot	0.054	0.055	0.055	0.042	0.047	0.043	0.037	0.032	0.045	0.025	0.048	0.02
Na(A)+K	0	0	0	0	0	0	0	0	0	0	0	0
SI+Na+K	2.081	2.083	2.106	2.154	2.148	2.137	2.101	2.138	2.103	2.254	2.134	2.245
Al(IV)+Ca	0.836	0.85	0.807	0.762	0.763	0.768	0.842	0.77	0.815	0.318	0.786	0.297
pyx components normalized to 1												
Ac: (Na)	0.097	0.098	0.133	0.164	0.168	0.149	0.12	0.157	0.117	0.299	0.16	0.234
En: (Mg/2)	0.029	0.029	0.029	0.023	0.025	0.023	0.019	0.017	0.024	0.017	0.025	0.014
Fs: (Fe(t)-Na)/	0.453	0.449	0.435	0.428	0.425	0.43	0.436	0.436	0.448	0.524	0.422	0.577
Wo: (Ca/2)	0.421	0.424	0.403	0.385	0.382	0.397	0.424	0.387	0.412	0.16	0.393	0.175
sum=	1	1	1	1	1	1	1	1	1	1	1	1
AEFplot error=	0.211	0.212	0.201	0.192	0.191	0.189	0.212	0.194	0.208	0.08	0.198	0.086
AFWplot error=	0.014	0.015	0.015	0.011	0.012	0.011	0.01	0.009	0.012	0.009	0.013	0.007
EFSplot error=	0.048	0.049	0.066	0.082	0.084	0.076	0.08	0.078	0.058	0.15	0.08	0.117
Ac: (Na)	0.091	0.093	0.125	0.154	0.158	0.141	0.117	0.147	0.11	0.217	0.151	0.165
En: (Mg)	0.054	0.055	0.055	0.042	0.047	0.043	0.037	0.032	0.045	0.025	0.048	0.02
Fs: (Fe(t)-Na)	0.854	0.852	0.82	0.803	0.796	0.815	0.846	0.821	0.845	0.758	0.801	0.815
cpx mormote												
Q=Ca+Mg+(Fe2	1.776	1.757	1.694	1.649	1.624	1.673	1.712	1.649	1.727	1.442	1.63	1.567
J=2*Na	0.19	0.193	0.263	0.322	0.334	0.293	0.239	0.31	0.23	0.553	0.316	0.435
J/Q+J	0.097	0.099	0.134	0.163	0.17	0.149	0.122	0.158	0.118	0.277	0.162	0.215
Ca Cpx J/J+Q < .2												
Wo -Ca	43.51	43.86	42.52	41.29	41.12	42.23	44.4	41.38	43.05	18.51	41.99	19.54
Fs-Fet+Mn	53.51	53.11	54.39	56.28	56.2	55.33	53.61	56.78	54.47	79.49	55.31	78.92
En - Mg	2.977	3.026	3.087	2.429	2.682	2.442	1.992	1.841	2.478	2.001	2.701	1.543
total	100	100	100	100	100	100	100	100	100	100	100	100
Na cpx J/J+Q >.8												
Na-Ca cpx .2<J/J+Q< .8												
2*Na**	0.097	0.099	0.134	0.163	0.17	0.149	0.122	0.158	0.118	0.277	0.162	0.215
Q**	0.903	0.901	0.866	0.837	0.83	0.851	0.878	0.842	0.882	0.723	0.838	0.785
Jd/Ae	0	0	0	0	0	0	0	0	0	2.195	0	8.465
Jd	0	0	0	0	0	0	0	0	0	0.609	0	1.821
Ae	0.097	0.099	0.134	0.163	0.17	0.149	0.122	0.158	0.118	-0.33	0.162	-1.61
total=Q+Ae+Jd	1	1	1	1	1	1	1	1	1	1	1	1

MAG-61	16 amb-r	17(16) amb-c	18 amb-c	19(16) amb-r
MGO	0.939	1.042	0.99	1.062
AL203	2.237	2.299	2.26	2.147
SIO2	46.35	46.624	46.352	45.919
CIO	7.372	6.946	6.587	6.458
TIO2	1.379	1.469	1.513	1.504
CR203	0.025	0.053	0	0.112
NIO	0	0	0	0
MNO	0.827	0.778	0.81	0.793
FED	34.061	34.504	35.002	35.502
NA2O	3.149	3.233	3.207	3.234
K2O	1.075	1.099	1.145	1.112
F	0.161	0.284	0.2	0.334
CL	0.031	0.087	0.113	0.098
SUM=	97.606	98.436	98.179	98.275
SI	7.4731	7.4313	7.3856	7.3142
AI(tot)	0.4251	0.4319	0.4244	0.4031
AI(IV)	0.4251	0.4319	0.4244	0.4031
AI(VI)	0	0	0	0
TI	0.1672	0.1785	0.1813	0.1802
Fe(tot)	4.5928	4.5994	4.6643	4.7294
Fe +3	0.5384	0.7467	0.969	1.1649
Fe +2	4.0545	3.8527	3.6952	3.5646
Mg	0.2256	0.2475	0.2351	0.2521
Mn	0.1129	0.1048	0.1093	0.107
NI	0	0	0	0
Cr	0.0049	0.0049	0.0049	0.0049
Ca	1.2736	1.1863	1.1246	1.1022
K	0.2211	0.2235	0.2326	0.226
Na(tot)	0.9845	0.9992	0.9908	0.9988
Na(M4)	0.7264	0.8137	0.8754	0.8978
Na(A)	0.2581	0.1854	0.1154	0.101
SUM=	15.481	15.407	15.353	15.316
Mg/(Mg-	0.0468	0.0511	0.048	0.0506
Na(A)+K	0.4792	0.4089	0.3482	0.327
SI+Na+K	8.6787	8.6539	8.6091	8.539
AI(IV)+C	1.6987	1.6182	1.549	1.5053

21-Sep-89											
meg 84-b	1	2(1)	8	9(8)	14	15(14)	41	42	3(1)	22	23(22)
	cpx-l	cpx-c	cpx-c	cpx-r	cpx-c	cpx-r	cpx	cpx	amb?-r	amb-c	amb-r
MGO	2.333	2.243	2.757	2.095	2.457	2.434	1.82	2.139	2.36	2.536	2.399
AL203	0.621	1.142	0.66	0.434	1.16	0.917	0.206	0.482	5.357	4.786	4.841
SIO2	48.34	48.21	48.98	48.1	48.08	48.33	48.588	47.84	43.83	43.94	44.33
CrO	20.48	20.17	20.47	19.57	20.43	20.25	20.007	19.447	9.821	8.985	9.745
TIO2	0.451	0.34	0.442	0.117	0.56	0.338	0.111	0.443	1.09	1.27	1.35
CR2O3	0.091	0.052	0.013	0.042	0	0	0.113	0.035	0.042	0	0
NiO	0	0	0	0	0	0	0	0	0	0	0
MNO	1.072	1.016	0.98	0.99	1.166	1.099	1.003	1.037	0.708	0.707	0.7
FEO	26.01	26.17	25.31	26.82	25.85	26.04	26.809	26.272	31.42	32.55	31.9
NA2O	0.542	0.483	0.565	0.673	0.635	0.52	0.564	0.711	1.706	1.78	1.586
K2O	0	0	0	0	0	0	0	0	0	0.935	0.98
F											
CL											
SUM=	99.94	99.83	100.1	98.84	100.1	99.92	99.221	98.406	96.33	97.49	97.81
SI	1.961	1.958	1.975	1.979	1.941	1.959	1.993	1.9723	7	6.954	7.056
Al(tot)	0.03	0.055	0.031	0.021	0.055	0.044	0.01	0.0234	1.009	0.893	0.871
Al(VI)	0.03	0.042	0.025	0.021	0.055	0.041	0.007	0.0234	1	0.893	0.871
Al(IV)	0	0.013	0.006	0	0	0.002	0.0029	0	0.009	0	0
TI	0.014	0.01	0.013	0.004	0.017	0.01	0.0034	0.0137	0.131	0.151	0.162
Fe(tot)	0.882	0.889	0.854	0.916	0.866	0.882	0.9197	0.9058	4.197	4.309	4.248
Fe +3	0.061	0.045	0.038	0.066	0.079	0.059	0.0384	0.0802	0.833	1.114	0.883
Fe +2	0.821	0.844	0.818	0.849	0.787	0.823	0.8813	0.8457	3.364	3.195	3.364
Mg	0.141	0.136	0.166	0.126	0.148	0.147	0.1113	0.1314	0.562	0.598	0.569
Mn	0.037	0.035	0.033	0.034	0.04	0.036	0.0348	0.0362	0.096	0.095	0.094
Ni	0	0	0	0	0	0	0	0	0	0	0
Cr	0.003	0.002	4E-04	0.001	0	0	0.0037	0.0011	0.003	0.003	0.003
Ca	0.89	0.878	0.885	0.863	0.864	0.879	0.8793	0.8591	1.681	1.524	1.662
K	0	0	0	0	0	0	0	0	0	0.189	0.195
Na(tot)	0.043	0.038	0.043	0.054	0.05	0.041	0.0449	0.0568	0.528	0.546	0.49
Na(M4)									0.319	0.476	0.338
Na(A)									0.209	0.07	0.152
SUM=	4	4	4	4	4	4	4	4	15.21	15.26	15.35
Mg/(Mg+Fe(tot))	0.138	0.132	0.163	0.123	0.146	0.143	0.1079	0.1267	0.118	0.122	0.118
Na(A)+K	0	0	0	0	0	0	0	0	0.209	0.259	0.347
SI+Na+K	2.003	1.996	2.018	2.033	1.99	1.999	2.0378	2.0291	7.529	7.689	7.742
Al(IV)+Ca	0.92	0.92	0.91	0.884	0.939	0.921	0.8863	0.8825	2.681	2.417	2.533
pyx components normalized to 1											
Ac: (Na)	0.044	0.039	0.045	0.055	0.051	0.042	0.0459	0.0582			
En: (Mg/2)	0.072	0.07	0.085	0.068	0.076	0.076	0.0569	0.0673			
Fs: (Fe(t)-Na)/2	0.429	0.439	0.416	0.44	0.419	0.432	0.4474	0.4347			
Wo: (Ca/2)	0.455	0.452	0.454	0.44	0.454	0.451	0.4498	0.4398			
sum=	1	1	1	1	1	1	1	1			
AEFplot error=	0.227	0.228	0.227	0.22	0.227	0.226	0.2249	0.2199			
AFWplot error=	0.036	0.035	0.043	0.033	0.038	0.036	0.0285	0.0336			
EFSplot error=	0.022	0.02	0.022	0.027	0.028	0.021	0.0229	0.0291			
Ac: (Na)	0.042	0.037	0.043	0.051	0.049	0.04	0.0435	0.0548			
En: (Mg)	0.138	0.132	0.163	0.123	0.146	0.143	0.1079	0.1267			
Fs: (Fe(t)-Na)	0.821	0.83	0.795	0.826	0.805	0.817	0.8486	0.8185			
cpx morimoto											
Q=Ca+Mg+(Fe2+	1.852	1.857	1.868	1.841	1.818	1.849	1.8716	1.8362			
J=2*Na	0.085	0.078	0.087	0.107	0.099	0.082	0.0897	0.1137			
J/Q+J	0.044	0.039	0.044	0.055	0.052	0.042	0.0457	0.0583			
Ca Cpx J/J+Q < .2											
Wo -Ca	45.83	45.3	45.67	44.44	45.61	45.17	45.207	44.453			
Fs-Fet+Mn	47.13	47.69	45.77	46.95	46.78	47.27	49.073	48.747			
En - Mg	7.231	7.007	8.555	8.616	7.629	7.563	5.7199	6.8006			
total	100	100	100	100	100	100	100	100			
Na cpx J/J+Q >.8											
Na-Ca cpx .2<J/J+Q< .8											
2*Na**	0.044	0.039	0.044	0.055	0.052	0.042	0.0457	0.0583			
Q**	0.956	0.961	0.956	0.945	0.948	0.958	0.9543	0.9417			
Jd/Ae	0	7.031	3.742	0	0	0.948	1.6781	0			
Jd	0	0.277	0.166	0	0	0.04	0.0767	0			
Ae	0.044	-0.24	-0.12	0.055	0.052	0.002	-0.031	0.0583			

24	21-Sep-89 mag 84-b	4	5(4)	10	18	19(18)	20(19	21(19)
amb		olv-c	olv-r	olv-c	plg	plg-c	sp-lam	sp-lam-c
2.326	MGO	0.791	0.77	0.772	0.027	0.015	0.042	0.046
5.013	AL203	0.192	0.116	0.166	21.67	21.21	20.25	18.41
43.8	SIO2	29.29	29.36	29.5	66.51	67.68	66.36	65.44
9.087	CAO	0.117	0.063	0.047	2.553	2.163	1.427	0.052
1.304	TIO2	0	0.067	0	0	0	0	0
0.054	CR2O3	0.056	0.091	0.125	0	0	0	0
0	NIO	0	0	0	0	0	0	0
0.72	MNO	2.981	3.021	3.018	0	0	0	0
32.37	FEO	66.23	66.13	66.11	0	0.198	0.11	0.121
1.969	NA2O	0	0	0	7.656	6.6	6.219	1.24
0.968	K2O	0	0	0	0.304	0.387	5.768	14.31
	F							
	CL							
97.63	SUM=	99.66	99.62	99.73	98.72	100.5	100.2	99.62
6.954	SI	0.99	0.993	0.996	3.021	3.002	2.98	3.029
0.938	Al(tot)	0.008	0.005	0.007	1.16	1.109	1.072	1.004
0.938	Al(VI)	0.008	0.005	0.004	0.979	0.998	1.02	0.971
0	Al(IV)	0	0	0.003	0.182	0.11	0.052	0.033
0.156	TI	0	0.002	0	0	0	0	0
4.298	Fe(tot)	1.872	1.87	1.867	0	0.007	0.004	0.005
0.935	Fe +3	0.012	0.003	0	-0.51	-0.33	-0.16	-0.11
3.363	Fe +2	1.86	1.867	1.869	0.511	0.341	0.164	0.11
0.55	Mg	0.04	0.039	0.039	0.002	1E-03	0.003	0.003
0.097	Mn	0.085	0.087	0.086	0	0	0	0
0	NI	0	0	0	0	0	0	0
0.003	Cr	0.001	0.002	0.003	0	0	0	0
1.546	Ca	0.004	0.002	0.002	0.124	0.103	0.069	0.003
0.198	K	0	0	0	0.018	0.022	0.33	0.845
0.612	Na(tot)	0	0	0	0.674	0.757	0.542	0.111
0.454	Na(M4)							
0.158	Na(A)							
15.35	SUM=							
0.114	Mg/(Mg+Fe(t	0.021	0.02	0.02				
0.354	Na(A)+K							
7.783	SI+Na+K							
2.484	Al(IV)+Ca							

pyx components normalized to 1
Ac: (Na)
En: (Mg/2)
Fs: (Fe(t)-Na)/2
Wo: (Ca/2)
sum=
AEFplot error=
AFWplot error=
EFSplot error=

plg comp normalized to 1

An:	0.162	0.117	0.073	0.003
Ab:	0.828	0.859	0.576	0.116
Or:	0.022	0.025	0.351	0.881

21-Sep-89 mag 91-1	2(3) Pyx-C	5 Pyx-R	8(5) Pyx-C	10 Pyx	88 cpx-i	96 cpx-c	97 cpx-i
MGO	1.591	1.243	4.555	1.291	1.399	4.564	4.913
AL203	0.104	0.164	1.261	0.103	0.207	0.325	1.208
SIO2	48.385	48.571	48.798	48.502	49.145	49.843	48.961
CIO	18.787	19.415	19.242	18.357	19.433	19.904	19.347
TIO2	1.68	0.274	0.702	0.198	0.028	0.283	0.688
CR203	0	0	0	0	0	0	0
NIO	0	0	0	0	0	0	0
MNO	0.757	0.856	0.609	0.76	0.771	0.686	0.642
FEO	27.868	27.672	22.329	28.132	27.194	22.409	21.584
NA2O	1.427	1.18	1.577	1.619	1.174	1.037	1.191
K2O	0	0	0	0	0	0	0
F							
CL							
SUM=	100.6	99.375	99.073	98.962	99.351	99.051	98.534
SI	1.9552	1.9869	1.9429	1.9862	2.0061	1.9957	1.9812
Al(tot)	0.005	0.0079	0.0592	0.005	0.01	0.0153	0.057
Al(IV)	0.005	0.0079	0.0571	0.005	-0.006	0.0043	0.0388
Al(VI)	0	0	0.002	0	0.0161	0.011	0.0182
TI	0.0511	0.0084	0.021	0.0061	0.0009	0.0085	0.0207
Fe(tot)	0.9418	0.9467	0.7435	0.9835	0.9284	0.7504	0.7231
Fe +3	0.0944	0.095	0.1348	0.1389	0.089	0.0587	0.0716
Fe +2	0.8475	0.8517	0.6087	0.8246	0.8594	0.6937	0.6515
Mg	0.0958	0.0758	0.2703	0.0788	0.0851	0.2723	0.2933
Mn	0.0259	0.0297	0.0205	0.0264	0.0267	0.0233	0.0218
NI	0	0	0	0	0	0	0
Cr	0	0	0	0	0	0	0
Ca	0.8135	0.851	0.8209	0.8055	0.85	0.8539	0.8304
K	0	0	0	0	0	0	0
Na(tot)	0.1118	0.0936	0.1217	0.1286	0.0929	0.0808	0.0925
Na(M4)							
Na(A)							
SUM=	4	4	4	4	4	4	4
Mg/(Mg+Fe(tot))	0.0923	0.0741	0.2666	0.0758	0.084	0.2663	0.2688
Na(A)+K	0	0	0	0	0	0	0
SI+Na+K	2.067	2.0805	2.0648	2.1148	2.099	2.0762	2.0637
Al(IV)+Ca	0.8184	0.8589	0.878	0.8105	0.8439	0.8582	0.8692
pyx components normalized to 1							
Ac: (Na)	0.1139	0.0952	0.1245	0.1301	0.095	0.0823	0.0954
En: (Mg/2)	0.0488	0.0385	0.1381	0.0399	0.0435	0.1392	0.1512
Fs: (Fe(t)-Na)/2	0.4226	0.4337	0.3178	0.4225	0.427	0.3423	0.3252
Wo: (Ca/2)	0.4144	0.4326	0.4198	0.4076	0.4345	0.4383	0.4282
sum=	1	1	1	1	1	1	1
AEFplot error=	0.2072	0.2163	0.2099	0.2038	0.2172	0.2182	0.2141
AFWplot error=	0.0244	0.0193	0.0691	0.0199	0.0218	0.0696	0.0758
EFWplot error=	0.057	0.0476	0.0822	0.065	0.0475	0.0411	0.0477
Ac: (Na)	0.1076	0.0916	0.1201	0.1233	0.0917	0.0787	0.091
DI	0.0923	0.0741	0.2666	0.0758	0.084	0.2663	0.2688
Hd	0.7998	0.8343	0.8133	0.8011	0.8243	0.865	0.8204
cpx morimoto							
Q=Ca+Mg+Fe2+	1.7567	1.7785	1.8998	1.7089	1.7945	1.8199	1.7751
J=2*Na	0.2236	0.1872	0.2435	0.2571	0.1858	0.161	0.185
J/Q+J	0.1129	0.0952	0.1253	0.1308	0.0938	0.0813	0.0944
Ca Cpx J/J+Q < .2	x	x	x	x	x	x	x
Wo	43.338	44.715	44.248	42.98	44.97	44.945	44.441
Fs	51.557	51.303	41.184	52.616	50.528	40.72	39.863
En	5.1047	3.9818	14.569	4.2041	4.5026	14.334	15.696
total	100	100	100	100	100	100	100
Na cpx J/J+Q >.8							
Na-Ca cpx .2<J/J+Q< .8							
2*Na**	0.1129	0.0952	0.1253	0.1308	0.0938	0.0813	0.0944
Q**	0.8871	0.9048	0.8747	0.8692	0.9062	0.9187	0.9056
Jd/Ae	0	0	0.1203	0	2.4833	2.3922	2.6984
Jd	0	0	0.0151	0	0.233	0.1944	0.2547
Ae	0.1129	0.0952	0.1102	0.1308	-0.139	-0.113	-0.16

21-Sep-89 mag 91-1	2(3) Pyx-C	Pyx-C	Pyx-C	Pyx-C	Pyx-C	Pyx-C	Pyx-C
MGO	1.591	1.243	4.555	1.291	1.399	4.564	4.913
AL203	0.104	0.164	1.261	0.103	0.207	0.325	1.208
SIO2	48.385	48.571	48.798	48.502	49.145	49.843	48.961
CIO	18.787	19.415	19.242	18.357	19.433	19.904	19.347
TIO2	1.68	0.274	0.702	0.198	0.028	0.283	0.688
CR203	0	0	0	0	0	0	0

NiO	0	0	0	0	0	0	0
MnO	0.757	0.856	0.609	0.76	0.771	0.886	0.642
FeO	27.868	27.872	22.329	28.132	27.194	22.409	21.584
Na2O	1.427	1.16	1.577	1.619	1.174	1.037	1.191
K2O	0	0	0	0	0	0	0
F							
Cl							
SUM=	100.6	99.375	99.073	98.962	99.351	99.051	98.534
Si	1.9707	2.0028	1.9849	2.0095	2.0177	2.0052	1.973
Al(tot)	0.005	0.008	0.0598	0.005	0.01	0.0154	0.0574
Al(IV)	0.005	-0.003	0.0351	-0.009	-0.018	-0.005	0.027
Al(VI)	0	0.0107	0.0248	0.0145	0.0277	0.0206	0.0304
Ti	0.0515	0.0085	0.0213	0.0082	0.0009	0.0086	0.0209
Fe(tot)	0.9493	0.9543	0.752	0.9746	0.9338	0.754	0.7274
Fe +3	2E-15	-2E-15	4E-15	-2E-15	-2E-15	2E-15	0
Fe +2	0.9493	0.9543	0.752	0.9746	0.9338	0.754	0.7274
Mg	0.0966	0.0764	0.2733	0.0797	0.0866	0.2736	0.2961
Mn	0.0261	0.0299	0.0208	0.0267	0.0268	0.0234	0.0219
Ni	0	0	0	0	0	0	0
Cr	0	0	0	0	0	0	0
Ca	0.8199	0.8578	0.8302	0.8149	0.8549	0.858	0.8354
K	0	0	0	0	0	0	0
Na(tot)	0.1127	0.0943	0.1231	0.1301	0.0935	0.0809	0.0931
Na(M4)							
Na(A)							
SUM=	4.0317	4.0319	4.0455	4.0469	4.0231	4.019	4.024
Mg/(Mg+Fe(tot))	0.0923	0.0741	0.2666	0.0756	0.084	0.2663	0.2886
Na(A)+K	0	0	0	0	0	0	0
Si+Na+K	2.0834	2.0971	2.0861	2.1396	2.1112	2.0861	2.068
Al(IV)+Ca	0.8249	0.855	0.8653	0.8054	0.8372	0.8528	0.8824
pyx components normalized to 1							
Ac: (Na)	0.1139	0.0952	0.1245	0.1301	0.095	0.0823	0.0954
En: (Mg/2)	0.0488	0.0385	0.1381	0.0399	0.0435	0.1392	0.1512
Fs: (Fe(t)-Na)/2	0.4228	0.4337	0.3178	0.4225	0.427	0.3423	0.3252
Wo: (Ca/2)	0.4144	0.4328	0.4196	0.4076	0.4345	0.4363	0.4282
sum=	1	1	1	1	1	1	1
AEFplot error=	0.2072	0.2163	0.2098	0.2038	0.2172	0.2182	0.2141
AFWplot error=	0.0244	0.0193	0.0691	0.0199	0.0218	0.0698	0.0756
EFWplot error=	0.057	0.0478	0.0622	0.065	0.0475	0.0411	0.0477
Ac: (Na)	0.1078	0.0918	0.1201	0.1233	0.0917	0.0787	0.091
Di	0.0923	0.0741	0.2666	0.0756	0.084	0.2663	0.2886
Hd	0.7999	0.8343	0.8133	0.8011	0.8243	0.855	0.8204
cpx morimoto							
Q=Ca+Mg+Fe2	1.8657	1.8684	1.8555	1.8694	1.8743	1.8858	1.8578
J=2*Na	0.2254	0.1887	0.2463	0.2601	0.1869	0.1618	0.1861
J/Q+J	0.1078	0.0908	0.1172	0.1222	0.0907	0.079	0.0911
Ca Cpx J/J+Q < .2	x	x	x	x	x	x	x
Wo	43.338	44.715	44.248	42.98	44.97	44.945	44.441
Fs	51.587	51.303	41.184	52.816	50.528	40.72	39.883
En	5.1047	3.9818	14.569	4.2041	4.5028	14.334	15.696
total	100	100	100	100	100	100	100
Na cpx J/J+Q >.8							
Na-Ca cpx .2<J/J+Q< .8							
2*Na**	0.1078	0.0908	0.1172	0.1222	0.0907	0.079	0.0911
Q**=Q/(Q+J)	0.8922	0.9092	0.8828	0.8778	0.9093	0.921	0.9089
Jd/Ae	0	-7E+13	8E+13	-7E+13	-2E+14	1E+14	#DIV/0!
Jd	0	-6E+12	7E+12	-6E+12	-2E+13	1E+13	#DIV/0!
Ae	0.1078	8E+12	-7E+12	8E+12	2E+13	-1E+13	#DIV/0!

25-May-89

mag 91-3	14 amb	15 amb	17 amb	11 coss(as p	11 pyx(as an	16 coss	18 felds	19 felds	13 opaq	91-3	12 cpx
MGO	0.575	0.529	0.602	0.065	0.095	0.091	0	0	0	MGO	0.229
AL203	1.154	1.128	1.076	0.405	0.39	0.372	18.22	14.95	0	AL203	0.125
SIO2	48.75	48.22	48.46	41.26	41.3	41.36	67.54	75.11	19	SIO2	49.2
CAO	5.063	4.895	4.616	0.326	0.314	0.341	0	0	0	CAO	14.81
TIO2	1.387	1.376	1.338	8.481	8.59	8.55	0	0	0.149	TIO2	0.267
CR2O3	0	0	0	0	0	0.031	0	0	0	CR2O3	0
NIO	0	0	0	0	0	0	0	0		NIO	0
MNO	0.547	0.783	0.696	0.967	0.923	0.973	0	0	0.029	MNO	0.713
FEO	35.28	34.61	35.16	41.36	41.05	42.34	0.803	0.522	61.97	FEO	28.99
NA2O	5.379	5.388	5.393	7.302	7.478	7.399	0.839	6.754	0	NA2O	4.787
K2O	1.269	1.402	1.587	0	0	0	13.88	0.102		K2O	0
F	0.819	0.774	0.929							F	
CL	0.027	0.061	0.037							CL	
SUM=	99.71	98.33	99.13	100.2	100.1	101.5	99.08	97.44		SUM=	99.11
SI	7.707	7.741	7.702	5.885	5.882	5.829	3.171	3.53		SI	1.97
AI(tot)	0.215	0.213	0.202	0.068	0.065	0.062	0.896	0.828		AI(tot)	0.006
AI(IV)	0.215	0.213	0.202	0.068	0.065	0.062	0.829	0.47		AI(IV)	0.006
AI(IV)	0	0	0	0	0	0	0.069	0.358		AI(IV)	0
TI	0.165	0.166	0.16	0.91	0.92	0.906	0	0		TI	0.008
Fe(tot)	4.665	4.646	4.673	4.936	4.889	4.99	0.024	0.021		Fe(tot)	0.971
Fe +3	0.422	0.324	0.518	0.362	0.396	0.465	-0.33	-1.27		Fe +3	0.409
Fe +2	4.242	4.322	4.155	4.575	4.493	4.505	0.356	1.287		Fe +2	0.562
Mg	0.135	0.127	0.143	0.014	0.02	0.019	0	0		Mg	0.014
Mn	0.113	0.106	0.121	0.117	0.111	0.116	0	0		Mn	0.024
Ni	0	0	0	0	0	0	0	0		NI	0
Cr	0.003	0.003	0.003	0	0	0.003	0	0		Cr	0
Ca	0.858	0.842	0.786	0.05	0.048	0.051	0	0		Ca	0.835
K	0.256	0.287	0.322	0	0	0	0.831	0.006		K	0
Na(tot)	1.849	1.877	1.862	2.02	2.065	2.022	0.076	0.615		Na(tot)	0.372
Na(M4)	1.142	1.158	1.214							Na(M4)	
Na(A)	0.506	0.519	0.448							Na(A)	
sum=	15.77	15.81	15.77	14	14	14	5	5		sum=	4
Mg/(Mg+Fe(tot))	0.028	0.027	0.03	2.507	2.398	2.575				Mg/(Mg+F	0.014
Na(A)+K	0.762	0.806	0.77	1.796	1.755	1.03				Na(A)+K	0
SI+Na+K	9.811	9.705	9.686	4.677	5.282	10.66				SI+Na+K	2.342
AI(IV)+Ca	1.073	1.055	0.988	9.012	8.006	9.374				AI(IV)+Ca	0.841
				82.01	82.56	76.14					
An:							0	0		pyx components nor	
Ab:							0.084	0.99		Ac: (Na)	0.373
Or:							0.916	0.01		En: (Mg/2	0.007
										Fs: (Fe(t	0.301
										Wo: (Ca/2	0.319
										sum=	1
										AEFplot a	0.16
										AFWplot a	0.003
										EFSplot a	0.187
										Ac: (Na)	0.376
										En: (Mg)	0.014
										Fs: (Fe(t)	0.609
										cpx morimoto	
										Q=Ca+Mg	1.211
										J=2*Na	0.743
										J/Q+J	0.38
										Ca Cpx J/J+Q < .2	
										Wo -Ca	38.64
										Fs-Fet+Mt	60.52
										En - Mg	0.831
										total	100
										Na cpx J/J+Q >.8	
										Na-Ca cpx .2<J/J+	
										2*Na**	0.38
										Q**	0.62
										Jd/Ae	0
										Jd	0
										Ae	0.38

21-Sep-89 mag 91-4	43' cpx-i	44(43) cpx-i	46(43) cpx-r	49 cpx	48 amb-c	55 amb-c	50 ksp-i-r	51(50) plg-i-r	52(50) ksp-i-c	53(50) plg-i-c
MGO	0.168	0.072	0.305	0.073	0.84	0.774	0	0	0	0.021
AL203	0.94	0.554	0.814	0.85	0.915	1.351	17.451	18.52	17.539	18.403
SIO2	51.84	51.699	52.325	51.831	48.92	48.387	65.627	69.66	64.658	70.038
CAO	0.205	0.104	0.155	0.041	1.978	1.964	0	0	0	0.043
TIO2	0.173	0.696	0.783	0.85	1.5	0.473	0	0	0	0
CR2O3	0.119	0.035	0.057	0.041	0.016	0.063	0	0	0	0
NIO	0	0	0	0	0	0	0	0	0	0
MNO	0.019	0.057	0	0.043	0.754	0.319	0	0	0	0
FEO	29.21	28.713	27.877	28.604	32.33	33.473	0.739	0.938	0.528	0.652
NA2O	13.42	13.883	13.753	13.645	8.929	8.372	0.391	11.02	0.471	10.909
K2O	0.384	0	0	0.018	1.642	1.504	15.183	0.088	15.272	0.115
F										
CL										
SUM=	96.5	96.013	96.069	95.796	95.82	94.69	99.391	100.2	98.468	100.38
SI	1.982	1.9838	2.0025	1.9878	7.942	7.881	3.0683	3.062	3.045	3.0767
Al(tot)	0.042	0.0251	0.0367	0.0386	0.175	0.2595	0.9617	0.96	0.9736	0.9529
Al(IV)	0.018	0.0164	-0.002	0.0122	0.058	0.119	0.9317	0.938	0.955	0.9233
Al(VI)	0.024	0.0088	0.0392	0.0264	0.118	0.1405	0.03	0.022	0.0186	0.0296
TI	0.005	0.0259	0.0225	0.0246	0.183	0.058	0	0	0	0
Fe(tot)	0.934	0.9213	0.8922	0.921	4.39	4.5615	0.0289	0.034	0.0208	0.0313
Fe +3	0.994	0.9878	0.9321	0.9549	0.362	0.8428	-0.157	-0.14	-0.103	-0.171
Fe +2	-0.06	-0.066	-0.04	-0.034	4.029	3.7187	0.1861	0.174	0.1238	0.202
Mg	0.011	0.0041	0.0174	0.0042	0.203	0.188	0	0	0	0.0014
Mn	6E-04	0.0019	0	0.0014	0.104	0.044	0	0	0	0
NI	0	0	0	0	0	0	0	0	0	0
Cr	0.004	0.0011	0.0017	0.0012	0.003	0.0035	0	0	0	0
Ca	0.008	0.0043	0.0064	0.0017	0.344	0.3429	0	0	0	0.002
K	0	0	0	0	0.34	0.3127	0.9058	0.005	0.9176	0.0084
Na(tot)	0.995	1.0328	1.0206	1.0186	2.182	2.0132	0.0354	0.939	0.043	0.9292
Na(M4)					1.656	1.6571				
Na(A)					0.526	0.3561				
SUM=	3.981	4	4	3.9991	15.87	15.664				
Mg/(Mg+Fe(tot))	0.011	0.0044	0.0191	0.0045	0.044	0.0398				
Na(A)+K	0	0	0	0	0.866	0.6688				
Si+Na+K	2.977	3.0164	3.023	3.0064	10.46	10.207				
Al(IV)+Ca	0.027	0.0207	0.0039	0.0139	0.402	0.4819				

pyx components normalized to 1				
Ac: (Na)	1.022	1.0525	1.054	1.0472
En: (Mg/2)	0.005	0.0021	0.009	0.0022
Fs: (Fe(t)-Na)/2	-0.03	-0.057	-0.066	-0.05
Wo: (Ca/2)	0.004	0.0022	0.0033	0.0009
sum=	1	1	1	1
AEFplot error=	0.002	0.0011	0.0016	0.0004
AFWplot error=	0.003	0.001	0.0045	0.0011
EFSplot error=	0.511	0.5263	0.527	0.5238
Ac: (Na)	1.053	1.118	1.1219	1.101
En: (Mg)	0.011	0.0044	0.0191	0.0045
Fs: (Fe(t)-Na)	-0.06	-0.12	-0.141	-0.106
cpx morimoto				
Q=Ca+Mg+(Fe2+	-0.04	-0.058	-0.016	-0.028
J=2*Na	1.99	2.0857	2.0411	2.0372
J/Q+J	1.021	1.0289	1.0079	1.0139
Ca Cpx J/J+Q < .2				
Wo -Ca	0.881	0.459	0.8939	0.1822
Fs-Fet+Mn	98	99.099	97.407	99.387
En - Mg	1.123	0.4419	1.8991	0.4512
total	100	100	100	100
Na cpx J/J+Q >.8				
Na-Ca cpx .2<J/J+Q< .8				
2*Na**	1.021	1.0289	1.0079	1.0139
Q**	-0.02	-0.029	-0.008	-0.014
Jd/Ae	0.024	0.0085	0.0417	0.0272
Jd	0.024	0.0085	0.0421	0.0276
Ae	0.997	1.0202	0.9859	0.9863

plg comp normalized to 1				
An:	0	0	0	0.0022
Ab:	0.0377	0.995	0.0448	0.991
Or:	0.9623	0.005	0.9552	0.0069

21-Sep-89	clot1								clot2
mag 125	33	34	35	25	26	27	31	32	36
	amb	amb	amb	plg-l-c	plg-l-c	ksp-l-c	ksp	alb	plg-l-r
MGO	2.873	2.841	2.791	0	0	0	0	0	0
AL203	0.764	1.054	0.904	21.48	21.57	17.99	17.77	18.48	23.98
SIO2	50.26	48.78	48.81	67.14	66.95	64.4	65.48	69.39	62.81
CAO	4.278	3.651	4.057	2.191	2.156	0.045	0.014	0	4.997
TIO2	1.3	1.236	1.206	0	0	0	0	0	0
CR203	0.029	0.044	0	0	0	0	0	0	0
NIO	0	0	0	0	0	0	0	0	0
MNO	0.721	0.688	0.632	0	0	0	0	0	0
FEO	31.12	31.74	30	0.023	0.105	0.127	0.717	0.633	0
NA2O	5.076	5.287	4.662	7.698	8.738	0.77	0.606	11.76	5.908
K2O	1.365	1.167	1.484	0.113	0.126	13.98	15.12	0.092	0.218
F									
CL									
SUM=	97.78	96.49	94.54	98.64	99.65	97.31	99.7	100.4	97.91
Si	7.864	7.701	7.876	3.055	2.992	3.064	3.046	3.027	2.903
Al(tot)	0.141	0.196	0.172	1.152	1.136	1.009	0.974	0.95	1.307
Al(VI)	0.136	0.196	0.124	0.945	1.008	0.936	0.954	0.95	1.097
Al(IV)	0.005	0	0.048	0.207	0.128	0.073	0.02	0	0.21
Ti	0.153	0.147	0.146	0	0	0	0	0	0
Fe(tot)	4.073	4.19	4.048	9E-04	0.004	0.005	0.028	0.023	0
Fe +3	0.574	1.014	0.616	-0.58	-0.36	-0.22	-0.11	0	-0.57
Fe +2	3.499	3.176	3.432	0.577	0.36	0.223	0.142	0.027	0.571
Mg	0.67	0.668	0.671	0	0	0	0	0	0
Mn	0.096	0.092	0.086	0	0	0	0	0	0
Ni	0	0	0	0	0	0	0	0	0
Cr	0.003	0.003	0.003	0	0	0	0	0	0
Ca	0.717	0.618	0.702	0.107	0.103	0.002	7E-04	0	0.248
K	0.273	0.235	0.306	0.007	0.007	0.849	0.897	0.005	0.013
Na(tot)	1.54	1.618	1.459	0.679	0.757	0.071	0.055	0.995	0.53
Na(M4)	1.283	1.382	1.298						
Na(A)	0.257	0.236	0.16						
SUM=	15.53	15.47	15.47						
Mg/(Mg+Fe(tot))	0.141	0.138	0.142						
Na(A)+K	0.53	0.471	0.466						
Si+Na+K	9.677	9.554	9.64						
Al(IV)+Ca	0.853	0.814	0.826						
pyx components normalized to 1									
Ac: (Na)									
En: (Mg/2)									
Fs: (Fe(t)-Na)/2									
Wo: (Ca/2)									
sum=									
AEFplot error=									
AFWplot error=									
EFWplot error=									
plg comp normalized to 1									
An:				0.135	0.119	0.002	7E-04	0	0.313
Ab:				0.857	0.873	0.077	0.057	0.995	0.67
Or:				0.008	0.008	0.92	0.942	0.005	0.016

37(36) ksp-l-r	38(36 plg-c	39(36) plg-c		21-Sep-89 mag 84-b	host 40 amb	28 plg-l	29 plg-l	30(29) or-l
0	0	0	MGO		2.556	0	0	0
23.23	21.82	21.16	AL203		1.035	18.67	18.94	18.2
63.79	65.46	65.43	SIO2		48.67	69.66	70.89	66.55
3.71	2.393	2.175	CAO		4.805	0	0	0
0	0	0	TIO2		1.489	0	0	0
0	0	0	CR2O3		0.038	0	0	0
0	0	0	NIO		0	0	0	0
0	0	0	MNO		0.599	0	0	0
0.104	0.16	0.047	FEO		30.5	0.677	0.4	0.048
8.389	8.898	10.01	NA2O		4.933	9.959	9.528	0.373
0.628	0.275	0.12	K2O		1.32	0.074	0.141	14.33
			F					
			CL					
99.84	99	98.95	SUM =		95.94	99.04	99.89	99.51
2.84	2.936	2.913	Si		7.825	3.12	3.159	3.108
1.219	1.153	1.111	Al(tot)		0.196	0.986	0.995	1.002
1.16	1.064	1.087	Al(VI)		0.175	0.88	0.841	0.892
0.059	0.089	0.024	Al(IV)		0.021	0.106	0.154	0.11
0	0	0	Ti		0.18	0	0	0
0.004	0.006	0.002	Fe(tot)		4.1	0.025	0.015	0.002
-0.14	-0.24	-0.07	Fe +3		0.326	-0.36	-0.48	-0.33
0.143	0.242	0.068	Fe +2		3.775	0.382	0.496	0.333
0	0	0	Mg		0.612	0	0	0
0	0	0	Mn		0.082	0	0	0
0	0	0	Ni		0	0	0	0
0	0	0	Cr		0.003	0	0	0
0.177	0.115	0.104	Ca		0.828	0	0	0
0.036	0.016	0.007	K		0.271	0.004	0.008	0.854
0.724	0.774	0.864	Na(tot)		1.538	0.865	0.823	0.034
			Na(M4)		1.172			
			Na(A)		0.366			
			SUM=		15.63			
			Mg/(Mg+Fe(t		0.13			
			Na(A)+K		0.636			
			Si+Na+K		9.633			
			Al(IV)+Ca		1.003			
			pyx components normalized to 1					
			Ac: (Na)					
			En: (Mg/2)					
			Fs: (Fe(t)-Na)/2					
			Wo: (Ca/2)					
			sum=					
			AEFplot error=					
			AFWplot error=					
			EFWplot error=					
			plg comp normalized to 1					
0.189	0.127	0.106	An:			0	0	0
0.773	0.855	0.887	Ab:			0.995	0.99	0.038
0.038	0.017	0.007	Or:			0.005	0.01	0.962

21-Sep-89 mag-155	70 cpx	71 cpx	72 cpx	74 cpx	69 amb		67 coss-c	68 coss-r
MGO	0.26	0.211	0.138	0.196	0.522		0.055	0.082
AL203	0.352	0.345	0.078	0.43	1.187		0.986	0.59
SIO2	48.729	49.293	49.379	49.065	47.354		39.532	42.14
CAO	16.629	15.679	15.086	15.67	4.839		0.826	0.376
TIO2	0.122	0.072	0.169	0.077	1.157		8.174	7.955
CR2O3	0.083	0	0.035	0.045	0.016		0.028	0.059
NIO	0	0.016	0	0	0		0	0
MNO	0.999	1.061	0.89	1.102	0.932		1.234	1.236
FEO	28.071	28.581	28.01	28.422	34.015		40.22	41.043
NA2O	3.235	3.4	4.221	3.619	4.884		7.15	7.377
K2O	0	0	0	0	1.207		0	0.033
F								
CL								
SUM =	98.48	98.658	98.006	98.626	96.113		98.205	100.89
Si	1.9869	2.0063	2.0081	1.9931	7.7287		5.7425	5.9527
Al(tot)	0.0169	0.0166	0.0037	0.0206	0.2284		0.1688	0.0982
Al(IV)	0.0131	-0.006	-0.008	0.0069	0.2284		0.1688	0.0473
Al(VI)	0.0038	0.0229	0.0118	0.0137	0		0	0.0509
Ti	0.0037	0.0022	0.0052	0.0024	0.142		0.893	0.8451
Fe(tot)	0.9572	0.9729	0.9526	0.9656	4.643		4.8862	4.8488
Fe +3	0.255	0.2347	0.3015	0.2721	0.5386		0.5708	0.3261
Fe +2	0.7023	0.7382	0.6512	0.6935	4.1044		4.3154	4.5226
Mg	0.0158	0.0128	0.0084	0.0119	0.127		0.0119	0.0173
Mn	0.0345	0.0366	0.0307	0.0379	0.1288		0.1518	0.1479
Ni	0	0.0005	0	0	0		0	0
Cr	0.0027	0	0.0011	0.0014	0.0035		0.0032	0.0066
Ca	0.7265	0.6836	0.6574	0.6821	0.8463		0.1286	0.0589
K	0	0	0	0	0.2513		0	0.0059
Na(tot)	0.2558	0.2683	0.3326	0.2851	1.5456		2.0139	2.0206
Na(M4)					1.1537			
Na(A)					0.3919			
SUM=	4	4	4	4	15.645		14	14
Mg/(Mg+Fe(tot))	0.0162	0.013	0.0087	0.0121	0.0266	Rh	0.0643	
Na(A)+K	0	0	0	0	0.6432	Fe3-Al	0.0403	
Si+Na+K	2.2426	2.2746	2.3409	2.2782	9.5257	Fe3-ts		
Al(IV)+Ca	0.7396	0.6775	0.6493	0.6889	1.0746	Ferri ideal		
pyx components normalized to 1								
Ac: (Na)	0.2616	0.2769	0.3412	0.2932				
En: (Mg/2)	0.0081	0.0066	0.0043	0.0061				
Fs: (Fe(t)-Na)/2	0.3588	0.3636	0.3176	0.35				
Wo: (Ca/2)	0.3716	0.3529	0.3369	0.3508				
sum=	1	1	1	1				
AEFplot error=	0.1858	0.1764	0.1685	0.1754				
AFWplot error=	0.004	0.0033	0.0021	0.0031				
EFWplot error=	0.1308	0.1385	0.1706	0.1468				
Ac: (Na)	0.2629	0.2722	0.3463	0.2916				
Di: (Mg)	0.0162	0.013	0.0087	0.0121				
Hd:(Fe(T)-Na)	0.7209	0.7148	0.645	0.6962				
cpx morimoto								
Q=Ca+Mg+(Fe2+	1.4446	1.4348	1.3169	1.3874				
J=2*Na	0.5115	0.5367	0.6657	0.5701				
J/Q+J	0.2615	0.2722	0.3358	0.2912				
Ca Cpx J/J+Q < .2 x								
Wo -Ca	41.897	40.08	39.884	40.182				
Fs-Fet+Mn	57.192	59.17	59.629	59.119				
En - Mg	0.9111	0.7502	0.5072	0.699				
total	100	100	100	100				
Na cpx J/J+Q >.8								
Na-Ca cpx .2<J/J+Q< .8								
2*Na**	0.2615	0.2722	0.3358	0.2912				
Q**	0.7385	0.7278	0.6642	0.7088				
Jd/Ae	0.0567	0.3579	0.1169	0.173				
Jd	0.0148	0.0974	0.0392	0.0504				
Ae	0.2467	0.1748	0.2985	0.2408				

21-Sep-89

73	mag 155	75	76	77	78(77)	79(77)	80(77)
coss		ksp-i	plg-i	plg-r	ksp-i	plg-i	ksp-i
0.071	MGO	0	0	0	0	0	0
0.739	AL203	17.538	18.791	19.625	18.542	19.17	17.411
40.256	SIO2	65.413	70.816	69.496	65.899	69.875	64.153
0.538	CRO	0	0	0.413	0.018	0	0.026
8.287	TIO2	0	0	0	0	0	0
0.043	CR2O3	0	0	0	0	0	0
0	NIO	0	0	0	0	0	0
1.185	MNO	0	0	0	0	0	0
40.483	FEO	0.533	0.752	0.084	0.117	0.241	0.676
7.283	NA2O	0.686	8.546	9.113	1.082	9.716	0.479
0	K2O	15.002	0.066	0.176	13.77	0.128	12.311
	F						
	CL						
98.885	SUM =	99.172	98.971	98.907	99.428	99.13	95.056
5.8067	SI	3.0567	3.2116	3.1295	3.064	3.1285	3.1477
0.1256	Al(tot)	0.966	1.0045	1.0416	1.0162	1.0117	1.0069
0.1256	Al(IV)	0.9433	0.7884	0.8705	0.936	0.8715	0.8523
0	Al(VI)	0.0226	0.2161	0.1711	0.0802	0.1402	0.1547
0.899	Ti	0	0	0	0	0	0
4.8836	Fe(tot)	0.0208	0.0285	0.0032	0.0045	0.009	0.0277
0.4952	Fe +3	-0.123	-0.672	-0.495	-0.23	-0.418	-0.486
4.3885	Fe +2	0.1436	0.701	0.4979	0.2344	0.4269	0.5139
0.0153	Mg	0	0	0	0	0	0
0.1448	Mn	0	0	0	0	0	0
0	Ni	0	0	0	0	0	0
0.0049	Cr	0	0	0	0	0	0
0.0832	Ca	0	0	0.0199	0.0009	0	0.0014
0	K	0.8944	0.0038	0.0101	0.8168	0.0073	0.7706
2.037	Na(tot)	0.0622	0.7515	0.7957	0.0975	0.8435	0.0456
	Na(M4)						
	Na(A)						
14	SUM=	5	5	5	5	5	5

Mg/(Mg+Fe(tot))
Na(A)+K
Si+Na+K
Al(IV)+Ca

pyx components normalized to 1
Ac: (Na)
En: (Mg/2)
Fs: (Fe(t)-Na)/2
Wo: (Ca/2)
sum=
AEFplot error=
AFWplot error=
EFWplot error=

plg comp normalized to 1

An:	0	0	0.0241	0.001	0	0.0017
Ab:	0.065	0.9949	0.9636	0.1066	0.9914	0.0557
Or:	0.935	0.0051	0.0122	0.8924	0.0086	0.9426

15-Jun-89

MAG 193	1	2(1)	3	4(3)	5	6(5)	7
	Amb-c	Amb-r	Amb-c	Amb-r	Amb-c	Amb-r	Amb
MGO	0.198	0.226	0.218	0.172	0.15	0.112	0.964
AL203	1.098	0.764	1.817	0.51	1.013	0.494	2.297
SIO2	48.61	48.31	47.43	50.43	48.87	49.5	46.68
CAO	2.46	2.761	2.963	0.351	4.478	3.001	7.003
TIO2	1.328	0.528	0.656	0.339	1.381	1.402	1.486
CR2O3	0	0.087	0.09	0.081	0.103	0.022	0
NIO	0	0	0	0	0	0	0
MNO	1.055	1.092	1.112	0.768	1.052	1.018	0.823
FEO	34.2	34.71	34.24	34.21	32.59	34.05	34.67
NA2O	6.59	6.339	6.076	7.654	6.305	6.458	3.081
K2O	2.069	1.033	1.69	1.146	1.553	1.899	1.053
F	0.263	0.47	0.337	0.443	0.85	0.375	0.362
CL	0.015	0	0	0	0	0	0.096
SUM =	97.88	96.32	96.63	96.1	98.35	98.33	98.52
Si	7.831	7.854	7.704	8.107	7.986	7.979	7.434
Al(tot)	0.209	0.146	0.348	0.097	0.195	0.094	0.431
Al(IV)	0.169	0.146	0.296	-0.11	0.014	0.021	0.431
Al(VI)	0.039	1E-04	0.051	0.204	0.181	0.072	0
Ti	0.161	0.065	0.08	0.041	0.17	0.17	0.178
Fe(tot)	4.608	4.719	4.651	4.599	4.454	4.589	4.617
Fe +3	0.475	0.831	0.778	0.855	-0.41	0.161	0.79
Fe +2	4.134	3.888	3.873	3.744	4.863	4.428	3.827
Mg	0.048	0.055	0.053	0.041	0.037	0.027	0.229
Mn	0.144	0.15	0.153	0.105	0.146	0.139	0.111
NI	0	0	0	0	0	0	0
Cr	0	0	0	0	0	0	0
Ca	0.425	0.481	0.516	0.06	0.784	0.518	1.195
K	0.425	0.214	0.35	0.235	0.324	0.39	0.214
Na(tot)	2.059	1.998	1.914	2.386	1.998	2.018	0.951
Na(M4)	1.575	1.519	1.484	1.94	1.216	1.482	0.805
Na(A)	0.483	0.479	0.429	0.446	0.782	0.536	0.146
SUM=	15.91	15.68	15.77	15.67	16.09	15.92	15.36
Mg/(Mg+Fe(t	0.01	0.011	0.011	0.009	0.008	0.006	0.047
Na(A)+K	0.909	0.693	0.779	0.681	1.106	0.927	0.36
Si+Na+K	10.31	10.07	9.967	10.73	10.31	10.39	8.599
Al(IV)+Ca	0.594	0.627	0.812	-0.05	0.798	0.54	1.626

APPENDIX III.IV

EXCEL MACROS
- PRBMAC
- PETMAC

	C_senig norm	cass	C_AMB norm	amb
result type	=RESULT(64)		=RESULT(64)	
input array assignment	=ARGUMENT("wt6",64)	wt6 input	=ARGUMENT("wt7",64)	
convert to mole proportions	=(INDEX(wt6,1,1)/40.32)	MGO	=(INDEX(wt7,1,1)/40.32)	MGO
	=((INDEX(wt6,2,1)/101.96)*2)	AL203	=((INDEX(wt7,2,1)/101.9	AL203
	=(INDEX(wt6,3,1)/60.09)	SIO2	=(INDEX(wt7,3,1)/60.09)	SIO2
	=(INDEX(wt6,4,1)/56.08)	CAO	=(INDEX(wt7,4,1)/56.08)	CAO
	=(INDEX(wt6,5,1)/79.9)	TIO2	=(INDEX(wt7,5,1)/79.9)	TIO2
	=(INDEX(wt6,6,1)/151.9902)*2	CR203	=(INDEX(wt7,6,1)/151.98(	CR203
	=(INDEX(wt6,7,1)/74.71)	NIO	=(INDEX(wt7,7,1)/74.71)	NIO
	=(INDEX(wt6,8,1)/70.94)	MNO	=(INDEX(wt7,8,1)/70.94)	MNO
	=(INDEX(wt6,9,1)/71.85)	FEO	=(INDEX(wt7,9,1)/71.85)	FEO
	=((INDEX(wt6,10,1)/61.98)*2)	NA2O	=((INDEX(wt7,10,1)/61.9(	NA2O
	=((INDEX(wt6,11,1)/94.2)*2)	K2O	=((INDEX(wt7,11,1)/94.2)	K2O
cation normalization factor	=14/SUM(B4:B14)		=13/(D4+D5+D6+D8+D9+[	
normalize to number of cations	=(B4*$I8)	MGO	=(D4*D15)	MGO
	=(B5*$I8)	AL203	=(D5*D15)	AL203
	=(B6*$I8)	SIO2	=(D6*D15)	SIO2
	=(B7*$I8)	CAO	=(D7*D15)	CAO
	=(B8*$I8)	TIO2	=(D8*D15)	TIO2
	=(B9*$I8)	CR203	=(D9*D15)	CR203
	=(B10*$I8)	NIO	=(D10*D15)	NIO
	=(B11*$I8)	MNO	=(D11*D15)	MNO
	=(B12*$I8)	FEO	=(D12*D15)	FEO
	=(B13*$I8)	NA2O	=(D13*D15)	NA2O
	=(B14*$I8)	K2O	=(D14*D15)	K2O
calc Al assignment to 4 or 6 fold sites	=prbmacIC_CoesAl(B16:B18)		=prbmacIC_AmbAL(D16:D18	
balance charges and calc Fe3+ and 2+	=prbmacIC_CoesAl(B16:B18)		=prbmacIC_AmbAL(D16:D18	
	=40-(B16*2+B17*3+B18*4+B19*2+B20*4+B2		=prbmacIC_Nam4(D16:D26)	
	=B24-B29		=prbmacIC_Nam4(D16:D26)	
assign output array	=SET.VALUE(INDEX(senig1,1,1),B16)	Si	=40-(D16*2+D17*3+D18*·	
	=SET.VALUE(INDEX(senig1,2,1),B17)	Al(tot)	=D24-D31	
	=SET.VALUE(INDEX(senig1,3,1),B27)	Al(IV)	=SET.VALUE(INDEX(amb,1,1	Si
	=SET.VALUE(INDEX(senig1,4,1),B28)	Al(IV)	=SET.VALUE(INDEX(amb,2,1	Al(tot)
	=SET.VALUE(INDEX(senig1,5,1),B20)	Ti	=SET.VALUE(INDEX(amb,3,1	Al(IV)
	=SET.VALUE(INDEX(senig1,6,1),B24)	Fe(tot)	=SET.VALUE(INDEX(amb,4,1	Al(IV)
	=SET.VALUE(INDEX(senig1,7,1),B29)	Fe +3	=SET.VALUE(INDEX(amb,5,1	Ti
	=SET.VALUE(INDEX(senig1,8,1),B30)	Fe +2	=SET.VALUE(INDEX(amb,6,1	Fe(tot)
	=SET.VALUE(INDEX(senig1,9,1),B10)	Mg	=SET.VALUE(INDEX(amb,7,1	Fe +3
	=SET.VALUE(INDEX(senig1,10,1),B23)	Mn	=SET.VALUE(INDEX(amb,8,1	Fe +2
	=SET.VALUE(INDEX(senig1,11,1),B22)	NI	=SET.VALUE(INDEX(amb,9,1	Mg
	=SET.VALUE(INDEX(senig1,12,1),B21)	Cr	=SET.VALUE(INDEX(amb,10	Mn
	=SET.VALUE(INDEX(senig1,13,1),B19)	Ca	=SET.VALUE(INDEX(amb,11	NI
	=SET.VALUE(INDEX(senig1,14,1),B26)	K	=SET.VALUE(INDEX(amb,12	Cr
	=SET.VALUE(INDEX(senig1,15,1),B25)	Na(tot)	=SET.VALUE(INDEX(amb,13	Ca
return output array	=RETURN(INDEX(senig1,1,1):INDEX(senig1,15,1))		=SET.VALUE(INDEX(amb,14	K
ouput array	8.8293887620443		=SET.VALUE(INDEX(amb,15	Na(tot)
	0.061788388468202		=SET.VALUE(INDEX(amb,16	Na(M4)
	0.061788388468202		=SET.VALUE(INDEX(amb,17	Na(A)
	0		=RETURN(INDEX(amb,1,1):I	
	0.906261184729G7		7.4150139747299	
	4.990368015406		0.53528713460612	
	0.485471243769Z9		0.53528713460612	
	4.504836771636B		0	
	0.019114146616690		0.11006316476327	
	0.116159788441Q1		3.6003186331885	
	0		0.748484708S2747	
	0.0034546984657974		2.8548638242611	
	0.061466820776139		1.2566297594975	
	0		0.08268743321473	
	2.0220202246612		0	
			0.0034546984657974	
			1.3954709548498	
			0	
			0.878133967780Q1	
			0.604520045150Q4	
			0.273613922630Z6	

subroutine for calc Al sites	C_CoesAl	C_AmbAL
	=RESULT(64)	=RESULT(64)
	=ARGUMENT("ctwt",64)	=ARGUMENT("ctwt2",64)
	=6-INDEX(ctwt,3,1)	=6-INDEX(ctwt2,3,1)
	=INDEX(ctwt,2,1)-B79	=INDEX(ctwt2,2,1)-D77
	=IF(Al<0,GOTO(else))	=IF(AmbAl<0,GOTO(else3))
	then	then
	=SET.VALUE(INDEX(Alres,1,1),(B79))	=SET.VALUE(INDEX(Alres1,
	=SET.VALUE(INDEX(Alres,2,1),(B80))	=SET.VALUE(INDEX(Alres1,
	=GOTO(continue)	=GOTO(continue3)
	else	else3
	=SET.VALUE(INDEX(Alres,1,1),INDEX(ctwt,2,1))	=SET.VALUE(INDEX(Alres1,
	=SET.VALUE(INDEX(Alres,2,1),0)	=SET.VALUE(INDEX(Alres1,:
	continue	continue3
	=RETURN(INDEX(Alres,1,1):INDEX(Alres,2,1))	=RETURN(INDEX(Alres1,1,1
	0.061788388468202	0.53528713460612
	0	0
		C_Na(m4)
		=RESULT(64)
		=ARGUMENT("catwt1",64)
		=2-INDEX(catwt1,4,1)
		=INDEX(catwt1,10,1)-D98
		=IF(Na_M4<=0,GOTO(else1))
		then
		=SET.VALUE(INDEX(NaRes,

```
=SET.VALUE(INDEX(NaRes,2
=GOTO(continue1)
else1
=SET.VALUE(INDEX(NaRes,
continue1
=RETURN(INDEX(NaRes,1,1)
0.60452004515014
0.27361392263028
```

```
C_bio_norm                    bio
=RESULT(64)
=ARGUMENT("wt8",64)
=(INDEX(wt8,1,1)/40.32)       MGO
=((INDEX(wt8,2,1)/101.9(      AL203
=(INDEX(wt8,3,1)/60.09)       SIO2
=(INDEX(wt8,4,1)/56.08)       CAO
=(INDEX(wt8,5,1)/79.9)        TIO2
=(INDEX(wt8,6,1)/151.99(      CR203
=(INDEX(wt8,7,1)/74.71)       NIO
=(INDEX(wt8,8,1)/70.94)       MNO
=(INDEX(wt8,9,1)/71.85)       FEO
=((INDEX(wt8,10,1)/61.9(      NA2O
=((INDEX(wt8,11,1)/94.2)      K2O
=8/SUM(F4:F14)
=(F4*F15)                     MGO
=(F5*F15)                     AL203
=(F6*F15)                     SIO2
=(F7*F15)                     CAO
=(F8*F15)                     TIO2
=(F9*F15)                     CR203
=(F10*F15)
=(F11*F15)                    MNO
=(F12*F15)                    FEO
=(F13*F15)                    NA2O
=(F14*F15)                    K2O
=prbmacIC_BioAL(F16:F18)
=prbmacIC_BioAL(F16:F18)
=22-(F16*2+F17*3+F18*4
=F24-F29
=SET.VALUE(INDEX(bio,1,1)     SI
=SET.VALUE(INDEX(bio,2,1)     AI(tot)
=SET.VALUE(INDEX(bio,3,1)     AI(IV)
=SET.VALUE(INDEX(bio,4,1)     AI(IV)
=SET.VALUE(INDEX(bio,5,1)     TI
=SET.VALUE(INDEX(bio,6,1)     Fe(tot)
=SET.VALUE(INDEX(bio,7,1)     Fe +3
=SET.VALUE(INDEX(bio,8,1)     Fe +2
=SET.VALUE(INDEX(bio,9,1)     Mg
=SET.VALUE(INDEX(bio,10,      Mn
=SET.VALUE(INDEX(bio,11,      NI
=SET.VALUE(INDEX(bio,12,      Cr
=SET.VALUE(INDEX(bio,13,      Ca
=SET.VALUE(INDEX(bio,14,      K
=SET.VALUE(INDEX(bio,15,      Na(tot)
=RETURN(INDEX(bio,1,1):IN
2.9287561479371
1.2753641530289
0.073243852062877
1.202120306966
0.20824879247813
1.9075232231598
-0.5408884412338E
2.44822266433634
0.63858344321881
0.036668333187826
0
0
0.0021613143729825
0.99980063254091
0.0050757600788973
```

```
C_pyx_norm                    Pyx
=RESULT(64)
=ARGUMENT("wt9",64)
=(INDEX(wt9,1,1)/40.32)       MGO
=((INDEX(wt9,2,1)/101.9(      AL203
=(INDEX(wt9,3,1)/60.09)       SIO2
=(INDEX(wt9,4,1)/56.08)       CAO
=(INDEX(wt9,5,1)/79.9)        TIO2
=(INDEX(wt9,6,1)/151.99(      CR203
=(INDEX(wt9,7,1)/74.71)       NIO
=(INDEX(wt9,8,1)/70.94)       MNO
=(INDEX(wt9,9,1)/71.85)       FEO
=((INDEX(wt9,10,1)/61.9(      NA2O
=((INDEX(wt9,11,1)/94.2)      K2O
=4/SUM(H4:H14)
=(H4*H15)                     MGO
=(H5*H15)                     AL203
=(H6*H15)                     SIO2
=(H7*H15)                     CAO
=(H8*H15)                     TIO2
=(H9*H15)                     CR203
=(H10*H15)                    NIO
=(H11*H15)                    MNO
=(H12*H15)                    FEO
=(H13*H15)                    NA2O
=(H14*H15)                    K2O
=prbmacIC_PyxAL(H16:H18)
=prbmacIC_PyxAL(H16:H18)
=12-(H16*2+H17*3+H18*4
=H24-H29
=SET.VALUE(INDEX(pyx,1,1      SI
=SET.VALUE(INDEX(pyx,2,1      AI(tot)
=SET.VALUE(INDEX(pyx,3,1      AI(IV)
=SET.VALUE(INDEX(pyx,4,1      AI(IV)
=SET.VALUE(INDEX(pyx,5,1      TI
=SET.VALUE(INDEX(pyx,6,1
=SET.VALUE(INDEX(pyx,7,1      Fe +3
=SET.VALUE(INDEX(pyx,8,1      Fe +2
=SET.VALUE(INDEX(pyx,9,1      Mg
=SET.VALUE(INDEX(pyx,10,      Mn
=SET.VALUE(INDEX(pyx,11,      NI
=SET.VALUE(INDEX(pyx,12,      Cr
=SET.VALUE(INDEX(pyx,13,      Ca
=SET.VALUE(INDEX(pyx,14,      K
=SET.VALUE(INDEX(pyx,15,      Na(tot)
=RETURN(INDEX(pyx,1,1):IN
1.9706922083833
0.0049927983637617
0.0049927983637617
0
0.051480362946336
0.94928887605038
1.7763568394003E-15
0.94928887605038
0.096673932068067
0.026110468732263
0
0
0.81989773858319
0
0.11269707778218
```

```
C_olv_norm                    olv
=RESULT(64)
=ARGUMENT("wt10",64)
=(INDEX(wt10,1,1)/40.32)      MGO
=((INDEX(wt10,2,1)/101.9      AL203
=(INDEX(wt10,3,1)/60.09)      SIO2
=(INDEX(wt10,4,1)/56.08)      CAO
=(INDEX(wt10,5,1)/79.9)       TIO2
=(INDEX(wt10,6,1)/151.91      CR203
=(INDEX(wt10,7,1)/74.71)      NIO
=(INDEX(wt10,8,1)/70.94)      MNO
=(INDEX(wt10,9,1)/71.85)      FEO
=((INDEX(wt10,10,1)/61.9      NA2O
=((INDEX(wt10,11,1)/94.2      K2O
=3/SUM(J4:J14)
=(J4*J15)                     MGO
=(J5*J15)                     AL203
=(J6*J15)                     SIO2
=(J7*J15)                     CAO
=(J8*J15)                     TIO2
=(J9*J15)                     CR203
=(J10*J15)                    NI
=(J11*J15)                    MNO
=(J12*J15)                    FEO
=(J13*J15)                    NA2O
=(J14*J15)                    K2O
=prbmacIC_OlvAL(J16:J18)
=prbmacIC_OlvAL(J16:J18)
=8-(J16*2+J17*3+J18*4
=J24-J29
=SET.VALUE(INDEX(olv,1,1)     SI
=SET.VALUE(INDEX(olv,2,1)     AI(tot)
=SET.VALUE(INDEX(olv,3,1)     AI(IV)
=SET.VALUE(INDEX(olv,4,1)     AI(IV)
=SET.VALUE(INDEX(olv,5,1)     TI
=SET.VALUE(INDEX(olv,6,1)     Fe(tot)
=SET.VALUE(INDEX(olv,7,1)     Fe +3
=SET.VALUE(INDEX(olv,8,1)     Fe +2
=SET.VALUE(INDEX(olv,9,1)     Mg
=SET.VALUE(INDEX(olv,10,      Mn
=SET.VALUE(INDEX(olv,11,      NI
=SET.VALUE(INDEX(olv,12,      Cr
=SET.VALUE(INDEX(olv,13,      Ca
=SET.VALUE(INDEX(olv,14,      K
=SET.VALUE(INDEX(olv,15,      Na(tot)
=RETURN(INDEX(olv,1,1):IN
1.0008789430988       SI
0.0063644382662886    AI(tot)
-0.0008789430988E-16  AI(IV)
0.0072413783647758    AI(IV)
0.0022502900845018    TI
1.8777855573018       Fe(tot)
-0.012917974894703    Fe +3
1.8907065316868       Fe +2
0.015901681181302     Mg
0.0003388033882784    Mn
0.00182140287896A1    NI
0.0002991349424385I   Cr
0.0045665531434335    Ca
0                     K
0                     Na(tot)
```

```
C_BioAL
=RESULT(64)
=ARGUMENT("ctwt3",64)
=3-INDEX(ctwt3,3,1)
=INDEX(ctwt3,2,1)-F73
=IF(BioAl1<0,GOTO(else4))
then
=SET.VALUE(INDEX(Alres2,
=SET.VALUE(INDEX(Alres2,
=GOTO(continue4)
else4
=SET.VALUE(INDEX(Alres2,
=SET.VALUE(INDEX(Alres2,:
continue4
=RETURN(INDEX(Alres2,1,1
0.073243852062877
1.202120306966
```

```
C_PyxAL
=RESULT(64)
=ARGUMENT("ctwt8",64)
=2-INDEX(ctwt8,3,1)
=INDEX(ctwt8,2,1)-H72
=IF(PyxAl1<0,GOTO(else6))
then
=SET.VALUE(INDEX(Alres5,
=SET.VALUE(INDEX(Alres5,
=GOTO(continue6)
else6
=SET.VALUE(INDEX(Alres5,
=SET.VALUE(INDEX(Alres5,:
continue6
=RETURN(INDEX(Alres5,1,1
0.0049927983637617
0
```

```
C_OlvAL
=RESULT(64)
=ARGUMENT("ctwt6",64)
=1-INDEX(ctwt6,3,1)
=INDEX(ctwt6,2,1)-J73
=IF(OlvAl<0,GOTO(else6))
then
=SET.VALUE(INDEX(Alres6
=SET.VALUE(INDEX(Alres6
=GOTO(continue6)
else6
=SET.VALUE(INDEX(Alres6,
=SET.VALUE(INDEX(Alres6,:
continue6
=RETURN(INDEX(Alres6,1,1
-0.0008789430988E-16
0.0072413783647758
```

```
C_pyx_ox_norm                 Pyx
=RESULT(64)
=ARGUMENT("wt9ox",64)
=(INDEX(wt9ox,1,1)/40.32      MGO-cat
=((INDEX(wt9ox,2,1)/101.      AL203
=(INDEX(wt9ox,3,1)/60.09      SIO2
=(INDEX(wt9ox,4,1)/56.08      CAO
=(INDEX(wt9ox,5,1)/79.9)      TIO2
=(INDEX(wt9ox,6,1)/151.9      CR203
=(INDEX(wt9ox,7,1)/74.71      NIO
```

```
=(INDEX(wt9ox,8,1)/70.94 MNO
=(INDEX(wt9ox,9,1)/71.85 FEO
=((INDEX(wt9ox,10,1)/61. NA2O
=((INDEX(wt9ox,11,1)/94. K2O
=(INDEX(wt9ox,1,1)/40.32 MGO-ox p
=((INDEX(wt9ox,2,1)/101. AL203
=(INDEX(wt9ox,3,1)/60.09 SIO2
=(INDEX(wt9ox,4,1)/58.08 CFO
=(INDEX(wt9ox,5,1)/79.9)' TIO2
=(INDEX(wt9ox,6,1)/151.9 CR2O3
=(INDEX(wt9ox,7,1)/74.71 NIO
=(INDEX(wt9ox,8,1)/70.94 MNO
=(INDEX(wt9ox,9,1)/71.85 FEO
=(INDEX(wt9ox,10,1)/61.9 NA2O
=(INDEX(wt9ox,11,1)/94.2 K2O
=6/SUM(H104:H114)
=(H93*H115)                MGO
=(H94*H115)                AL203
=(H95*H115)                SIO2
=(H96*H115)                CFO
=(H97*H115)                TIO2
=(H98*H115)                CR2O3
=(H99*H115)                NIO
=(H100*H115)               MNO
=(H101*H115)               FEO
=(H102*H115)               NA2O
=(H103*H115)               K2O
=prbmacIC_PyxAL(H115:H1
=prbmacIC_PyxAL(H115:H1
=12-(H116*2+H117*3+H1
=H124-H129
=SET.VALUE(INDEX(pyxox,1 SI
=SET.VALUE(INDEX(pyxox,2 Al(tot)
=SET.VALUE(INDEX(pyxox,3 Al(IV)
=SET.VALUE(INDEX(pyxox,4 Al(IV)
=SET.VALUE(INDEX(pyxox,5 TI
=SET.VALUE(INDEX(pyxox,6
=SET.VALUE((INDEX(pyxox,7 Fe +3
=SET.VALUE(INDEX(pyxox,8 Fe +2
=SET.VALUE(INDEX(pyxox,9 Mg
=SET.VALUE(INDEX(pyxox,1 Mn
=SET.VALUE(INDEX(pyxox,1 NI
=SET.VALUE(INDEX(pyxox,1 Cr
=SET.VALUE(INDEX(pyxox,1 Ca
=SET.VALUE(INDEX(pyxox,1 K
=SET.VALUE(INDEX(pyxox,1 Na(tot)
=RETURN(INDEX(pyxox,1,1)
2.1467248700881
0.020476835274767
-0.1467248700881
0.167204708360B7
0.0023514081183527
1.6991717340199
-0.2958707114478B
1.9951424484678
0.018443446006335
0.07366E530666368
0
0.0006357167B617038
0.018043068603308
0
0.023297400003949
```

```
C_PyxAL
=RESULT(64)
=ARGUMENT("ctwt8",64)
=2-INDEX(ctwt8,3,1)
=INDEX(ctwt8,2,1)-H172
=IF(PyxAl1<0,GOTO(else6))
then
=SET.VALUE(INDEX(Alres6,
=SET.VALUE(INDEX(Alres6,
=GOTO(continue6)
else6
=SET.VALUE(INDEX(Alres6,
=SET.VALUE(INDEX(Alres6,2
continue6
=RETURN(INDEX(Alres6,1,1
-0.1467248700881
0.167204708360B7
```

C_felds_norm	felds
=RESULT(64)	
=ARGUMENT("wt11",64)	
=(INDEX(wt11,1,1)/40.32)	MGO
=((INDEX(wt11,2,1)/101.9	AL203
=(INDEX(wt11,3,1)/60.09)	SIO2
=(INDEX(wt11,4,1)/56.08)	CAO
=(INDEX(wt11,5,1)/79.9)	TIO2
=(INDEX(wt11,6,1)/151.9(	CR203
=(INDEX(wt11,7,1)/74.71)	NIO
=(INDEX(wt11,8,1)/70.94)	MNO
=(INDEX(wt11,9,1)/71.85)	FEO
=((INDEX(wt11,10,1)/61.9	NA2O
=((INDEX(wt11,11,1)/94.2	K2O
=5/SUM(L4:L14)	
=(L4*L15)	MGO
=(L5*L15)	AL203
=(L6*L15)	SIO2
=(L7*L15)	CAO
=(L8*L15)	TIO2
=(L9*L15)	CR203
=(L10*L15)	NI
=(L11*L15)	MNO
=(L12*L15)	FEO
=(L13*L15)	NA2O
=(L14*L15)	K2O
=prbmacIC_FeldsAL(L16:L1E	
=prbmacIC_FeldsAL(L16:L1E	
=16-(L16*2+L17*3+L18*4	
=L24-L29	
=SET.VALUE(INDEX(olv,1,1)	SI
=SET.VALUE(INDEX(olv,2,1)	Al(tot)
=SET.VALUE(INDEX(olv,3,1)	Al(IV)
=SET.VALUE(INDEX(olv,4,1)	Al(IV)
=SET.VALUE(INDEX(olv,5,1)	TI
=SET.VALUE(INDEX(olv,6,1)	Fe(tot)
=SET.VALUE(INDEX(olv,7,1)	Fe +3
=SET.VALUE(INDEX(olv,8,1)	Fe +2
=SET.VALUE(INDEX(olv,9,1)	Mg
=SET.VALUE(INDEX(olv,10,'	Mn
=SET.VALUE(INDEX(olv,11,'	NI
=SET.VALUE(INDEX(olv,12,'	Cr
=SET.VALUE(INDEX(olv,13,'	Ca
=SET.VALUE(INDEX(olv,14,'	K
=SET.VALUE(INDEX(olv,15,'	Na(tot)
=RETURN(INDEX(olv,1,1):I	
1.5766268572785	SI
0.087572820872624	Al(tot)
-0.57662685727645	Al(IV)
0.6441996781508	Al(IV)
0.003383350450151	TI
1.2531526755675	Fe(tot)
-1.2275532363288	Fe +3
2.4807058118974	Fe +2
0.029245440739651	Mg
0.028770362517521	Mn
0	NI
0	Cr
0.041268472573988	Ca
0	K
0	Na(tot)

Amb_name	
=(INDEX(cat,1,1))	SI
=(INDEX(cat,2,1))	Al(tot)
=(INDEX(cat,3,1))	Al(IV)
=(INDEX(cat,4,1))	Al(IV)
=(INDEX(cat,5,1))	TI
=(INDEX(cat,6,1))	Fe(tot)
=(INDEX(cat,7,1))	Fe +3
=(INDEX(cat,8,1))	Fe +2
=(INDEX(cat,9,1))	Mg
=(INDEX(cat,10,1))	Mn
=(INDEX(cat,11,1))	NI
=(INDEX(cat,12,1))	Cr
=(INDEX(cat,13,1))	Ca
=(INDEX(cat,14,1))	K
=(INDEX(cat,15,1))	Na(tot)
=(INDEX(cat,16,1))	Na(M4)
=(INDEX(cat,17,1))	Na(A)
=N11/(N11+N10)	
=IF((N18+N15)<1.34,goto n	
then	
=IF(N15>=0.67,go to noise2)	
then	
=IF(N7<0.5,goto noise3)	
then	
noise2	
noise1	
=return	
=continue1	

C_Ilm_norm	felds
=RESULT(64)	
=ARGUMENT("wt12",64)	
=(INDEX(wt12,1,1)/40.32)	MGO
=((INDEX(wt12,2,1)/101.1	AL203
=(INDEX(wt12,3,1)/60.09)	SIO2
=(INDEX(wt12,4,1)/56.08)	CAO
=(INDEX(wt12,5,1)/79.9)	TIO2
=(INDEX(wt12,6,1)/151.9(	CR203
=(INDEX(wt12,7,1)/74.71)	NIO
=(INDEX(wt12,8,1)/70.94)	MNO
=(INDEX(wt12,9,1)/71.85)	FEO
=((INDEX(wt12,10,1)/61.9	NA2O
=((INDEX(wt12,11,1)/94.2	K2O
=2/SUM(P4:P14)	
=(P4*P15)	MGO
=(P5*P15)	AL203
=(P6*P15)	SIO2
=(P7*P15)	CAO
=(P8*P15)	TIO2
=(P9*P15)	CR203
=(P10*P15)	NI
=(P11*P15)	MNO
=(P12*P15)	FEO
=(P13*P15)	NA2O
=(P14*P15)	K2O
=16-(P16*2+P17*3+P18*	
=P24-P27	
=SET.VALUE(INDEX(Ilm,1,1	SI
=SET.VALUE(INDEX(Ilm,2,1	Al(tot)
=SET.VALUE(INDEX(Ilm,2,1	Al(IV)
=SET.VALUE(INDEX(Ilm,2,1	Al(IV)
=SET.VALUE(INDEX(Ilm,5,1	TI
=SET.VALUE(INDEX(Ilm,6,1	Fe(tot)
=SET.VALUE(INDEX(Ilm,7,1	Fe +3
=SET.VALUE(INDEX(Ilm,8,1	Fe +2
=SET.VALUE(INDEX(Ilm,9,1	Mg
=SET.VALUE(INDEX(Ilm,10,	Mn
=SET.VALUE(INDEX(Ilm,11,	NI
=SET.VALUE(INDEX(Ilm,12,	Cr
=SET.VALUE(INDEX(Ilm,13,	Ca
=SET.VALUE(INDEX(Ilm,14,	K
=SET.VALUE(INDEX(Ilm,15,	Na(tot)
=RETURN(INDEX(Ilm,1,1):II	

C_FeldsAL	
=RESULT(64)	
=ARGUMENT("ctwt7",64)	
=4-INDEX(ctwt7,3,1)	
=INDEX(ctwt7,2,1)-L73	
=IF(FeldsAl<0,GOTO(else7))	
then	
=SET.VALUE(INDEX(Alree7,	
=SET.VALUE(INDEX(Alree7,	
=GOTO(continue7)	
else7	
=SET.VALUE(INDEX(Alree7,	
=SET.VALUE(INDEX(Alree7,:	
continue7	
=RETURN(INDEX(Alree7,1,1	
1.1858206686721	
0.00688459154106826	

```
Larsen_DI_7_not used
=ARGUMENT("SiO2")
=ARGUMENT("K2O")
=ARGUMENT("MnO")
=ARGUMENT("MgO")
=ARGUMENT("CaO")
=0.33*SiO2+K2O-0.9*MnO-MgO-CaO
=RETURN(A7)

Cwt2mol
=RESULT(64)
=ARGUMENT("wt",64)

=INDEX(wt,1,1)/60.09
=INDEX(wt,2,1)/79.9
=INDEX(wt,3,1)/101.96
=INDEX(wt,4,1)/71.85
=INDEX(wt,5,1)/159.69
=INDEX(wt,6,1)/70.94
=INDEX(wt,7,1)/40.32
=INDEX(wt,8,1)/56.08
=INDEX(wt,9,1)/61.98
=INDEX(wt,10,1)/94.2
=INDEX(wt,11,1)/141.95
=SUM(A14:A24)
=A14/A25
=A15/A25
=A16/A25
=A17/A25
=A18/A25
=A19/A25
=A20/A25
=A21/A25
=A22/A25
=A23/A25
=A24/A25
=SET.VALUE(INDEX(molares,1),A26)
=SET.VALUE(INDEX(molares,2),A27)
=SET.VALUE(INDEX(molares,3),A28)
=SET.VALUE(INDEX(molares,4),A29)
=SET.VALUE(INDEX(molares,5),A30)
=SET.VALUE(INDEX(molares,6),A31)
=SET.VALUE(INDEX(molares,7),A32)
=SET.VALUE(INDEX(molares,8),A33)
=SET.VALUE(INDEX(molares,9),A34)
=SET.VALUE(INDEX(molares,10),A36)
=SET.VALUE(INDEX(molares,11),A36)
=RETURN(INDEX(molares,1):INDEX(ma
#REFI
#REFI
#REFI
#REFI
#REFI
#REFI
#REFI
#REFI
#REFI
#REFI

Larsen_DI
=ARGUMENT("wt6",64)

=INDEX(wt6,1,1)/3+INDEX(wt6,1,10)
=RETURN(A66)

AL(IV)_CA
=ARGUMENT("catwt",64)
=8-INDEX(catwt,3,1)
=INDEX(catwt,2,1)-A70
=IF(Al<0,GOTO(else))
then
=SET.VALUE(Alres,(A70+INDEX(catwt,
=GOTO(continue)
else
=SET.VALUE(Alres,(INDEX(catwt,2,1)+
continue
=RETURN(Alres)
1.3236

Rwt2mol
=RESULT(64)
=ARGUMENT("wt1",64)

=INDEX(wt1,1,1)/60.09
=INDEX(wt1,1,2)/79.9
=INDEX(wt1,1,3)/101.96
=INDEX(wt1,1,4)/71.85
=INDEX(wt1,1,5)/159.69
=INDEX(wt1,1,6)/70.94
=INDEX(wt1,1,7)/40.32
=INDEX(wt1,1,8)/56.08
=INDEX(wt1,1,9)/61.98
=INDEX(wt1,1,10)/94.2
=INDEX(wt1,1,11)/141.95
=SUM(B14:B24)
=(B14/B25)*100
=(B15/B25)*100
=(B16/B25)*100
=(B17/B25)*100
=(B18/B25)*100
=(B19/B25)*100
=(B20/B25)*100
=(B21/B25)*100
=(B22/B25)*100
=(B23/B25)*100
=(B24/B25)*100
=SET.VALUE(INDEX(molares
=SET.VALUE(INDEX(molares
=SET.VALUE(INDEX(molares
=SET.VALUE(INDEX(molares
=SET.VALUE(INDEX(molares
=SET.VALUE(INDEX(molares
=SET.VALUE(INDEX(molares
=SET.VALUE(INDEX(molares
=SET.VALUE(INDEX(molares
=SET.VALUE(INDEX(molares
=SET.VALUE(INDEX(molares
=RETURN(INDEX(molares1,
83.43392755169B          0.1(8.1(0    0.8+0.0(0.8(0.4(3,1(3.2(0.0(

C_Na(mt)
=RESULT(64)
=ARGUMENT("catwt1",64)
=2-INDEX(catwt1,4,1)
=INDEX(catwt1,9,1)-B64
=IF(Na_M4<=0,GOTO(else1)
then
=SET.VALUE(INDEX(NaRes,
=SET.VALUE(INDEX(NaRes,
=GOTO(continue1)
else1
=SET.VALUE(INDEX(NaRes,
=SET.VALUE(INDEX(NaRes,
continue1
=RETURN(INDEX(NaRes,1,1)
0.9724                   0.21

R_REECHON
=RESULT(64)
=ARGUMENT("REE",64)
=INDEX(REE,1,1)/0.33
=INDEX(REE,1,2)/0.68
=INDEX(REE,1,3)/0.6
=INDEX(REE,1,4)/0.181
=INDEX(REE,1,5)/0.069
=INDEX(REE,1,6)/0.047
=INDEX(REE,1,7)/0.2
=INDEX(REE,1,8)/0.034
=SET.VALUE(INDEX(REEres
=SET.VALUE(INDEX(REEres
=SET.VALUE(INDEX(REEres
=SET.VALUE(INDEX(REEres
=SET.VALUE(INDEX(REEres
=SET.VALUE(INDEX(REEres
=SET.VALUE(INDEX(REEres
=SET.VALUE(INDEX(REEres
=RETURN(INDEX(REEres,1,
#N/A                  #N/ #N/ #N/ #N/ #N/ #N/ #N/

R_wt2CATwt
=RESULT(64)
=ARGUMENT("wt1",64)
=(INDEX(wt1,1,1)/60.09)*
=(INDEX(wt1,1,2)/79.9)*4
=((INDEX(wt1,1,3)/101.9
=(INDEX(wt1,1,4)/71.85)*
=((INDEX(wt1,1,5)/159.6
=(INDEX(wt1,1,6)/70.94)*
```

```
=(INDEX(wt1,1,7)/40.32)*
=(INDEX(wt1,1,8)/56.08)*
=((INDEX(wt1,1,9)/61.98)
=((INDEX(wt1,1,10)/94.2)
=((INDEX(wt1,1,11)/141.1
=SUM(B94:B104)
=(B94/$B$105)*100
=(B95/$B$105)*100
=(B96/$B$105)*100
=(B97/$B$105)*100
=(B98/$B$105)*100
=(B99/$B$105)*100
=(B100/$B$105)*100
=(B101/$B$105)*100
=(B102/$B$105)*100
=(B103/$B$105)*100
=(B104/$B$105)*100
=SET.VALUE(INDEX(catwtre
=SET.VALUE(INDEX(catwtre
=SET.VALUE(INDEX(catwtre
=SET.VALUE(INDEX(catwtre
=SET.VALUE(INDEX(catwtre
=SET.VALUE(INDEX(catwtre
=SET.VALUE(INDEX(catwtre
=SET.VALUE(INDEX(catwtre
=SET.VALUE(INDEX(catwtre
=SET.VALUE(INDEX(catwtre
=SET.VALUE(INDEX(catwtre
=RETURN(INDEX(catwtree,1
70.6347178644          0.1213.20   2.8:0.010.310.5:4.4:7.7:0.0(
```

```
C_Rone
=ARGUMENT("wt2",64)
=4*((INDEX(wt2,1,1)/60.C
=RETURN(M3)
C_Rtwo
=ARGUMENT("wt3",64)
=6*((INDEX(wt3,8,1)/56.C
=RETURN(M7)
```

```
R_Rone
=ARGUMENT("wt4",64)
=4*((INDEX(wt4,1,1)/60.C
=RETURN(N3)
R_Rtwo
=ARGUMENT("wt5",64)
=6*((INDEX(wt5,1,8)/56.C
=RETURN(N7)

R_O
=ARGUMENT("wt7",64)
=(((INDEX(wt7,1,1)/60.05
=RETURN(N12)
R_F
=ARGUMENT("wt8",64)
=((INDEX(wt8,1,10)/94.2)
=RETURN(N16)
```

```
R_Chon_Norm
=RESULT(64)
=ARGUMENT("ree",
=INDEX(REE,1,1)/C la
=INDEX(REE,1,2)/C ce
=INDEX(REE,1,3)/C pr
=INDEX(REE,1,4)/C nd
=INDEX(REE,1,5)/C sm
=INDEX(REE,1,6)/C eu
=INDEX(REE,1,7)/C gd
=INDEX(REE,1,8)/C tb
=INDEX(REE,1,9)/C dy
=SET.VALUE(INDEX
=SET.VALUE(INDEX
=SET.VALUE(INDEX
=SET.VALUE(INDEX
=SET.VALUE(INDEX
=SET.VALUE(INDEX
=SET.VALUE(INDEX
=SET.VALUE(INDEX
=RETURN(INDEX(R
```

```
viscosity
                                    calculated at 1(
=ARGUMENT("wt9",64)

=INDEX(wt9,1,1)/60.09               si
=INDEX(wt9,1,2)/79.9                ti
=(INDEX(wt9,1,3)/101.96)*2          al
=INDEX(wt9,1,4)/71.85               fe
=(INDEX(wt9,1,5)/159.69)*2          fe3+
=INDEX(wt9,1,6)/70.94               mn
=INDEX(wt9,1,7)/40.32               mg
=INDEX(wt9,1,8)/56.08               ca
=(INDEX(wt9,1,9)/61.98)*2           na
=(INDEX(wt9,1,10)/94.2)*2           k
=(INDEX(wt9,1,11)/141.95)*2         p
=SUM(O5:O15)
=O5/O16                             si
=O6/O16                             ti
=O7/O16                             al
=O8/O16                             fe
=O9/O16                             fe3+
=O10/O16                            mn
=O11/O16                            mg
=O12/O16                            ca
=O13/O16                            na
=O14/O16                            k
=O15/O16                            p
=O20+O21+O22+O23                    feT+mn+mg
=O26+O25                            k+na
=O17+O18+O19+O28+O24+(O29+
=O19*6.7*O17
=O28*3.4*O17
=(O24+O18)*4.5*O17
=O29*1.4*O17
=(O31+O32+O33+O34)
=O35/(1-O17)
=O36*(10000/(1200+273))-O36
=EXP(O37)
=RETURN(O38)
```

```
density
=ARGUMENT("wt9",64)

=INDEX(wt9,1,1)/60.09
=INDEX(wt9,1,2)/79.9
=(INDEX(wt9,1,3)/101.96)
=INDEX(wt9,1,4)/71.85
=(INDEX(wt9,1,5)/159.69)
=INDEX(wt9,1,6)/70.94
=INDEX(wt9,1,7)/40.32
=INDEX(wt9,1,8)/56.08
=(INDEX(wt9,1,9)/61.98)
=(INDEX(wt9,1,10)/94.2)
=(INDEX(wt9,1,11)/141.98)
=S5*27.03
=1200*0.00001
=S6*22.6*(1+temp*26.7)
=S7*36.63/2*(1+temp*14.7)
=S9*43.73/2*(1+temp*12.2)
=(S8+S10)*13.85*(1+temp*31
=S11*11.43*(1+temp*9.4)
=S12*16.32*(1+temp*36.4)
=S13*14.39*(1+temp*23.5)
=S13*22.965*(1+temp*24.9)
=100/(S16+S18+S19+S20+S21
=RETURN(S26)
```

```
Rwt2catprop
=RESULT(64)
=ARGUMENT("wt10",64)

=INDEX(wt10,1,1)/60.09
=INDEX(wt10,1,2)/79.9
=(INDEX(wt10,1,3)/101.96)"
=INDEX(wt10,1,4)/71.85
=(INDEX(wt10,1,5)/159.69)"
=INDEX(wt10,1,6)/70.94
=INDEX(wt10,1,7)/40.32
=INDEX(wt10,1,8)/56.08
=(INDEX(wt10,1,9)/61.98)"2
=(INDEX(wt10,1,10)/94.2)"2
=(INDEX(wt10,1,11)/141.95)
=SUM(U5:U15)
=U5/U16
=U6/U16
=U7/U16
=U8/U16
=U9/U16
=U10/U16
=U11/U16
=U12/U16
=U13/U16
=U14/U16
=U15/U16
=SET.VALUE(INDEX(catrest,1,1
=SET.VALUE(INDEX(catrest,1,2
=SET.VALUE(INDEX(catrest,1,3
=SET.VALUE(INDEX(catrest,1,4
=SET.VALUE(INDEX(catrest,1,5
=SET.VALUE(INDEX(catrest,1,6
=SET.VALUE(INDEX(catrest,1,7
=SET.VALUE(INDEX(catrest,1,8
=SET.VALUE(INDEX(catrest,1,9
=SET.VALUE(INDEX(catrest,1,
=SET.VALUE(INDEX(catrest,1,
=RETURN(INDEX(catrest,1,1))
0.672538726819371          0.003(0.183(0.01170      0      0.002(0.015(0.0685
```

APPENDIX III.V

Trace element models

-Explanation of spread sheets

- III.V.I SQSZ
- III.V.II Alkalic syenites
- III.V.III Alkalic granite to Quartz Syenite
- III.V.IV Aegirine granites

Example of trace element model.

Both pages of EXCELL spread sheet are shown. Variables are defined on bottom of first page and on the second page. References for trace element distribution coefficients are on top of second page. Geochemistry for parent and product are pasted from corresponding geochemical spread sheet. These analyses extend off page two but are not shown.

Kd*	heden	emph	fay	tiMt.2s	plg	san	apt	Zir	Tit
U	0.09	0.45	0.14	0.29	0.04	0.07	0	300	1
Th	1.6	0.11	0.49	0.39	3E-04	0.05	0	62	1
Zr	0	0.5	0.66	1.8	0.008	0.07	0	1500	1
Hf	0.95	0.84	0.09	2.51	0.03	0.08	0	1000	1
Ta	0.47	1.02	0.14	2.55	0.03	0.05	0	40	70
La	0.66	0.85	0.4	0.87	0.23	0.24	12	0.8	10
Eu	0.87	3.2	0	0.4	2	1.13	2	2.5	30
Tb	3	3.67	0.52	1.72	0.06	0.09	21	15	40
Co	5.3	16.7	14.6	41.7	0.08	0.29	0	9	1
Sc	30	5.3	0.5	2.5	0	0.1	0	60	1
Rb	0.03	0.08	0.007	0	0.02	0.42	0	0	1
Sr	0.04	0.3	0	0.04	5.2	2.9	2	0	1
Ba	0.1	0.8	0.05	0.1	1.4	6	1	0	1

	SAMPLE #	REF.	SiO2	TiO2	Al2O3	FeO	Fe2O3	MnO	MgO	CaO
parent	MAG-91-1	Perlit(L	60.18	0.82	14.78	0	9.59	0.24	0.43	2.89
product	MAG-51D	Perlit(L	62.86	0.61	15.26	0	7.8	0.19	0.33	1.21

	cpx	amph	oiv	tiMt.2s	plg	ksp	apt	zir	tit
least squares input	0.055	0	0.0847	0.011	0.1605	0.291	0	4E-04	0
% cummulate	0.091	0	0.14056	0.018	0.2663	0.483	0	5E-04	0

	D	f	Co	Cl	Cr	san	Cs-inst	Cs-avg	um com	oxides
U	0.228	0.398	3.99	8.13	5.90	3.1145	1.85	1.25	41.20	sio2
Th	0.277		13.11	25.51	18.92	13.33	7.07	4.91	1.10	tio2
Zr	0.912		271	294.01	283.44	268	268	255.8	8.89	al2o3
Hf	0.692		9.58	12.73	11.20	10.712	8.80	7.50	12.46	fe2o3
Ta	0.161		4.85	10.50	7.42	7.944	1.69	1.11	0.59	mno
La	0.310		47.088	88.93	66.84	59.116	27.56	19.43	0.57	mgo
Eu	1.166		4.6968	4.03	4.32	2.63	4.70	5.14	1.94	cao
Tb	0.445		1.3978	2.33	1.85	1.5918	1.04	0.78	3.22	na2o
Co	3.463		1.26	0.13	0.36	1199	0.45	2.01	3.40	k20
Sc	2.932		13.14	2.22	4.93	3.877	6.50	20.36	0.00	p205
Rb	0.212		105	217.04	156.64	134	45.98	30.93		
Sr	2.790		138	26.53	55.64	87.9	74.02	211.70		
Ba	3.288		2439	296.22	783.6	552	974.08	3856		

	D*(I)	D**(r)	D*(I)/D	D**(r)/D	Co/Cl	San/Cl	San/Cr
U	1.27	1.49	5.57	6.54	1.28	0.38	0.53
Th	0.98	0.97	3.54	3.49	0.98	0.52	0.70
Zr	1.01	1.02	1.11	1.12	1.01	0.91	0.95
Hf	0.88	0.78	1.27	1.13	0.89	0.84	0.93
Ta	0.46	0.03	2.88	0.17	0.61	0.76	1.07
La	0.75	0.55	2.43	1.78	0.80	0.66	0.88
Eu	1.83	2.14	1.40	1.64	1.79	0.65	0.61
Tb	0.86	0.74	1.93	1.67	0.88	0.68	0.86
Co	-6.44	-12.51	-1.86	-3.61	0.00	####	####
Sc	2.32	3.41	0.79	1.16	3.39	1.75	0.79
Rb	0.74	0.52	3.47	2.45	0.78	0.62	0.86
Sr	1.49	1.89	0.53	0.68	1.57	3.31	1.58
Ba	2.61	3.93	0.79	1.19	4.42	1.86	0.72

D*(I) and D**(r)- back calculated D from Cl and Cr f*=f for perfectly incompatible elements

Kd*-source for Kd by print style-((Lemarchard et al., 1987, *(Nelson,1987)*) Apt(Watson and Green ,1981))

	sio2	heden	amb	fay	ti-mag	pig	ksp	apt	zir
	tio2	48.27	0	30.56	0.02	0	67.27	0	32.5
	al2o3	0.37	0	0.72	53.03	0	0	0	0
	fe2o3	0.2	0	0.09	0	0	18.35	0	0.21
	mno	28.54	0	60.9	46.82	0	0.92	0.2	0.08
	mgo	0.91	0	3.43	1.6	0	0	1.52	0
	cao	0.92	0	3.47	0	0	0	0.54	0
	na2o	18.7	0	1.13	0.32	0	0.15	52.4	0.01
	k20	1.19	0	0	0	0	6.45	0	*0.2*
	p205	0	0	0	0	0	7.05	0	0
		0	0	0	0	0	0	45.34	0

compositions of cumulate minerals

Na2O	K2O	P2O5	LOI	CO2	SUM	Rb	*Cs*	Sr	Ba	*Sc*	Y	Zr	*Hf*	V
5.87	4.64	0.22	0.15		99.66	105	2.77	138	2439	13.14	33.3	271	9.58	11.9
6.34	5.24	0.09	0.3		99.47	154	2.109	28.7	192	2.793	43.1	397	10.34	9.29

etc.

Cl=Co*(f^(D-1))=liquid composition for Rayleigh fractional crystallization
Cr=Co((1-f)^(D-1))=residue of Rayleigh fractional crystallization

Cs-inst=D*Cl=instantaneous solid
Cs-avg=Co((1-f^D)/(1-f))=mean concentration in cummulate

where D=bulk distribution coefficient
f= proportion of liquid
Cl and Cr from Cox, Bell and Pankhurst (1979)
Cs and Cr from Allegre and Minster (1978)

APPENDIX III.V.I

SQSZ

Mix'n'Mac file : 91-1 to 51-d m'n'm
Date: 04-05-1990 Time: 08:20:31

	Parent	Daughter	Phases					
	mag 51-d	mag91-1	cpx	olig	fayalite	ksp	ilm	apt
Variables								
SiO2	60.18	62.90	48.80	64.10	30.56	67.50	0.51	0.00
TiO2	0.82	0.61	0.70	0.00	0.72	0.00	50.02	0.00
Al2O3	14.74	15.28	1.26	22.66	0.09	16.22	0.00	0.00
Fe2O3	9.59	7.80	20.09	0.20	54.07	0.60	46.00	0.21
MnO	0.24	0.19	0.61	0.00	3.43	0.00	1.44	1.52
MgO	0.43	0.33	4.55	0.25	3.47	0.00	0.46	0.54
CaO	2.89	1.21	19.24	3.26	1.13	0.00	0.71	52.40
Na2O	5.87	6.64	1.58	9.89	0.00	5.00	0.00	0.00
K2O	4.64	4.91	0.00	0.00	0.00	8.00	0.00	0.00
P2O5	0.22	0.12	0.00	0.00	0.00	0.00	0.00	45.33

Oxides recalculated to 100%

RESULTS:

	Parent observed	Parent estimated	Residuals
SiO2	60.41	60.50	-0.0909
TiO2	0.82	0.89	-0.0712
Al2O3	14.80	14.61	0.1841
Fe2O3	9.63	9.54	0.0857
MnO	0.24	0.45	-0.2051
MgO	0.43	0.74	-0.3130
CaO	2.90	2.68	0.2203
Na2O	5.89	5.74	0.1539
K2O	4.66	4.30	0.3560
P2O5	0.22	0.46	-0.2441
			0.4532 = sum of squared residuals

Component	Proportion
mag 51-d	0.3403
cpx	0.0549
olig	0.1771
fayalite	0.0861
ksp	0.3200
ilm	0.0115
apt	0.0094

model 1

Kd*	hoden	amph	fay	tiMt.29	plg	san	apt	Zir	Tit
U	0.09	0.45	0.14	0.29	0.04	0.07	0	300	1
Th	*1.6*	*0.11*	*0.49*	*0.39*	*3E-04*	*0.05*	0	62	1
Zr	*0*	*0.5*	*0.66*	*1.8*	*0.008*	*0.07*	0	1500	1
Hf	0.95	0.84	0.09	2.51	0.03	0.08	0	1000	1
Ta	0.47	1.02	0.14	2.55	0.03	0.05	0	40	70
La	0.66	0.85	0.4	0.87	0.23	0.24	12	0.8	10
Eu	*0.87*	*3.2*	*0*	*0.4*	*2*	*1.13*	2	2.5	30
Tb	3	3.67	0.52	1.72	0.06	0.09	21	15	40
Co	5.3	16.7	14.6	41.7	0.08	0.29	0	9	1
Sc	*30*	*5.3*	*0.5*	*2.5*	*0*	*0.1*	0	60	1
Rb	*0.03*	*0.08*	*0.007*	*0*	*0.02*	*0.42*	0	0	1
Sr	*0.04*	*0.3*	*0*	*0.04*	*5.2*	*2.9*	2	0	1
Ba	0.1	0.8	0.05	0.1	1.4	6	1	0	1

	SAMPLE #	REF.	SIO2	TIO2	Al2O3	FeO	Fe2O3	MnO	MgO	CaO
parent	MAG-91-1	Perfit(L	60.18	0.82	14.78	0	9.59	0.24	0.43	2.89
product	MAG-51D	Perfit(L	62.86	0.61	15.28	0	7.8	0.19	0.33	1.21

	cpx	amph	olv	tiMt.29	plg	ksp	apt	zir	tit
least squares input	0.055	0	0.0847	0.011	0.1605	0.291	0	4E-04	0
% cummulate	0.091	0	0.14056	0.018	0.2663	0.483	0	5E-04	0

	D	f	Co	Cl	Cr	son	Cs-inst	Cs-avg	um com	oxides
U	0.228	0.398	3.99	8.13	5.90	3.1145	1.85	1.25	41.20	sio2
Th	0.277		13.11	25.51	18.92	*13.33*	7.07	4.91	1.10	tio2
Zr	0.912		271	294.01	283.44	*268*	268	255.8	8.89	al2o3
Hf	0.692		9.58	12.73	11.20	10.712	8.80	7.50	12.46	fe2o3
Ta	0.161		4.85	10.50	7.42	7.944	1.69	1.11	0.59	mno
La	0.310		47.088	88.93	66.84	59.116	27.56	19.43	0.57	mgo
Eu	1.166		4.6968	4.03	4.32	*2.63*	4.70	5.14	1.94	cao
Tb	0.445		1.3978	2.33	1.85	1.5918	1.04	0.78	3.22	na2o
Co	3.463		1.26	0.13	0.36	1199	0.45	2.01	3.40	k20
Sc	2.932		13.14	2.22	4.93	*3.877*	6.50	20.36	0.00	p205
Rb	0.212		105	217.04	156.64	*134*	45.98	30.93		
Sr	2.790		138	26.53	55.64	*87.9*	74.02	211.70		
Ba	3.288		2439	296.22	763.6	*552*	974.08	3856		

	D*(I)	D**(r	D*(I)/D	D**(r)/D	%Ce/C	Son/Cl	Son/Cr
U	1.27	1.49	5.57	6.54	1.28	0.38	0.53
Th	0.98	0.97	3.54	3.49	0.98	0.52	0.70
Zr	1.01	1.02	1.11	1.12	1.01	0.91	0.95
Hf	0.88	0.78	1.27	1.13	0.89	0.84	0.96
Ta	0.46	0.03	2.88	0.17	0.61	0.76	1.07
La	0.75	0.55	2.43	1.78	0.80	0.66	0.88
Eu	1.63	2.14	1.40	1.84	1.79	0.65	0.61
Tb	0.86	0.74	1.93	1.67	0.88	0.68	0.86
Co	-6.44	-12.51	-1.86	-3.61	0.00	####	####
Sc	2.32	3.41	0.79	1.16	3.39	1.75	0.79
Rb	0.74	0.52	3.47	2.45	0.78	0.82	0.86
Sr	1.49	1.89	0.53	0.68	1.57	3.31	1.58
Ba	2.61	3.93	0.79	1.19	4.42	1.86	0.72

D*(I) and D**(r)- back calculated D from Cl and Cr f*=f for perfectly incompatible elements

Mix'n'Mac file : 91-1 TO 91-2
Date: 04-05-1990 Time: 08:24:21

	Parent	Daughter	Phases					
	mag91-2	mag91-cpx	olig	fayalite	ksp	ilm	apt	
Variables								
SiO2	60.18	63.30	48.80	64.10	30.56	67.50	0.51	0.00
TiO2	0.82	0.56	0.70	0.00	0.72	0.00	50.02	0.00
Al2O3	14.74	14.50	1.26	22.66	0.09	16.22	0.00	0.00
Fe2O3	9.59	7.52	20.09	0.20	54.07	0.60	46.00	0.21
MnO	0.24	0.18	0.61	0.00	3.43	0.00	1.44	1.52
MgO	0.43	0.10	4.55	0.25	3.47	0.00	0.46	0.54
CaO	2.89	1.05	19.24	3.26	1.13	0.00	0.71	52.40
Na2O	5.87	6.29	1.58	9.89	0.00	5.00	0.00	0.00
K2O	4.64	5.36	0.00	0.00	0.00	8.00	0.00	0.00
P2O5	0.22	0.04	0.00	0.00	0.00	0.00	0.00	45.33

Oxides recalculated to 100%

RESULTS:

	Parent observed	Parent estimated	Residuals
SiO2	60.41	60.51	-0.1014
TiO2	0.82	0.90	-0.0749
Al2O3	14.80	14.59	0.2069
Fe2O3	9.63	9.54	0.0890
MnO	0.24	0.46	-0.2226
MgO	0.43	0.68	-0.2498
CaO	2.90	2.67	0.2296
Na2O	5.89	5.71	0.1783
K2O	4.66	4.26	0.4020
P2O5	0.22	0.48	-0.2551
			0.4898 = sum of squared residuals

Component	Proportion
mag91-2	0.2940
cpx	0.0508
olig	0.2128
fayalite	0.0939
ksp	0.3239
ilm	0.0123
apt	0.0102

model 1

Kd*	heden	amph	fay	tiMt.28	plg	san	apt	Zir	Tit
U	0.09	0.45	0.14	0.29	0.04	0.07	0	300	1
Th	1.6	0.11	0.49	0.39	3E-04	0.05	0	62	1
Zr	0	0.5	0.66	1.8	0.008	0.07	0	1500	1
Hf	0.95	0.84	0.09	2.51	0.03	0.08	0	1000	1
Ta	0.47	1.02	0.14	2.55	0.03	0.05	0	40	70
La	0.66	0.85	0.4	0.87	0.23	0.24	12	0.8	10
Eu	0.87	3.2	0	0.4	2	1.13	2	2.5	30
Tb	3	3.67	0.52	1.72	0.06	0.09	21	15	40
Co	5.3	16.7	14.6	41.7	0.08	0.29	0	9	1
Sc	30	5.3	0.5	2.5	0	0.1	0	60	1
Rb	0.03	0.08	0.007	0	0.02	0.42	0	0	1
Sr	0.04	0.3	0	0.04	5.2	2.9	2	0	1
Ba	0.1	0.8	0.05	0.1	1.4	6	1	0	1

	SAMPLE #	REF.	SiO2	TiO2	Al2O3	FeO	Fe2O3	MnO	MgO	CaO
parent	MAG-91-1	Perlit(L	60.18	0.82	14.78	0	9.59	0.24	0.43	2.89
product	MAG- 91-2	Perlit(L	63.25	0.56	14.5	0	7.52	0.18	0.1	1.05

	cpx	amph	olv	tiMt.28	plg	ksp	apt	zir	tit
least squares input	0.051	0	0.0938	0.012	0.2127	0.324	0	0	0
% cummulate	0.074	0	0.13526	0.017	0.3067	0.467	0	0	0

	D	f	Co	Cl	Cr	son	Cs-inst	Cs-avg	um com	oxides
U	0.076	0.295	3.99	12.33	5.51	5.46	0.93	0.50	39.11	sio2
Th	0.214		13.11	34.22	17.25	25.97	7.33	4.28	1.04	tio2
Zr	0.156		271	759.74	364.05	430	118.2	66.49	8.60	al2o3
Hf	0.172		9.58	26.32	12.80	16.588	4.53	2.57	11.58	fe2o3
Ta	0.130		4.85	14.02	6.57	7.0723	1.83	1.01	0.56	mno
La	0.300		47.088	110.62	60.13	69.977	33.23	20.50	0.54	mgo
Eu	1.212		4.6968	3.62	4.36	1.66	4.39	5.15	1.60	cao
Tb	0.361		1.3978	2.98	1.74	2.3265	1.13	0.74	3.10	na2o
Co	3.246		1.26	0.08	0.57	0.4358	0.26	1.75	3.29	k20
Sc	2.364		13.14	2.49	8.16	1	5.88	17.60	0.00	p205
Rb	0.206		105	276.96	138.61	198	56.92	33.05		
Sr	2.953		138	12.71	69.72	25.9	37.55	190.43		
Ba	3.249		2439	156.73	1111	67.2	509.13	3394		

	D*(I)	D**(r)	D*(I)/D	D**(r)/I	f*=Co/C	Son/Cl	Son/Cr
U	0.74	0.10	9.84	1.36	0.73	0.44	0.99
Th	0.44	-0.96	2.08	-4.46	0.50	0.76	1.51
Zr	0.62	-0.32	4.00	-2.06	0.63	0.57	1.18
Hf	0.55	-0.57	3.20	-3.32	0.58	0.63	1.30
Ta	0.69	-0.08	5.31	-0.61	0.69	0.50	1.08
La	0.68	-0.13	2.25	-0.44	0.67	0.63	1.16
Eu	1.85	3.98	1.53	3.28	2.83	0.46	0.38
Tb	0.58	-0.46	1.53	-1.20	0.60	0.78	1.34
Co	1.87	4.04	0.58	1.24	2.89	5.37	0.76
Sc	3.11	8.37	1.32	3.54	13.14	0.40	0.12
Rb	0.48	-0.81	2.34	-3.96	0.53	0.71	1.43
Sr	2.37	5.79	0.80	1.96	5.33	2.04	0.37
Ba	3.94	11.27	1.21	3.47	36.29	0.43	0.06

D*(I) and D**(r)- back calculated D from Cl and Cr f*=1 for perfectly incompatible elements

Mix'n'Mac file : 91-1 to 139 m'n'm
Date: 04-05-1990 Time: 08:22:17

	Parent	Daughter	Phases					
	mag 139	mag91-cpx	olig	fayalite	ksp	ilm	phase 6	
Variables								
SiO2	60.18	62.11	48.80	64.10	30.56	67.50	0.51	0.00
TiO2	0.82	0.54	0.70	0.00	0.72	0.00	50.02	0.00
Al2O3	14.74	14.58	1.26	22.66	0.09	16.22	0.00	0.00
Fe2O3	9.59	8.00	20.09	0.20	54.07	0.60	46.00	0.00
MnO	0.24	0.22	0.61	0.00	3.43	0.00	1.44	0.00
MgO	0.43	0.13	4.55	0.25	3.47	0.00	0.46	0.00
CaO	2.89	1.46	19.24	3.26	1.13	0.00	0.71	0.00
Na2O	5.87	6.34	1.58	9.90	0.00	5.00	0.00	0.00
K2O	4.64	5.24	0.00	0.00	0.00	8.00	0.00	0.00
P2O5	0.22	0.09	0.00	0.00	0.00	0.00	0.00	0.00

Oxides recalculated to 100%

RESULTS:

	Parent observed	Parent estimated	Residuals	
SiO2	60.41	60.54	-0.1281	
TiO2	0.82	0.91	-0.0845	
Al2O3	14.80	14.49	0.3098	
Fe2O3	9.63	9.53	0.0966	
MnO	0.24	0.41	-0.1733	
MgO	0.43	0.69	-0.2580	
CaO	2.90	2.62	0.2792	
Na2O	5.89	5.83	0.0625	
K2O	4.66	4.22	0.4420	
P2O5	0.22	0.04	0.1850	
			0.5368	= sum of squared residuals

Component	Proportion
mag 139	0.3934
cpx	0.0669
olig	0.1891
fayalite	0.0729
ksp	0.2588
ilm	0.0116

model 1

Kd*	heden	amph	fay	tiMt.29	pig	san	apt	Zir	Tit
U	0.09	0.45	0.14	0.29	0.04	0.07	0	300	1
Th	*1.6*	*0.11*	*0.49*	*0.39*	*3E-04*	*0.05*	0	62	1
Zr	*0*	*0.5*	*0.66*	*1.8*	*0.008*	*0.07*	0	1500	1
Hf	0.95	0.84	0.09	2.51	0.03	0.08	0	1000	1
Ta	0.47	1.02	0.14	2.55	0.03	0.05	0	40	70
La	0.66	0.85	0.4	0.87	0.23	0.24	12	0.8	10
Eu	*0.87*	*3.2*	*0*	*0.4*	*2*	*1.13*	2	2.5	30
Tb	3	3.67	0.52	1.72	0.06	0.09	21	15	40
Co	5.3	16.7	14.6	41.7	0.08	0.29	0	9	1
Sc	*30*	*5.3*	*0.5*	*2.5*	*0*	*0.1*	0	60	1
Rb	*0.03*	*0.08*	*0.007*	*0*	*0.02*	*0.42*	0	0	1
Sr	*0.04*	*0.3*	*0*	*0.04*	*5.2*	*2.9*	2	0	1
Ba	0.1	0.8	0.05	0.1	1.4	6	1	0	1

	SAMPLE #	REF.	SiO2	TiO2	Al2O3	FeO	Fe2O3	MnO	MgO	CaO
parent	MAG-91-1	Perfit(L	60.18	0.82	14.78	0	9.59	0.24	0.43	2.89
product	MAG-139	Perfit(L	62.11	0.54	14.58	0	8.76	0.22	0.13	1.46

	cpx	amph	olv	tiMt.29	pig	ksp	apt	zir	tit
least squares input	0.068	0	0.075	0.012	0.1929	0.271	0	0	0
% cummulate	0.11	0	0.12118	0.019	0.3117	0.438	0	0	0

	D	f	Co	Cl	Cr	son	Cs-inst	Cs-avg	um com	oxides
U	0.076	0.374	3.99	9.90	6.15	2.6348	0.75	0.46	38.46	sio2
Th	0.265		13.11	27.02	18.50	*10.77*	7.15	4.80	1.16	tio2
Zr	0.148		271	626.43	403.91	*397*	92.73	58.65	8.07	al2o3
Hf	0.206		9.58	20.87	13.86	10.34	4.35	2.84	11.83	fe2o3
Ta	0.149		4.85	11.20	7.22	4.9621	1.67	1.06	0.55	mno
La	0.315		47.088	92.39	64.91	63.971	29.07	20.02	0.52	mgo
Eu	1.222		4.6968	3.78	4.23	*2.282*	4.61	5.25	2.26	cao
Tb	0.484		1.3978	2.32	1.78	1.521	1.12	0.85	2.96	na2o
Co	3.312		1.26	0.13	0.43	0.7033	0.43	1.94	3.09	k20
Sc	3.449		13.14	1.18	4.17	*2.793*	4.08	20.28	0.00	p205
Rb	0.194		105	231.92	153.14	*154*	45.06	29.17		
Sr	2.896		138	21.39	56.79	*28.7*	61.93	207.67		
Ba	3.083		2439	314.54	919.5	*192*	969.61	3708		

	D*(I)	D**(r)	D*(I)/D	D**(r)/I	I*=Co/C	Son/Cl	Son/Cr
U	1.42	1.89	18.81	24.95	1.51	0.27	0.43
Th	1.20	1.42	4.53	5.36	1.22	0.40	0.58
Zr	0.61	0.18	4.13	1.25	0.68	0.63	0.98
Hf	0.92	0.84	4.43	4.02	0.93	0.50	0.74
Ta	0.98	0.95	6.54	6.37	0.98	0.44	0.69
La	0.69	0.35	2.19	1.10	0.74	0.69	0.99
Eu	1.73	2.54	1.42	2.08	2.06	0.60	0.54
Tb	0.91	0.82	1.89	1.69	0.92	0.66	0.85
Co	1.59	2.24	0.48	0.68	1.79	5.42	1.65
Sc	2.57	4.31	0.75	1.25	4.70	2.36	0.67
Rb	0.61	0.18	3.14	0.94	0.68	0.66	1.01
Sr	2.60	4.35	0.90	1.50	4.81	1.34	0.51
Ba	3.58	6.43	1.16	2.08	12.70	0.61	0.21

D*(I) and D**(r)- back calculated D from Cl and Cr I*=I for perfectly incompatible elements

model 2

Kd*	heden	amph	fay	tiMt.28	pig	san	apt	Zir	Tit
U	0.09	0.45	0.14	0.29	0.04	0.07	0	300	1
Th	*1.6*	*0.11*	*0.49*	*0.39*	*3E-04*	*0.05*	0	62	1
Zr	*0*	*0.5*	*0.66*	*1.8*	*0.008*	*0.07*	0	1500	1
Hf	0.95	0.84	0.09	2.51	0.03	0.08	0	1000	1
Ta	0.47	1.02	0.14	2.55	0.03	0.05	0	40	70
La	0.66	0.85	0.4	0.87	0.23	0.24	12	0.8	10
Eu	*0.87*	*3.2*	*0*	*0.4*	*2*	*1.13*	2	2.5	30
Tb	3	3.67	0.52	1.72	0.06	0.09	21	15	40
Co	5.3	16.7	14.6	41.7	0.08	0.29	0	9	1
Sc	*30*	*5.3*	*0.5*	*2.5*	*0*	*0.1*	0	60	1
Rb	*0.03*	*0.08*	*0.007*	*0*	*0.02*	*0.9*	0	0	1
Sr	*0.04*	*0.3*	*0*	*0.04*	*5.2*	*2*	2	0	1
Ba	0.1	0.8	0.05	0.1	1.4	7.5	1	0	1

	SAMPLE #	REF.	SiO2	TiO2	Al2O3	FeO	Fe2O3	MnO	MgO	CaO
parent	MAG-91-1	Perlit(L	60.18	0.82	14.78	0	9.59	0.24	0.43	2.89
product	MAG- 91-2	Perlit(L	63.25	0.56	14.5	0	7.52	0.18	0.1	1.05

	cpx	amph	olv	tiMt.28	pig	ksp	apt	zir	tit
least squares input	0.051	0	0.0938	0.012	0.2127	0.324	0	0	0
% cummulate	0.074	0	0.13526	0.017	0.3067	0.467	0	0	0

	D	f	Co	Cl	Cr	son	Cs-inst	Cs-avg	um com	oxides
U	0.076	0.295	3.99	12.33	5.51	5.46	0.93	0.50	39.11	sio2
Th	0.214		13.11	34.22	17.25	*25.97*	7.33	4.28	1.04	tio2
Zr	0.156		271	759.74	364.05	*430*	118.2	66.49	8.60	al2o3
Hf	0.172		9.58	26.32	12.80	16.588	4.53	2.57	11.58	fe2o3
Ta	0.130		4.85	14.02	6.57	7.0723	1.83	1.01	0.56	mno
La	0.300		47.088	110.62	60.13	69.977	33.23	20.50	0.54	mgo
Eu	1.212		4.6968	3.62	4.36	*1.66*	4.39	5.15	1.60	cao
Tb	0.381		1.3978	2.98	1.74	2.3265	1.13	0.74	3.10	na2o
Co	3.246		1.26	0.08	0.57	0.4358	0.26	1.75	3.29	k20
Sc	2.364		13.14	2.49	8.16	*1*	5.88	17.60	0.00	p205
Rb	0.430		105	210.63	128.16	*198*	90.52	60.80		
Sr	2.533		138	21.24	80.76	*25.9*	53.80	186.86		
Ba	3.949		2439	66.62	869.9	*67.2*	263.10	3432		

	D*(l)	D**(r	D*(l)/D	D**(r)/D	f*=Co/C	Son/Cl	Son/Cr
U	0.74	0.10	9.84	1.38	0.73	0.44	0.99
Th	0.44	-0.98	2.06	-4.46	0.50	0.76	1.51
Zr	0.62	-0.32	4.00	-2.06	0.63	0.57	1.18
Hf	0.55	-0.57	3.20	-3.32	0.58	0.63	1.30
Ta	0.69	-0.08	5.31	-0.61	0.69	0.50	1.08
La	0.68	-0.13	2.25	-0.44	0.67	0.63	1.16
Eu	1.85	3.98	1.53	3.28	2.83	0.46	0.38
Tb	0.58	-0.46	1.53	-1.20	0.60	0.78	1.34
Co	1.87	4.04	0.58	1.24	2.89	5.37	0.76
Sc	3.11	8.37	1.32	3.54	13.14	0.40	0.12
Rb	0.48	-0.81	1.12	-1.90	0.53	0.94	1.54
Sr	2.37	5.79	0.94	2.28	5.33	1.22	0.32
Ba	3.94	11.27	1.00	2.85	36.29	1.01	0.08

D*(l) and D**(r)- back calculated D from Cl and Cr f*=l for perfectly incompatible elements

model 2

Kd*	heden	amph	fay	tiMt.29	plg	san	apt	Zir	Tit
U	0.09	0.45	0.14	0.29	0.04	0.07	0	300	1
Th	1.6	0.11	0.49	0.39	3E-04	0.05	0	62	1
Zr	0	0.5	0.66	1.8	0.008	0.07	0	1500	1
Hf	0.95	0.84	0.09	2.51	0.03	0.08	0	1000	1
Ta	0.47	1.02	0.14	2.55	0.03	0.05	0	40	70
La	0.66	0.85	0.4	0.87	0.23	0.24	12	0.8	10
Eu	0.87	3.2	0	0.4	2	1.13	2	2.5	30
Tb	3	3.67	0.52	1.72	0.06	0.09	21	15	40
Co	5.3	16.7	14.6	41.7	0.08	0.29	0	9	1
Sc	30	5.3	0.5	2.5	0	0.1	0	60	1
Rb	0.03	0.08	0.007	0	0.02	0.9	0	0	1
Sr	0.04	0.3	0	0.04	5.2	2	2	0	1
Ba	0.1	0.8	0.05	0.1	1.4	7.5	1	0	1

	SAMPLE #	REF.	SiO2	TiO2	Al2O3	FeO	Fe2O3	MnO	MgO	CaO
parent	MAG-91-1	Perfit(L	60.18	0.82	14.78	0	9.59	0.24	0.43	2.89
product	MAG-51D	Perfit(L	62.86	0.61	15.28	0	7.8	0.19	0.33	1.21

	cpx	amph	oiv	tiMt.29	plg	ksp	apt	zir	tit
least squares input	0.055	0	0.0847	0.011	0.1605	0.291	0	0.0004	0
% cummulate	0.091	0	0.140558	0.01825	0.2663	0.483	0	0.0007	0

	D	f	Co	Cl	Cr	son	Cs-inst	Cs-avg	cum com	oxides
U	0.277	0.398	3.99	7.77	5.76	3.1145	2.15	1.49	41.21	sio2
Th	0.287		13.11	25.28	18.82	13.33	7.26	5.07	1.10	tio2
Zr	1.157		271	234.45	250.21	268	271.3	295.2	8.89	al2o3
Hf	0.858		9.58	10.94	10.31	10.712	9.36	8.68	12.46	fe2o3
Ta	0.168		4.85	10.44	7.40	7.944	1.75	1.15	0.59	mno
La	0.310		47.088	88.92	66.83	59.116	27.57	19.43	0.57	mgo
Eu	1.167		4.6968	4.03	4.32	2.63	4.70	5.14	1.94	cao
Tb	0.448		1.3978	2.33	1.85	1.5918	1.04	0.78	3.22	na2o
Co	3.464		1.26	0.13	0.36	1199	0.45	2.01	3.40	k20
Sc	2.942		13.14	2.20	4.90	3.877	6.46	20.38	0.00	p205
Rb	0.444		105	175.30	139.25	134	77.78	58.52		
Sr	2.355		138	39.60	69.37	87.9	93.25	203.06		
Ba	4.013		2439	151.98	528.699	552	609.85	3951		

	D*(l)	D**(r	D*(l)/D	D**(r)/D	f*=Co/Cl	Son/Cl	Son/Cr
U	1.27	1.49	4.58	5.38	1.28	0.40	0.54
Th	0.98	0.97	3.42	3.36	0.98	0.53	0.71
Zr	1.01	1.02	0.87	0.88	1.01	1.14	1.07
Hf	0.88	0.78	1.03	0.91	0.89	0.98	1.04
Ta	0.46	0.03	2.77	0.17	0.61	0.76	1.07
La	0.75	0.55	2.43	1.78	0.80	0.66	0.88
Eu	1.63	2.14	1.40	1.84	1.79	0.65	0.61
Tb	0.86	0.74	1.92	1.66	0.88	0.68	0.86
Co	-6.44	-12.51	-1.86	-3.61	0.00	#####	#####
Sc	2.32	3.41	0.79	1.16	3.39	1.77	0.79
Rb	0.74	0.52	1.66	1.17	0.78	0.76	0.96
Sr	1.49	1.89	0.63	0.80	1.57	2.22	1.27
Ba	2.61	3.93	0.65	0.98	4.42	3.63	1.04

D*(l) and D**(r)- back calculated D from Cl and Cr f*=l for perfectly incompatible elements

model 2

Kd*	heden	amph	fay	tiMt.2s	pig	san	apt	Zir	Tit
U	0.09	0.45	0.14	0.29	0.04	0.07	0	300	1
Th	*1.6*	*0.11*	*0.49*	*0.39*	*3E-04*	*0.05*	0	62	1
Zr	*0*	*0.5*	*0.66*	*1.8*	*0.008*	*0.07*	0	1500	1
Hf	0.95	0.84	0.09	2.51	0.03	0.08	0	1000	1
Ta	0.47	1.02	0.14	2.55	0.03	0.05	0	40	70
La	0.66	0.85	0.4	0.87	0.23	0.24	12	0.8	10
Eu	*0.87*	*3.2*	*0*	*0.4*	*2*	*1.13*	2	2.5	30
Tb	3	3.67	0.52	1.72	0.06	0.09	21	15	40
Co	5.3	16.7	14.6	41.7	0.08	0.29	0	9	1
Sc	*30*	*5.3*	*0.5*	*2.5*	*0*	*0.1*	0	60	1
Rb	*0.03*	*0.08*	*0.007*	*0*	*0.02*	*0.9*	0	0	1
Sr	*0.04*	*0.3*	*0*	*0.04*	*5.2*	*2*	2	0	1
Ba	0.1	0.8	0.05	0.1	1.4	7.5	1	0	1

	SAMPLE #	REF.	SIO2	TIO2	Al2O3	FeO	Fe2O3	MnO	MgO	CaO
parent	MAG-91-1	Perlit(L	60.18	0.82	14.78	0	9.59	0.24	0.43	2.89
product	MAG-139	Perlit(L	62.11	0.54	14.58	0	8.76	0.22	0.13	1.46

	cpx	amph	olv	tiMt.2s	pig	kap	apt	zir	tit
least squares input	0.068	0	0.075	0.012	0.1929	0.271	0	0	0
% cummulate	0.11	0	0.12118	0.019	0.3117	0.438	0	0	0

	D	f	Co	Cl	Cr	san	Cs-inst	Cs-avg	um com	oxides
U	0.076	0.374	3.99	9.90	6.15	2.6348	0.75	0.46	38.46	sio2
Th	0.265		13.11	27.02	18.50	*10.77*	7.15	4.80	1.16	tio2
Zr	0.148		271	626.43	403.91	*397*	92.73	58.65	8.07	al2o3
Hf	0.208		9.58	20.87	13.88	10.34	4.35	2.84	11.83	fe2o3
Ta	0.149		4.85	11.20	7.22	4.9621	1.67	1.06	0.55	mno
La	0.315		47.088	92.39	64.91	63.971	29.07	20.02	0.52	mgo
Eu	1.222		4.6968	3.78	4.23	*2.282*	4.61	5.25	2.26	cao
Tb	0.484		1.3978	2.32	1.78	1.521	1.12	0.85	2.96	na2o
Co	3.312		1.26	0.13	0.43	0.7033	0.43	1.94	3.09	k20
Sc	3.449		13.14	1.18	4.17	*2.793*	4.08	20.28	0.00	p205
Rb	0.404		105	188.61	138.78	*154*	76.29	55.05		
Sr	2.502		138	31.51	68.30	*28.7*	78.83	201.62		
Ba	3.739		2439	164.87	676	*192*	616.51	3798		

	D*(l)	D**(r	D*(l)/D	D**(r)/	f*=Co/C	San/Cl	San/Cr
U	1.42	1.89	18.81	24.95	1.51	0.27	0.43
Th	1.20	1.42	4.53	5.36	1.22	0.40	0.58
Zr	0.61	0.18	4.13	1.25	0.68	0.63	0.98
Hf	0.92	0.84	4.43	4.02	0.93	0.50	0.74
Ta	0.98	0.95	6.54	6.37	0.98	0.44	0.69
La	0.69	0.35	2.19	1.10	0.74	0.69	0.99
Eu	1.73	2.54	1.42	2.08	2.06	0.60	0.54
Tb	0.91	0.82	1.89	1.69	0.92	0.66	0.85
Co	1.59	2.24	0.48	0.68	1.79	5.42	1.65
Sc	2.57	4.31	0.75	1.25	4.70	2.36	0.67
Rb	0.61	0.18	1.51	0.45	0.68	0.82	1.11
Sr	2.60	4.35	1.04	1.74	4.81	0.91	0.42
Ba	3.58	6.43	0.96	1.72	12.70	1.16	0.28

D*(l) and D**(r)- back calculated D from Cl and Cr f*=f for perfectly incompatible elements

Mix'n'Mac file : 91-1 to 37b.m'n'm
Date: 05-07-1990 Time: 11:59:00

	Parent	Daughter	Phases					
	mag 37b	mag91-1	cpx	olig	fayalite	ksp	ilm	phase 6
Variables								
SiO2	60.18	64.00	48.80	64.10	30.56	67.50	0.51	0.00
TiO2	0.82	0.28	0.70	0.00	0.72	0.00	50.02	0.00
Al2O3	14.74	16.50	1.26	22.66	0.09	16.22	0.00	0.00
Fe2O3	9.59	5.00	20.09	0.20	54.07	0.60	46.00	0.00
MnO	0.24	0.15	0.61	0.00	3.43	0.00	1.44	0.00
MgO	0.43	0.18	4.55	0.25	3.47	0.00	0.46	0.00
CaO	2.89	1.17	19.24	3.26	1.13	0.00	0.71	0.00
Na2O	5.87	6.08	1.58	9.90	0.00	5.00	0.00	0.00
K2O	4.64	5.67	0.00	0.00	0.00	8.00	0.00	0.00
P2O5	0.22	0.05	0.00	0.00	0.00	0.00	0.00	0.00

Oxides recalculated to 100%

RESULTS:

	Parent observed	Parent estimated	Residuals
SiO2	60.41	60.48	-0.0668
TiO2	0.82	0.83	-0.0075
Al2O3	14.80	14.75	0.0460
Fe2O3	9.63	9.62	0.0112
MnO	0.24	0.26	-0.0164
MgO	0.43	0.51	-0.0800
CaO	2.90	2.87	0.0318
Na2O	5.89	6.00	-0.1101
K2O	4.66	4.66	-0.0067
P2O5	0.22	0.10	0.1198
			0.0409 = sum of squared residuals

Component	Proportion
mag 37b	2.0027
cpx	0.0622
olig	-0.2171
fayalite	-0.0250
ksp	-0.8268
ilm	0.0047

Mix'n'Mac file : 91-2 TO 120.M'N'M 2
Date: 04-05-1990 Time: 08:32:06

	Parent mag91-2	Daughter mag 120	Phases fayalite	hedenbergite	ksp	ti-mag	phase 5	phase 6
Variables								
SiO2	63.30	67.58	30.56	48.27	67.27	0.02	0.00	0.00
TiO2	0.56	0.41	0.72	0.37	0.00	53.03	0.00	0.00
Al2O3	14.50	15.97	0.09	0.23	18.35	0.00	0.00	0.00
FeO	7.52	4.97	60.90	28.54	0.92	46.82	0.00	0.00
MnO	0.18	0.12	3.43	0.91	0.00	1.60	0.00	0.00
MgO	0.10	0.25	3.47	0.92	0.00	0.00	0.00	0.00
CaO	1.05	1.15	1.13	18.70	0.15	0.32	0.00	0.00
Na2O	6.29	5.73	0.00	1.19	6.45	0.00	0.00	0.00
K2O	5.36	5.58	0.00	0.00	7.05	0.00	0.00	0.00
P2O5	0.04	0.08	0.00	0.00	0.00	0.00	0.00	0.00

Oxides recalculated to 100%

RESULTS:

	Parent observed	Parent estimated	Residuals
SiO2	64.00	63.97	0.0359
TiO2	0.57	0.57	-0.0027
Al2O3	14.66	15.12	-0.4583
FeO	7.60	7.60	0.0079
MnO	0.18	0.29	-0.1090
MgO	0.10	0.37	-0.2720
CaO	1.06	1.20	-0.1363
Na2O	6.36	5.41	0.9496
K2O	5.42	5.43	-0.0131
P2O5	0.04	0.05	-0.0132
			1.2179 = sum of squared residuals

Component	Proportion
mag 120	0.6832
fayalite	0.0547
hedenbergite	0.0174
ksp	0.2401
ti-mag	0.0048

Mix'n'Mac file : 91-2 TO 49 M'N'M
Date: 04-05-1990 Time: 08:33:59

	Parent	Daughter	Phases					
	mag49	mag91-2px	olig	fayalite	ksp	ilm	apt	
Variables								
SiO2	63.30	70.90	48.80	64.10	30.56	67.50	0.51	0.00
TiO2	0.56	0.33	0.70	0.00	0.72	0.00	50.02	0.00
Al2O3	14.50	11.80	1.26	22.66	0.09	16.22	0.00	0.00
Fe2O3	7.52	5.08	20.09	0.20	54.07	0.60	46.00	0.21
MnO	0.18	0.00	0.61	0.00	0.43	0.00	1.44	1.52
MgO	0.10	0.10	4.55	0.25	3.47	0.00	0.46	0.54
CaO	1.05	0.34	19.24	3.26	1.13	0.00	0.71	52.40
Na2O	6.29	4.93	1.58	9.89	0.00	5.00	0.00	0.00
K2O	5.36	4.39	0.00	0.00	0.00	8.00	0.00	0.00
P2O5	0.04	0.08	0.00	0.00	0.00	0.00	0.00	45.33

Oxides recalculated to 100%

RESULTS:

	Parent observed	Parent estimated	Residuals
SiO2	64.00	64.05	-0.0431
TiO2	0.57	0.61	-0.0457
Al2O3	14.66	14.97	-0.3097
Fe2O3	7.60	7.54	0.0588
MnO	0.18	0.38	-0.2025
MgO	0.10	0.45	-0.3538
CaO	1.06	0.98	0.0798
Na2O	6.36	5.39	0.9681
K2O	5.42	5.04	0.3794
P2O5	0.04	0.12	-0.0815
			1.3636 = sum of squared residuals

Component	Proportion
mag49	0.1793
cpx	0.0032
olig	0.1863
fayalite	0.0996
ksp	0.5154
ilm	0.0094
apt	0.0024

Mix'n'Mac file : 51-D TO 120 M'N'M
Date: 04-05-1990 Time: 08:41:28

	Parent	Daughter	Phases					
	51-D	120	cpx	olig	fayalite	ksp	ilm	apt
Variables								
SiO2	62.90	67.50	48.80	64.10	30.56	67.50	0.51	0.00
TiO2	0.61	0.41	0.70	0.00	0.72	0.00	50.02	0.00
Al2O3	15.28	15.97	1.26	22.66	0.09	16.22	0.00	0.00
Fe2O3	7.80	4.97	20.09	0.20	54.07	0.60	46.00	0.21
MnO	0.19	0.12	0.61	0.00	3.43	0.00	1.44	1.52
MgO	0.33	0.25	4.55	0.25	3.47	0.00	0.46	0.54
CaO	1.21	1.15	19.24	3.26	1.13	0.00	0.71	52.40
Na2O	6.64	5.73	1.58	9.89	0.00	5.00	0.00	0.00
K2O	4.91	5.58	0.00	0.00	0.00	8.00	0.00	0.00
P2O5	0.12	0.08	0.00	0.00	0.00	0.00	0.00	45.33

None

RESULTS:

	Parent observed	Parent estimated	Residuals
SiO2	62.90	62.89	0.0067
TiO2	0.61	0.62	-0.0115
Al2O3	15.28	15.70	-0.4224
Fe2O3	7.80	7.78	0.0208
MnO	0.19	0.39	-0.2044
MgO	0.33	0.49	-0.1647
CaO	1.21	1.25	-0.0430
Na2O	6.64	5.70	0.9361
K2O	4.91	4.71	0.1963
P2O5	0.12	0.06	0.0584
			1.1681 = sum of squared residuals

Component	Proportion
120	0.3680
cpx	0.0021
olig	0.1951
fayalite	0.0981
ksp	0.3325
ilm	0.0080
apt	0.0007

APPENDIX III.V.II

ALKALIC SYENITE

Kd*	heden	amph	fay	tiMt.29	plg	san	apt	Zir	Tit
U	0.09	0.45	0.14	0.29	0.04	0.07	0	300	1
Th	1.6	0.11	0.49	0.39	3E-04	0.05	0	62	1
Zr	0	0.5	0.66	1.8	0.008	0.07	0	1500	1
Hf	0.95	0.84	0.09	2.51	0.03	0.08	0	1000	1
Ta	0.47	1.02	0.14	2.55	0.03	0.05	0	40	70
La	0.66	0.85	0.4	0.87	0.23	0.24	12	0.8	10
Eu	0.87	3.2	0	0.4	2	1.13	2	2.5	30
Tb	3	3.67	0.52	1.72	0.06	0.09	21	15	40
Co	5.3	16.7	14.6	41.7	0.08	0.29	0	9	1
Sc	30	5.3	0.5	2.5	0	0.1	0	60	1
Rb	0.03	0.08	0.007	0	0.02	1.8	0	0	1
Sr	0.04	0.3	0	0.04	5.2	2	2	0	1
Ba	0.1	0.8	0.05	0.1	1.4	7.5	1	0	1

	SAMPLE #	REF.	SiO2	TiO2	Al2O3	FeO	Fe2O3	MnO	MgO	CaO
PARENT	MAG-37b	Ridley(U	64	0.28	16.5	0	5	0.15	0.18	1.17
PRODUCT	MAG-61B	Perfit(L	65.11	0.42	16.69	0	4.78	0.13	0.13	1.14

	cpx	amph	oiv	tiMt.29	plg	kap	apt	zir	tit
least squares input	0.03	0	0.025	0.001	0	0.488	0	9E-04	0
% cummulate	0.055	0	0.04588	0.002	0	0.895	0	0.002	0

	D	f	Co	Cl	Cr	son	Cs-inst	Cs-avg	um_com	oxides
U	0.543	0.445	4.899	7.10	6.41	0	3.85	3.14	64.35	sio2
Th	0.253		24.387	44.67	37.85	0	11.30	8.14	0.16	tio2
Zr	2.437		533	166.44	228.86	160	405.6	826.7	16.45	al2o3
Hf	1.693		24.069	13.73	18.01	0	23.24	32.35	5.28	fe2o3
Ta	0.145		9.0668	18.13	15.00	0	2.62	1.81	0.21	mno
La	0.273		119.12	214.74	182.76	0	58.54	42.52	0.21	mgo
Eu	1.064		0.431	0.41	0.41	0	0.44	0.45	1.22	cao
Tb	0.297		1.902	3.36	2.88	0	1.00	0.73	5.84	na2o
Co	1.320		0.5783	0.45	0.48	0.892	0.59	0.68	6.31	k20
Sc	1.863		2.557	1.27	1.54	0	2.37	3.59	0.00	p205
Rb	1.614		155	94.27	108.01	110	152.13	203.66		
Sr	1.793		24	12.62	15.05	35.3	22.63	33.12		
Ba	6.724		23	0.22	0.792	56.9	1.50	41.25		

	D*(i)	D**(r	D*(i)/C	D**(r)/C	f*	Son/Cl	Son/Cr
U	#NUM!	#NUM!	#NUM!	#NUM!	####	0.00	0.00
Th	#NUM!	#NUM!	#NUM!	#NUM!	####	0.00	0.00
Zr	2.49	3.05	1.02	1.25	3.33	0.96	0.70
Hf	#NUM!	#NUM!	#NUM!	#NUM!	####	0.00	0.00
Ta	#NUM!	#NUM!	#NUM!	#NUM!	####	0.00	0.00
La	#NUM!	#NUM!	#NUM!	#NUM!	####	0.00	0.00
Eu	#NUM!	#NUM!	#NUM!	#NUM!	####	0.00	0.00
Tb	#NUM!	#NUM!	#NUM!	#NUM!	####	0.00	0.00
Co	0.47	0.26	0.35	0.20	0.65	2.00	1.86
Sc	#NUM!	#NUM!	#NUM!	#NUM!	####	0.00	0.00
Rb	1.42	1.58	0.88	0.98	1.41	1.17	1.02
Sr	0.52	0.34	0.29	0.19	0.68	2.80	2.35
Ba	-0.12	-0.54	-0.02	-0.08	0.40	255.45	71.81

D*(i) and D**(r)- back calculated D from Cl and Cr f*=Co/Cl= f for perfectly incompatible elements

Mix'n'Mac file : 37 TO 3.M'N'M
Date: 04-05-1990 Time: 08:51:03

	Parent mag37	Daughter mag 3	Phases KSP	hedenbergite	FAY	ti-mag	phase 5	phase 6
Variables								
SiO2	64.00	66.99	67.27	48.27	30.56	0.02	0.00	0.00
TiO2	0.28	0.35	0.00	0.37	0.72	53.03	0.00	0.00
Al2O3	16.50	16.99	18.35	0.23	0.09	0.00	0.00	0.00
FeO	5.00	5.75	0.92	28.54	60.90	46.82	0.00	0.00
MnO	0.15	0.17	0.00	0.91	3.43	1.60	0.00	0.00
MgO	0.18	0.17	0.00	0.92	3.47	0.00	0.00	0.00
CaO	1.17	1.36	0.15	18.70	1.13	0.32	0.00	0.00
Na2O	6.08	5.50	7.05	1.19	0.00	0.00	0.00	0.00
K2O	5.67	5.88	6.45	0.00	0.00	0.00	0.00	0.00
P2O5	0.05	0.02	0.00	0.00	0.00	0.00	0.00	0.00

Oxides recalculated to 100%

RESULTS:

	Parent observed	Parent estimated	Residuals
SiO2	64.59	64.59	0.0056
TiO2	0.28	0.29	-0.0045
Al2O3	16.65	16.58	0.0747
FeO	5.05	5.04	0.0055
MnO	0.15	0.18	-0.0303
MgO	0.18	0.18	0.0034
CaO	1.18	1.16	0.0163
Na2O	6.14	6.15	-0.0156
K2O	5.72	5.80	-0.0778
P2O5	0.05	0.00	0.0455
			0.0152 = sum of squared residuals

Component	Proportion
mag 3	0.2580
KSP	0.6726
hedenbergite	0.0366
FAY	0.0294
ti-mag	0.0032

Kd*	heden	amph	fay	tiMt.29	plg	san	apt	Zir	Tit
U	0.09	0.45	0.14	0.29	0.04	0.07	0	300	1
Th	*1.6*	*0.11*	*0.49*	*0.39*	*3E-04*	*0.05*	0	62	1
Zr	*0*	*0.5*	*0.66*	*1.8*	*0.008*	*0.07*	0	1500	1
Hf	0.95	0.84	0.09	2.51	0.03	0.08	0	1000	1
Ta	0.47	1.02	0.14	2.55	0.03	0.05	0	40	70
La	0.66	0.85	0.4	0.87	0.23	0.24	12	0.8	10
Eu	*0.87*	*3.2*	*0*	*0.4*	*2*	*1.13*	2	2.5	30
Tb	3	3.67	0.52	1.72	0.06	0.09	21	15	40
Co	5.3	16.7	14.6	41.7	0.08	0.29	0	9	1
Sc	*30*	*5.3*	*0.5*	*2.5*	*0*	*0.1*	0	60	1
Rb	*0.03*	*0.08*	*0.007*	*0*	*0.02*	*1.8*	0	0	1
Sr	*0.04*	*0.3*	*0*	*0.04*	*5.2*	*2*	2	0	1
Ba	0.1	0.8	0.05	0.1	1.4	7.5	1	0	1

	SAMPLE #	REF.	SiO2	TiO2	Al2O3	FeO	Fe2O3	MnO	MgO	CaO
parent	MAG-37b	Ridley(U	64	0.28	16.5	0	5	0.15	0.18	1.17
product	MAG-3	BROOKS	66.99	0.351	16.99	0	5.75	0.174	0.17	1.36

	cpx	amph	olv	tiMt.29	plg	ksp	apt	zir	tit
least squares input	0.029	0	0.0248	0.003	0.1605	0.577	0	0.001	0
% cummulate	0.037	0	0.03116	0.004	0.2017	0.725	0	0.002	0

	D	f	Co	Cl	Cr	son	Cs-inst	Cs-avg	um com	oxides
U	0.520	0.365	4.899	7.95	6.09	1.6255	4.13	3.15	51.55	sio2
Th	0.205		24.387	54.32	34.98	*8.93*	11.16	7.18	0.24	tio2
Zr	2.342		533	137.88	289.82	*126.9*	322.9	760.1	13.32	al2o3
Hf	1.619		24.069	12.90	18.17	4.612	20.86	30.49	3.79	fe2o3
Ta	0.134		9.0668	21.70	13.44	3.806	2.91	1.80	0.15	mno
La	0.262		119.12	250.71	166.58	39.756	65.60	43.48	0.14	mgo
Eu	1.260		0.431	0.33	0.38	*0.74*	0.42	0.49	0.83	cao
Tb	0.233		1.902	4.12	2.69	0.943	0.96	0.63	4.72	na2o
Co	1.047		0.5783	0.55	0.57	0.8385	0.58	0.59	5.11	k20
Sc	1.293		2.557	1.90	2.24	*1.785*	2.46	2.93	0.00	p205
Rb	1.310		155	113.36	134.62	*111.2*	148.55	178.94		
Sr	2.500		24	5.29	12.14	*7.2*	13.23	34.75		
Ba	5.726		23	0.20	2.689	*25.4*	1.12	36.11		

	D*(i)	D**(r)	D*(i)/D	D**(r)/D	f*	Son/Cl	Son/Cr
U	2.09	3.43	4.03	6.60	3.01	0.20	0.27
Th	2.00	3.21	9.72	15.63	2.73	0.16	0.26
Zr	2.42	4.16	1.04	1.78	4.20	0.92	0.44
Hf	2.64	4.64	1.63	2.86	5.22	0.36	0.25
Ta	1.86	2.91	13.90	21.74	2.38	0.18	0.28
La	2.09	3.42	7.98	13.06	3.00	0.16	0.24
Eu	0.46	-0.19	0.37	-0.15	0.58	2.23	1.93
Tb	1.70	2.54	7.28	10.92	2.02	0.23	0.35
Co	0.63	0.18	0.60	0.17	0.69	1.52	1.48
Sc	1.36	1.79	1.05	1.39	1.43	0.94	0.80
Rb	1.33	1.73	1.01	1.32	1.39	0.98	0.83
Sr	2.19	3.65	0.88	1.46	3.33	1.36	0.59
Ba	0.90	0.78	0.16	0.14	0.91	129.32	9.44

D*(i) and D**(r)- back calculated D from Cl and Cr f*=Co/Cl= f for perfectly incompatible elements

Mix'n'Mac file : 37 to 135 m'n'm
Date: 04-05-1990 Time: 08:55:51

	Parent mag37	Daughter mag 135	Phases KSP	hedenbergite	FAY	ti-mag	phase 5	phase 6
Variables								
SiO2	64.00	68.40	67.27	48.27	30.56	0.02	0.00	0.00
TiO2	0.28	0.35	0.00	0.37	0.72	53.03	0.00	0.00
Al2O3	16.50	15.20	18.35	0.23	0.09	0.00	0.00	0.00
FeO	5.00	3.92	0.92	28.54	60.90	46.82	0.00	0.00
MnO	0.15	0.10	0.00	0.91	3.43	1.60	0.00	0.00
MgO	0.18	0.10	0.00	0.92	3.47	0.00	0.00	0.00
CaO	1.17	0.47	0.15	18.70	1.13	0.32	0.00	0.00
Na2O	6.08	5.93	7.05	1.19	0.00	0.00	0.00	0.00
K2O	5.67	5.32	6.45	0.00	0.00	0.00	0.00	0.00
P2O5	0.05	0.03	0.00	0.00	0.00	0.00	0.00	0.00

Oxides recalculated to 100%

RESULTS:

	Parent observed	Parent estimated	Residuals
SiO2	64.59	64.62	-0.0213
TiO2	0.28	0.29	-0.0102
Al2O3	16.65	16.45	0.1988
FeO	5.05	5.03	0.0127
MnO	0.15	0.19	-0.0421
MgO	0.18	0.19	-0.0071
CaO	1.18	1.13	0.0532
Na2O	6.14	6.38	-0.2438
K2O	5.72	5.78	-0.0545
P2O5	0.05	0.00	0.0487
			0.1097 = sum of squared residuals

Component	Proportion
mag 135	0.0589
KSP	0.8486
hedenbergite	0.0491
FAY	0.0397
ti-mag	0.0043

Kd*	heden	amph	fay	tiMt.29	plg	san	apt	Zlr	Tit
U	0.09	0.45	0.14	0.29	0.04	0.07	0	300	1
Th	*1.6*	*0.11*	*0.49*	*0.39*	*3E-04*	*0.05*	0	62	1
Zr	*0*	*0.5*	*0.66*	*1.8*	*0.008*	*0.07*	0	1500	1
Hf	0.95	0.84	0.09	2.51	0.03	0.08	0	1000	1
Ta	0.47	1.02	0.14	2.55	0.03	0.05	0	40	70
La	0.66	0.85	0.4	0.87	0.23	0.24	12	0.8	10
Eu	*0.87*	*3.2*	*0*	*0.4*	*2*	*1.13*	2	2.5	30
Tb	3	3.67	0.52	1.72	0.06	0.09	21	15	40
Co	5.3	16.7	14.6	41.7	0.08	0.29	0	9	1
Sc	*30*	*5.3*	*0.5*	*2.5*	*0*	*0.1*	0	60	1
Rb	*0.03*	*0.08*	*0.007*	*0*	*0.02*	*1.8*	0	0	1
Sr	*0.04*	*0.3*	*0*	*0.04*	*5.2*	*2*	2	0	1
Ba	0.1	0.8	0.05	0.1	1.4	7.5	1	0	1

	SAMPLE #	REF.	SIO2	TIO2	Al2O3	FeO	Fe2O3	MnO	MgO	CaO
PARENT	MAG-37b	Ridley(U	64	0.28	16.5	0	5	0.15	0.18	1.17
PRODUCT	MAG-135	Perfit(L	68.43	0.35	15.2	0	3.92	0.1	0.1	0.47

	cpx	amph	oiv	tiMt.29	plg	ksp	apt	zlr	tit
least squares input	0.05	0	0.0399	0.004	0	0.859	0	7E-04	0
% cummulate	0.052	0	0.04185	0.005	0	0.9	0	7E-04	0

	D	f	Co	Cl	Cr	son	Cs-inst	Cs-avg	um com	oxides
U	0.295	0.048	4.899	41.47	5.07	1.84	12.24	3.04	64.41	sio2
Th	0.197		24.387	278.19	25.38	*11.21*	54.72	11.51	0.29	tio2
Zr	1.200		533	290.77	527.75	*226*	348.9	545.3	16.54	al2o3
Hf	0.871		24.069	35.57	24.22	6.3787	30.99	23.49	5.08	fe2o3
Ta	0.116		9.0668	131.93	9.47	5.0748	15.36	2.83	0.20	mno
La	0.272		119.12	1081.72	123.49	49.55	294.20	70.27	0.19	mgo
Eu	1.067		0.431	0.35	0.43	*0.463*	0.38	0.44	1.16	cao
Tb	0.279		1.902	16.91	1.97	1.168	4.72	1.14	5.87	na2o
Co	1.345		0.5783	0.20	0.57	0.6092	0.27	0.60	6.35	k20
Sc	1.739		2.557	0.27	2.47	*0.719*	0.47	2.67	0.00	p205
Rb	1.623		155	23.49	150.29	*146*	38.11	161.67		
Sr	1.803		24	2.10	23.06	*23*	3.79	25.11		
Ba	6.761		23	0.00	17.29	*12*	0.00	24.17		

	D°(I)	D°°(r)	D°(I)/D	D°°(r)/D	f°	Son/Cl	Son/Cr
U	1.32	20.78	4.48	70.41	2.66	0.04	0.36
Th	1.26	16.69	6.39	84.85	2.17	0.04	0.44
Zr	1.28	18.33	1.07	15.28	2.36	0.78	0.43
Hf	1.44	27.82	1.65	31.94	3.77	0.18	0.26
Ta	1.19	12.72	10.24	109.31	1.79	0.04	0.54
La	1.29	18.72	4.74	68.83	2.40	0.05	0.40
Eu	0.98	-0.45	0.92	-0.42	0.93	1.32	1.08
Tb	1.16	10.85	4.16	38.91	1.63	0.07	0.59
Co	0.98	-0.05	0.73	-0.04	0.95	2.99	1.07
Sc	1.42	26.63	0.82	15.31	3.56	2.84	0.29
Rb	1.02	2.21	0.63	1.36	1.06	6.22	0.97
Sr	1.01	1.86	0.56	1.03	1.04	10.93	1.00
Ba	1.21	14.14	0.18	2.09	1.92	####	0.69

D°(I) and D°°(r)- back calculated D from Cl and Cr f°=Co/Cl= 1 for perfectly incompatible elements

Mix'n'Mac file : 72b to 37b m'n'm
Date: 04-05-1990 Time: 08:46:07

	Parent	Daughter	Phases					
	mag 37b	mag842HED	ksp	fayalite	ILM	phase 5	phase 6	
Variables								
SiO2	62.49	64.00	48.96	67.50	30.56	0.51	0.00	0.00
TiO2	0.54	0.28	0.44	0.00	0.72	50.02	0.00	0.00
Al2O3	17.09	16.50	0.66	16.22	0.09	0.00	0.00	0.00
FeO	5.00	5.00	28.12	0.60	54.07	44.19	0.00	0.00
MnO	0.13	0.15	0.96	0.00	3.43	1.44	0.00	0.00
MgO	0.50	0.18	2.76	0.00	3.47	0.46	0.00	0.00
CaO	1.71	1.17	20.47	0.00	1.13	0.71	0.00	0.00
Na2O	6.09	6.08	0.56	9.00	0.00	0.00	0.00	0.00
K2O	6.20	5.67	0.00	6.00	0.00	0.00	0.00	0.00
P2O5	0.13	0.05	0.00	0.00	0.00	0.00	0.00	0.00

Oxides recalculated to 100%

RESULTS:

	Parent observed	Parent estimated	Residuals
SiO2	62.56	62.82	-0.2526
TiO2	0.54	0.64	-0.1044
Al2O3	17.11	16.58	0.5330
FeO	5.01	4.90	0.1106
MnO	0.13	0.11	0.0180
MgO	0.50	0.14	0.3620
CaO	1.71	1.34	0.3721
Na2O	6.10	5.58	0.5174
K2O	6.21	5.62	0.5845
P2O5	0.13	0.06	0.0713
			1.2553 = sum of squared residuals

Component	Proportion
mag 37b	1.1661
84 HED	-0.0009
ksp	-0.1738
fayalite	-0.0199
ILM	0.0064

Mix'n'Mac file : 37 TO 120 M'N'M
Date: 04-05-1990 Time: 08:53:48

	Parent mag37	Daughter mag 120	Phases KSP	hed 84	FAY	ti-mag	phase 5	phase 6
Variables								
SiO2	64.00	67.58	67.27	48.96	30.56	0.02	0.00	0.00
TiO2	0.28	0.41	0.00	0.44	0.72	53.03	0.00	0.00
Al2O3	16.50	15.97	18.35	0.66	0.09	0.00	0.00	0.00
FeO	5.00	4.97	0.92	28.12	60.90	46.82	0.00	0.00
MnO	0.15	0.12	0.00	0.96	3.43	1.60	0.00	0.00
MgO	0.18	0.25	0.00	2.76	3.47	0.00	0.00	0.00
CaO	1.17	1.15	0.15	20.47	1.13	0.32	0.00	0.00
Na2O	6.08	5.73	7.05	0.56	0.00	0.00	0.00	0.00
K2O	5.67	5.58	6.45	0.00	0.00	0.00	0.00	0.00
P2O5	0.05	0.08	0.00	0.00	0.00	0.00	0.00	0.00

Oxides recalculated to 100%

RESULTS:

	Parent observed	Parent estimated	Residuals
SiO2	64.59	64.67	-0.0781
TiO2	0.28	0.32	-0.0400
Al2O3	16.65	16.33	0.3252
FeO	5.05	5.00	0.0456
MnO	0.15	0.18	-0.0319
MgO	0.18	0.27	-0.0848
CaO	1.18	1.04	0.1395
Na2O	6.14	6.17	-0.0354
K2O	5.72	5.72	0.0002
P2O5	0.05	0.02	0.0290
			0.1453 = sum of squared residuals

Component	Proportion
mag 120	0.2732
KSP	0.6564
hed 84	0.0299
FAY	0.0345
ti-mag	0.0034

APPENDIX III.V.III

ALKALIC GRANITE

Mix'n'Mac file : 120 to 135 m'n'm
Date: 04-05-1990 Time: 08:57:46

	Parent mag120	Daughter mag 135	Phases fayalite	hedenbergite	ksp	ti-mag	phase 5	phase 6
Variables								
SiO2	67.58	68.46	30.56	48.27	67.27	0.02	0.00	0.00
TiO2	0.41	0.35	0.72	0.37	0.00	53.03	0.00	0.00
Al203	15.97	15.20	0.09	0.23	18.35	0.00	0.00	0.00
FeO	4.97	3.50	60.90	28.54	0.92	46.82	0.00	0.00
MnO	0.12	0.10	3.43	0.91	0.00	1.60	0.00	0.00
MgO	0.25	0.10	3.47	0.92	0.00	0.00	0.00	0.00
CaO	1.15	0.47	1.13	18.70	0.15	0.32	0.00	0.00
Na20	5.73	5.93	0.00	1.19	6.45	0.00	0.00	0.00
K20	5.58	5.32	0.00	0.00	7.05	0.00	0.00	0.00
P205	0.08	0.03	0.00	0.00	0.00	0.00	0.00	0.00

Oxides recalculated to 100%

RESULTS:

	Parent observed	Parent estimated	Residuals
SiO2	66.36	66.35	0.0070
TiO2	0.40	0.40	0.0064
Al203	15.68	15.55	0.1328
FeO	4.88	4.89	-0.0052
MnO	0.12	0.17	-0.0519
MgO	0.25	0.17	0.0799
CaO	1.13	1.13	0.0039
Na20	5.63	5.82	-0.1940
K20	5.48	5.70	-0.2167
P205	0.08	0.02	0.0628
			0.1154 = sum of squared residuals

Component	Proportion
mag 135	0.5231
fayalite	0.0214
hedenbergite	0.0419
ksp	0.4118
ti-mag	0.0035

Kd*	heden	amph	fay	tiMt.29	plg	san	apt	Zir	Tit
U	0.09	0.45	0.14	0.29	0.04	0.07	0	300	1
Th	1.6	0.11	0.49	0.39	3E-04	0.05	0	62	1
Zr	0	0.5	0.66	1.8	0.008	0.07	0	1500	1
Hf	0.95	0.84	0.09	2.51	0.03	0.08	0	1000	1
Ta	0.47	1.02	0.14	2.55	0.03	0.05	0	40	70
La	0.66	0.85	0.4	0.87	0.23	0.24	12	0.8	10
Eu	0.87	3.2	0	0.4	2	1.13	10	2.5	30
Tb	3	3.67	0.52	1.72	0.06	0.09	21	15	40
Co	5.3	16.7	14.6	41.7	0.08	0.29	0	9	1
Sc	30	5.3	0.5	2.5	0	0.1	0	60	1
Rb	0.03	0.08	0.007	0	0.02	1.9	0	0	1
Sr	0.04	0.3	0	0.04	5.2	3	2	0	1
Ba	0.1	0.8	0.05	0.1	1.4	7	1	0	1

	SAMPLE #	REF.	SiO2	TiO2	Al2O3	FeO	Fe2O3	MnO	MgO	CaO
PARENT	MAG-120	Perlit(L	67.58	0.41	15.97	0	4.97	0.12	0.25	1.15
PRODUCT	MAG-135	Perlit(L	68.43	0.35	15.2	0	3.92	0.1	0.1	0.47

	cpx	amph	olv	tiMt.29	plg	ksp	apt	zir	tit
least squares input	0.042	0	0.0213	0.004	0	0.408	0	6E-04	0
% cummulate	0.088	0	0.04479	0.007	0	0.859	0	0.001	0

	D	f	Co	Cl	Cr	son	Cs-inst	Cs-avg	um com	oxides
U	0.455	0.527	5.1783	7.34	7.78	1.84	3.34	2.77	63.42	sio2
Th	0.286		21.284	33.63	36.30	11.21	9.63	7.54	0.46	tio2
Zr	1.996		440	232.39	208.93	228	463.8	671	15.78	al2o3
Hf	1.436		14.411	10.89	10.40	6.3787	15.65	18.32	6.37	fe2o3
Ta	0.160		7.8502	13.45	14.72	5.0748	2.15	1.61	0.25	mno
La	0.289		97.162	153.24	165.33	49.55	44.34	34.76	0.24	mgo
Eu	1.053		1.4577	1.41	1.40	0.463	1.48	1.51	1.82	cao
Tb	0.395		2.1902	3.23	3.44	1.168	1.28	1.04	5.64	na2o
Co	1.686		0.9209	0.59	0.55	0.6092	1.00	1.29	6.06	k20
Sc	2.833		2.7468	0.85	0.70	0.719	2.40	4.86	0.00	p205
Rb	1.635		215	143.11	133.72	146	233.97	295.00		
Sr	2.580		59.8	21.71	18.33	23	56.02	102.19		
Ba	6.024		332	13.25	7.745	12	79.83	686.7		

	D*(I)	D**(r	D*(I)/D	D**(r)/D	f*=Co/C	Son/Cl	Son/Cr
U	2.61	2.38	5.75	5.24	2.81	0.25	0.24
Th	2.00	1.86	6.98	6.48	1.90	0.33	0.31
Zr	2.04	1.89	1.02	0.95	1.95	0.97	1.08
Hf	2.27	2.09	1.58	1.45	2.26	0.59	0.61
Ta	1.68	1.58	10.52	9.92	1.55	0.38	0.34
La	2.05	1.90	7.09	6.57	1.96	0.32	0.30
Eu	2.79	2.53	2.65	2.41	3.15	0.33	0.33
Tb	1.98	1.84	5.01	4.66	1.88	0.36	0.34
Co	1.64	1.55	0.98	0.92	1.51	1.03	1.11
Sc	3.09	2.79	1.09	0.99	3.82	0.85	1.03
Rb	1.80	1.52	0.98	0.93	1.47	1.02	1.09
Sr	2.49	2.28	0.97	0.88	2.60	1.06	1.25
Ba	6.18	5.44	1.03	0.90	27.67	0.91	1.55

D*(I) and D**(r)- back calculated D from Cl and Cr f*=f for perfectly incompatible elements

Mix'n'Mac file : 120 to 26 m'n'm
Date: 04-05-1990 Time: 08:59:26

	Parent mag120	Daughter mag 26	Phases fayalite	hedenbergite	ksp	ti-mag	phase 5	phase 6
Variables								
SiO2	67.58	70.95	30.56	48.27	67.27	0.02	0.00	0.00
TiO2	0.41	0.24	0.72	0.37	0.00	53.03	0.00	0.00
Al2O3	15.97	14.43	0.09	0.23	18.35	0.00	0.00	0.00
FeO	4.97	3.12	60.90	28.54	0.92	46.82	0.00	0.00
MnO	0.12	0.07	3.43	0.91	0.00	1.60	0.00	0.00
MgO	0.25	0.12	3.47	0.92	0.00	0.00	0.00	0.00
CaO	1.15	0.53	1.13	18.70	0.15	0.32	0.00	0.00
Na2O	5.73	5.60	0.00	1.19	6.45	0.00	0.00	0.00
K2O	5.58	5.27	0.00	0.00	7.05	0.00	0.00	0.00
P2O5	0.08	0.02	0.00	0.00	0.00	0.00	0.00	0.00

Oxides recalculated to 100%

RESULTS:

	Parent observed	Parent estimated	Residuals
SiO2	66.36	66.37	-0.0072
TiO2	0.40	0.40	-0.0004
Al2O3	15.68	15.49	0.1871
FeO	4.88	4.88	0.0021
MnO	0.12	0.17	-0.0539
MgO	0.25	0.18	0.0621
CaO	1.13	1.11	0.0145
Na2O	5.63	5.69	-0.0613
K2O	5.48	5.85	-0.3678
P2O5	0.08	0.00	0.0712
			0.1861 = sum of squared residuals

Component	Proportion
mag 26	0.3704
fayalite	0.0288
hedenbergite	0.0425
ksp	0.5545
ti-mag	0.0053

Kd*	heden	amph	fay	tiMt.29	plg	sen	apt	Zir	Tit
U	0.09	0.45	0.14	0.29	0.04	0.07	0	300	1
Th	*1.6*	*0.11*	*0.49*	*0.39*	*3E-04*	*0.05*	0	62	1
Zr	*0*	*0.5*	*0.66*	*1.8*	*0.008*	*0.07*	0	1500	1
Hf	0.95	0.84	0.09	2.51	0.03	0.08	0	1000	1
Ta	0.47	1.02	0.14	2.55	0.03	0.05	0	40	70
La	0.66	0.85	0.4	0.87	0.23	0.24	12	0.8	10
Eu	*0.87*	*3.2*	*0*	*0.4*	*2*	*2*	10	2.5	30
Tb	3	3.67	0.52	1.72	0.06	0.09	21	15	40
Co	5.3	16.7	14.6	41.7	0.08	0.29	0	9	1
Sc	*30*	*5.3*	*0.5*	*2.5*	*0*	*0.1*	0	60	1
Rb	*0.03*	*0.08*	*0.007*	*0*	*0.02*	*1.5*	0	0	1
Sr	*0.04*	*0.3*	*0*	*0.04*	*5.2*	*1.8*	2	0	1
Ba	0.1	0.8	0.05	0.1	1.4	3	1	0	1

	SAMPLE #	REF.	SiO2	TiO2	Al2O3	FeO	Fe2O3	MnO	MgO	CaO
PARENT	MAG-120	Perlit(L	67.58	0.41	15.97	0	4.97	0.12	0.25	1.15
PRODUCT	MAG-26	Perlit(L	70.95	0.24	14.43	0	3.12	0.07	0.12	0.53

	cpx	amph	oiv	tiMt.28	plg	ksp	apt	zir	tit
least squares input	0.043	0	0.0288	0.005	0	0.556	0	7E-04	0
% cummulate	0.068	0	0.04546	0.008	0	0.878	0	0.001	0

	D	f	Co	Cl	Cr	son	Cs-inst	Cs-avg	um com	oxides
U	0.408	0.368	5.1783	9.36	6.80	0	3.81	2.74	63.74	sio2
Th	0.246		21.284	45.17	30.09	*0*	11.13	7.35	0.48	tio2
Zr	1.763		440	205.36	309.86	*227*	362.1	576.9	16.12	al2o3
Hf	1.264		14.411	11.08	12.77	0	14.00	16.36	5.88	fe2o3
Ta	0.146		7.8502	18.41	11.62	0	2.70	1.69	0.23	mno
La	0.281		97.162	199.14	135.18	76.7	56.03	37.68	0.22	mgo
Eu	1.820		1.4577	0.64	1.00	*0*	1.17	1.93	1.45	cao
Tb	0.336		2.1902	4.25	2.97	0	1.43	0.99	5.74	na2o
Co	1.617		0.9209	0.50	0.69	0.65	0.80	1.17	6.19	k20
Sc	2.233		2.7468	0.80	1.56	*0*	1.79	3.88	0.00	p205
Rb	1.319		215	156.37	185.70	*141*	206.23	249.20		
Sr	1.583		59.8	33.41	45.75	*34*	52.89	75.19		
Ba	2.643		332	64.37	156.1	*61.9*	170.11	488.1		

	D*(l)	D**(r	D*(l)/D	D**(r)/	f*=Co/C	Son/Cl	Son/Cr
U	#NUM!	#NUM!	#NUM!	#NUM!	####	0.00	0.00
Th	#NUM!	#NUM!	#NUM!	#NUM!	####	0.00	0.00
Zr	1.66	2.44	0.94	1.38	1.94	1.11	0.73
Hf	#NUM!	#NUM!	#NUM!	#NUM!	####	0.00	0.00
Ta	#NUM!	#NUM!	#NUM!	#NUM!	####	0.00	0.00
La	1.24	1.51	4.40	5.38	1.27	0.39	0.57
Eu	#NUM!	#NUM!	#NUM!	#NUM!	####	0.00	0.00
Tb	#NUM!	#NUM!	#NUM!	#NUM!	####	0.00	0.00
Co	1.35	1.76	0.83	1.09	1.42	1.31	0.94
Sc	#NUM!	#NUM!	#NUM!	#NUM!	####	0.00	0.00
Rb	1.42	1.92	1.08	1.45	1.52	0.90	0.76
Sr	1.57	2.23	0.99	1.41	1.76	1.02	0.74
Ba	2.68	4.66	1.01	1.76	5.36	0.96	0.40

D*(l) and D**(r)- back calculated D from Cl and Cr f*=f for perfectly incompatible elements

Mix'n'Mac file : 120 to 23 m'n'm
Date: 04-05-1990 Time: 09:01:41

	Parent mag120	Daughter mag 23	Phases fayalite	hedenbergite	ksp	ilm	apt	phase 6
Variables								
SiO2	67.58	75.60	30.56	48.27	67.27	0.51	0.00	0.00
TiO2	0.41	0.09	0.72	0.37	0.00	50.02	0.00	0.00
Al2O3	15.97	13.20	0.09	0.23	18.35	0.00	0.00	0.00
FeO	4.97	0.63	60.90	28.54	0.92	44.19	0.21	0.00
MnO	0.12	0.03	3.43	0.91	0.00	1.44	1.52	0.00
MgO	0.25	0.13	3.47	0.92	0.00	0.46	0.54	0.00
CaO	1.15	0.21	1.13	18.70	0.15	0.71	52.40	0.00
Na2O	5.73	4.77	0.00	1.19	6.45	0.00	0.00	0.00
K2O	5.58	4.47	0.00	0.00	7.05	0.00	0.00	0.00
P2O5	0.08	0.02	0.00	0.00	0.00	0.00	45.33	0.00

Oxides recalculated to 100%

RESULTS:

	Parent observed	Parent estimated	Residuals
SiO2	66.36	66.37	-0.0108
TiO2	0.40	0.41	-0.0048
Al2O3	15.68	15.54	0.1412
FeO	4.88	4.87	0.0078
MnO	0.12	0.20	-0.0847
MgO	0.25	0.22	0.0271
CaO	1.13	1.12	0.0090
Na2O	5.63	5.54	0.0876
K2O	5.48	5.83	-0.3524
P2O5	0.08	0.09	-0.0080
			0.1600 = sum of squared residuals

Component	Proportion
mag 23	0.2203
fayalite	0.0419
hedenbergite	0.0437
ksp	0.6876
ilm	0.0066
apt	0.0018

Kd*	heden	amph	fay	tiMt.29	plg	san	apt	Zir	Tit
U	0.09	0.45	0.14	0.29	0.04	0.07	0	300	1
Th	*1.6*	*0.11*	*0.49*	*0.39*	*3E-04*	*0.05*	0	62	1
Zr	*0*	*0.5*	*0.66*	*1.8*	*0.008*	*0.07*	0	1500	1
Hf	0.95	0.84	0.09	2.51	0.03	0.08	0	1000	1
Ta	0.47	1.02	0.14	2.55	0.03	0.05	0	40	70
La	0.66	0.85	0.4	0.87	0.23	0.24	12	0.8	10
Eu	*0.87*	*3.2*	*0*	*0.4*	*2*	*2*	10	2.5	30
Tb	3	3.67	0.52	1.72	0.06	0.09	21	15	40
Co	5.3	16.7	14.6	41.7	0.08	0.29	0	9	1
Sc	*30*	*5.3*	*0.5*	*2.5*	*0*	*0.1*	0	60	1
Rb	*0.03*	*0.08*	*0.007*	*0*	*0.02*	*1.5*	0	0	1
Sr	*0.04*	*0.3*	*0*	*0.04*	*5.2*	*1.8*	2	0	1
Ba	0.1	0.8	0.05	0.1	1.4	3	1	0	1

	SAMPLE #	REF.	SiO2	TiO2	Al2O3	FeO	Fe2O3	MnO	MgO	CaO
PARENT	MAG-120	Perlit(L	67.58	0.41	15.97	0	4.97	0.12	0.25	1.15
PRODUCT	MAG-23	Perlit(L	75.64	0.09	13.2	0	0.63	0.03	0.13	0.21

	cpx	amph	oiv	tiMt.29	plg	ksp	apt	zir	tit
least squares input	0.037	0	0.0446	0.007	0	0.666	0	9E-04	0
% cummulate	0.049	0	0.05905	0.009	0	0.882	0	0.001	0

	D	f	Co	Cl	Cr	son	Cs-inst	Cs-avg	um com	oxides
U	0.435	0.243	5.1783	11.53	6.06	0	5.01	3.14	63.51	sio2
Th	0.229		21.284	63.37	26.38	*0*	14.51	7.78	0.55	tio2
Zr	1.904		440	122.34	342.10	*118*	233	541.9	16.19	al2o3
Hf	1.337		14.411	8.95	13.12	0	11.96	16.16	6.24	fe2o3
Ta	0.146		7.8502	26.27	9.95	0	3.85	1.94	0.26	mno
La	0.277		97.162	270.48	118.83	22	74.79	41.56	0.25	mgo
Eu	1.812		1.4577	0.40	1.16	*0*	0.84	1.78	1.12	cao
Tb	0.291		2.1902	5.97	2.67	0	1.74	0.98	5.74	na2o
Co	1.770		0.9209	0.31	0.74	1.84	0.55	1.12	6.21	k20
Sc	1.686		2.7468	1.04	2.27	*0*	1.75	3.29	0.00	p205
Rb	1.324		215	135.90	196.46	*168*	179.96	240.38		
Sr	1.589		59.8	25.98	50.76	*40*	41.29	70.65		
Ba	2.653		332	31.99	209.6	*22.5*	84.89	428.3		

	D*(I)	D**(r)	D*(I)/D	D**(r)/f	f*=Co/Cl	Son/Cl	Son/Cr
U	#NUM!	#NUM!	#NUM!	#NUM!	####	0.00	0.00
Th	#NUM!	#NUM!	#NUM!	#NUM!	####	0.00	0.00
Zr	1.93	5.73	1.01	3.01	3.73	0.96	0.34
Hf	#NUM!	#NUM!	#NUM!	#NUM!	####	0.00	0.00
Ta	#NUM!	#NUM!	#NUM!	#NUM!	####	0.00	0.00
La	2.05	6.34	7.41	22.92	4.42	0.08	0.19
Eu	#NUM!	#NUM!	#NUM!	#NUM!	####	0.00	0.00
Tb	#NUM!	#NUM!	#NUM!	#NUM!	####	0.00	0.00
Co	0.51	-1.49	0.29	-0.84	0.50	5.94	2.48
Sc	#NUM!	#NUM!	#NUM!	#NUM!	####	0.00	0.00
Rb	1.17	1.89	0.89	1.42	1.28	1.24	0.86
Sr	1.28	2.45	0.81	1.54	1.50	1.54	0.79
Ba	2.90	10.67	1.09	4.02	14.76	0.70	0.11

D*(I) and D**(r)- back calculated D from Cl and Cr f*=I for perfectly incompatible elements

APPENDIX III.V.IV

AEGIRINE GRANITE

Mix'n'Mac file : 49 TO 48.M'N'M
Date: 04-05-1990 Time: 09:04:21

	Parent mag49	Daughter mag 48	Phases TI-MAG	AEG	ksp	phase 4	phase 5	phase 6
Variables								
SiO2	70.90	73.80	0.21	51.84	67.27	0.00	0.00	0.00
TiO2	0.33	0.18	53.03	0.17	0.00	0.00	0.00	0.00
Al2O3	11.80	9.79	0.00	0.94	18.35	0.00	0.00	0.00
FeO	5.08	5.60	46.82	32.46	0.92	0.00	0.00	0.00
MnO	0.00	0.08	1.60	0.02	0.00	0.00	0.00	0.00
MgO	0.10	0.10	0.00	0.19	0.00	0.00	0.00	0.00
CaO	0.34	0.26	0.32	0.20	0.15	0.00	0.00	0.00
Na2O	4.93	4.67	0.00	13.42	6.45	0.00	0.00	0.00
K2O	4.39	4.17	0.00	0.38	7.05	0.00	0.00	0.00
P2O5	0.05	0.05	0.00	0.00	0.00	0.00	0.00	0.00

Oxides recalculated to 100%

RESULTS:

	Parent observed	Parent estimated	Residuals
SiO2	72.41	72.41	-0.0009
TiO2	0.34	0.42	-0.0781
Al2O3	12.05	11.83	0.2169
FeO	5.19	5.10	0.0902
MnO	0.00	0.07	-0.0685
MgO	0.10	0.08	0.0248
CaO	0.35	0.24	0.1115
Na2O	5.03	5.25	-0.2202
K2O	4.48	4.85	-0.3695
P2O5	0.05	0.04	0.0136
			0.2642 = sum of squared residuals

Component	Proportion
mag 48	0.7387
TI-MAG	0.0053
AEG	0.0134
ksp	0.2454

Kd*	heden	amph	fay	tiMt.29	plg	san	apt	Zir	Tit
U	0.09	0.45	0.14	0.29	0.04	0.07	0	300	1
Th	*1.6*	*0.11*	*0.49*	*0.39*	*3E-04*	*0.05*	0	62	1
Zr	*0*	*0.5*	*0.66*	*1.8*	*0.008*	*0.07*	0	1500	1
Hf	0.95	0.84	0.09	2.51	0.03	0.08	0	1000	1
Ta	0.47	1.02	0.14	2.55	0.03	0.05	0	40	70
La	0.66	0.85	0.4	0.87	0.23	0.24	12	0.8	10
Eu	*0.87*	*3.2*	*0*	*0.4*	*2*	*1.13*	2	2.5	30
Tb	3	3.67	0.52	1.72	0.06	0.09	21	15	40
Co	5.3	16.7	14.6	41.7	0.08	0.29	0	9	1
Sc	*30*	*5.3*	*0.5*	*2.5*	*0*	*0.1*	0	60	1
Rb	*0.03*	*0.08*	*0.007*	*0*	*0.02*	*0.9*	0	0	1
Sr	*0.04*	*0.3*	*0*	*0.04*	*5.2*	*2*	2	0	1
Ba	0.1	0.8	0.05	0.1	1.4	7.5	1	0	1

	SAMPLE #	REF.	SIO2	TIO2	AI2O3	FeO	Fe2O3	MnO	MgO	CaO
parent	MAG-49	Ridley(U	70.9	0.33	11.8	0	5.08	0.09	0.1	0.34
product	MAG-48	Ridley(U	73.8	0.18	9.79	0	5.6	0.08	0.1	0.26

	cpx	amph	oiv	tiMt.29	plg	ksp	apt	zir	tit
least squares input	0.017	0	0	0.0005	0	0.259	0	0.0005	0
% cummulate	0.061	0	0	0.00181	0	0.935	0	0.0018	0

	D	f	Co	Cl	Cr	son	Cs-inst	Cs-avg	cum com	oxides
U	0.613	0.723	6.897	7.82	11.33	3.44	4.79	4.49	65.92	sio2
Th	0.258		38.48	48.96	99.81	*10.85*	12.61	11.13	0.12	tio2
Zr	2.776		1151	646.94	117.70	*519*	1796	2467	17.17	al2o3
Hf	1.943		35.08	25.84	10.46	26.23	50.20	59.20	2.70	fe2o3
Ta	0.152		18.63	24.52	55.31	8.11	3.74	3.24	0.06	mno
La	0.268		128.63	163.10	329.22	46.08	43.70	38.65	0.06	mgo
Eu	1.115		1.78	1.71	1.54	*0.609*	1.91	1.95	1.29	cao
Tb	0.298		3.92	4.92	9.65	1.53	1.47	1.31	6.10	na2o
Co	0.688		0.343	0.38	0.51	0.6132	0.26	0.25	6.59	k20
Sc	2.047		0.401	0.29	0.10	*0.218*	0.58	0.70	0.00	p205
Rb	0.843		340	357.72	415.73	*362*	301.69	293.75		
Sr	1.873		29	21.85	9.46	*24*	40.92	47.66		
Ba	7.019		41	5.82	0.01808	*32*	40.85	132.8		

	D*(I)	D**(r	D*(I)/D	D**(r)/D	f*=Co/Cl	Son/Cl	Son/Cr
U	3.14	1.54	5.13	2.52	2.00	0.44	0.30
Th	4.90	1.99	19.04	7.71	3.55	0.22	0.11
Zr	3.46	1.62	1.24	0.58	2.22	0.80	4.41
Hf	1.90	1.23	0.98	0.63	1.34	1.02	2.51
Ta	3.56	1.65	23.39	10.81	2.30	0.33	0.15
La	4.17	1.80	15.55	6.72	2.79	0.28	0.14
Eu	4.31	1.84	3.86	1.65	2.92	0.36	0.40
Tb	3.90	1.73	13.07	5.81	2.56	0.31	0.16
Co	-0.79	0.55	-1.15	0.80	0.56	1.62	1.20
Sc	2.68	1.47	1.41	0.72	1.84	0.76	2.09
Rb	0.81	0.95	0.96	1.13	0.94	1.01	0.87
Sr	1.58	1.15	0.85	0.61	1.21	1.10	2.54
Ba	1.76	1.19	0.25	0.17	1.28	5.50	####

D*(I) and D**(r)- back calculated D from Cl and Cr f*=f for perfectly incompatible elements

Plate 2.1
Lithotectonic overlay

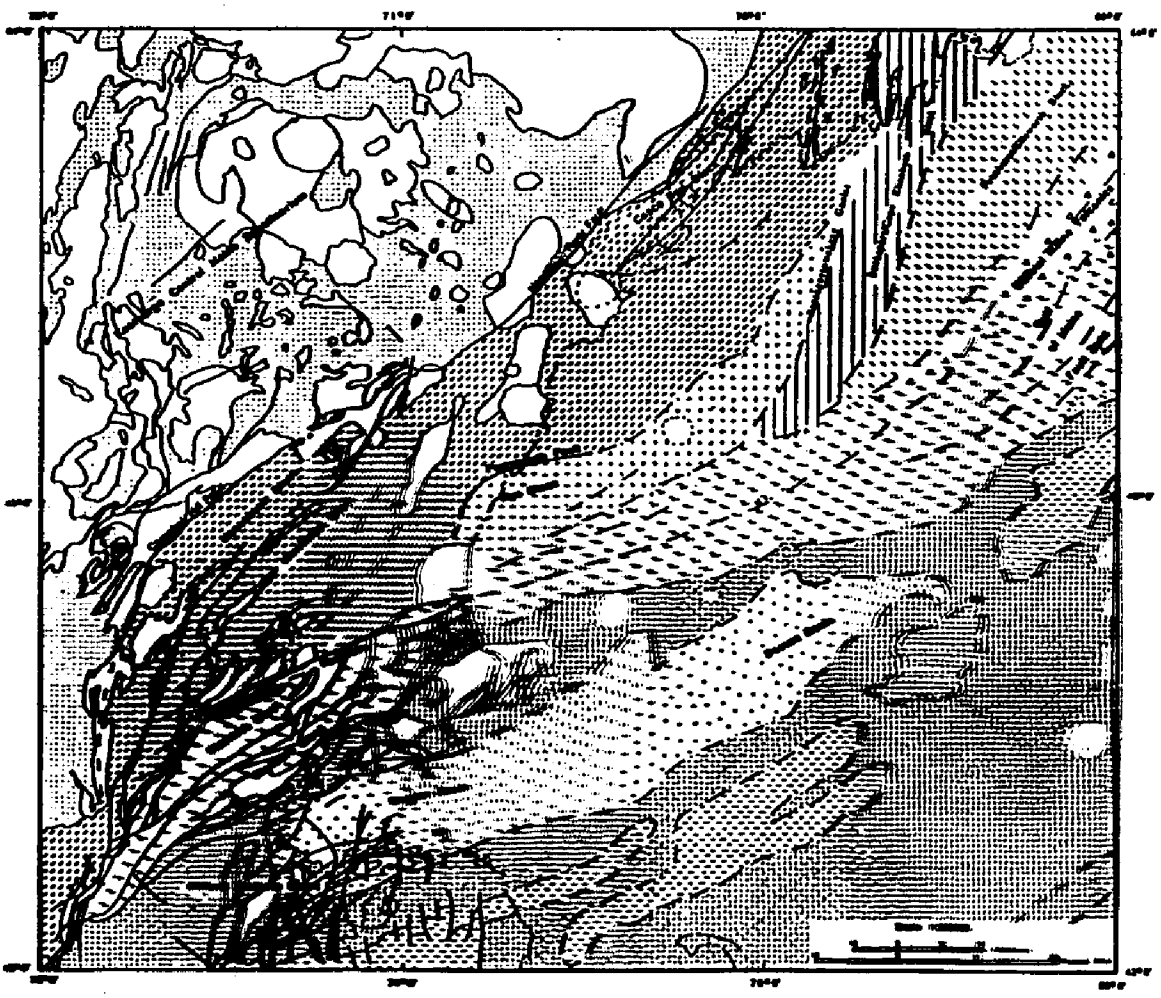

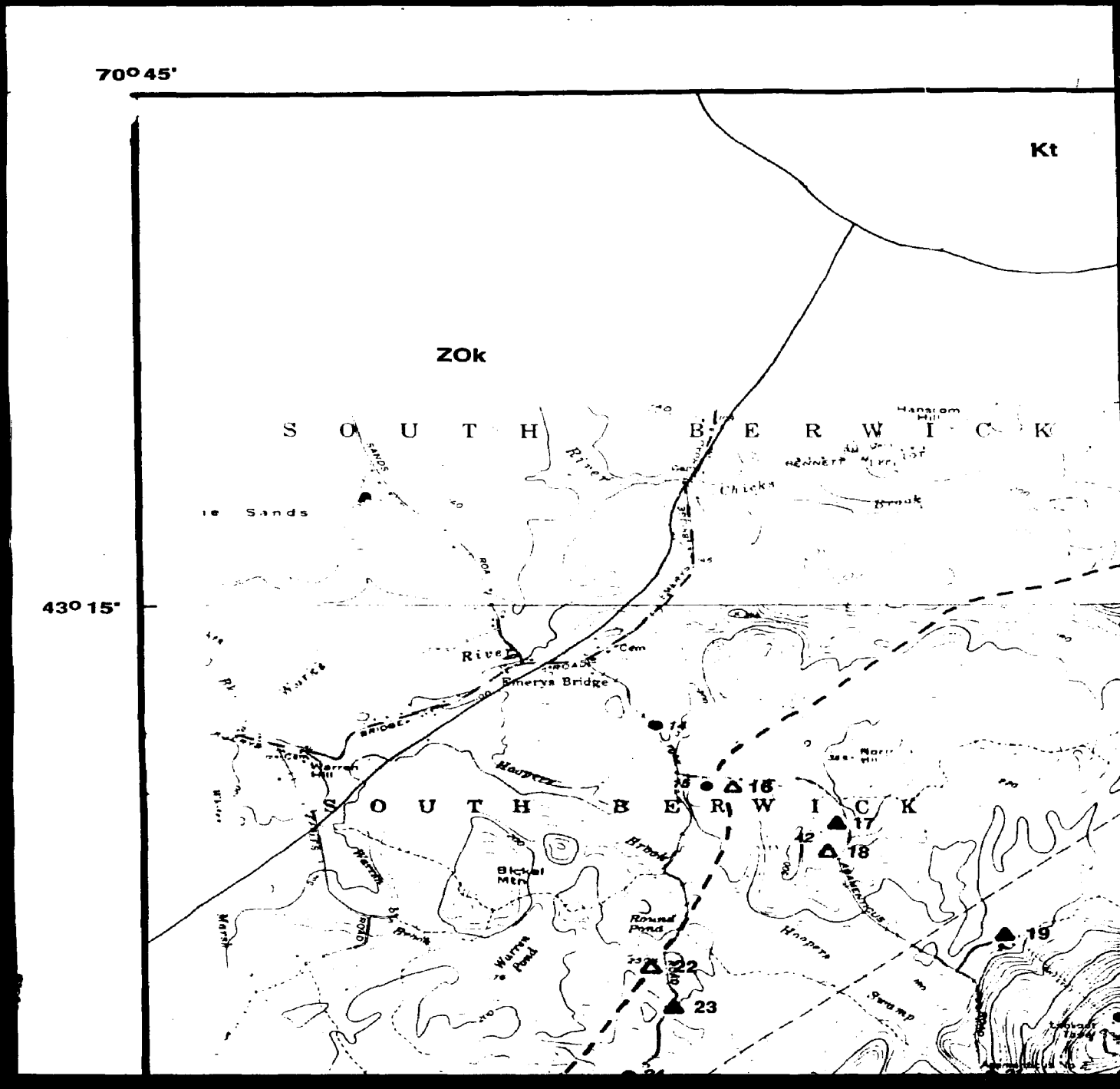
70° 45'
Kt
ZOk
S O U T H B E R W I C K
Sands
River
Brook
43° 15'
Emerys Bridge
Cem
Harper
Hooper
Round Pond
Warren Pond
Swamp
Hooper
16
17
18
19
22
23

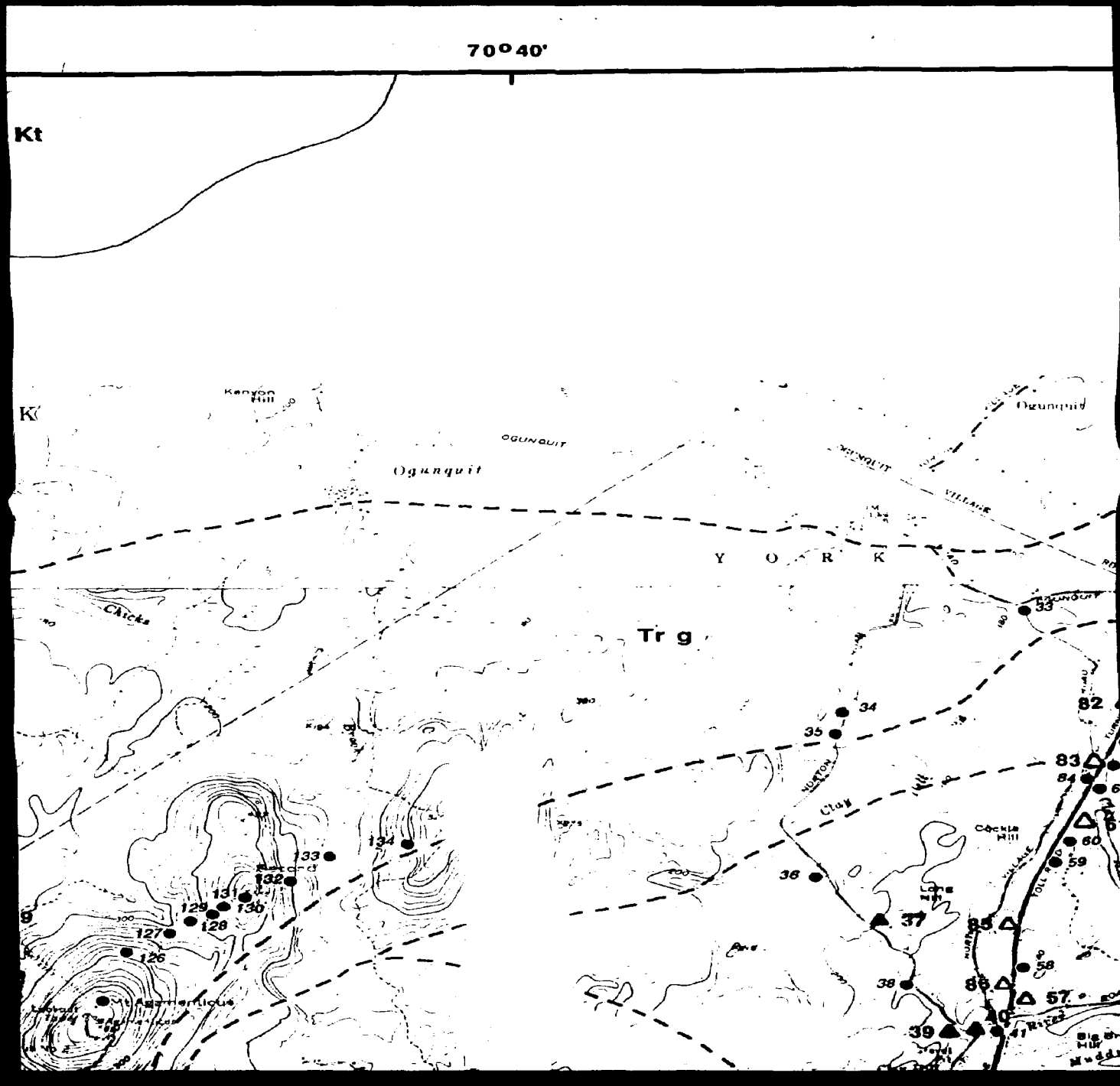
70°40'
Kt
Kenyon Hill
Ogunquit
OGUNQUIT
Ogunquit
Y O R K
Chicks
Tr g
Clay
Cocks Hill
Mt Agamenticus
33
34
35
36
37
38
39
40
41
82
83
84
85
86
57
58
59
60
126
127
128
129
130
131
132
133
134

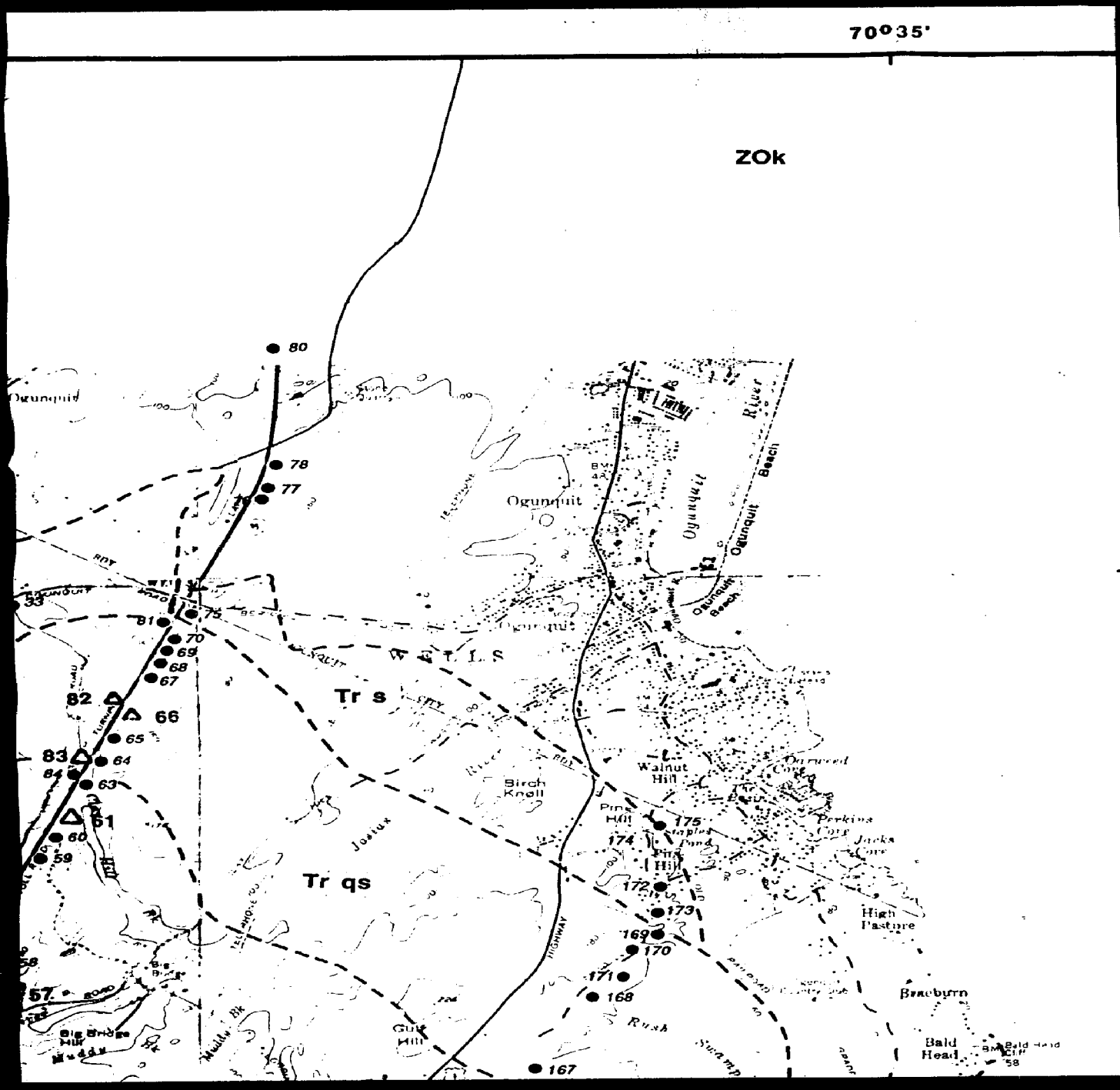
70°35'
ZOk
Ogunquit
Ogunquit River
Ogunquit Beach
Tr s
Tr qs
W E L S
Walnut Hill
Pine Hill
Birch Knoll
Josiux
Gulf Hill
Big Brook
High Pasture
Perkins Cove
Jacks Cove
Bald Head
Bald Head Cliff
Brackburn
Runk
Swamp
Highway
80
78
77
75
70
69
68
67
66
65
64
63
61
60
59
58
57
175
174
173
172
170
169
168
167
171

70°35'

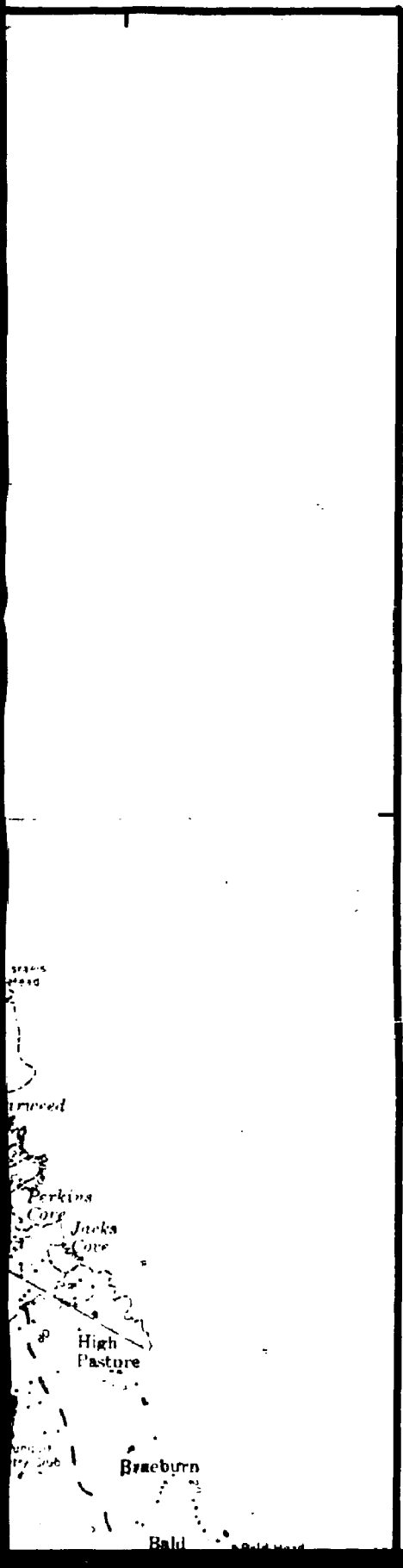

43° 15'

Plate 3.1

Sample locations

Legend (After Hussey, 1962 and 1985)

Metamorphic Rocks

ZOe- Eliot Formation
ZOk- Kittery Formation

Igneous Rocks

Kcn - Cape Neddick Complex
Kt- Tatnic Complex - undifferentiated
Tr g- Alkalic granite
Tr s- Alkalic syenite
Tr bg- Biotite granite
Tr qs- Quartz syenite
D g- Webhannet Pluton

--- Contacts within the Agamenticus Complex

—.—.— Contacts of country rocks

• Sample location

Δ Samples with thin-sections

▲ Samples with thin-sections and geochemical analyses

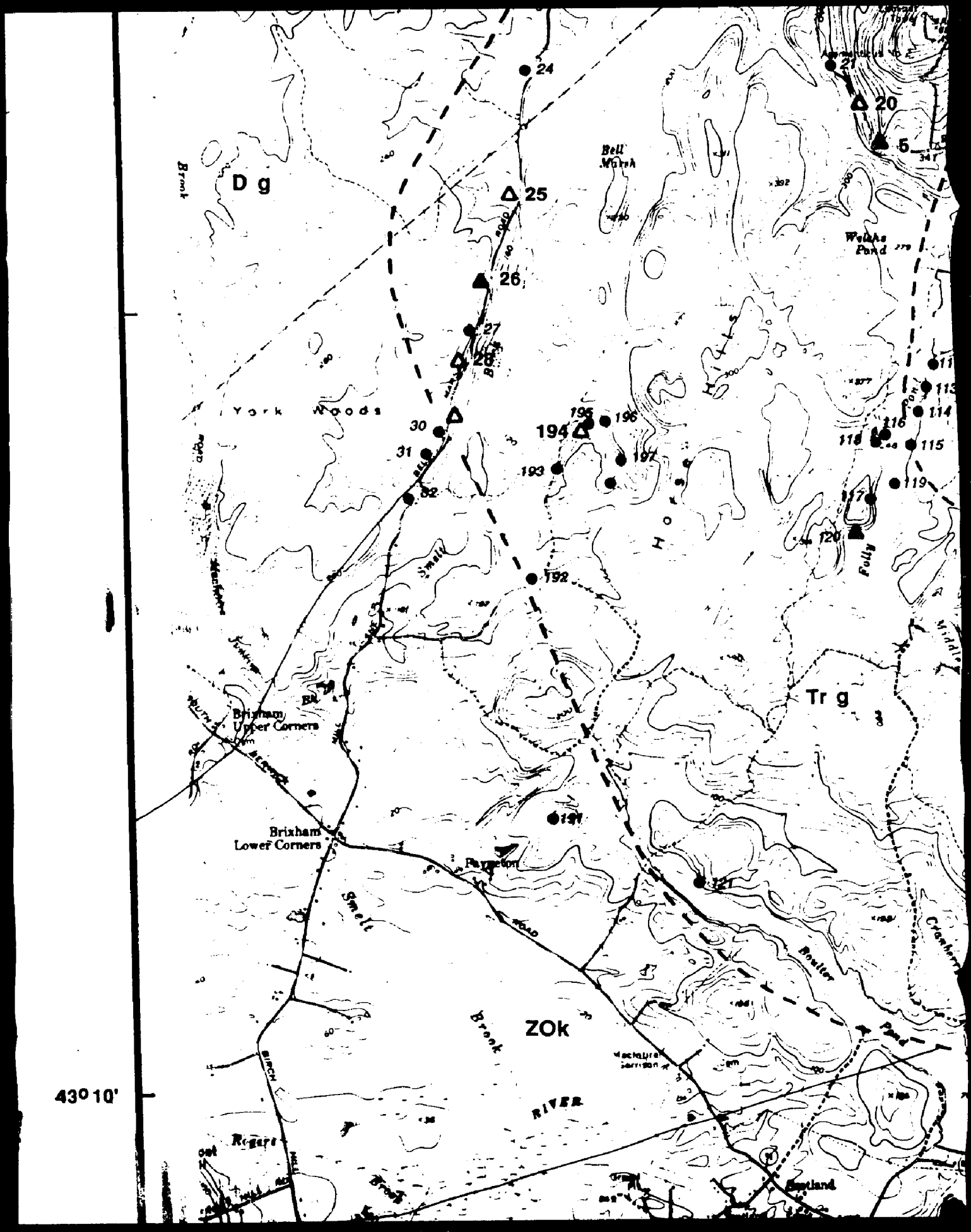
Dg
Tr g
ZOk
York Woods
Brixham Upper Corners
Brixham Lower Corners
Smelt
Brook
RIVER
Bell Marsh
Wallis Pond
Boulter Pond
Cranberry
Middle
Finley
Eastland
43° 10'
24
25
26
27
28
30
31
32
192
193
194
195
196
197
198
199
120
121
20
5
11
113
114
115
116
117
118
119

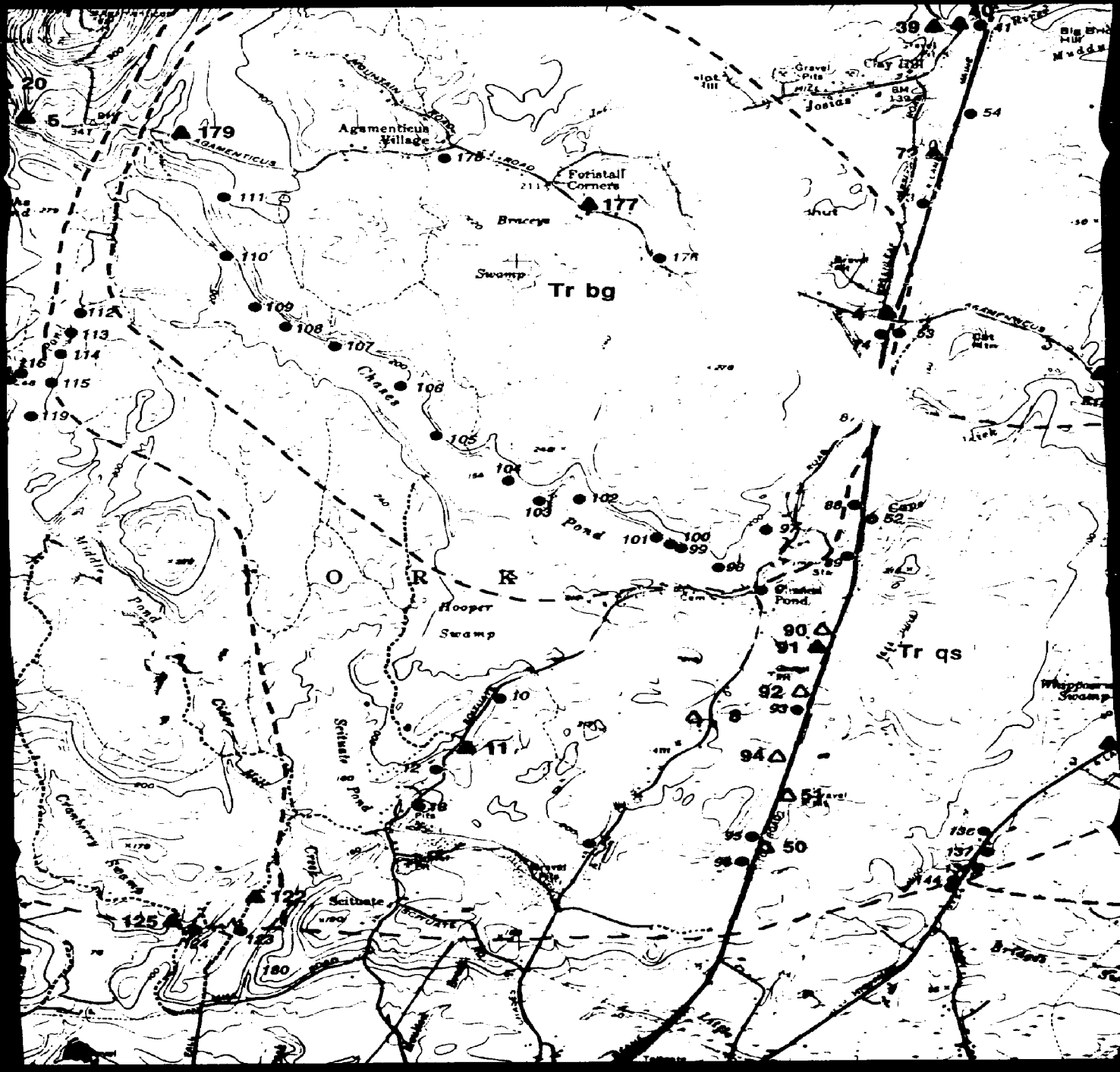
Agamenticus Village
Fortistall Corners
Swamp
Tr bg
Tr qs
Pond
Hooper Swamp
Chases
Scituate
Gravel Pits
Clay Pits
Josias
Capes
Whipple Swamp
Bridges
Agamenticus
Mountain Road
179
177
178
20
5
39
54
52
50
51
90
91
92
93
94
95
96
97
98
99
100
101
102
103
105
106
107
108
109
110
111
112
113
114
115
119
124
125
126
127
135
136
180

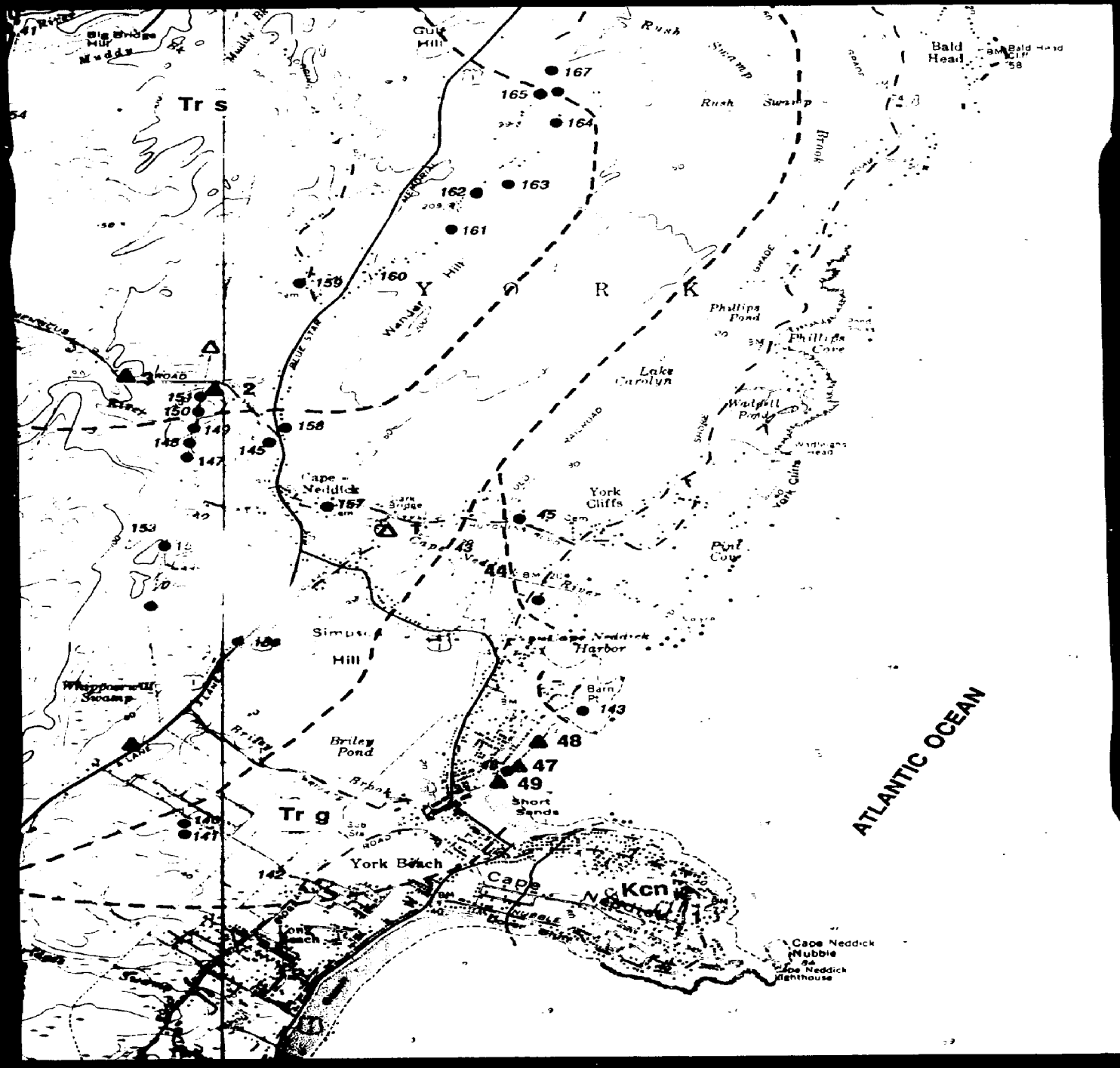
Tr s
Tr g
Kcn
ATLANTIC OCEAN
Bald Head
Gulf Hill
Rush Swamp
Brook
Y O R K
Phillips Pond
Phillips Cove
Lake Carolyn
Walpole Pond
Cape Neddick
York Cliffs
Pond Cove
Simpson Hill
Whipporwill Swamp
Briley Pond
Barn Pt.
Short Sands
York Beach
Cape Neddick Nubble
Cape Neddick Lighthouse
167
165
164
163
162
161
160
159
158
157
153
152
151
150
149
148
147
145
143
142
141
140
49
48
47
45
44
43
2

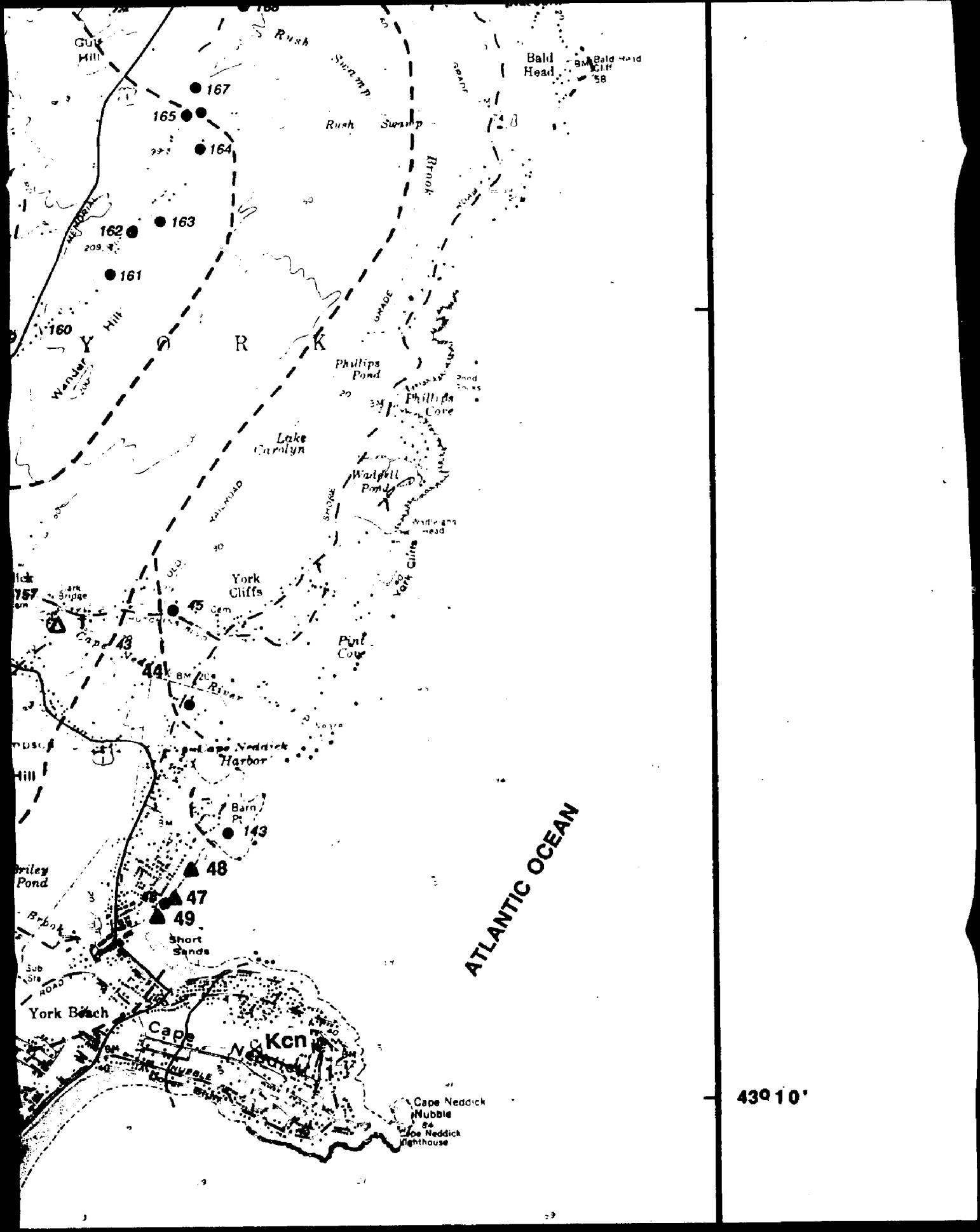
Gulf Hill
Rush Swamp
Bald Head
Bald Head Cliff
167
165
164
Rush Swamp
Brook
163
162
161
160
Hill
Y O R K
Wander
Phillips Pond
Phillips Cove
Lake Carolyn
Walpole Pond
York Cliffs
York Cliffs
Pool Cove
45
43
44
Cape Neddick Harbor
Barn Pt
143
48
47
49
Short Sands
ATLANTIC OCEAN
York Beach
Cape Neddick
Kcn
Cape Neddick Nubble
Cape Neddick Lighthouse
43° 10'

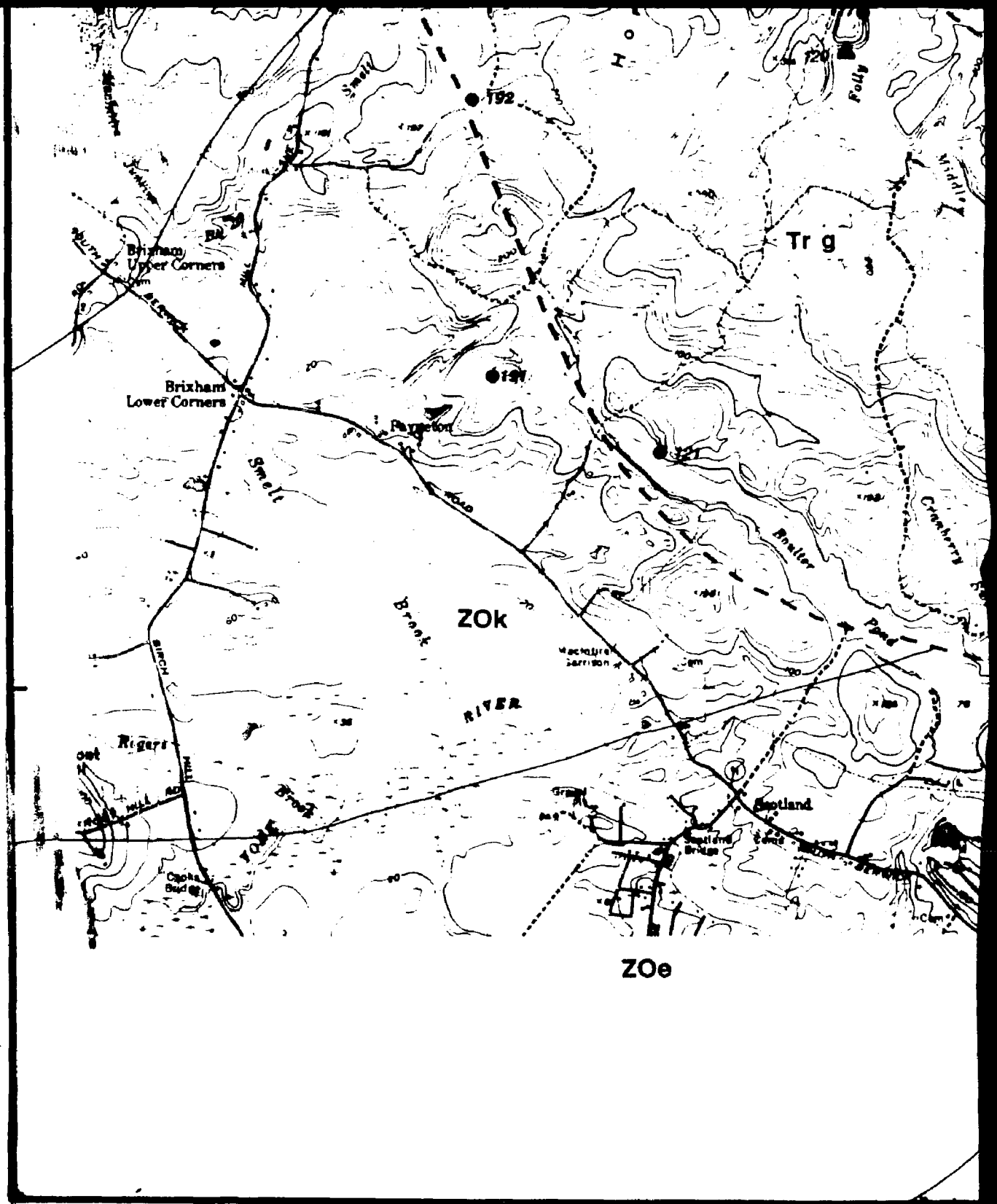
192
Tr g
Brixham
Upper Corners
Brixham
Lower Corners
191
Pepperton
Smelt
Brook
ZOk
Brattler
Pond
Cranberry
RIVER
Rogers
Scotland
ZOe
43°10'
70°45'

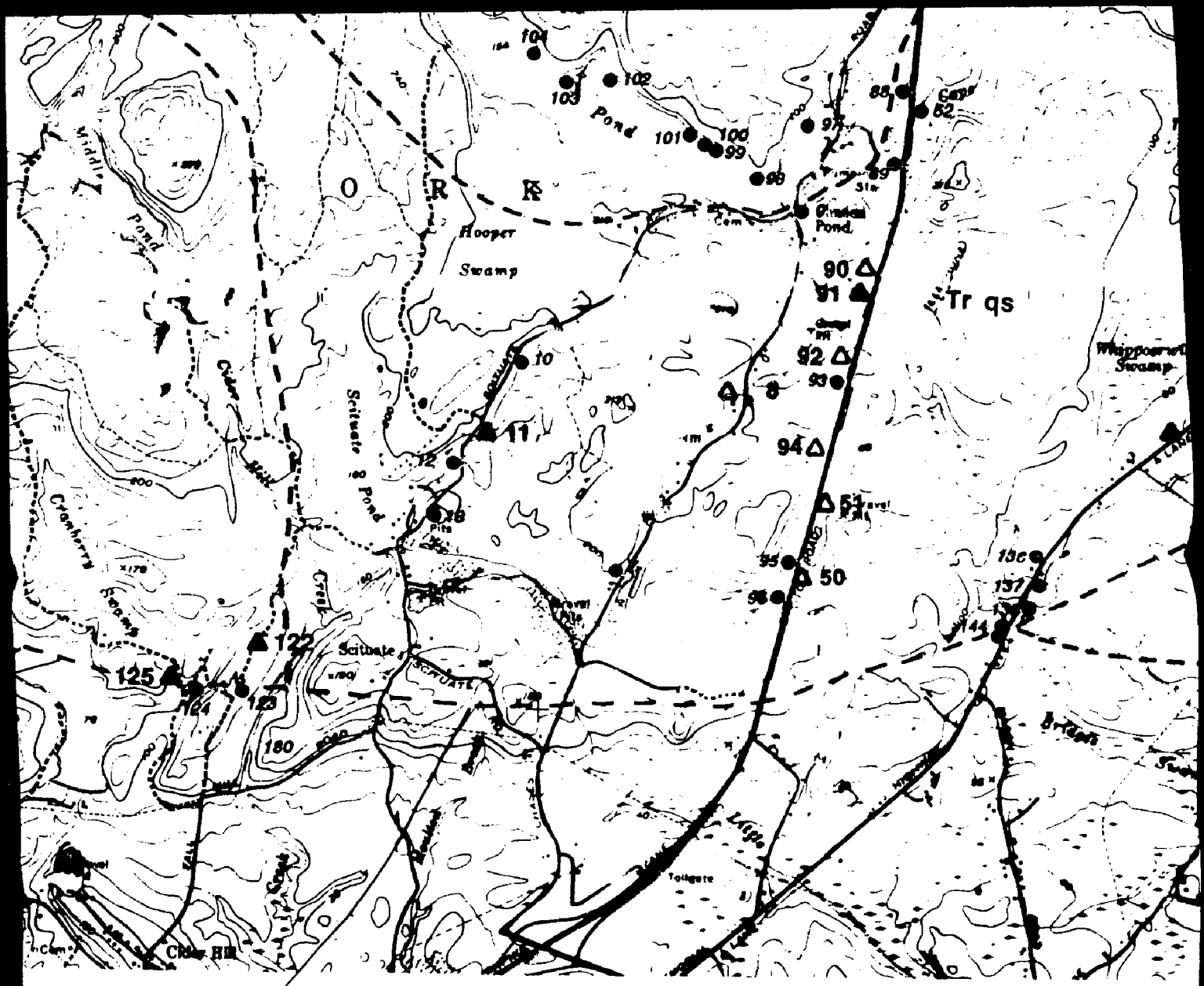
Hooper
Swamp
Pond
Scituate
Tr qs
ZOk
Cider Hill
70°40'

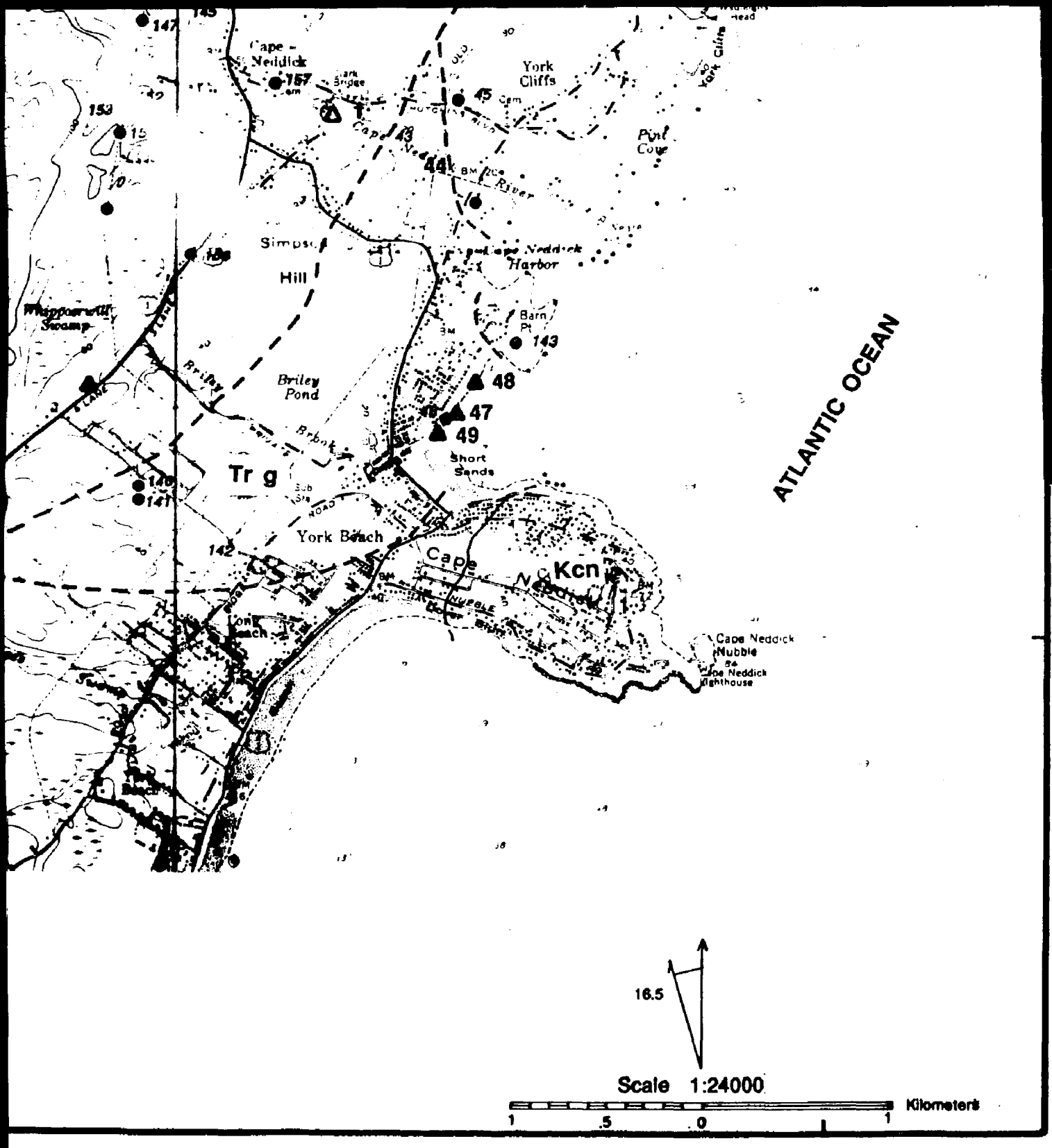
Cape Neddick
York Cliffs
Pine Cove
Simpson Hill
Cape Neddick Harbor
Barn Pt.
Whippoorwill Swamp
Briley Pond
Short Sands
ATLANTIC OCEAN
Tr g
York Beach
Cape Neddick Nubble
Cape Neddick Lighthouse
16.5
Scale 1:24000
1 .5 0 1 Kilometers
70°35'


York Cliffs
Pine Cove
Simpson Hill
Cape Neddick Harbor
Barn Pt
143
Briley Pond
48
47
49
Short Sands
York Beach
Cape Neddick
Nubble
Cape Neddick Lighthouse
ATLANTIC OCEAN
43°10'
16.5
Scale 1:24000
Kilometers
1 .5 0 1
70°35'

43°15'

Plate 3.2

Geology of the Agamenticus Complex

Legend

Agamenticus Complex

Tr bg- Biotite granite
Tr ag- Aegirine granite
Tr g- Alkalic granite


-quartz syenite

Tr s- Alkalic syenite


-fine grained alkalic syenite

Tr SQSZ- Syenite to Quartz Syenite zone


Tr as- Aegirine syenite


Region with abundant alkalic syenite xenoliths


Region with abundant xenoliths of country rocks.

- - - Lithic contacts

Dikes

unlabeled - basalt
a - aegirine
g - fine-grained alkalic granite
m - mafic syenite
p - pegmatite
r - rhyolite
t - trachyte

Dikes of basalt dike swarm

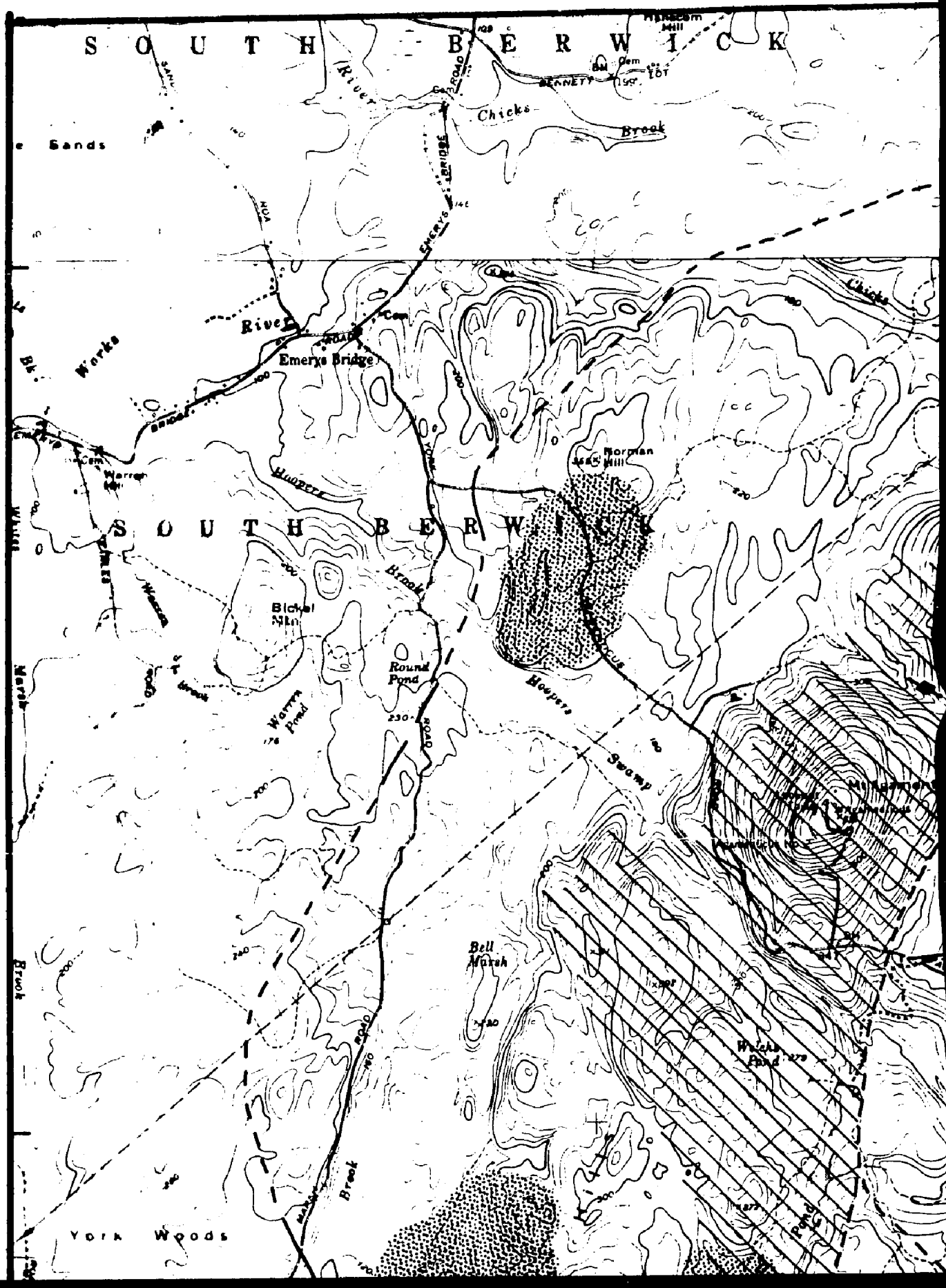
SOUTH BERWICK
Chicks Brook
Emerys Bridge
Emerys Bridge Road
Hoopers Swamp
Round Pond
Warren Pond
Bell Marsh
Norman Hill
Bickel Hill
York Woods
SOUTH BERWICK

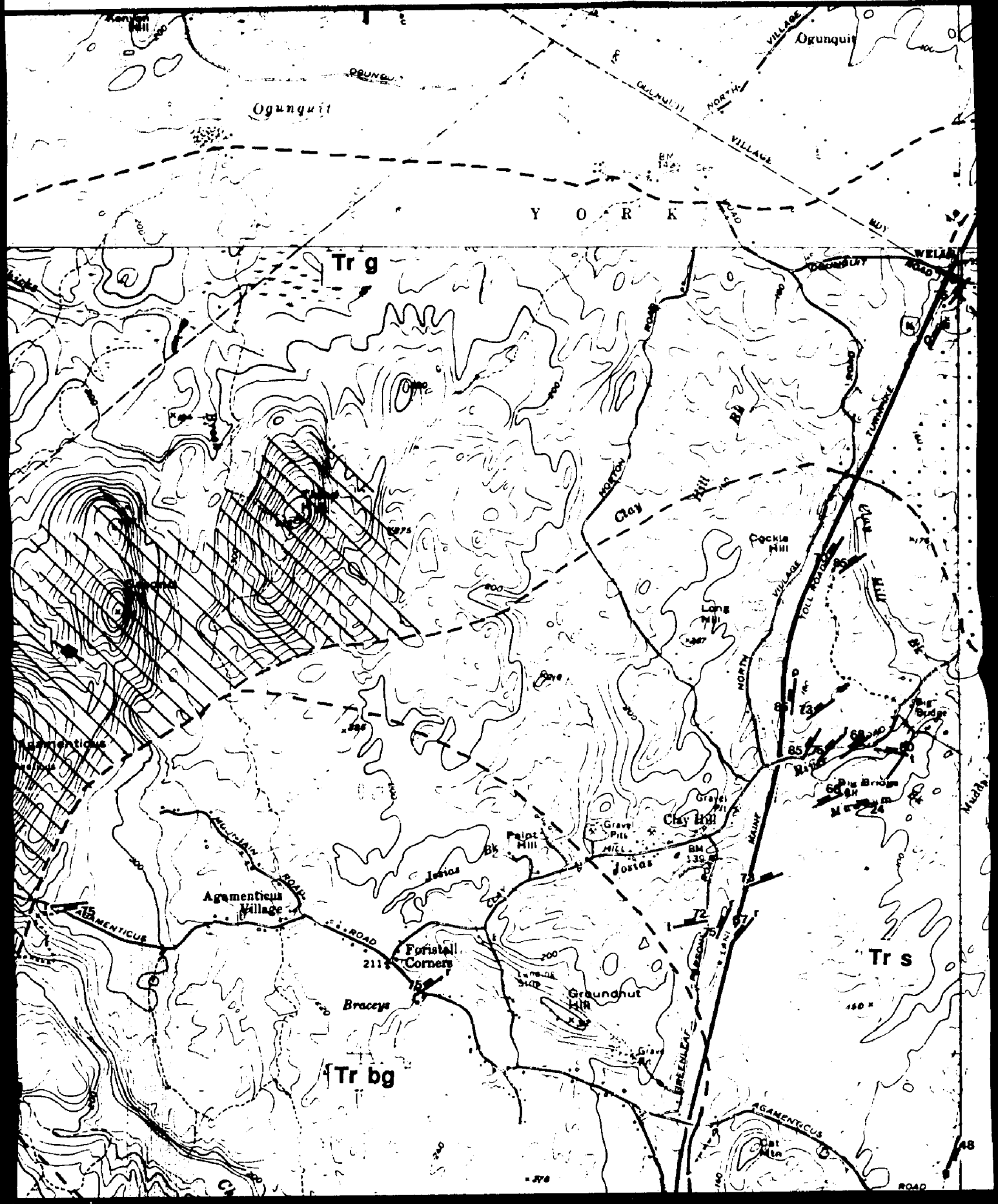
Kenyon Hill
Ogunquit
Ogunquit
OGUNQUIT NORTH VILLAGE ROAD
BM 142
Cem
Y O R K
WELLS
Tr g
NORTON ROAD
Clay Hill
Cockle Hill
Long Hill
NORTH VILLAGE ROAD
TOLL ROAD
TURNPIKE
Agamenticus
Agamenticus Village
MOUNTAIN ROAD
AGAMENTICUS ROAD
Foristall Corners
211
Braceys
Tr bg
Paint Hill
Josias
Gravel Pits
Clay Hill
BM 139
Groundnut Hill
GREENLEAF PARSONS LANE
MAINE
Big Bridge
Tr s
Cat Mtn
AGAMENTICUS ROAD
86
85
73
85
76
68
60
66
24
75
72
75
67
75
75
48

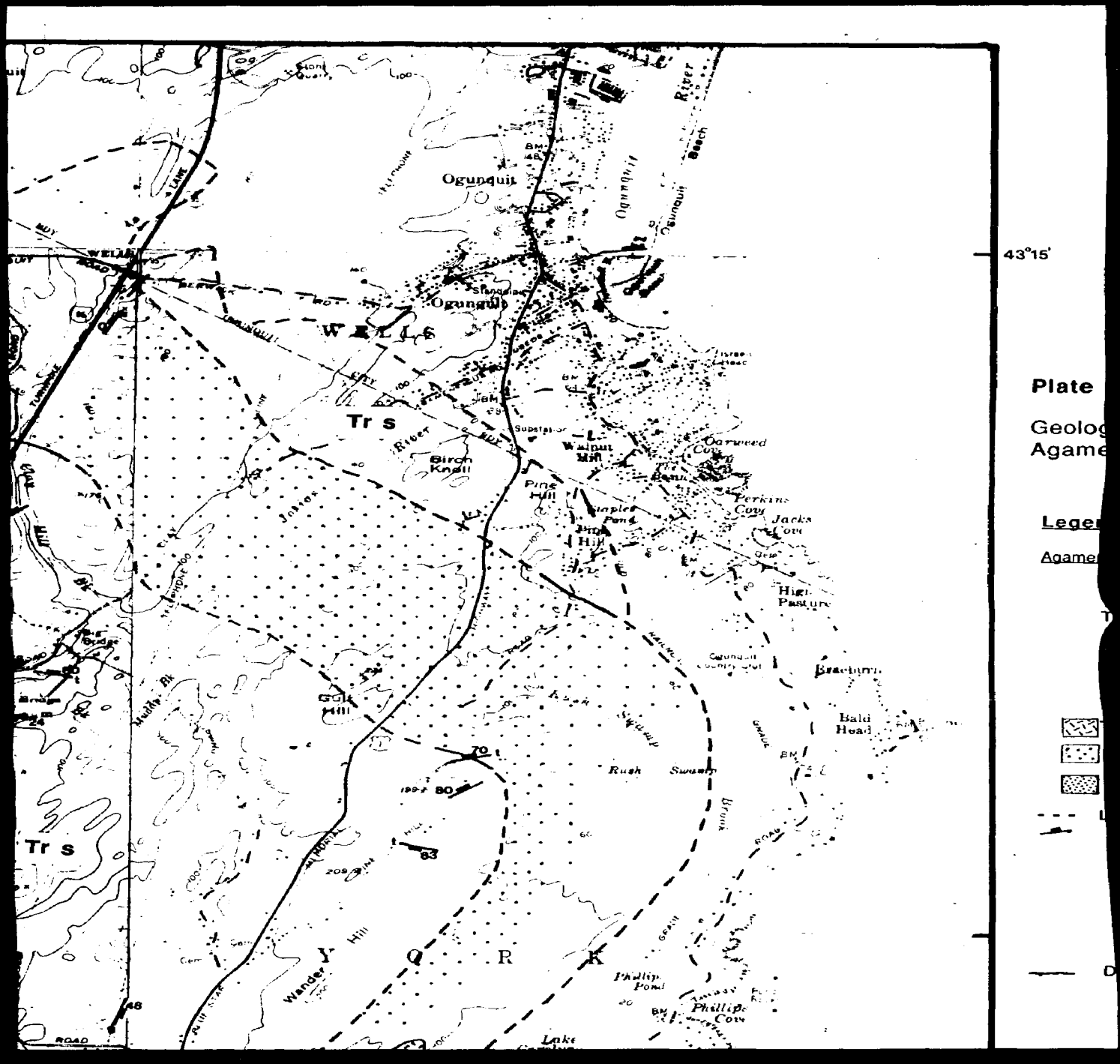
Ogunquit
Ogunquit River
Ogunquit Beach
WELLS
Tr s
Tr s
Birch Knoll
Pine Hill
Walnut Hill
Oarweed Cove
Perkins Cove
Jacks Cove
High Pasture
Bald Head
Rush Swamp
Gulf Hill
Wander Hill
Phillips Pond
Phillips Cove
Lake
Josiah
Mt. Hope
Mill Stream
Branch
Brook
Road
43°15'
Plate
Geolog
Agame
Leger
Agame

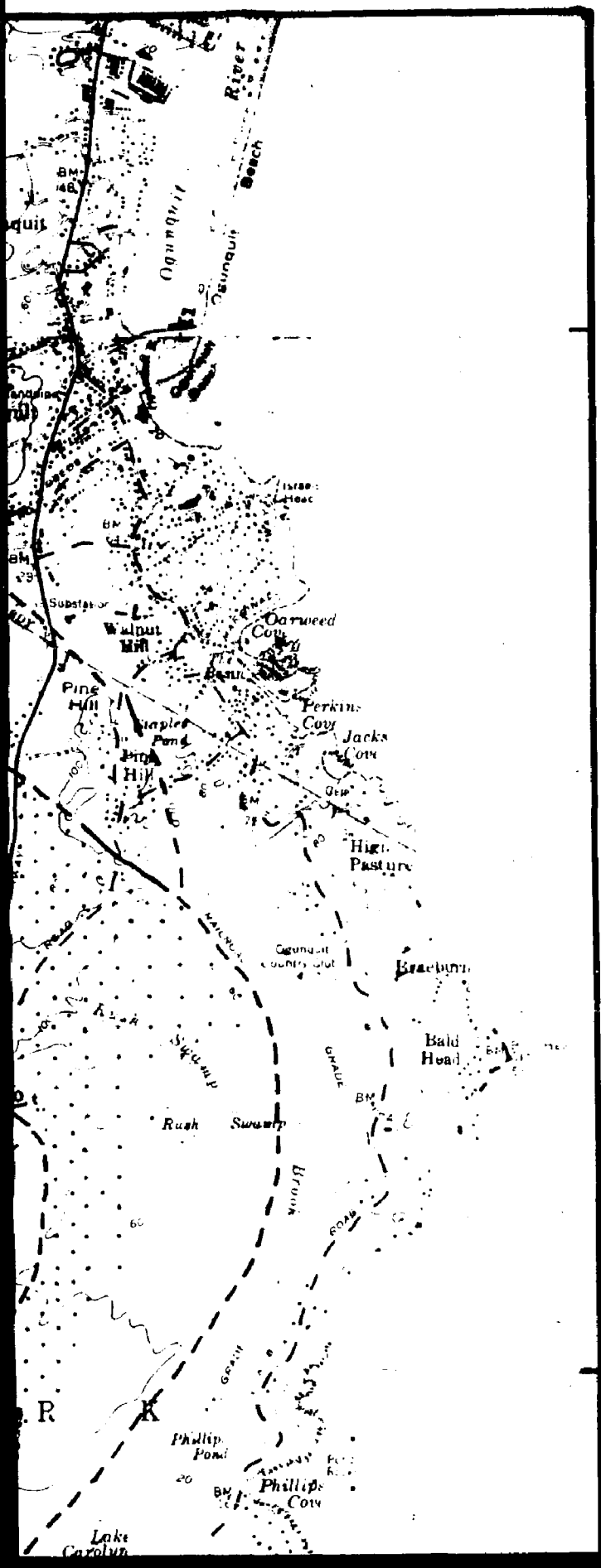

Plate 3.2

Geology of the Agamenticus Complex

Legend

Agamenticus Complex

- Tr bg- Biotite granite
- Tr ag- Aegirine granite
- Tr g- Alkalic granite
- -quartz syenite
- Tr s- Alkalic syenite
- -fine grained alkalic syenite
- Tr SQSZ- Syenite to Quartz Syenite zone
- Tr as- Aenigmatite syenite
- Region with abundant alkalic syenite xenoliths
- Region with abundant xenoliths of country rocks.
- Lithic contacts
- Dikes
  - unlabeled - basalt
  - a - aegirine
  - g - fine-grained alkalic granite
  - m - mafic syenite
  - p - pegmatite
  - r - rhyolite
  - t - trachyte
- Dikes of basalt dike swarm

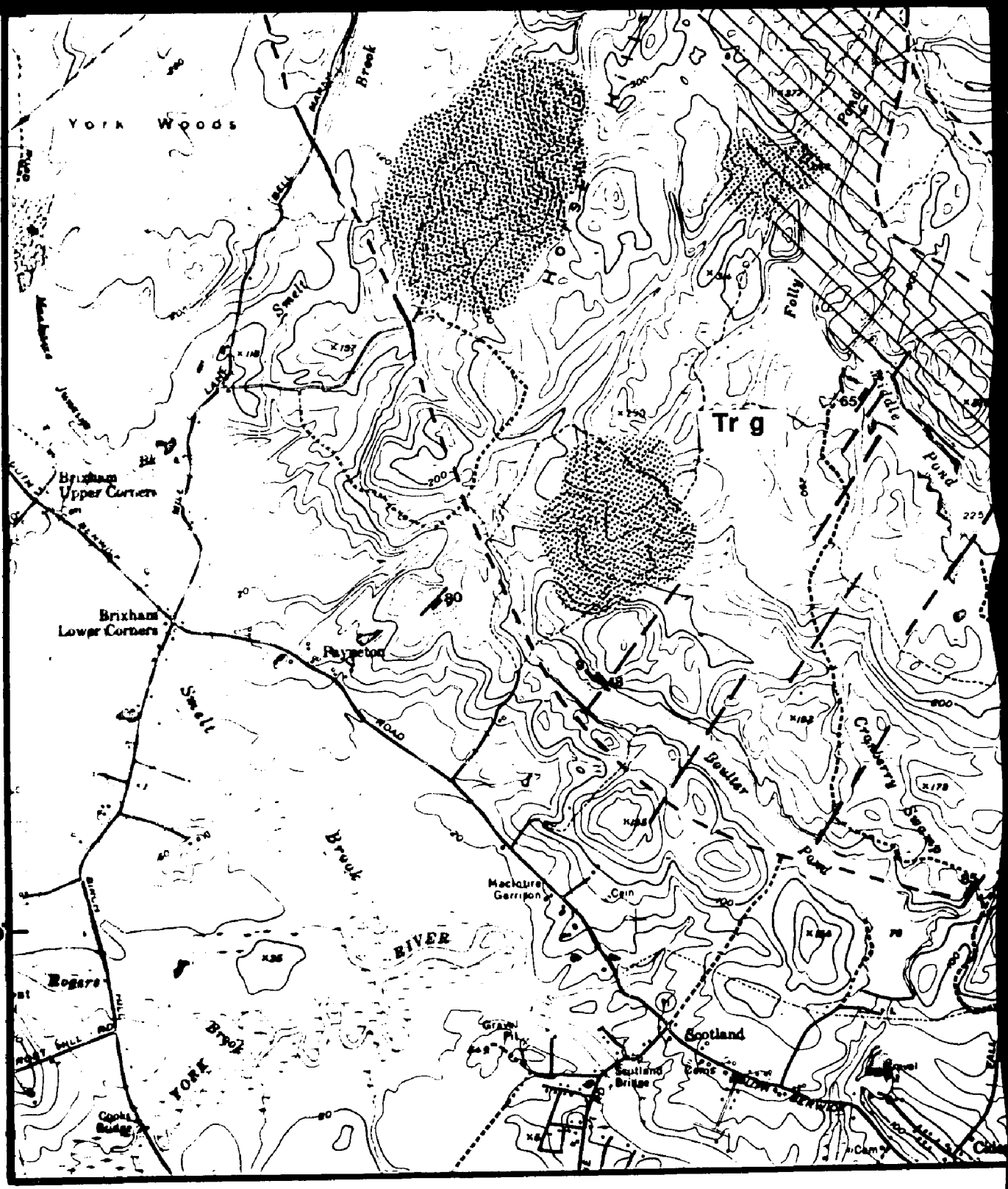
York Woods
Brixham Upper Corners
Brixham Lower Corners
Paynetop
Mackaye Garrison
Scotland
Scotland Bridge
Cooks Bridge
Rogers
Tr g
Folly Pond
Cranberry Swamp
Boulder Pond
Smelt Brook
York Brook
RIVER
43°10'


Tr SQSZ
Pond
Mooper
Swamp
Young Hill
Tollgate
Bridgett
Swamp
Agamenticus
Road
Nedelick
Capt
Chases
Pond
Scituate
Cliff Hill
70°40'

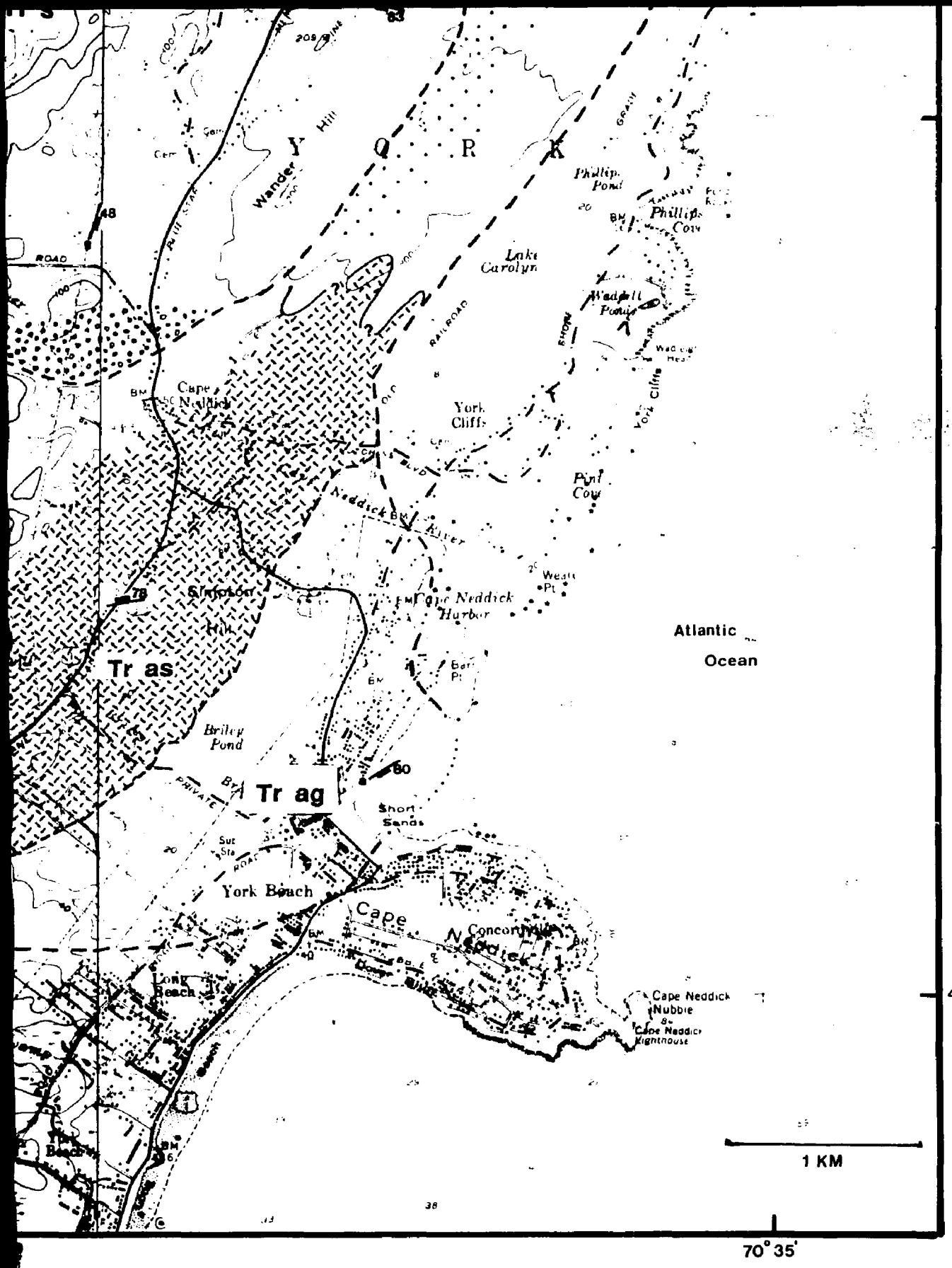
Dik
Y O R K
Wander Hill
Phillips Pond
Lake Carolyn
Waddell Pond
Cape Neddick
York Cliffs
Pine Cove
Neddick River
Cape Neddick Harbor
Atlantic Ocean
Tr as
Briley Pond
Tr ag
Short Sands
York Beach
Cape Neddick
Cape Neddick Nubble
Cape Neddick Lighthouse
1 KM
43°10'
70°35'

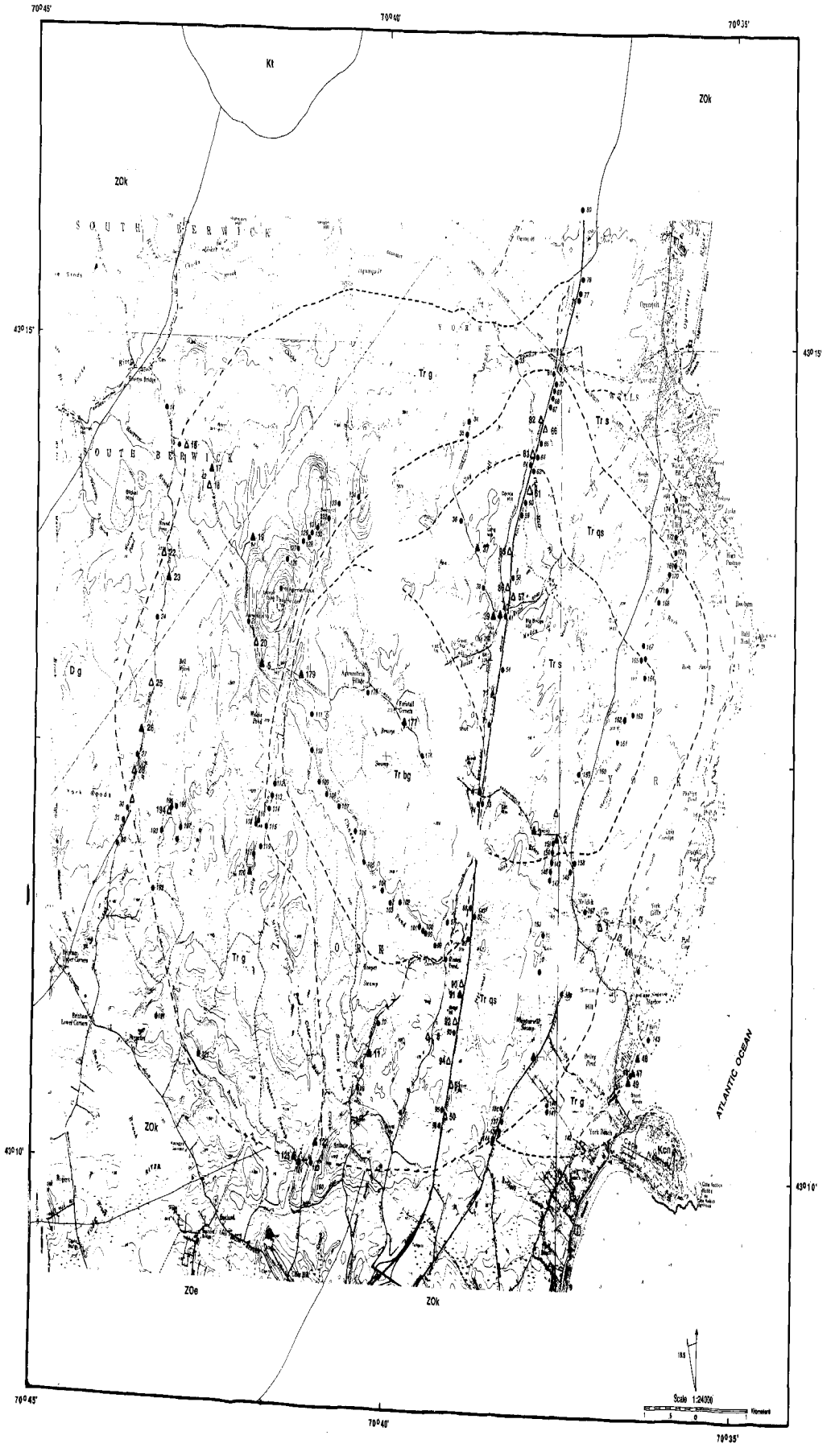

Plate 3.1

Sample locations

Legend (After Hussey 1969 and 1985)

Metamorphic Rocks

ZOe- Eliot Formation
ZOk- Kittery Formation

Igneous Rocks

Kcn - Capa Neddick Complex
Kt - Tonic Complex - undifferentiated
Tr g - Alkalic granite
Tr s - Alkalic syenite
Tr bg - Biotite granite
Tr qs - Quartz syenite
D g - Wohlomet Pluton

--- Contacts within the Agamenticus Complex
---- Contacts of country rocks
• Sample location
Δ Samples with thin-sections
▲ Samples with thin-sections and geochemical analyses

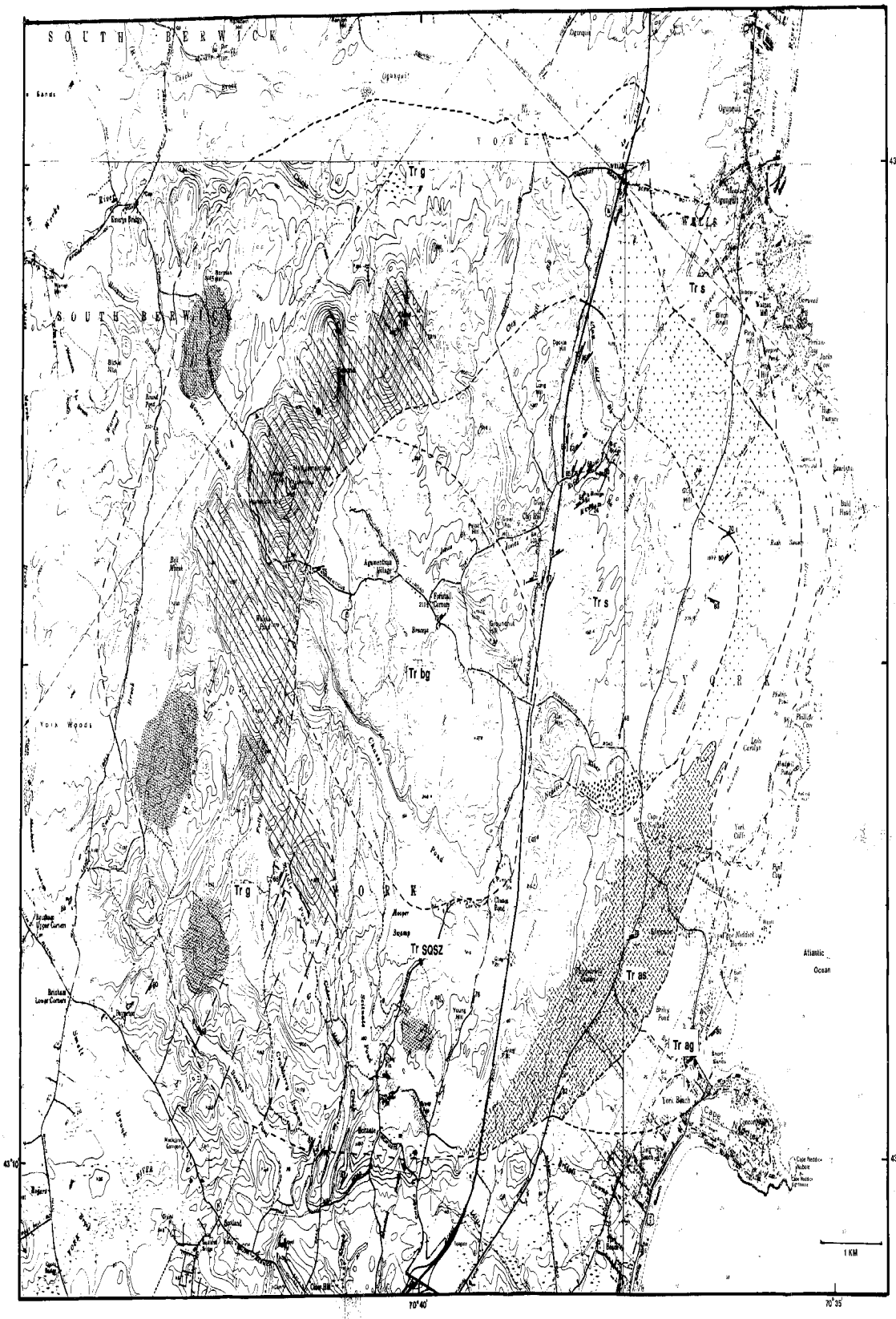

Plate 3.2

Geology of the
Agamenticus Complex

Legend

Agamenticus Complex

- Tr bg- Biotite granite
- Tr ag- Aegirine granite
- Tr g- Alkalic granite
- -quartz syenite
- Tr s- Alkalic syenite
- -fine grained alkalic syenite
- Tr SQSZ- Syenite to Quartz Syenite zone
- Tr as- Aegirinalite syenite
- Region with abundant alkalic syenite xenoliths
- Region with abundant xenoliths of country rocks.

- Lithic contacts
- Dikes
  - unlabeled - basalt
  - a - aegirine
  - g - fine-grained alkalic granite
  - m - mafic syenite
  - p - pegmatite
  - r - rhyolite
  - t - trachyte
- Dikes of basalt dike swarm